

INVESTIGATION OF FLOWSLIDES
FROM THE FAILURE OF
MINE TAILINGS' DAMS

BY

K.J. SPENCE

B.Eng (Hons)

A thesis submitted to the Department of Civil and Structural Engineering

in partial fulfilment of the requirements for the

Degree of Doctor of Philosophy

University of Sheffield

September 1992

SUMMARY

Progress to further understand the complex nature of the flowslides has, in the past, been restricted by a shortage of good quality experimental and field data. This thesis describes a series of small scale laboratory flowslide experiments, using a realistic test material of fine sand and water, which was performed to elucidate aspects of this phenomenon.

Following initiation of the flowslide, liquefaction of the static material occurred and the flowslide accelerated under the influence of gravitational driving forces without any segregation of the components of the two-phase material. It was observed that movement of the flowing material was not arrested 'en masse', but unsteady deposition of sand and pore fluid at the lower flow boundary occurred, being dependent on deceleration of the flowslide. This resulted in thinning of the flowing layer. The rate of deposition also increased with the solid volume concentration of the flowing material. The final stages of flowslide motion were influenced by the presence of surface water derived from consolidated material.

It was established that excess pore pressures were present during flowslide motion. Within the limitations of experimental measurement, the magnitude of these excess pore water pressures at the lower flow boundary was such that the intergranular friction was sufficiently reduced to allow motion. This reduction of intergranular friction explained the fluid-like motion observed at bed slopes lower than the equilibrium slope of the granular fluid. Some shear resistance mechanism other than Coulomb friction must therefore play an important role in bringing the flowslide to a halt.

ACKNOWLEDGEMENTS

This research project was conducted within the Department of Civil and Structural Engineering at the University of Sheffield, over the period October 1987 to December 1990. Financial support of this project was provided by a University Scholarship, in the form of a Hossein Famy award. This beneficiary kindly donated funds in thanks for the education received at this establishment. The main requirement of this award was that the research was related to the mining industry. This has been faithfully followed. I am also grateful to the Department of Civil and Structural Engineering for permission to use their facilities during preparation of this thesis.

Completion of this project was possible due to the arrival of both Professor A.J. Saul and Dr. I. Guymer to this Department. Without their moral support and the kind loan of laboratory equipment, I would most certainly have become yet another casualty of the acrimonious disputes that raged here at that time. I fully respect the time and effort that Dr. Guymer has devoted to this project. I would also like to thank all the Technical staff within the Department, in particular Glen Brawn, Shane Smith and Stuart Richards. The discussions with Dr. C.C.Hird were also helpful and appreciated.

Finally, I would like to mention Diane Foster and Harry Davis for their important contributions; I cannot thank you enough.

Life's but a walking shadow, a poor player
that struts and frets his hour upon the stage,
and then is heard no more.

[Shakespeare (1606): Macbeth Act V, Scene V, vs 24-26]

DECLARATION

Except where specific reference has been made to the work of others, this thesis was entirely the result of my own work. No part of this thesis has been submitted to any University or other educational establishment for a Degree, Diploma or other qualification.

.....

K.J.Spence

.....

Dr. I Guymer (Supervisor)

CONTENTS:

Summary	ii
Acknowledgements	iii
Declaration	v
Contents	vi
Notation	x
List of tables	xiv
List of figures	xv
1 INTRODUCTION	1
2 LITERATURE REVIEW	4
2.1 Mineral processing and mine tailings	4
2.2 Types and characteristics of tailings	6
2.3 Disposal of tailings	6
2.4 Failure of tailings' dams	10
2.5 Soil behaviour during liquefaction	13
2.51 Steady state and critical state soil mechanics	13
2.52 Undrained monotonic loading	18
2.53 Undrained cyclic loading	20
2.54 Relative density and confining pressure	22
2.55 Initial shear stress	24
2.56 Particle angularity	25
2.6 The flowslide event	25
2.7 Analysis of flowslide motion	28
2.71 Introduction	28

2.72	Dispersive pressures	31
2.73	Fluid turbulence	40
2.74	Laminar flow without dispersive pressures	43
2.75	Flow classification	48
2.8	Conclusions	50
3	PRELIMINARY EXPERIMENTS	52
3.1	Introduction	52
3.2	Selection of the test material	52
3.3	Experimental apparatus	54
3.4	Results of the preliminary experiments	57
3.41	Test sample preparation	57
3.42	The laboratory flowslide	61
3.43	Limitations of the preliminary apparatus	65
3.5	Conclusions	66
4	DEVELOPMENT OF THE EXPERIMENTAL APPARATUS	67
4.1	Perspex channel	67
4.2	Sluice gate	69
4.3	Measurement of pore water pressure	71
4.4	Equipment used for depth measurements	79
4.5	Measurement of the flowslide wave tip velocity	83
5	ANALYSIS OF PORE WATER PRESSURE	85
5.1	Introduction	85
5.2	Flowing sand and water mixture	86
5.3	Surface water and static material	90

5.4	Total pore water pressure	91
5.6	Sensitivity calculations	92
6	SECOND SERIES OF FLOWSLIDE EXPERIMENTS	94
6.1	Introduction	94
6.2	Flowslide motion	95
6.3	Comparison of measured and calculated pore water pressures	102
6.4	Conclusions	106
7	FURTHER INSTRUMENTATION	107
7.1	Pressure transducers and pre-test calibration	107
7.2	Video cameras	110
7.3	Still photography (35mm)	111
	7.31 Plan photography	111
	7.32 Side elevation photography	112
8	THIRD SERIES OF FLOWSLIDE EXPERIMENTS	119
8.1	Introduction	119
8.2	Additional experimental data	120
	8.21 Three-dimensional flow	120
	8.22 Surface slopes of the flowslide's layers	123
8.3	Comparison of measured and calculated pore water pressures	125
8.4	Implications of the laboratory results	134

9 CONCLUSIONS AND FURTHER WORK	137
9.1 Conclusions from experimental investigation	137
9.2 Further work	139
APPENDICES	143
A 1 Infinite landslide model	143
A 2 Experimental data	145
A 2.1 Laboratory tests performed	145
A 2.2 Side elevations of initial sample and flowslide after all motion has ceased	149
A 2.3 Temporal variation of the flowslide surface angle	155
A.3 References	156

NOTATION

Ba = Bagnold number

C = solid volume concentration

C_0 = maximum possible static solid volume concentration

C_{res} = resedimented concentration

CSL = critical state line

CSR = critical stress ratio

CVR = critical void ratio

D = particle diameter

D_{10} = particle diameter attained by 10% of grains on a size distribution curve

D_{50} = median particle diameter

D_r = relative density

DVM = digital volt meter

F = factor of safety

G_s = specific gravity

H_d = vertical height of test sample at sluice gate site

IF = interslice force

M = soil constant of CSL equation

M_s = mass of dry sand

N = total number of layers

NF = normal reaction force

P = dispersive or grain normal stress

Re = Reynold's number

SF = shear resistance force

SSL = steady state line

SSE = steady state envelope

T = dispersive or grain shear stress

- V = specific volume
- V_s = volume of solids
- V_t = total volume
- V_v = volume of voids
- W = weight of vertical element of a flowslide
- W_s = settling velocity of the grains
- W_{s0} = settling velocity of a grain in still water
- b = length of vertical element of a flowslide
- e = void ratio
- h_f = vertical flow depth
- h_s = vertical depth of static material
- h_{s2} = vertical height to secondary surface from channel bed
- h_{sw} = vertical depth of surface water
- h_z = depth of element of sand and water mixture in z direction
- k = permeability
- l = mixing length
- m = exponent that is a function of the Reynold's number
- n = porosity
- t = time
- p' = effective confining pressure
- q = deviator stress
- u = pore water pressure
- v = velocity in flow's longitudinal direction
- v_d = depth averaged velocity in flow's longitudinal direction
- v_s = velocity of resedimentation surface
- x = co-ordinate in longitudinal direction of flow
- y = co-ordinate transverse to direction of flow

- z = co-ordinate normal to direction of flow
- Γ = soil constant of CSL equation
- $\epsilon_{y,a}$ = apparent vertical diffusivity
- α = slope of flowslide's surface
- β = channel bed slope
- β_b = slip surface slope
- ϕ' = effective angle of friction
- ϕ_d = dynamic angle of friction
- γ = shear strain
- η = fluid viscosity as modified by the presence of grains
- λ = linear grain concentration
- λ = slope of isotropic virgin compression line
- μ = dynamic viscosity
- ρ_g = grain density
- ρ_{sat} = saturated bulk density
- ρ_w = density of water
- σ = total stress
- σ'_1 = major principal effective stress
- σ'_2 = intermediate principal effective stress
- σ'_3 = minor principal effective stress
- σ'_n = normal effective stress
- σ_{n-1} = standard deviation
- σ'_{vo} = vertical effective confining pressure
- τ = shear stress
- τ_B = Bingham yield stress
- τ_{cy} = cyclic shear stress
- τ_0 = initial static shear stress

Subscripts (independent values)

b = basal

crit = critical state

expt = experimentally measured

max = maximum

min = minimum

mob = mobilised

pred = predicted

prep = for preparation of test sample

ss = steady state

t = total

LIST OF TABLES

- 2.1 Summary of tailings' physical characteristics
- 2.2 Dynamic friction angles measured in ring shear tests
- 2.3 Residual friction angles measured in ring shear and flume tests
- 3.1 Test material's angle of repose
- 4.1 Pressure transducer data
- 4.2 Stability of transducers' power supplies
- 5.1 Accuracy of measured variables
- 6.1 Experimental data from the second series of flowslide tests
- 7.1 Pressure transducer data
- 8.1 Experimental data from the third series of flowslide tests

LIST OF FIGURES

- 2.1 Schematic diagram of sequential raising of an upstream embankment
- 2.2 Schematic diagram of sequential raising of a downstream embankment
- 2.3 Schematic diagram of sequential raising of a centreline embankment
- 2.4 The stable state boundary surface in (p', V, q) space
- 2.5 The critical state line in (p', V, q) space
- 2.6 Monotonic undrained behaviour (schematic):
 - a) State diagram
 - b) Stress path plot
- 2.7 Undrained behaviour under cyclic shear stresses smaller than the steady state strength (schematic):
 - a) State diagram
 - b) Stress path plot
- 2.8 Undrained behaviour under cyclic shear stresses larger than the steady state strength (schematic):
 - a) Flow deformation
 - b) Limited flow deformation
- 2.9 Effect of confining pressure on liquefaction resistance of sands at various initial relative densities
- 2.10 Effective stress paths for a soil element with an initial static shear stress (schematic)
- 2.11 Stationary granular fluid wave
- 2.12 Concentration distribution in a granular fluid wave
- 2.13 Grain pathlines in a granular fluid wave
- 2.14 Vertical velocity distribution in the body of a granular fluid wave
- 2.15 Definition sketch for resedimentation model

- 2.16 Classification matrix of granular fluids
- 3.1 Particle size distribution curve for laboratory flowslide material
- 3.2 General view of preliminary apparatus
- 3.3 Schematic diagram showing upstream section of channel
- 3.4 Side elevations of channel showing preparation of test sample
 - a) Levels of the sand surface during test sample preparation
 - b) Settled sand surface at the end of test sample preparation
- 3.5 Schematic diagram of apparatus used for column of sand experiments
- 3.6 Schematic diagram showing the failure of the test sample at various time intervals after sluice gate removal
- 4.1 Schematic diagram of experimental apparatus
- 4.2 General view of raising and lowering mechanism for laboratory channel
- 4.3 Schematic diagram of sluice gate
- 4.4 Schematic diagram of sluice gate frame
- 4.5 Schematic diagram of a pressure transducer fitting
- 4.6 Schematic diagram showing side elevation of apparatus used to test performance of pressure transducers under a sudden head increase
- 4.7 Pressure transducer response time to a sudden head increase
- 4.8 Schematic diagram of laboratory apparatus showing positions of pressure transducers and wave transmitters
- 4.9 Noise registered on pressure transducer due to sluice gate removal
- 5.1 Schematic diagram of a vertical element of a flowslide
- 5.2 Variation in basal pore water pressures with slip surface slope
- 5.3 Variation of percentage change in total predicted pore water pressure ($u_{t,pred}$) with channel bed slope for a 1% increase in each measured variable
- 6.1 Movement of a wave front past an observation site 0.3m from the sluice gate site (Test 4M, bed slope = 9 degrees)

- a) Time = 10 seconds from sluice gate removal
- b) Time = 10.55 seconds from sluice gate removal
- c) Time = 11.05 seconds from sluice gate removal
- d) Time = 11.5 seconds from sluice gate removal
- e) Time = 11.95 seconds from sluice gate removal
- f) Time = 12.45 seconds from sluice gate removal

6.2 Legend for figures 6.3-6.10

6.3 Temporal variations of depths of flowslide material (Test 8S) at 0.1 m from the sluice gate site, channel bed slope = 0 degrees

6.4 Temporal variations of depths of flowslide material (Test 15S) at 0.1 m from the sluice gate site, channel bed slope = 0 degrees

6.5 Temporal variations of depths of flowslide material (Test 12S) at 0.1 m from the sluice gate site, channel bed slope = 6 degrees

6.6 Temporal variations of depths of flowslide material (Test 13S) at 0.1 m from the sluice gate site, channel bed slope = 6 degrees

6.7 Temporal variations of depths of flowslide material (Test 16S) at 0.5 m from the sluice gate site, channel bed slope = 9 degrees

6.8 Temporal variations of depths of flowslide material (Test 19S) at 0.5 m from the sluice gate site, channel bed slope = 9 degrees

6.9 Temporal variations of depths of flowslide material (Test 9S) at 0.1 m from the sluice gate site, channel bed slope = 12 degrees

6.10 Temporal variations of depths of flowslide material (Test 10S) at 0.1 m from the sluice gate site, channel bed slope = 12 degrees

6.11 Side elevation of settled test sample and corresponding flowslide after all movement has ceased, channel bed slope = 0 degrees

6.12 Side elevations of test sample and corresponding flowslide after all movement has ceased, at various channel bed slopes

6.13 Side elevations of flowslides after all movement has ceased

- 6.14 Longitudinal variation of flowslide wave tip with time for tests at different channel bed slopes
- a) Channel bed slope = 0 degrees
 - b) Channel bed slope = 6 degrees
 - c) Channel bed slope = 9 degrees
 - d) Channel bed slope = 12 degrees
- 6.15 Comparison of longitudinal variation of flowslide wave tip with time for tests at different channel bed slopes
- 6.16 Legend for figures 6.17-6.24
- 6.17 Measured and calculated pore water pressures (Test 8S) at 0.1 m from the sluice gate site, channel bed slope = 0 degrees
- 6.18 Measured and calculated pore water pressures (Test 15S) at 0.1 m from the sluice gate site, channel bed slope = 0 degrees
- 6.19 Measured and calculated pore water pressures (Test 12S) at 0.1 m from the sluice gate site, channel bed slope = 6 degrees
- 6.20 Measured and calculated pore water pressures (Test 13S) at 0.1 m from the sluice gate site, channel bed slope = 6 degrees
- 6.21 Measured and calculated pore water pressures (Test 16S) at 0.5 m from the sluice gate site, channel bed slope = 9 degrees
- 6.22 Measured and calculated pore water pressures (Test 19S) at 0.5 m from the sluice gate site, channel bed slope = 9 degrees
- 6.23 Measured and calculated pore water pressures (Test 9S) at 0.5 m from the sluice gate site, channel bed slope = 12 degrees
- 6.24 Measured and calculated pore water pressures (Test 10S) at 0.5 m from the sluice gate site, channel bed slope = 12 degrees
- 7.1 Plan photograph showing positions of pressure transducer fittings, photographic and video cameras

- 7.2 Plan photograph showing light streaks obtained from timed exposure photography (Test 7M, channel bed slope = 9 degrees)
- 7.3 Side elevation of the surface of the flowing sand and water mixture of a flowslide, before the arrival of surface water
- 7.4 Side elevation of the surface of the flowing sand and water mixture of a flowslide, before the arrival of surface water
- 7.5 Side elevation of a flowslide at the 0.3 m observation sight after the arrival of surface water (Test 7M at a bed slope of 9 degrees)
- 7.6 Side elevation of a flowslide at the 0.1 m observation site showing light streaks obtained from photography of light reflective particles (Test 8M at a bed slope of 9 degrees)
- 8.1 Transverse section photographs of flowslide material after all movement has ceased (Test 7M, bed slope = 9 degrees)
 - a) Longitudinal distance = 0.08 m from the sluice gate site
 - b) Longitudinal distance = 0.07 m from the sluice gate site
 - c) Longitudinal distance = -0.014 m from the sluice gate site
 - d) Longitudinal distance = -0.03 m from the sluice gate site
- 8.2 Comparison of depths of depths of flowslide material observed at each channel wall at the 0.3 m observation site (Test 7M, channel bed slope = 9 degrees)
- 8.3 Plan photograph showing light streaks obtained from timed exposure photography (Test 7M, channel bed slope = 9 degrees)
- 8.4 Variation in depths of flowslide material with time at the three observation sites during Test 7M, bed slope = 9 degrees
- 8.5 Comparison of flowslide surface slopes at the three observation sites (Test 7M, channel bed slope = 9 degrees)
- 8.6 Comparison of flowslide and static material slopes at the 0.3 m observation site (Test 7M, channel bed slope = 9 degrees)

- 8.7 Legend for figures 8.8(a)-8.13(b)**
- 8.8 Test 3M at 0.3 m from the sluice gate site, channel bed slope = 6 degrees
(video records)**
- a) Temporal variation in depths of flowslide material**
 - b) Comparison of measured and calculated pore water pressures**
- 8.9 Test 4M at 0.5 m from the sluice gate site, channel bed slope = 9 degrees
(video records)**
- a) Temporal variation in depths of flowslide material**
 - b) Comparison of measured and calculated pore water pressures**
- 8.10 Test 7M at 0.1 m from the sluice gate site, channel bed slope = 9 degrees
(video records)**
- a) Temporal variation in depths of flowslide material**
 - b) Comparison of measured and calculated pore water pressures**
- 8.11 Test 7M at 0.3 m from the sluice gate site, channel bed slope = 9 degrees
(video records)**
- a) Temporal variation in depths of flowslide material**
 - b) Comparison of measured and calculated pore water pressures**
- 8.12 Test 7M at 0.3 m from the sluice gate site, channel bed slope = 9 degrees
(photographic records)**
- a) Temporal variation in depths of flowslide material**
 - b) Comparison of measured and calculated pore water pressures**
- 8.13 Test 7M at 0.5 m from the sluice gate site, channel bed slope = 9 degrees
(video records)**
- a) Temporal variation in depths of flowslide material**
 - b) Comparison of measured and calculated pore water pressures**
- 8.14 Comparison of the measured and predicted total pore water pressures at
three observation sites during flowslide test 7M; channel bed slope = 9
degrees**

- 8.15 Comparison of measured and predicted total pore water pressures, illustrating reduction in calculated values when flow over the channel bed was expected (Test 7M, channel bed slope = 9 degrees)
- 8.16 Average surface velocities measured above the three observation sites during flowslide test 7M; channel bed slope = 9 degrees
- 8.17 Comparison of measured and calculated pore water pressures, illustrating effect of change in bed slope (Test 7M, channel bed slope = 9 degrees, 0.3 m site: photographic records)
- 8.18 Comparison of average surface velocities and flow depths during flowslide test 7M; channel bed slope = 9 degrees
- a) Temporal variation of average surface velocities in the centre of the channel
 - b) Temporal variation of flow depth at the three observation sites
- 8.19 Side elevation of settled test sample and corresponding flowslide after all motion has ceased, for flowslide tests at various bed slopes
- 8.20 Side elevations of flowslides after all movement has ceased (channel bed slope = 6 degrees)
- 8.21 Side elevations of flowslides after all movement has ceased (channel bed slope = 9 degrees)
- A.1 Schematic diagram of a vertical element of soil considered during infinite landslide analysis

CHAPTER 1:

INTRODUCTION

Tailings are the waste product from the extraction of valuable mineral elements from their parent ores. They are often sand sized particles and are stored behind dams. These dams are therefore known as tailings' dams, and are often 20 to 50 metres high. Larger heights are also being considered. Unfortunately, economical pressure and a genuine lack of knowledge have resulted in construction of tailings' dams that are susceptible to a particular type failure known as flowslides. Flowslides have been recognised as a natural phenomenon whereby large volumes of material can be transported large distances at high velocities. Flowslide events from tailings' dams have involved more than a million cubic metres of material and have caused immense damage to property and significant loss of life.

Flowslides are triggered by liquefaction, which results in collapse of the soil structure. An increase in the pore water pressure occurs during this process, with a corresponding decrease in effective stresses and a considerable reduction of the soil's shear strength. Hence, the term flowslide is reserved for that distinctive form of disintegrating slide where a temporary transfer of part of the total normal stress onto the fluids of the voids' space has taken place [Bishop (1973)].

Liquefaction and flowsliding have not been limited to the failure of tailings' dams. Whilst under construction in 1938, the Fort Peck Dam failed and 10 million cubic yards of fill and foundation sands moved out on a level surface to a distance of 1400 feet in 3 minutes, killing 80 construction workers [Bishop (1973)]. Colliery spoil tips have also suffered, illustrated by the failure of Tip No 7 at Aberfan (1966)

where 144 people were killed [Bishop 1973]). Subaqueous flowslides have also occurred [Seed (1968)], for example, in the Norwegian fjords [Bjerrum (1971): cited Bishop (1973)] and off the Netherlands' coast during sand fill dam construction [De Groot et al (1988), Mastbergen et al (1988), Winterwerp et al (1990)]. More recently, a flowslide occurred at the Wheel Renfree tip in Cornwall containing china-clay waste [New Civil Engineer (1990)] and at a sewage sludge tip in Yorkshire [Fowler/Russell (1992)], illustrating the contemporary relevance of this phenomenon.

The ultimate objective would be identification of the potential hazard area downstream of any soil deposit that poses the flowslide threat. At present, this is a distant prospect because, despite the prevalence of such flows, the dynamic behaviour is poorly understood. The theory of plasticity has been applied to the problem of incipient failure and extended into the range of fully developed flow. Various rheological models have also been invoked to describe certain aspects of deformation beyond failure. These approaches are adaptations of theories developed in solid and fluid mechanics. Attention has also been focused on the behaviour of granular materials by considering grain interactions at a microscopic level and on the general principles of continuum mechanics. It has been noted that with today's advanced analytical and computer methods, too much research effort is expended in this direction and too little on physical investigations on which to base advanced analyses [Klemes (1986): cited Davies (1988)].

Field data pertaining to the flowslide event are very limited, usually being restricted to quantities measured after motion has ceased. Laboratory flowslide data are also scarce. Despite the many experimental difficulties associated with study of granular fluids, there is a definite need to improve the physical description of flowslide motion. Therefore, the objective of this research was to explore flowslide behaviour, both qualitatively and quantitatively, by conducting small scale

laboratory tests using a realistic test material of sand and water. Although uncertainty exists at present concerning model scale effects, this research allowed identification of features in a relatively inexpensive apparatus that indicated promising directions for further work.

CHAPTER 2:

LITERATURE REVIEW

2.1 MINERAL PROCESSING AND MINE TAILINGS

The mining industry exists to abstract valuable minerals from their parent ores. The methods by which this is achieved can be as diverse as the minerals themselves, but some of the fundamental steps are the same. Once the ore-body has been mined from the ground, the rock fragments produced are reduced from mine run size by crushing, followed by grinding to achieve the final stage in the physical reduction in size. The particle size distribution depends on both the degree of particle breakdown incurred during the above processes and the clay content of the parent ore. The optimum degree of grinding will depend on the type of mineral extraction process used. The individual particles produced by grinding vary in mineral content, and those with high mineral values (concentrate) are separated from the lower ones (tailings) by a process known as concentration. This process may vary according to ore type, but there are three general methods in use; gravity separation, magnetic separation, and froth flotation.

Gravity separation is used when the mineral and the parent rock have considerably different specific gravities; as occurs with coal, iron, tin or gold for example. This process is usually performed with water, and the lighter (or heavier) particles are collected, leaving the remaining particles as tailings. Magnetic separation is useful for the extraction of iron from magnetic ores such as magnetite and magnetic taconite. Magnetic particles are collected from a belt or

drum separator, whilst the non-magnetic particles remain as tailings. The most common method of concentration is by froth flotation, and is a highly complex physiochemical process. This is the first step in the mineral processing sequence in which chemical reagents are introduced. These reagents are very specific to the type of mineral or minerals being separated. Basically, individual mineral bearing particles are made water repellent and attractive to air bubbles, which rise to the surface as a froth. The froth is skimmed off and the remaining barren particles become tailings. The production of concentrate is the final stage of many milling operations, the concentrate being taken to a smelter for refining or to the user, in the case of coal. Other processes may replace or supplement concentration, such as heating (principally to obtain oil from oil sands, and phosphoric acid fertiliser from phosphate rock concentrate) or leaching. Leaching removes the mineral values from the other particles by direct contact with a solvent, usually a strong acid or alkali depending on the type of ore. The use of chemicals during the extraction process may produce mill effluent that is toxic, and this potential hazard must be assessed when designing how to dispose of the mill waste.

Once the mineral values have been extracted, the final stage in the milling process is that of dewatering. Some, but not all, of the water and chemical reagents are recovered from the tailings–water slurry for reuse in the mill process where possible. This is commonly performed by thickeners. Recycling of the used process water is not feasible in some cases because of the presence of contaminants that would reduce extraction efficiency, for example in acid leach uranium mills. This obviously has important environmental implications for tailings' disposal.

The tailings collected from the dewatering process are almost always transported in slurry form to the disposal area or to be impounded behind a tailings' dam. The slurry is sometimes transported in open channels by gravity

flow, but more often in pipes, either with or without pumping depending on the geographical location of the mill relative to the disposal area.

2.2 TYPES AND CHARACTERISTICS OF TAILINGS

The nature of the tailings depends on the type of ore being milled and the processing operation used. The index properties by which tailings are classified on a general basis are particle size distribution, specific gravity and plasticity.

The particle size can vary from coarse/medium sands down to silts or clays. The particle size distribution can also be quite variable. Generalisation is difficult because not only do tailings vary with differing parent ore, but tailings within any one ore type may vary according to the nature of the ore body and the mill process used. The particles tend to be highly angular, even down to silt sizes, reflecting the extreme violence of the crushing and grinding of the mill process. Because coarse and fine particles tend to settle in different areas of the tailing's impoundment, the coarser particles are known as sands, whilst the area where the material is mainly less than the 75 µm sieve size is called the slimes zone. Table 2.1 [Vick (1983)] divides tailings into four general categories according to gradation and plasticity.

2.3 DISPOSAL OF TAILINGS

The most common and important type of disposal method is storage of tailings behind dams or embankments. Other types of disposal include underground backfill, open pit backfill, offshore disposal and thickened discharge methods. When tailings are deposited behind dams, they are discharged into the impoundment area from a pipe running along the top of the embankment. This can

TABLE 2.1

SUMMARY OF TAILINGS' PHYSICAL CHARACTERISTICS

[FROM VICK (1983)]

Category	General character
Soft-rock tailings	
Fine coal refuse Trona insols Potash	Contain both sand and slime fractions, but slimes may dominate overall properties because of presence of clay.
Hard-rock tailings	
Lead-zinc Copper Gold-silver Molybdenum Nickel (sulphide)	May contain both sand and slime fractions, but slimes are usually of low plasticity to nonplastic. Sands usually control overall properties for engineering purposes.
Fine tailings	
Phosphatic clays Bauxite red muds Fine taconite tailings Slimes from tar sands tailings	Sand fraction generally small or absent. Behaviour of material, particularly sedimentation-consolidation characteristics, dominated by silt or clay sized particles and may pose disposal volume problems.
Coarse tailings	
Tar sands tailings Uranium tailings Gypsum tailings Coarse taconite tailings Phosphate sand	Contain either principally sands or nonplastic silt sized particles exhibiting sand-like behaviour and generally favourable engineering characteristics.

be performed either as a single point discharge from the end of the pipe, with the end of the pipe being periodically relocated to form a series of adjacent and overlapping deltas, or by spigotting. In the latter, the tailings' slurry is discharged through closely spaced, individually valved spigots (outlets) in the pipeline (15 to 50 m apart), avoiding the need for frequent relocation of the pipeline or disconnection of pipe segments.

There are two general classes of surface impoundments used for tailings:— water retention type dams and raised embankments. The former differ little from ordinary water storage dams in design and construction, being built to their full height prior to tailings' discharge. These dams are best suited to tailings' impoundments that require high storage of water, for example where large storm water runoffs are expected or where the discharged mill effluent cannot be recirculated and requires storage.

The raised embankments are most common and construction, with its associated costs, is staged over the working lifetime of the impoundment. This gives them a significant economical advantage over the water retention type dams. A starter dyke is constructed initially, usually of natural soil borrow, and often sized to impound the first two or three years' output of tailings from the mill. The embankment is then raised sequentially to keep pace with tailings' production. This allows more choice in embankment construction material, for example mine waste rock or sand tailings, which are essentially free materials. Sand tailings can be obtained from whole tailings by cycloning. Cyclones are simple devices that function on a centrifugal separation principle with no moving parts. The whole tailings' slurry is fed into the top of a cylindrical chamber under pressure. The coarser sand particles in the slurry spiral downwards through an inverted conical section and out through the bottom of the chamber. The finer fraction and most of the slurry water (principally slimes) rise up and out of the top of the feed chamber.

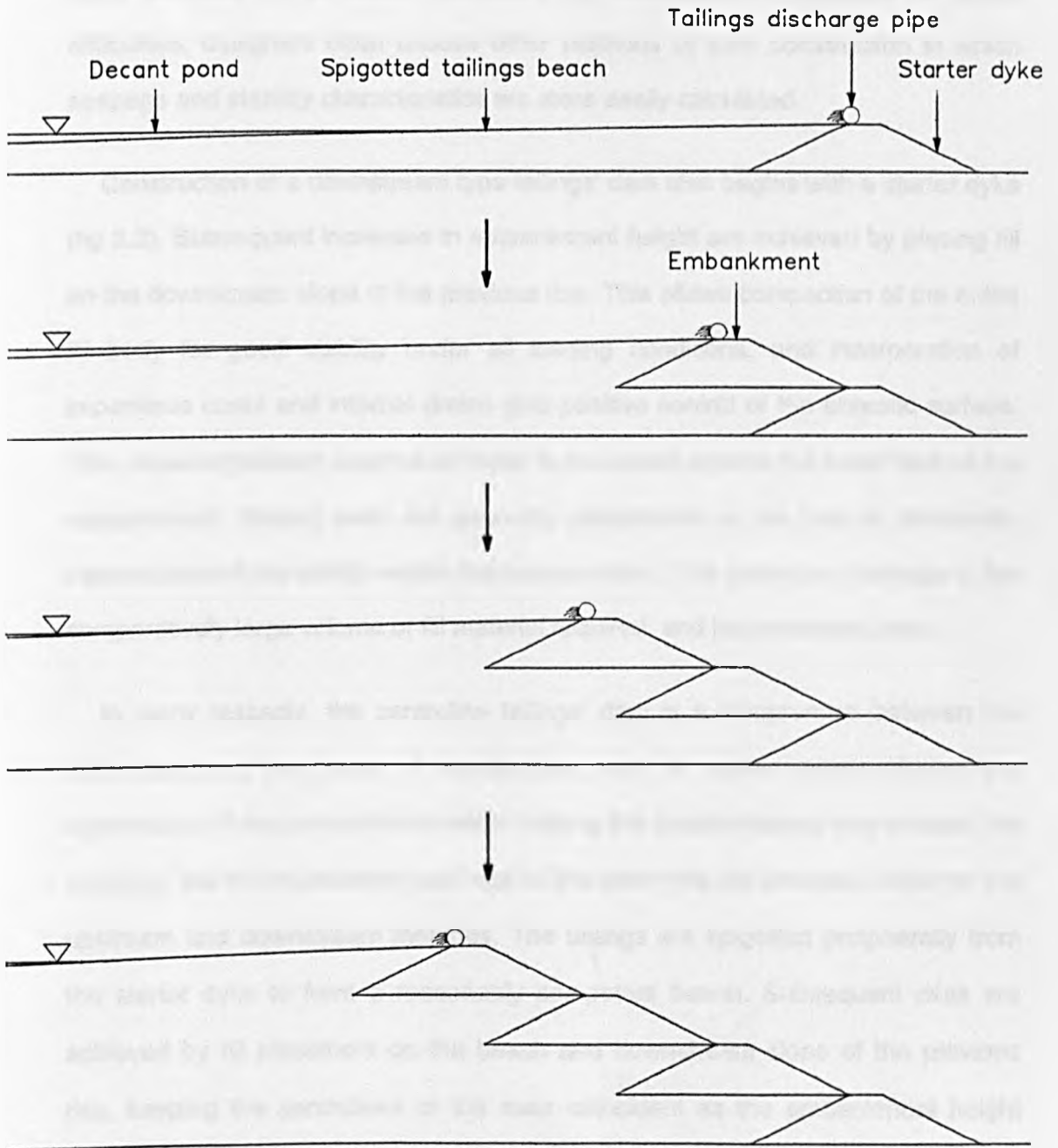
Regardless of the material used for construction, these embankments fall into three categories; upstream, centreline and downstream. These descriptions refer to the direction in which the dam crest moves in relation to the starter dyke as the dam height increases.

An upstream tailings' dam requires no less than 40-60% sand in the discharged whole tailings (with reference to Table 2.1, those tailings in the soft rock and fine categories cannot be used). A starter dyke is constructed initially and tailings are discharged peripherally from the crest, forming a beach. This beach then becomes the foundation for the second perimeter dyke, and the process continues as the impounded area is filled (fig 2.1). The advantage of this method is that only minimal volumes of mechanically placed fill are required for this simple construction, beach tailings often being a convenient source of material, and large dam heights can be achieved at very low cost.

Unfortunately, this type of dam is limited to very specific conditions and incorporates a number of inherent disadvantages. These include difficulty of control of the phreatic surface within the dam and a limited water storage capacity. To calculate the position of the phreatic surface for the upstream method of construction is far more difficult than other types of impoundment structure. It depends on pond location, variation of lateral and vertical permeability of the spigotted tailings, anisotropic permeability of the tailings' deposit, boundary conditions such as permeable starter dykes and underdrains, and other factors. The beach width or distance from the pond water to the dam crest is a factor that is not easily controlled by the designer when considering stability of the embankment. Because of the low slope of the tailings' deposit (typically 1%), a small increase in the depth of pond water will result in a dramatic reduction of the beach width and elevation of the phreatic surface. Stability of the upstream type of construction is most affected by changes in seepage conditions because of its

FIG 2.1

SCHEMATIC DIAGRAM OF SEQUENTIAL RAISING OF AN UPSTREAM EMBANKMENT [FROM VICK (1983)]



poor drainage facilities, thus the possibility of large storm water runoffs into the impoundment area should be avoided in this case by the use of diversion dykes. The rate at which the dam can be raised is also limited to about 5-10 m/year. Rapid rises can produce excess pore water pressures, particularly in the slimes zone because of its lower coefficient of consolidation. Because of these difficulties, designers often choose other methods of dam construction in which seepage and stability characteristics are more easily calculated.

Construction of a downstream type tailings' dam also begins with a starter dyke (fig 2.2). Subsequent increases in embankment height are achieved by placing fill on the downstream slope of the previous rise. This allows compaction of the entire fill body for good stability under all loading conditions, and incorporation of impervious cores and internal drains give positive control of the phreatic surface. This allows significant volumes of water to be stored against the inner face of the embankment. Raising rates are generally unrestricted as the dam is structurally independent of the tailings within the impoundment. The main disadvantage is the comparatively large volume of fill material required, and its associated costs.

In many respects, the centreline tailings' dam is a compromise between the aforementioned two ways of construction, and to some degree shares the advantages of the two methods whilst making the disadvantages less severe. For example, the fill requirements and cost of this dam type are between those for the upstream and downstream methods. The tailings are spigotted peripherally from the starter dyke to form a reasonably competent beach. Subsequent rises are achieved by fill placement on the beach and downstream slope of the previous rise, keeping the centrelines of the rises coincident as the embankment height increases (fig 2.3).

Due to the provision of internal drainage systems within the embankment,

FIG 2.2

SCHEMATIC DIAGRAM OF SEQUENTIAL RAISING
OF A DOWNSTREAM EMBANKMENT [FROM VICK (1983)]

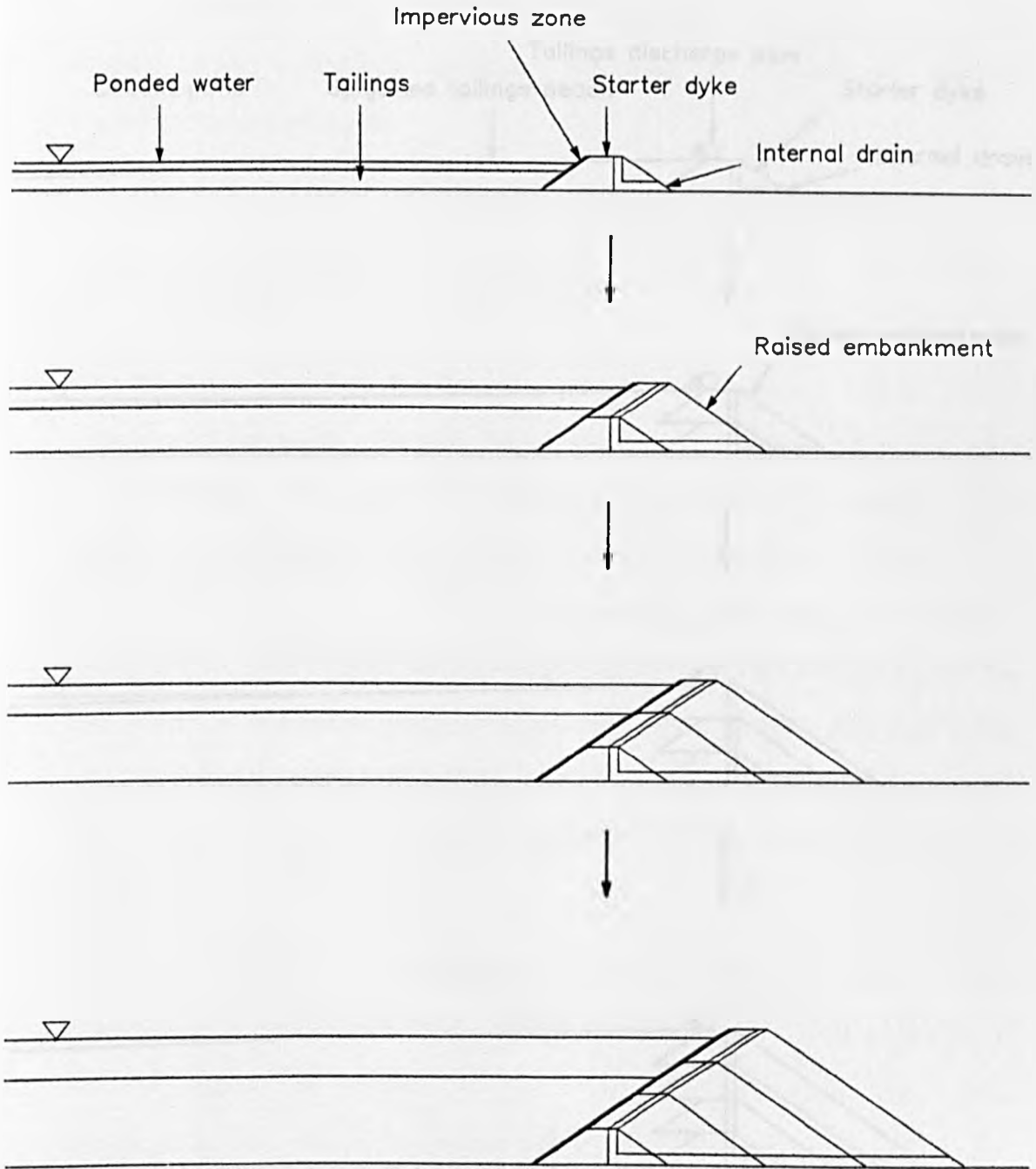
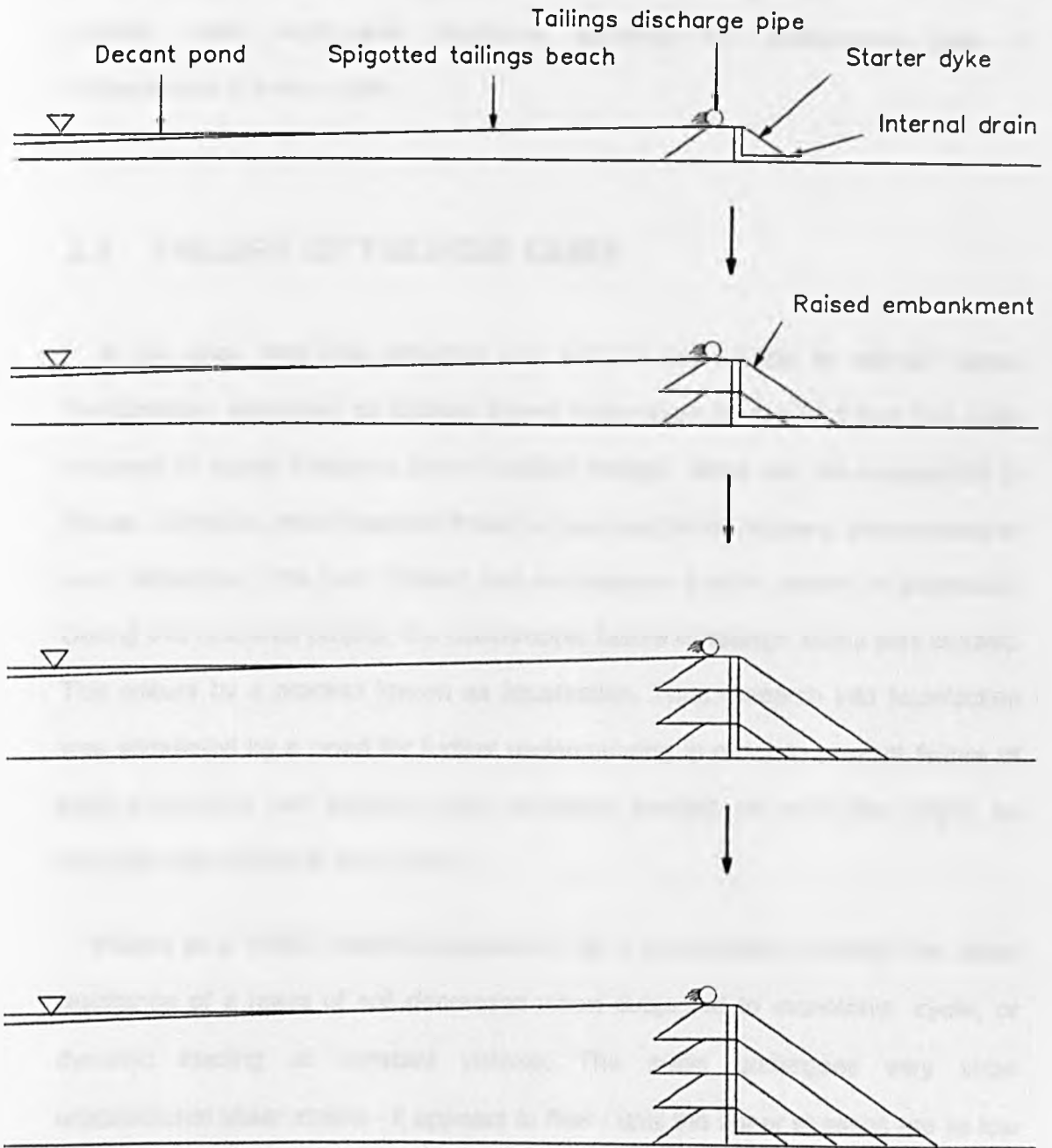


FIG 2.3

SCHEMATIC DIAGRAM OF SEQUENTIAL RAISING
OF A CENTRELIN EMBANKMENT [FROM VICK (1983)]



control of the phreatic surface is not as sensitive to the position of the pond water relative to the dam crest as it is in the upstream method. Even so, the stability of the dam is not sufficient to store large depths of water permanently, but the water level can be allowed to rise temporarily during floods because of the drainage zones. These drains in conjunction with fill compaction give good embankment stability under earthquake conditions, although the downstream type of embankment is more stable.

2.4 FAILURE OF TAILINGS' DAMS

In the past, very little attention was paid to the stability of tailings' dams. Documented examples of failures forced recognition of the fact that the large volumes of sandy materials stored behind tailings' dams can be susceptible to failure, posing a great potential threat to any people or property downstream of such structures. The term 'failure' can encompass a wide variety of behaviour. During this research project, the catastrophic failure of tailings' dams was studied. This occurs by a process known as liquefaction. Thus research into liquefaction was stimulated by a need for further understanding in order to prevent failure of both man-made soil deposits and structures erected on soils that might be naturally susceptible to liquefaction.

Poulos et al (1985) defined liquefaction as 'a phenomenon wherein the shear resistance of a mass of soil decreases when subjected to monotonic, cyclic, or dynamic loading at constant volume. The mass undergoes very large unidirectional shear strains - it appears to flow - until the shear stresses are as low or lower than the reduced shear resistance'. The motion of this fluid-like mass of great destructive power has been called a flowslide. Bishop (1973) stated that the

term 'flowslide' is reserved for that distinctive form of disintegrating slide where a temporary transfer of part of the total normal stress onto the fluids of the void space has taken place.

Other definitions of liquefaction have been used which have led to confusion. For example, Poulos et al (1985) noted that 'it has been customary to use the term 'liquefaction' to mean 5% strain in a cyclic load test. This use of the term might give a layman the impression that a flowslide will develop in situ if the cyclic loading that caused 5% strain in the laboratory were to occur during an earthquake in situ. But a strain of 5% in situ bears no relation to whether or not liquefaction will occur. The only factual statement consistent with the laboratory-measured strain of 5% is that a similar strain may occur in situ if the test is a proper model for in situ conditions if the test errors are not excessive. Five percent strain in a cyclic load test has the same implication as 5% strain in a monotonic test. Neither is related to whether or not liquefaction will occur'.

The triggering of liquefaction leading to flowslide behaviour occurs after the peak strength of the material has been attained, and Eckersley (1990) stated that liquefaction is generally a consequence of instability, rather than the cause of it. At failure, a point of instability is reached, and the pore water pressure and deformation of soil increases rapidly. This increased value of the pore water pressure (an excess pore water pressure) occurs as the soil collapses and more of the total normal stress is carried by the interstitial fluid, causing a reduction in the shear strength of the material. The generation of these excess pore water pressures is rapid in comparison to the ability of the material to dissipate them through its drainage capacity. This condition is commonly referred to as undrained loading.

Undrained monotonic loading can occur in the field, for example, if the height of

an upstream type embankment is raised too fast. Rapid raising can produce excess pore water pressures, as the application of load is rapid in comparison to the ability of the tailings to dissipate excess pore water pressures by the process of consolidation. This particularly applies to the slimes zone because of its lower coefficient of consolidation. Loading at the crest of the dam will also increase the initial shear stress of anisotropically consolidated specimens near the embankment face, which can lead to failure if the peak strength of the material is exceeded. Changes in shear stress causing failure are not just limited to applied loading at the crest of the dam, they can also be caused by removal of material from the toe of the dam.

Consideration of the performance of tailings' dams under seismic activity, which produces undrained cyclic loading of the soil, is important because the geological zones that produce mine ores are also often associated with tectonic activity and earthquakes. This is the case for many of the mining districts in west USA, Canada, Mexico, Central and South America. Damage can occur from two sources; ground rupture beneath the dam and seismic shaking. Cyclic loading can also be used to investigate soil behaviour under wave loading.

Examples of tailings' dams that have suffered liquefaction due to seismic loading and subsequent flowsliding include the upstream type Barahona dam in Chile 1928 resulting in 54 deaths [Aguero (1929): cited in Lucia (1981)], the upstream type El Cobre (old dam), Hierro Viejo, Los Marquis, La Patagua, Cerro Negro, Bellavista and Ramayana dams in Chile 1965 [Dobry/Alvarez (1967)], where the run out of the flowslides varied between 0.6 and 7.5 miles. The failure of the old El Cobre dam, together with the new El Cobre dam, which was of the downstream type using cyclone construction, resulted in the deaths of over 200 people.

Whilst the generation of excess pore water pressures during liquefaction is an undrained loading phenomenon, loading of the soil may be essentially drained (meaning that the loading rate is slow enough to ensure that no excess pore water pressures are generated) up to the point of failure. Drained monotonic loading leading to liquefaction and subsequent flowsliding was illustrated by Eckersley (1990) in his laboratory experiments where a deposit of coal failed purely as a result of slowly increasing the seepage of water through the embankment. Upstream type embankments have suffered failures attributed to seepage more often than the other types of construction due to their poorer drainage facilities. For example, Kleiner (1976) reported that the failure of an upstream type Gypsum tailings dam in S.E. Texas in December 1966 was due to poorly designed drainage provisions. Other failures of the upstream type of construction due to seepage include a carbide tailings' dam at Louisville in 1962, a copper tailings' dam in S.W. USA in 1973 and a platinum tailings' dam at Bafokeng, South Africa in 1974 [Lucia (1981)].

2.5 SOIL BEHAVIOUR DURING LIQUEFACTION

2.51 STEADY STATE AND CRITICAL STATE SOIL MECHANICS

The potential effects of a flowslide following liquefaction are related to the difference between the magnitude of applied shear stress and the shear strength of the soil that remains after liquefaction. The factors that affect this shear strength of the soil under both undrained monotonic and cyclic loading are now discussed.

The failure states of soil can be considered in terms of the effective stress parameters; effective confining pressure, p' , the deviator stress, q , and void ratio,

e , or specific volume, V . These are the appropriate invariant quantities for a study of a triaxial test, where:

$$p' = \frac{(\sigma_1' + \sigma_2' + \sigma_3')}{3} \quad (2.1)$$

$$q = \sigma_1' - \sigma_3' = \sigma_1 - \sigma_3 \quad (2.3)$$

$$e = \frac{V_v}{V_s} \quad (2.4)$$

$$V = 1 + e \quad (2.5)$$

σ_1' = major principal effective stress

σ_2' = intermediate principal effective stress

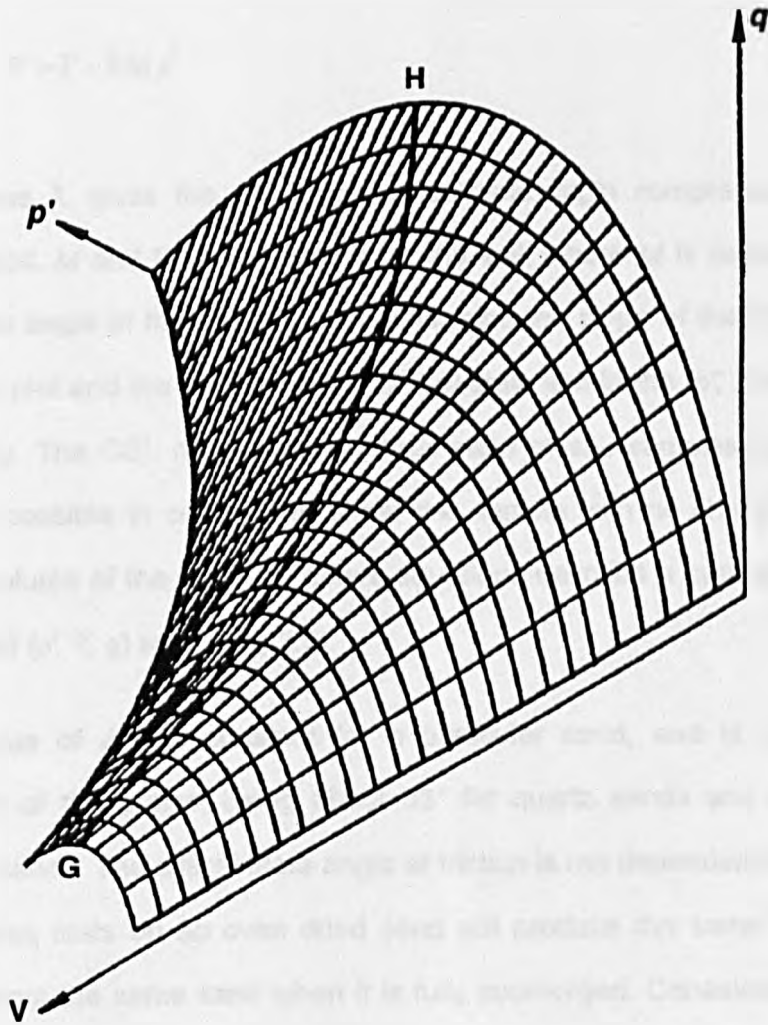
σ_3' = minor principal effective stress

V_v = volume of voids

V_s = volume of solids

In critical state soil mechanics, which was developed from the application of the plasticity theory to soil mechanics, state diagrams and stress path plots are used to represent the behaviour of a soil element of in three dimensional (p' , V , q) stress space. It is a powerful tool to aid understanding. A stable state boundary surface can be plotted in three dimensional stress space (fig 2.4). When the state of a specimen of soil can be represented by a point below the surface, then the soil behaviour is elastic. Soil states on the surface indicate yielding, whilst it is impossible for soil samples to exist in states equivalent to points above the surface. When soil samples are sheared until they flow as a frictional fluid, they

FIG 2.4 THE STABLE STATE BOUNDARY SURFACE IN (p' , v , q) SPACE [Britto/Gunn (1987)]



will reach the critical state line (CSL). The equations of the CSL are:

$$q = Mp' \quad (2.6)$$

$$V = \Gamma - \lambda \ln p' \quad (2.7)$$

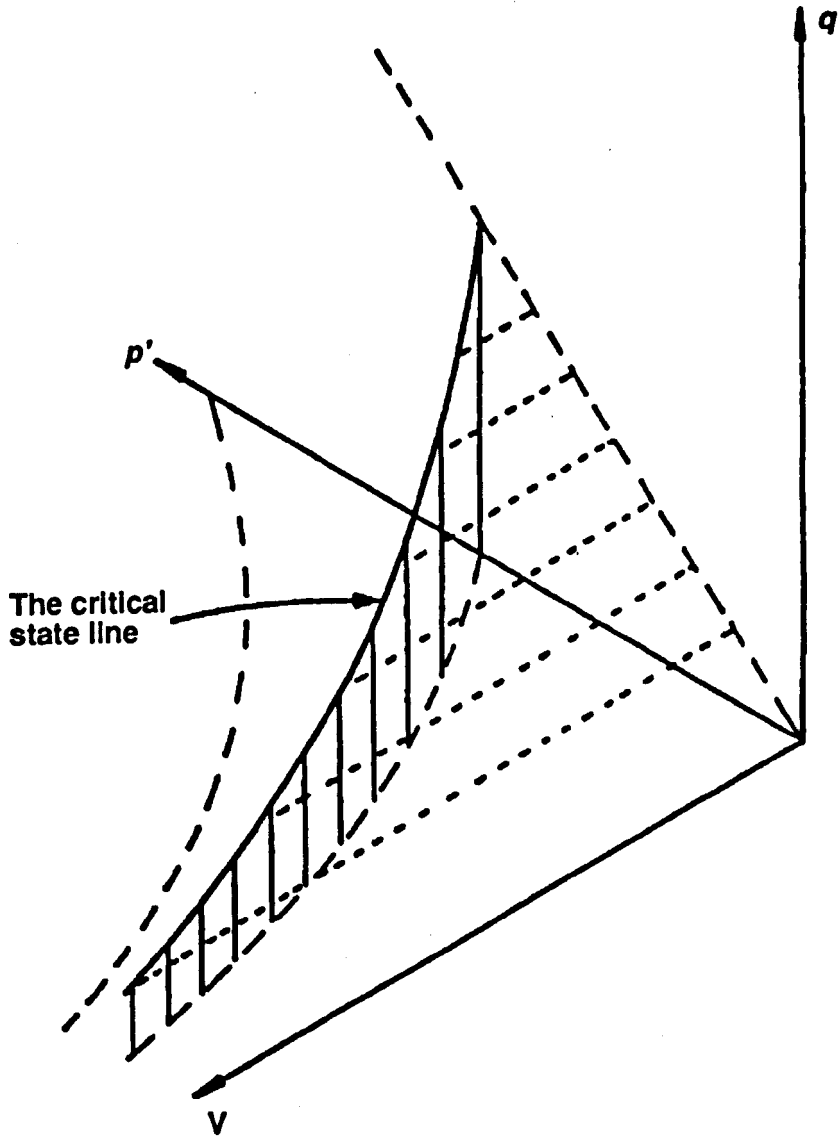
The value λ gives the slope of the isotropic virgin compression line for a particular soil. M and Γ are constants for the soil, where M is dependent on the critical state angle of friction, ϕ'_{crit} , and determine the slope of the CSL in a (p', q) stress path plot and the location of the critical state line in the (p', V) state diagram respectively. The CSL represents the final state of soil samples in triaxial tests when it is possible to continue to shear the sample with no change in imposed stress or volume of the soil. The above equations describe a curved line in three-dimensional (p', V, q) space (fig 2.5).

The value of ϕ'_{crit} is constant for a particular sand, and is dependent on mineralogy of the grains, being about 33° for quartz sands and about 40° for felspathic sands. The critical state angle of friction is not dependent on the degree of saturation; tests on an oven dried sand will produce the same value as that obtained from the same sand when it is fully submerged. Cohesionless materials such as sands are composed of relatively hard minerals and generally do not suffer particle degradation with large strains [Bishop (1973)] and hence ϕ'_{crit} will be unaffected. For materials such as colliery waste, very large strains may be necessary before a critical state is reached.

Post liquefaction behaviour for laboratory soil specimens has been described in terms of steady state deformation [Poulos (1981)]. The shear strength of the soil during steady state deformation is referred to as the steady state strength. The description of the soil behaviour at the steady state using state diagrams and

FIG 2.5

THE CRITICAL STATE LINE IN (p' , V , q) SPACE
[Britto/Gunn (1987)]



stress path plots is very similar to that of critical state soil mechanics.

Castro/Poulos (1977) concluded that the steady state line (SSL) represented the locus of states in which a soil could flow at constant void ratio, constant effective minor principal stress (or constant normal effective stress), constant shear stress and constant velocity. The SSL is a property that is unique to each soil. The SSL defines a straight line in (p', q) stress space that has been called the steady state (large strain) envelope, or more simply, the steady state envelope, SSE. The gradient of the SSL is related to a steady state angle of friction, ϕ'_{ss} , in a similar way to critical state theory. The SSL is curved on the (p', V) or (p', e) state diagram and defines a straight line on the $(\ln(p'), V)$ or $(\ln(p'), e)$ state diagram, in the same way as that described by critical state theory. Castro/Poulos (1977) have suggested that the gradient is affected chiefly by the shape of the grains in a given a soil, whilst the vertical position of the line is affected by even small differences in grain size distribution.

Although the critical and steady states are quite similar, there are some differences between them. The behaviour of very loose, strain softening soils during liquefaction mimics the behaviour the critical state behaviour expected of dense soils. Schofield/Wroth (1968) suggested, in their original description of the critical state, one should:

'Consider a random aggregate of irregular solid particles of diverse sizes which tear, rub, scratch, chip, and even bounce against each other during the process of continuous deformation. If the motion were viewed at close range we could see a stochastic process of random movements, but we keep our distance and see a continuous flow. At close range we would expect to find many complicated causes of power dissipation and some damage to particles; however, we stand back from the small details and loosely describe the whole process of power dissipation as

friction, neglecting the possibilities of degradation or of orientation of particles.'

Poulos (1981) proposed that this definition does not define continuous deformation at constant velocity, which is a necessary condition of the steady state. Data for critical state soil mechanics are obtained from conventional relatively slow tests, whereas the rate of deformation in load controlled liquefaction tests is about 10000 times faster [Casagrande (1971)]. The difference in the deformation rate of strain controlled compared to load controlled tests has been used to explain why the SSL from the former type of test is parallel to that from the latter type, but lies slightly above it on the $(\ln(p'), e)$ state diagram [Casagrande (1971), Hird/Hassona (1990)]. This implies differing steady state strengths depending on the strain rate. It has also been said that the steady states reached at the end of strain controlled tests may be justly termed critical states and used to define a CSL [Hird/Hassona (1986)].

Even so, the difference in the position of SSL depending on the type of test is disputed by Poulos et al (1985), who suggested that the SSL is unique. Any difference that may be observed in the position of the SSL from the results of strain controlled tests compared to the SSL from load controlled tests is because the former type of triaxial test may not provide sufficient strains for most soils to reach the steady state [Poulos et al (1985)]. Thus there is no general agreement on the effect of strain rate during liquefaction tests at present and this point remains unresolved.

Another variation between the critical state and the steady state approach is that in critical state soil mechanics, particle breakage and orientation are neglected, whereas Poulos (1981) suggested that the steady state can only be achieved after grain orientation (in sands as well as clays) and grain breakage is complete. The idea of grain orientation is part of the concept of a flow structure at

the steady state. When a sand is flowing, it must have a different structure to when it is static. Casagrande (1971) considered that each grain was constantly rotating in relation to all surrounding rotating grains during flow, so as to offer minimal frictional resistance. It was postulated that such a flow structure spreads by chain reaction, exists only during flow, and then in the moment that flow stops, the grains revert to a static structure. These arguments are somewhat difficult to support, as at present there is no detailed information on the arrangement of grains in a flow structure. Logically, the flow structure must be different to a static structure, supported by the fact that observations of flowslides, in both the laboratory and the field, indicate fluid-like behaviour. Also of interest to the concept of a flow structure, is that flows have been observed to 'jam', reverting from a flow to a static structure, when the void ratio was not high enough to allow rotation and flow of the grains [Bagnold (1955)].

The behaviour of a granular soil under both undrained monotonic and cyclic loading is now described. This is illustrated using the schematic diagrams produced by Alarcon-Guzman et al (1988), as the relation between monotonic and cyclic loading has been clearly presented (figs 2.6-2.8). It should be noted that their results have been presented in terms of void ratio, average of the major and minor principal effective stresses, and half the deviator stress. The latter two effective stress parameters can be legitimately used to present the steady state line, but are not usually defined as p' and q respectively.

2.52 UNDRAINED MONOTONIC LOADING

For monotonic undrained conditions, a sand has been observed to exhibit three different types of behaviour; strain softening (contractive), strain softening followed by strain hardening (dilative), and strain hardening behaviour. The type of

behaviour observed was dependent on the soil's initial state and the effective stress path during loading.

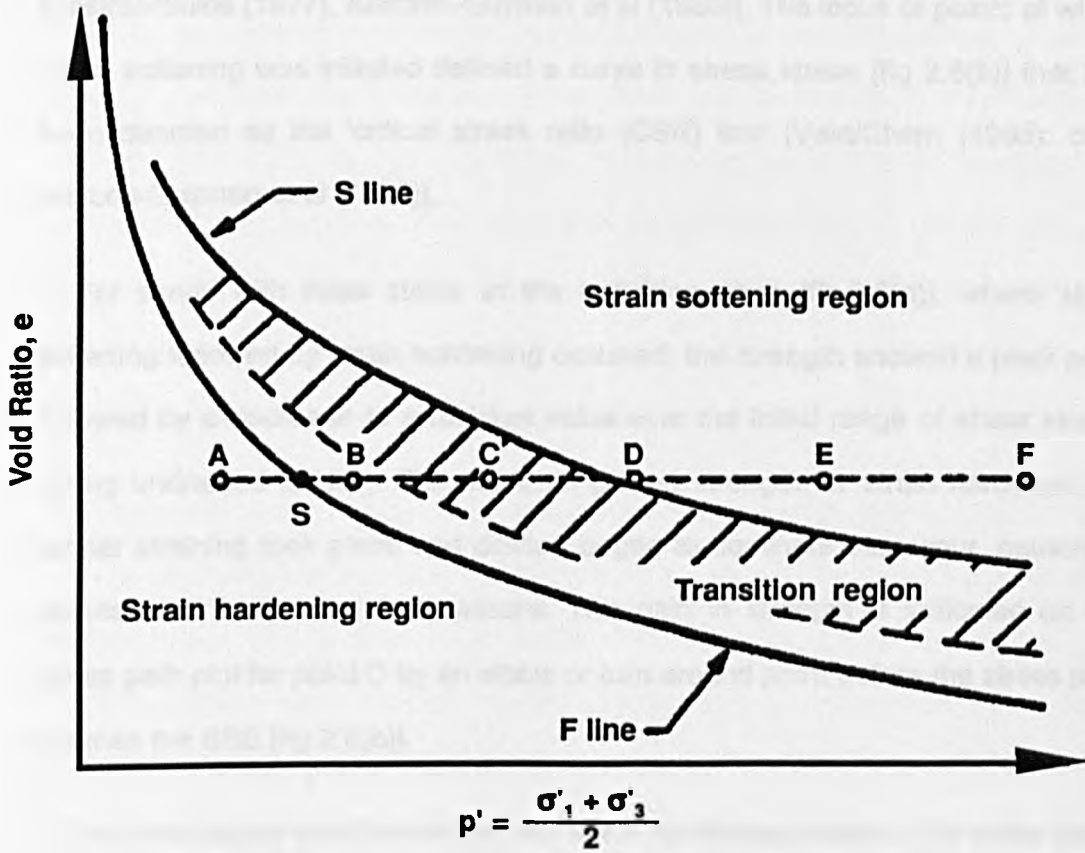
For a sand at a particular void ratio, strain softening followed by strain hardening occurred for initial states to the right of the SSL [on a (p', e) state diagram [point C, fig 2.6(a), where SSL has been denoted as F line], whilst solely strain softening occurred for initial states further to right [points D, E, and F, fig 2.6(a)]. It has been assumed that the initial states at which a sand will exhibit unlimited flow deformation under steady state conditions can be separated from those initial states where the sand exhibits only limited flow deformation followed by strain hardening behaviour. The position and name of the line that separates these two different types of behaviour have not been fully agreed on at present. Alarcon-Guzman et al (1988) postulated that this transition line, denoted as the S line [fig 2.6(a)], appeared to correspond to the critical void ratio line (CVR line) from drained tests. The critical void ratio line, was defined by Casagrande (1971) as the line joining void ratios during constant-volume deformation at different effective normal or minor principal stresses, originally obtained from drained direct shear and consolidated drained triaxial tests. Poulos et al (1988) disagreed with this point and have shown that there was no effect of drained versus undrained shear on a sample of Syncrude tailings, hence the CVR line and SSL were the same. Instead, these authors proposed that the transition line corresponded to something called the 'DC-boundary', which was thought to be probably dependent on the soil structure, state, and loading method [Poulos (1971): cited in Poulos et al (1985)]. Thus, this point remains unresolved at present.

Considering a sand that only exhibited strain softening behaviour, a marked reduction in strength was observed after the peak point of the stress strain curve was reached following a small strain. This reduction in strength was caused by a decrease in the normal effective stress within the sand as the pore water pressure

FIG 2.6

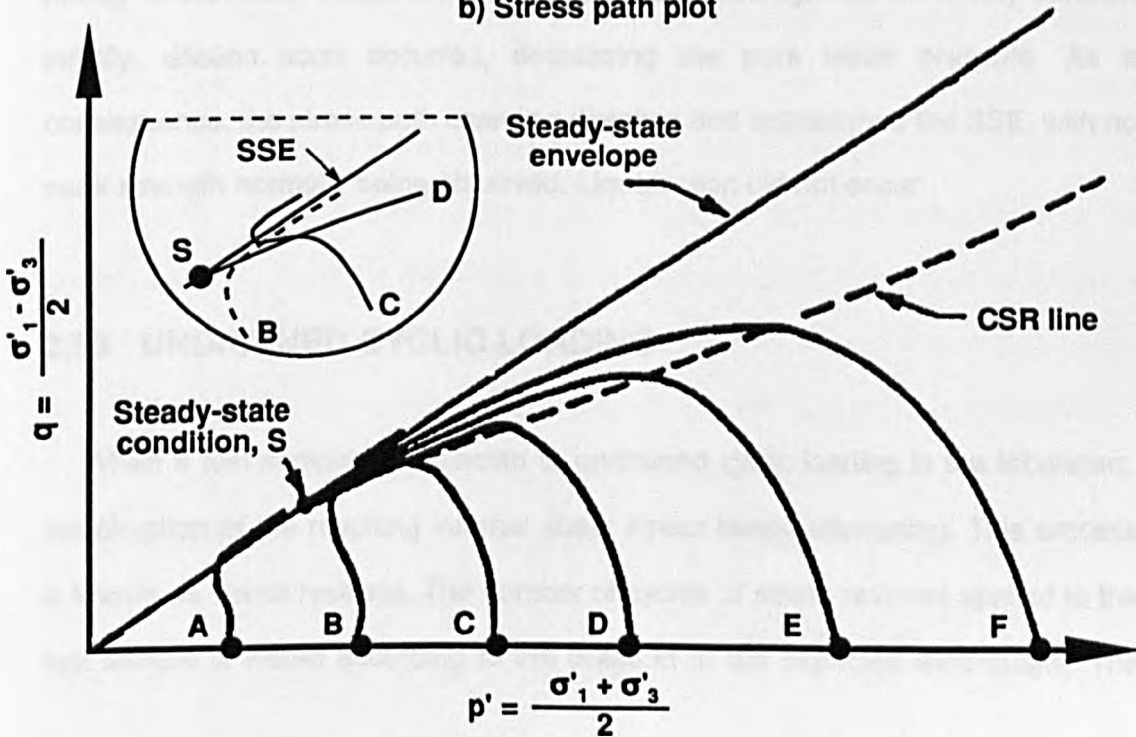
MONOTONIC UNDRAINED BEHAVIOUR (SCHEMATIC)
 [Alarcon-Guzman et al (1988)]

a) State diagram



$$p' = \frac{\sigma'_1 + \sigma'_3}{2}$$

b) Stress path plot



$$p' = \frac{\sigma'_1 + \sigma'_3}{2}$$

increased. The stress stabilised at the steady state strength during steady state deformation [point S, fig 2.6(b)]. No volume change occurred during this process [Castro/Poulos (1977), Alarcon-Guzman et al (1988)]. The locus of points at which strain softening was initiated defined a curve in stress space [fig 2.6(b)] that has been denoted as the 'critical stress ratio (CSR) line' [Vaid/Chern (1985): cited Alarcon-Guzman et al (1988)].

For sands with initial states in the transition zone [fig 2.6(a)], where strain softening followed by strain hardening occurred, the strength showed a peak point followed by a decrease to a residual value over the initial range of shear strains during undrained loading. The soil then gained strength, or strain hardened, as further straining took place and dilation began to dominate behaviour, causing a decrease in the pore water pressure. This gain in strength is indicated on the stress path plot for point C by an elbow or turn around point before the stress path reaches the SSE [fig 2.6(b)].

The final region was that where only strain hardening occurred [for initial states mainly to the left or below the F line, fig 2.6(a)]. Although the sand may contract initially, dilation soon occurred, decreasing the pore water pressure. As a consequence, the stress path changed direction and approached the SSE, with no peak strength normally being observed. Liquefaction did not occur.

2.53 UNDRAINED CYCLIC LOADING

When a test sample is subjected to undrained cyclic loading in the laboratory, the direction of the resulting internal shear stress keeps alternating. This process is known as stress reversal. The number of cycles of stress reversal applied to the test sample is varied according to the duration of the expected earthquake. The

level of stress applied during the test, or cyclic shear stress, is related to the acceleration of the earthquake being modelled.

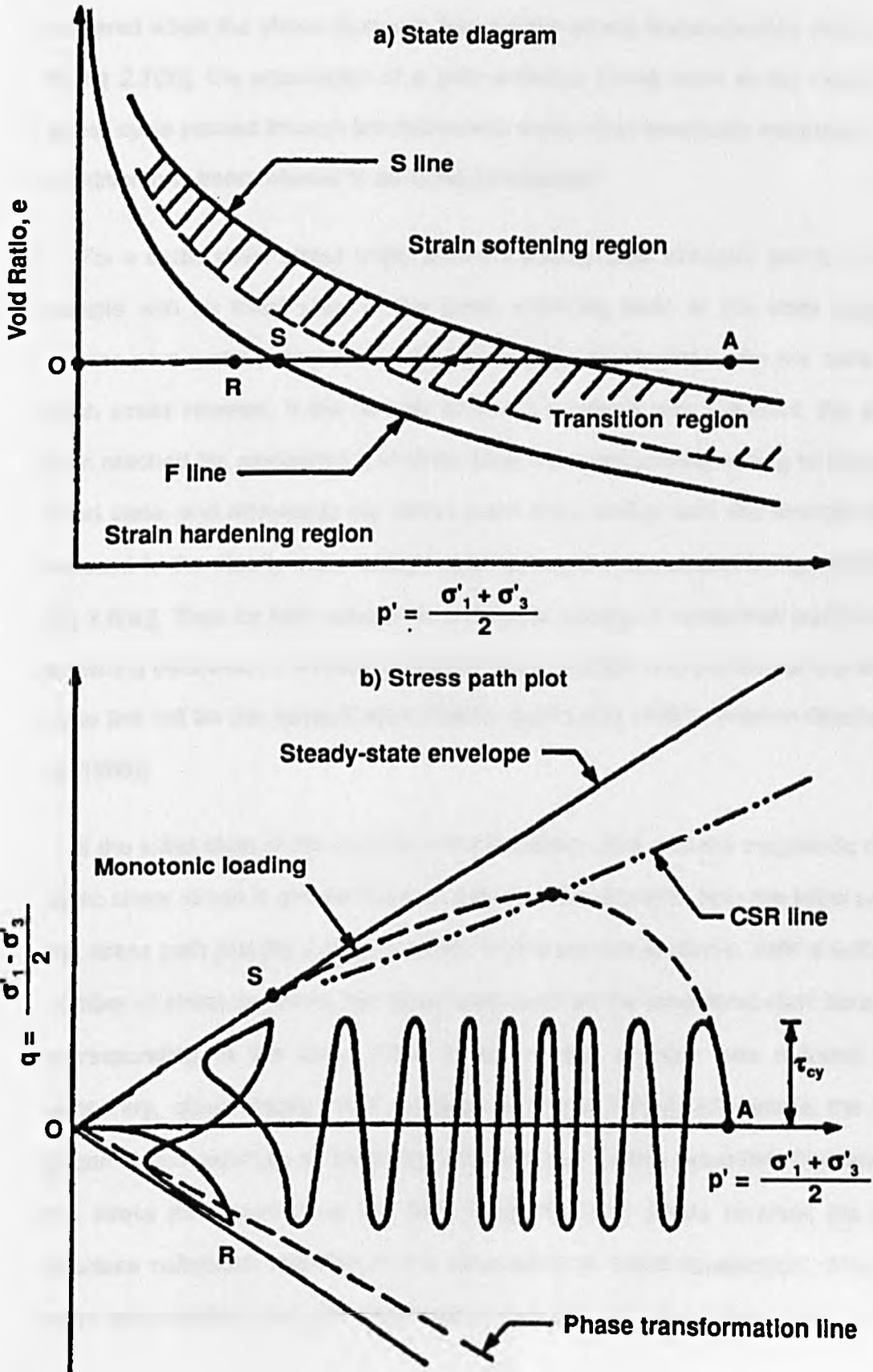
When an element of saturated soil is subjected to seismic shaking, it will be deformed by cyclic shear stresses. In the field, the magnitude of these stresses will vary from cycle to cycle because of the irregular nature of loading from earthquakes. Excess pore water pressures are generated during each application of cyclic stress reversal, and the effects become cumulative during the duration of the shaking. The rise in pore water pressure can result in liquefaction if the magnitude and duration of the shaking are large enough.

The behaviour and resulting deformation of a sand sample under cyclic loading is dependent on its initial state, the number of cyclic stress reversals and whether the magnitude of the cyclic shear stress imposed is greater or smaller than the undrained steady state strength, as determined from a sand sample at the same initial state under monotonic undrained conditions.

For a sand sample at an initial state in the strain softening zone [point A, fig 2.7(a)], undergoing a cyclic shear stress smaller than the steady state strength, Alarcon-Guzman et al (1988) noted that excess pore water pressures were generated during the stress reversals, but the stress path traversed below the point S and continued towards the SSE because of the small magnitude of the applied shear stress [fig 2.7(b)]. When the effective principal stress ratio reached a critical value, dilation began to prevail, causing a 'turn around' in the stress path [fig 2.7(b)]. Upon the next stress reversal, the number of contact points between neighbouring grains was reduced, causing a tendency for the sand to collapse and an increase in the excess pore water pressure. This was reflected by the stress path moving towards the origin of stress space [point O, fig 2.7(b)]. The 'phase transformation' lines are equal to the values of the mobilised effective friction

FIG 2.7

UNDRAINED BEHAVIOUR UNDER CYCLIC SHEAR STRESSES
SMALLER THAN THE STEADY STATE STRENGTH (SCHEMATIC)
[Alarcon-Guzman et al (1988)]



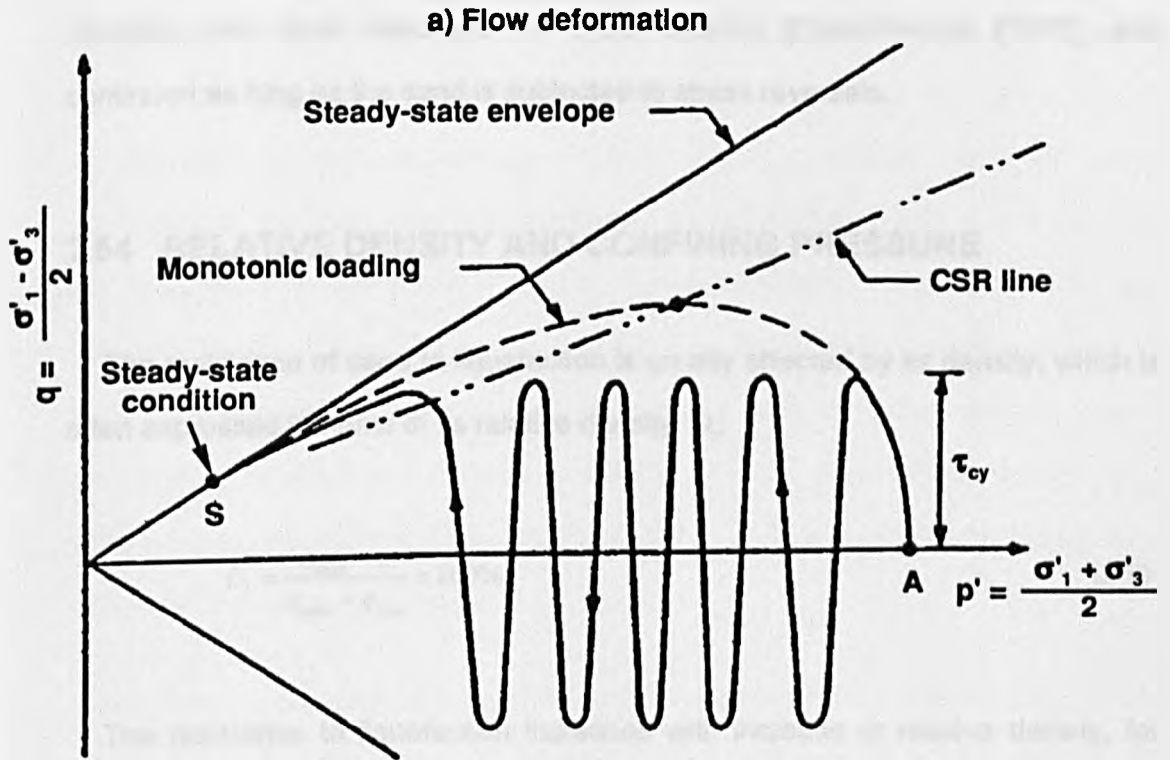
angle that correspond to the principal stress ratios at which dilation occurs on loading within the strain hardening region of the state diagram. If a stress reversal occurred when the stress path was beyond the phase transformation lines [point R, fig 2.7(b)], the occurrence of a zero effective stress state at the instant the stress cycle passed through the hydrostatic stress state eventually happened. This condition has been referred to as 'initial liquefaction'.

For a cyclic shear stress larger than the steady state strength, and for a sand sample with an initial state in the strain softening zone of the state diagram, excess pore water pressures were progressively developed within the sand with each stress reversal. If the number of stress reversals was sufficient, the stress path reached the monotonic undrained state boundary corresponding to the same initial state, and afterwards the stress paths were similar, with the strength being reduced to the steady state strength and unlimited shear strains being developed [fig 2.8(a)]. Thus for both monotonic and cyclic loading of sands that exhibit strain softening behaviour, the resultant steady state strength and position of the steady state line will be the same [Castro (1969): cited Lucia (1981), Alarcon-Guzman et al (1988)].

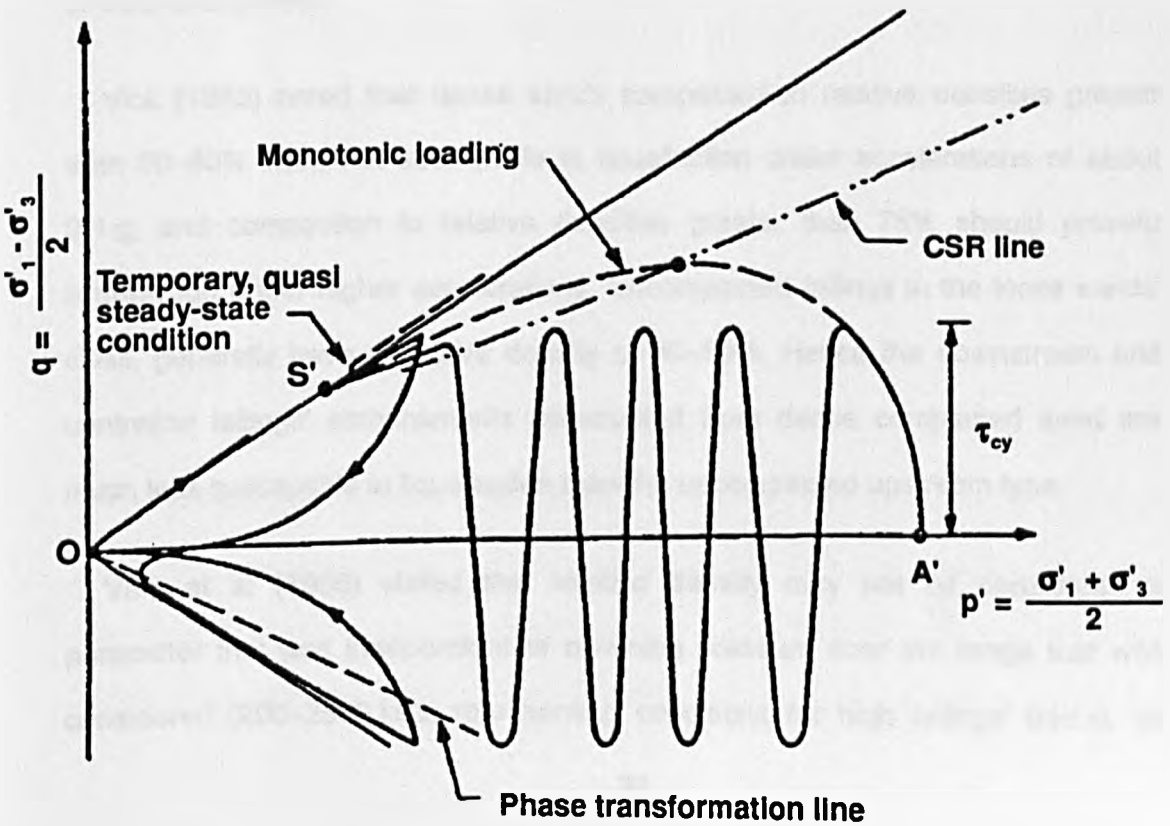
If the initial state of the sand is in the transition zone and the magnitude of the cyclic shear stress is greater than the steady state strength, then the initial part of the stress path plot [fig 2.8(b)] is similar to that described above. With a sufficient number of stress reversals, the stress path reached the monotonic state boundary corresponding to the same initial state and the strength was reduced to a temporary, quasi steady state condition at S' [fig 2.8(b)]. Afterwards, the sand began to gain strength as shearing continued and dilation prevailed, illustrated by the stress path moving up the SSL. Upon the next stress reversal, the sand structure collapsed, resulting in the occurrence of 'initial liquefaction'. After this point was reached, the soil continued to behave with alternating cycles of zero

FIG 2.8

UNDRAINED BEHAVIOUR UNDER CYCLIC SHEAR STRESSES LARGER THAN THE STEADY STATE STRENGTH (SCHEMATIC)
 [Alarcon-Guzman et al (1988)]



b) Limited flow deformation



effective stress state and associated large deformations, followed by stiffening upon shearing in the opposite direction [Alarcon-Guzman et al (1988)]. This last condition has been described as cyclic mobility [Casto/Poulos (1977)] and continued as long as the sand is subjected to stress reversals.

2.54 RELATIVE DENSITY AND CONFINING PRESSURE

The resistance of sand to liquefaction is greatly affected by its density, which is often expressed in terms of its relative density, D_r :

$$D_r = \frac{e_{\max} - e}{e_{\max} - e_{\min}} \times 100\% \quad (2.8)$$

The resistance to liquefaction increases with increase in relative density, for example, as illustrated in the laboratory experiments of soil liquefaction under monotonic loading conducted by Kramer/Seed (1988), and the cyclic loading tests of Vaid et al (1985).

Vick (1983) noted that dense sands compacted to relative densities greater than 50–60% were not susceptible to liquefaction under accelerations of about 0.1 g, and compaction to relative densities greater than 75% should prevent liquefaction under higher accelerations. Uncompacted tailings in the loose sands' class, generally have a relative density of 30–50%. Hence the downstream and centreline tailings' embankments constructed from dense compacted sand are much less susceptible to liquefaction than the uncompacted upstream type.

Vaid et al (1985) stated that relative density may not be considered a parameter that was independent of confining pressure over the range that was considered (200–2500 kPa: representing conditions for high tailings' dams), as

liquefaction resistance generally decreased with increase in confining pressure. The effect of confining pressure on some screened copper tailings prepared at various initial relative densities for comparison is shown (fig 2.9). The curves illustrate the net influence of these two factors. It should be noted that a considerable increase in density of the sample inevitably occurred under application of the large confining pressures. Kramer/Seed (1988) also noted that the resistance to liquefaction increased approximately in proportion to the confining pressure over the range 4.9–490 kPa for an initial relative density of 35%. This agreed with the results of Vaid et al (1985) over that stress range. It should also be noted that Vaid et al (1985) used the cyclic stress ratio (τ_o/σ'_{vo}) required to cause a shear strain amplitude of 5% in 10 stress reversal cycles as a definition of liquefaction (section 2.4).

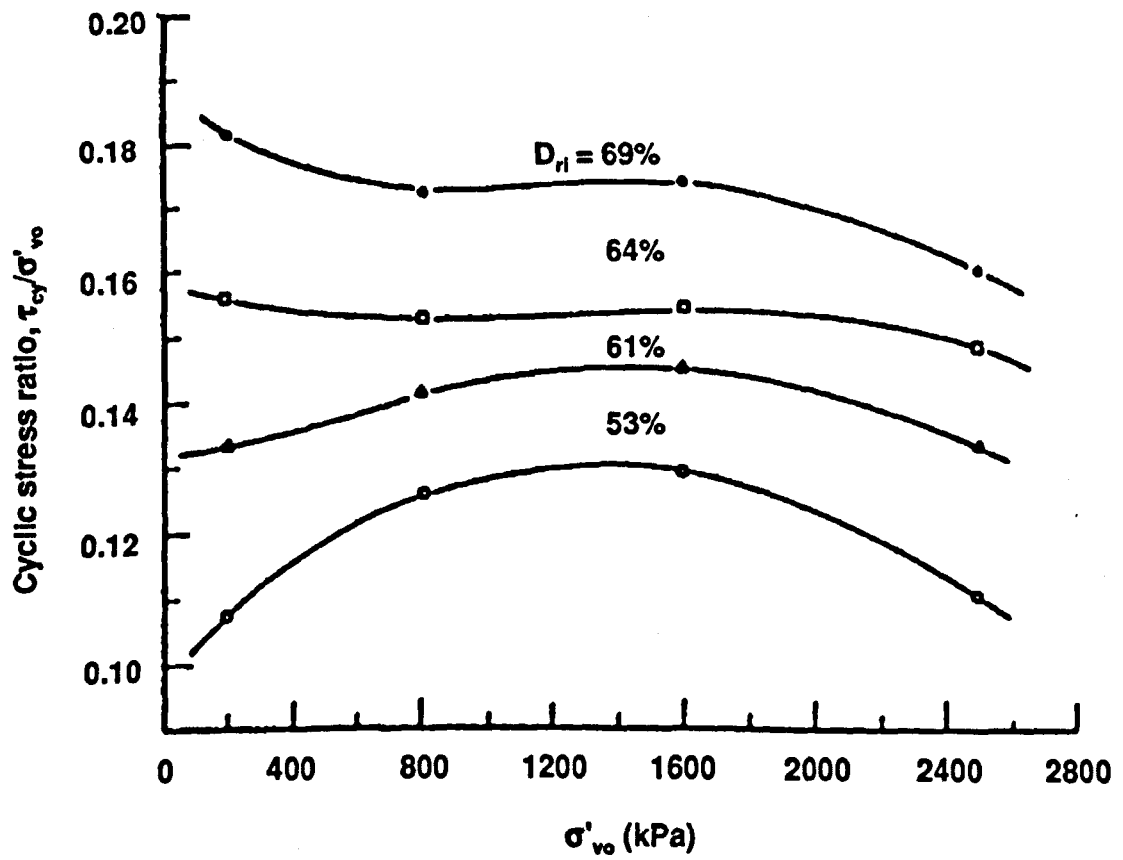
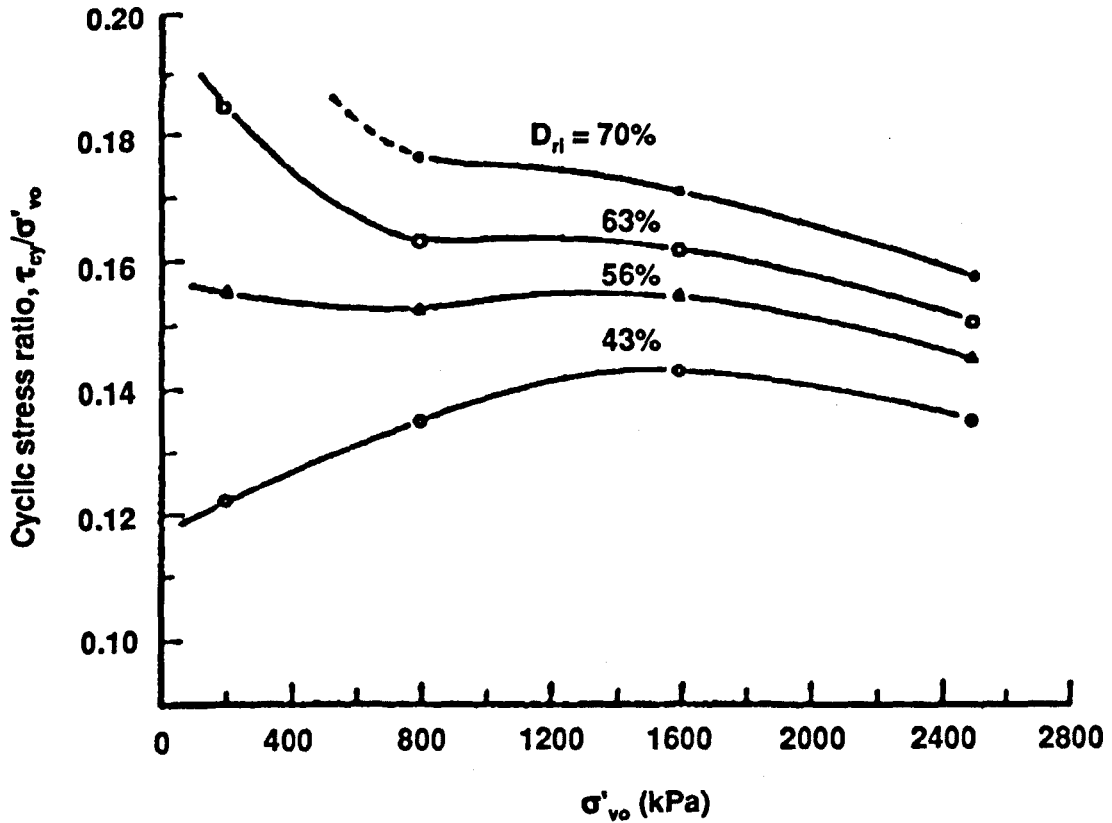
Liquefaction susceptibility of tailings can be greater than natural soils at the same relative density due to grain characteristics and gradation, causing cyclic stress ratios required for initial liquefaction to vary by +/- 20%. Also, the method of soil deposition can cause the liquefaction cyclic stress ratio to vary by as much as 200% [Vick (1983)]. Sedimentation under water, similar to tailings' deposition causes the greatest liquefaction susceptibility. The time a deposit has experienced a sustained loading is also influential, the younger soil deposits such as tailings being more susceptible to failure.

2.55 INITIAL SHEAR STRESS

The presence of an initial shear stress, τ_o , within a soil element is the result of anisotropic consolidation and is determined by the principal stress ratio. Lucia (1981) noted that the principal stress ratio of a soil element near the toe of an upstream type tailings' dam increases as the height of the dam increases and the

FIG 2.9

**EFFECT OF CONFINING PRESSURE ON LIQUEFACTION
RESISTANCE OF SANDS AT VARIOUS INITIAL RELATIVE DENSITIES**
[Vald et al (1985)]



crest moves upstream relative to the element under consideration. The initial shear stress has no effect on the steady state strength [Castro (1969): cited Lucia (1981)], but significantly influences the additional shear stress required to initiate liquefaction (fig 2.10), which decreases as the principal effective stress ratio increases [Kramer/Seed (1988)].

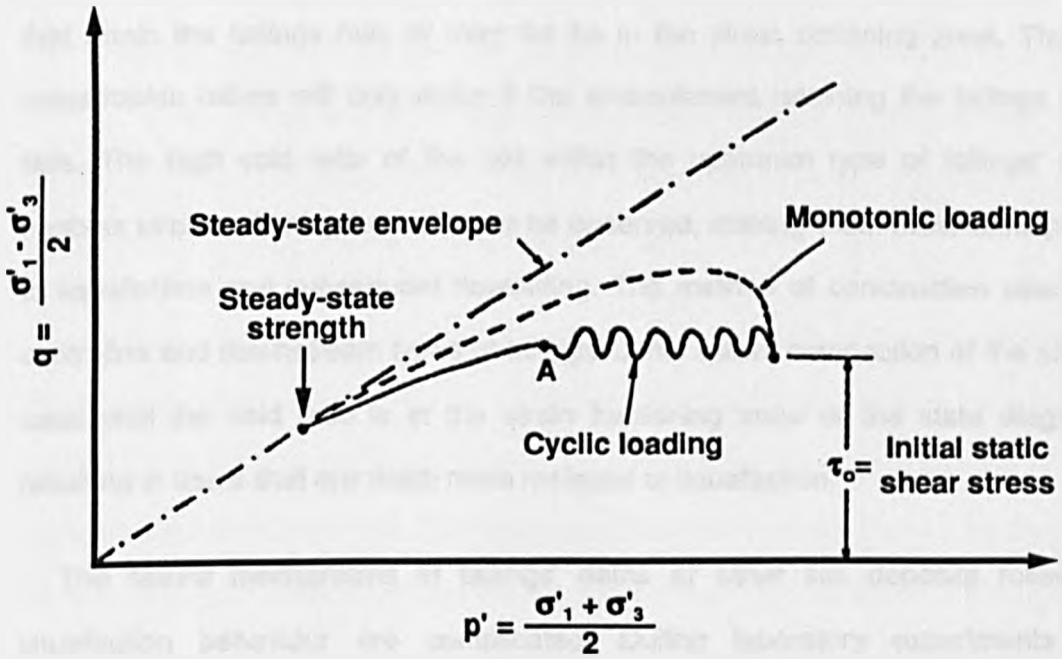
This indicates that liquefaction may be initiated in sand deposits that have been subjected to high shear stress levels during drained loading by very small changes in shear stress during undrained loading [Bishop (1973), Kramer/Seed (1988)]. The potential for liquefaction may therefore be very high at high levels of initial shear stress. This effect may be responsible for the cases of 'spontaneous' liquefaction where no source of loading of any kind was observed.

2.56 PARTICLE ANGULARITY

Vaid et al (1985) tested two sands of virtually identical gradation but one was rounded and the other an angular tailings' sand. The angular sand was more resistant to liquefaction over almost the entire range of relative densities considered for confining pressures less than 400 kPa. Above this confining pressure it was noted that the angular sand suffered breakage of its sharp edges, but no gross particle crushing, due to consolidation and subsequent shearing during liquefaction. The consequence of this particle breakage is analogous to increased compressibility, resulting in accelerated pore water pressure rise in liquefaction tests. Under higher confining pressures, the resistance of the angular sand was either larger or smaller than that of the rounded sand, depending on the range of relative densities considered.

FIG 2.10

EFFECTIVE STRESS PATHS FOR A SOIL ELEMENT WITH AN INITIAL STATIC SHEAR STRESS (SCHEMATIC)
[Aarcon/Leonards (1988)]



2.6 THE FLOWSLIDE EVENT

Tailings deposited hydraulically behind tailings' dams are nearly always loose enough to be in the strain softening zone of the state diagram, whilst the dams that retain the tailings may or may not be in the strain softening zone. Thus a catastrophic failure will only occur if the embankment retaining the tailings also fails. The high void ratio of the soil within the upstream type of tailings' dam enables strain softening behaviour to be observed, making them most susceptible to liquefaction and subsequent flowsliding. The method of construction used for centreline and downstream types of tailings' dams allows compaction of the sands used until the void ratio is in the strain hardening zone of the state diagram, resulting in dams that are much more resistant to liquefaction.

The failure mechanisms of tailings' dams or other soil deposits following liquefaction behaviour are complicated. During laboratory experiments on subaqueous flowslides, Silvis et al (1988) observed that immediately following failure of the sample, a kind of negative wave travelled upstream into the previously unaffected area. During these experiments, the most significant changes of the pore water pressure occurred when the negative wave approached the piezometers, which indicated that almost the full height of the sand mass was in a state of liquefaction when this occurred. This negative wave is reminiscent of water dam break flood waves, as described by St. Venant equations [Whitham (1955)], where a negative wave travels upstream into the impoundment area and a positive wave travels downstream. Further possible failure mechanisms identified during laboratory experiments on coal stockpiles [Eckersley (1990)], given in order of increasing bulk density of the soil, are:

- a) compound slide and retrogressive compound sliding

b) non-circular slide and retrogressive non-circular sliding

c) retrogressive cracking, toppling and rotational sliding

As the depth of material downstream of the slip provides a resisting force to the next potential slip surface, the rate of propagation of retrogressive slipping will depend on the shear strength of the intact material and the velocity at which the previously failed material moves away from the next potential slip surface. The retrogressive slip surfaces are three dimensional.

The final run-out distance and flow velocity of an individual flowslide event are important parameters in assessing of the potential hazard area from such a failure. These depend on the material's properties, the volume involved in the failure and the topography downstream. The maximum potential volume of material that can be involved in the flow depends on the total volume stored behind the tailings' dam. The size and erosion rate of a breach in a tailings' dam will affect the volume of material involved in a failure. The topography downstream of a tailings' dam will influence the distance travelled by a flowslide. Field data indicate that if the bed is flat and has a low slope, the flowslide is likely is to spread in the lateral as well as the longitudinal direction. When the bed slope is higher, Rouse (1984) suggested that the debris of a flowslide may follow a straight and narrow track that forms a bulbous lobe, with lateral ridges or levees of static material containing the moving material of the flowslide along its margins. These features have been reproduced in the laboratory at a small scale during the study of debris flows [Johnson/Rodine (1984)]. Additional material may be introduced to the flowslide through erosion of the bed and through side wall failures, caused by undercutting by the flow. Flowing material may be lost from the flowslide by the formation of lateral ridges along the margins of flow and by deposition at the bed. Such changes in the flow mass over the distance travelled will affect the final run out distance of the

flowslide. Rouse (1984) stated that the length of the flowslide often exceeds the width and depth by several orders of magnitude. This is reflected by the low difference between the flowslide's surface angle and the bed slope. The flow is capable of travelling great distances along a narrow track at high velocities.

Further information has been gained from the shearing of solid grains and water in a moving bed apparatus [Davies (1988)]. The non-depositing wave created may be similar to a flowslide along its longitudinal axis, with minimal side friction, during some stages of motion. It consisted of a sharply curved front or 'head', followed by a 'body' of uniform depth and ending with a uniformly sloping 'tail' (fig 2.11). The transition between the body and the tail was quite sharp, occurring within a few grain diameters. The angle made by the surface of the tail with the horizontal was very consistent at $7^\circ \pm 0.5^\circ$, which did not vary significantly with bed slope, bed speed (or mean grain velocity) or total grain volume.

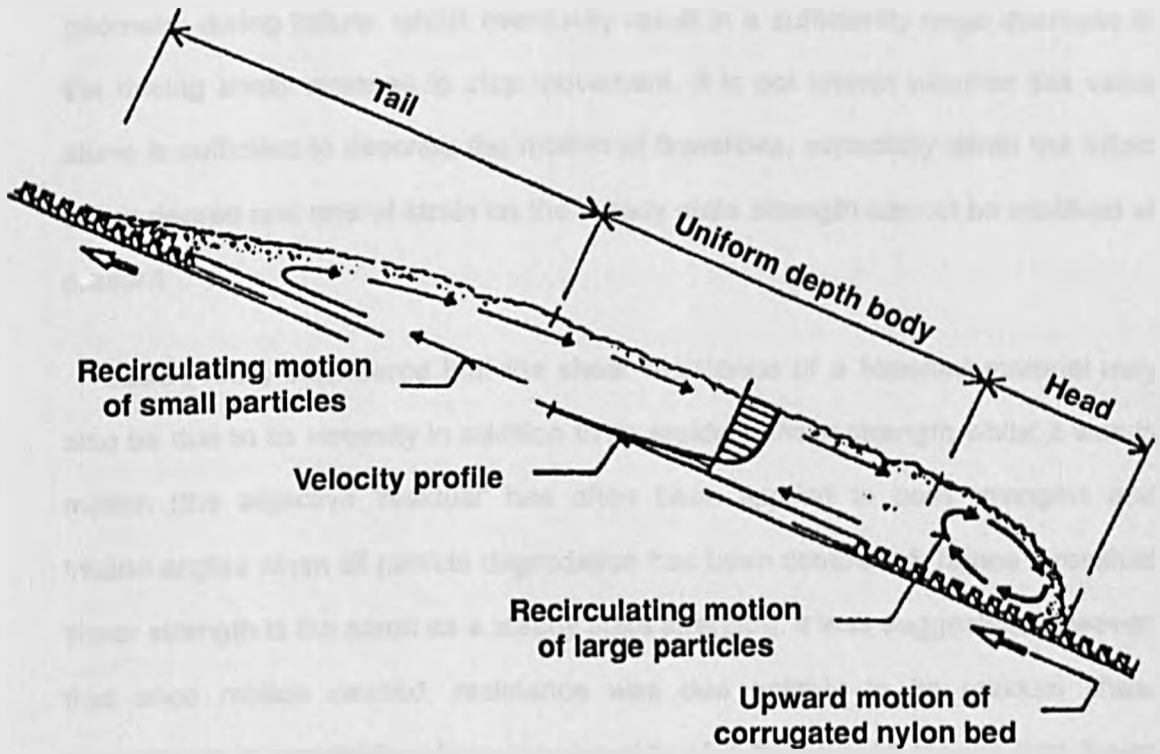
2.7 ANALYSIS OF FLOWSLIDE MOTION

2.71 INTRODUCTION

It has been shown that the value of steady state strength of a liquefied soil is dependent on the initial void ratio and the position of the steady state line in (p', e, q) stress space (section 2.5). The value of steady state strength will indicate whether large deformations are likely to occur after the peak strength has been reached. Thus, if the soil is in the strain softening zone of the state diagram, a considerable reduction in the shear strength will occur during liquefaction, meaning that the applied stresses can no longer be sustained and this will result in

FIG 2.11

STATIONARY GRANULAR FLUID WAVE
[Davies (1988): cited Savage (1989)]



rapid acceleration and large shear deformations of the soil [Eckersley (1990)].

Application of the steady state concept to flowslide motion was postulated by Poulos et al (1985), who stated that strains are limited only by the changes in geometry during failure, which eventually result in a sufficiently large decrease in the driving shear stresses to stop movement. It is not known whether this value alone is sufficient to describe the motion of flowslides, especially when the effect of the degree and rate of strain on the steady state strength cannot be resolved at present.

Lucia (1981) considered that the shear resistance of a liquefied material may also be due to its viscosity in addition to its residual shear strength whilst it was in motion (the adjective 'residual' has often been applied to both strengths and friction angles when all particle degradation has been completed, hence a residual shear strength is the same as a steady state strength). It was suggested, however, that once motion ceased, resistance was due entirely to its residual shear strength, as a contribution from the viscosity of a fluid would require that it was moving. Considering the moment when the material just stops moving, it was found that the mode of sliding that required the greatest shear strength was a liquefied wedge, with shear along the base and active pressure at the back of the wedge. Analysis of this wedge enabled a dimensionless graph to be produced. A value of the residual shear strength of a failure could be estimated, using back-calculated strengths estimated from similar materials. Even though this value was approximate, it was then possible to predict the flow distance by comparing an estimate of the flow volume against the wedge's strength by graphical means. This analysis of a liquefied wedge may be unrealistic as it assumes that all the material stops at the same time and ignores the dynamic behaviour of the liquefied soil whilst it was in motion.

Further information concerning the dynamic behaviour of soil, under different conditions other than idealised triaxial tests, has been obtained during the study of granular fluids. Flowslides are part of this diverse subject area of granular fluids. Other examples include rockfalls on the moon, landslides, snow avalanches, debris flows, mudflows, hyperconcentrated flows and flows of slurries in pipelines.

A granular fluid is a two phase material whose flow essentially consists of solid grains shearing over one another, and over a stationary boundary or bed. The interstitial fluid may be of negligible density, such as air, or of non-negligible density, such as mud or water. A body force component due to gravity pulls the grains towards the bed, whilst a tangential force is the driving force maintaining their shearing motion. The tangential force may consist of a body force component, as in a rockfall down the side of a mountain, or it may be almost exclusively a fluid force, as in the driving of grains over a bed by a stream of wind or water.

Bagnold (1956) called the movement of solid grains in response to the gravity-driven flow of water past them the 'stream case'. This is usually considered for the transport of sediment by rivers. The flow energy of the fluid has to be transferred from the fluid to the grains by means of a fluid drag on the individual dispersed grains, caused by an associated relative motion or 'slip' in the direction of flow. Thus in this case, a drag coefficient is involved, as the movement of the grains requires that the system be regarded as a fluid-dynamic transporting machine, requiring efficiency to be considered [Bagnold (1956)].

Experiments have shown that the behaviour of debris flows [Davies (1988)] and flowslides [Eckersley (1990)] is fundamentally different to the 'stream case'. Davies (1988) observed that the water and solids formed a single heterogeneous fluid in which all components were acted on by gravity to maintain the flow. There

was no significant segregation of any component; water and grains of all sizes were distributed uniformly throughout the flow, and all components of the flow moved at the same velocity, or distribution of velocities.

During the deformation of the bulk material of a granular fluid, individual solid particles typically acquire more or less random translational fluctuation velocities and spins, as a result of collisions and particle overriding, in addition to their mean translational motion [Savage (1989)]. For a dry granular material, there are three main mechanisms by which stresses can be generated during bulk deformations; Coulomb-type friction, momentum transport by particle translation and by collisional interactions. When the interstitial fluid is of non-negligible density, such as mud or water, analysis is further complicated by the resistance to shear of the fluid itself, the effect of the fluid on particle interactions and the difficulty in quantifying these effects. This is the case in flowslide motion. De Groot et al (1987) considered that for a flowslide, three types of flow could be possible;

- a) flow governed by dispersive pressures, or grain-grain interactions.
- b) turbulent flow
- c) laminar flow without dispersive pressures.

2.72 DISPERSIVE PRESSURES

Bagnold (1954,1956) regarded a mass of concentrated grains that was dispersed in a flowing fluid medium to be a fluid. The grains were not regarded as having been transported by the fluid stress exerted by the interstitial fluid. Dispersion describes a mass of scattered solid particles in a fluid medium. It was reasoned that a static grain mass cannot flow without some degree of dispersion.

Bagnold (1956) stated that when the grains were a diameter apart (volume concentration >9% for spheres), the probability of a collision approaches one. The grains must push or knock each other out the way, depending on whether or not the fluid viscosity outweighs the effect of the inertia of the grains. Both types of encounter must involve displacements of the grain normal to planes of shear. Bagnold (1954) thought it probable that the required normal dispersive stress between the sheared grains might arise from the influence of grain particle on grain particle. These encounters would also give rise to an associated shear resistance additional to that provided by the pore fluid. A dispersion of large neutrally buoyant solid spheres in a Newtonian fluid was sheared in the annular space between two concentric drums [Bagnold (1954)]. The experimental results showed that the presence of grains greatly increased the shear stress and the normal stress measured at the boundary. This was due to the interaction between grains under shear, or dispersive pressures. Davies (1988) stated that the existence of this dispersive pressure is beyond question. Bagnold (1954) found two distinct regions of behaviour existed; a grain inertia and a macroviscous zone, separated by a transition region. The empirical relations found for the grain shear stress in the macroviscous and inertia zones, $T_{viscous}$ & $T_{inertial}$, were:

$$T_{viscous} = 2.2\lambda^{2/3}\mu\frac{dv_d}{dz} \quad (2.9)$$

$$T_{inertial} = 0.013\rho_g(\lambda D)^2\left(\frac{dv_d}{dz}\right)^2 \quad (2.10)$$

ρ_g = grain density

μ = viscosity of the interstitial fluid

D = particle diameter

λ = linear grain concentration

$\frac{dv_d}{dz}$ = mean shear rate

The linear grain concentration, λ , was defined as the ratio of the grain diameter to mean free dispersion distance. This was related geometrically to the solid volume concentration C by:

$$C = \frac{V_s}{V_t} \quad (2.11)$$

$$\lambda = \left[\left(\frac{C_0}{C} \right)^{1/3} - 1 \right]^{-1} \quad (2.12)$$

V_s = volume of solids

V_t = total volume

C_0 = maximum possible static solid volume concentration

It has been found that $C_0 = 0.65$ (approximately.) for natural reasonably rounded and uniform sand grains [Bagnold (1956)]. It has also been noted that the expression for the inertial shear stress is analogous to $\rho l^2 (dv/dz)^2$, which expresses the shear stress in a pure turbulent fluid [Bagnold (1956)]. The expression for the viscous shear stress is similar to that for water undergoing laminar flow, where the viscosity of the granular fluid depends on the linear grain concentration, λ . The ratio of inertial to viscous shear stress was used to characterise the flow into a particular region under given conditions. This ratio is similar to a Reynold's number and was called a Bagnold number (Ba) by Mastbergen et al (1988):

$$Ba = \frac{\rho_s \lambda^{1/2} D^2}{\mu} \frac{dv_d}{dz} \quad (2.13)$$

It was found that the flow was macroviscous when $Ba < 40$, and was in the grain

inertia zone when $Ba > 450$.

Bagnold (1954) stated that the shear stress measured in the inertial zone was purely a grain stress, to be regarded as additive to any fluid shear stress that may persist by virtue of residual fluid turbulence. Davies (1988) stated that in this zone, the dominant means of momentum and energy transport was by nearly instantaneous collisions or impulsive contacts and was not at all transferred to the interstitial or intergranular fluid between successive grain contacts. Thus the viscosity of the interstitial fluid had very little effect on the boundary stresses. Examples of flow in this region are the motion of gravel in chutes or channels and the transport of sand by wind.

In the macroviscous zone, the shear stress was a mixed shear stress due to the effect of fluid viscosity as modified by the presence of grains, and it was suggested that it could not legitimately be split into grain and fluid elements [Bagnold (1954)]. In this zone, Mastbergen et al (1988) stated that the intermediate fluid phase played an important role in the momentum and stress transfer. Davies (1988) suggested that grain momentum resulting from a collision was entirely dissipated by fluid friction before the next collision. The boundary stresses were significantly affected by fluid properties.

Bagnold (1954) proposed that the ratio of grain shear stress T to normal stress P measured in his experiments was related by:

$$T = P \tan \phi_d \quad (2.14)$$

ϕ_d = dynamic angle of friction

The term dynamic angle of friction has been used to differentiate this angle from that measured in static or quasi static experiments [Savage (1989)]. Other

researchers have interpreted the shear and normal stresses in terms of the Coulomb yield criterion and have expressed the stress ratio in terms of a residual angle of friction [eg Hungr/Morgenstern (1984)].

Bagnold (1954) assumed this stress relationship to be valid throughout the granular fluid and as such is not equivalent to the Coulomb yield criterion, which defines regions of shearing from regions of static equilibrium [Bailard/Inman (1979)]. Insufficient information is available regarding the stresses within the interior of the shearing material and hence discussions should be restricted to the boundaries of flow, which is consistent with the use of Coulomb's law.

Although the initial experiments of Bagnold (1954) involved the shearing of neutrally buoyant spheres, it was reasoned that the value of the dispersive normal stress at the base of the flow, generated during shearing in a gravity field, must be equal to the normal immersed or buoyant weight component of all the grains moving over unit bed area, no matter how they are dispersed and what the flow conditions may be above the boundary [Bagnold (1956)]. This was assuming steady flow and the absence of grain suspension by eddies of fluid turbulence.

Subsequent researchers have used a variety of cohesionless materials, with both air and water as the interstitial fluid, to verify the work of Bagnold (1954) and to investigate further the behaviour of granular fluids. These experiments have typically been performed using annular shear cells or rotating drums similar to that used by Bagnold (1954). Experiments have been difficult to duplicate however, even using similar apparatus. Hanes/Inman (1985) noted that several complications may arise due to the geometrical constraints of a particular apparatus and that it has been unclear how to compare data obtained in differing apparatus, or even how to compare different sized material in the same apparatus. These authors also note that the exact values of the Bagnold number that define

each of the flow regions may vary, depending on the material used and the geometry of the testing apparatus.

Different results have been obtained, depending on test conditions. In the inertial region, if a constant mean solid volume concentration was maintained, both the shear and normal stress varied in proportion to the square of the mean shear rate [Savage/Sayed (1984), Hanes/Inman (1985)]. These results were in accordance with the results of Bagnold (1954). Hanes/Inman (1985) obtained results in Bagnold's transition zone and found that the shear and normal stresses were proportional to the shear rate. If, however, the tests were performed such that the shear rate was increased whilst the normal stress remained constant by allowing the granular material to dilate freely, it was found that the shear stress was independent of the shear rate [Hungri/Morgenstern (1984)].

The results of these two types of tests are apparently different, but the ratio of the shear to normal stress or dynamic angle of friction was nearly constant in each case [Savage (1989)]. Bagnold (1954) originally found that the T/P stress ratio for the inertial region approached a constant value of 0.32, which he assumed to be identical to the residual effective angle of friction [Bagnold (1966)]. The stress ratio gradually increased through the transition region, reaching another constant value of 0.75 in the macroviscous zone. This higher value was assumed to be the result of additional fluid friction [Bagnold (1966)]. Although additional research has not fully resolved the exact value of the dynamic angle of friction, it has been shown that the value was closer to the material's angle of repose throughout a range of shearing conditions than was obtained by Bagnold (1954).

Bagnold (1954) assumed that the neutrally buoyant spheres were uniformly dispersed within the fluid medium. Experiments conducted since have shown that whilst full shearing of all the grains can occur, it is also possible for a region of

close packed non-shearing spheres to exist, resulting in a partial shearing of the grains [Baillard (1978): cited Baillard/Inman (1979), Hanes/Inman (1985)].

Baillard/Inman (1979) rederived equations to obtain the T/P stress ratio for Bagnold's rotating drum experiment, taking into account the possible presence of a static layer of grains within the drum. Although no exact values could be obtained for the inertial and macroviscous flow regions, the possible range of values was much reduced and closer to the angle of repose of the material used. Hanes/Inman (1985) found that a higher value of the dynamic angle of friction was obtained during the full shearing compared to the partial shearing experiments (Table 2.2). These researchers observed that the higher values for the fully shearing experiments implied a smaller value of the normal stress. This could have been caused by the fact that the solid lower boundary, although fully stressed from above, could not partake in the granular fluctuations. Thus there was a deficiency in the normal stress, causing the stress ratios for the fully shearing flows to be higher than those for partial shearing. (These authors compared these angles to a dynamic angle of repose (Table 2.2), although the difference between an angle of repose and a dynamic angle of repose is not clear).

Hanes/Inman (1985) suggested that the type and roughness of boundary were therefore important and may strongly influence the dynamics of flow. Data obtained during open channel experiments [Augenstein/Hogg (1978)] also indicated that angle of friction at the bed was characteristic of the nature of the particles and of the surface over which they were flowing. The influence of the fixed grain bed, as compared to the movable grains at the flow boundary in the partially shearing experiments, requires further study.

Inconsistency in the value of the stress ratio for a material, depending on whether the interstitial fluid is air or water, has also been obtained. Hanes/Inman

TABLE 2.2 DYNAMIC FRICTION ANGLES MEASURED IN RING SHEAR TESTS
[FROM HANES/INMAN (1985)]

Material	Mean measured dynamic friction angles (degrees)		Dynamic angle of repose (degrees)
	In air	In water	In air
1.1mm spheres fully shearing	32	33	26
partially shearing	24	24	—
1.85mm spheres fully shearing	28	31	28
partially shearing	22	28	—

TABLE 2.3 RESIDUAL FRICTION ANGLES MEASURED IN RING SHEAR AND FLUME TESTS [FROM HUNGR/MORGENSTERN (1984)]

Material	Residual friction angle (degrees)		
	Very slow (0.1 cm/s)	Slow (16 cm/s)	Fast (98 cm/s)
10-14 dry sand	29	29	29
10-14 sand in water	26	26	26
4:1 sand-flour mixture	31	31	29
4:2 sand-flour mixture	31	31	31
8-10 dry sand	30	30	—
Polystyrene beads	21	21	stick slip
Ottawa sand in flume tests	25.5		
Polystyrene beads in flume tests	21.8 25		

(1985) reported that the dynamic angle of friction of glass spheres was higher for the larger particle size tested, when submerged, whilst no difference in the stress ratio was observed for a smaller particle size (Table 2.2). With air as the interstitial fluid, the flow was in the inertial region, whilst flows with water as the interstitial fluid ranged from the transitional to the inertial region. Hungr/Morgenstern (1984) observed a decrease in the residual angle of friction (Table 2.3).

The deformation of the water generates a much higher shear stress than that of air. The grain encounters resulted in a shearing resistance, T , that was additional to that provided by the interstitial fluid, giving a higher stress ratio. The viscosity and hence the shearing resistance provided by the interstitial fluid was found to be increased by the presence of grains at low concentrations [Einstein (1906): cited Bagnold (1956)]. Even so, in both the grain inertia and macroviscous regions, the residual fluid shear stress element became insignificant compared to the grain element T at high concentrations. Almost all of the overall stress was due to the grain encounters [Bagnold (1956)]. Therefore, this explanation for the increased dynamic friction is inadequate. Hanes/Inman (1985) also suggested that it is possible that granular vibrations are dampened by the viscosity of the interstitial fluid and this contributes to the higher stress ratio. Centrifugal forces could also have a significant effect upon the dynamics of the interstitial fluid.

Hanes/Inman (1985) stated that the values of the friction angle obtained for the submerged sand were affected by the inability of water to be introduced freely into the apparatus as the granular fluid material dilated when shearing commenced, and therefore regarded this data to be of poor quality. Hungr/Morgenstern (1984) did not discuss any difficulty with introduction of water to the sample when dilation occurs. At present, these conflicting results cannot be resolved.

Experiments have also been performed in open channels to investigate the

dynamic angle of friction. Augenstein/Hogg (1974) obtained results for powder flows that showed that the angle of friction was independent of the velocity of the particles and of the bed angle. This led to constant acceleration or deceleration depending on whether the bed angle was greater or less than the measured angle of friction. Constant velocity only occurred when the bed angle was equal to the dynamic angle of friction.

Other less conclusive results have been obtained during open channel experiments. Hungr/Morgenstern (1984) found for polystyrene beads an increase of the value of the friction angle with velocity occurred up to about 3 m/s, the value finishing in the region of that measured in a rotating drum experiment [Carrigy (1970): cited Hungr/Morgenstern (1984)]. For further increases in velocity, only a very slight rate dependence could be observed, and although the data was much more scattered, the friction angle was around that measured in the rotating drum experiment.

Hungr/Morgenstern (1984) performed the same experiments on Ottawa sand, but substantial experimental scatter exceeding the estimated error limits was observed. No trend with velocity was observed and the friction angle generally less than that measured in rotating drum experiments. These authors could not explain the degree of scatter, but presumed that the friction angle and also the density of the flow could be, to a certain extent, random in flowing sand although not in the more regularly shaped beads. The angle of friction from tests performed on an angular sand and a sand/rock flour showed scatter and a lack of trend with velocity, similar to the results of the Ottawa sand.

Hungr/Morgenstern (1984) also noted that very thin flows (< 30 mm) of dry granular fluids tended to decelerate at bed angles considerably above the angle of friction. This was also observed by Savage [(1979): cited Savage/Hutter (1989)]

and Bailard [(1978): cited Bailard/Inman (1979)]. Savage/Hutter (1989) noted that in small-scale laboratory tests using small particles, air drag effects may become significant, restraining the particles when vigorous saltation and a low-density cloud of particles are present at the flow's surface. This can give rise to a rate-dependence that is not likely to be present in geophysical-scale field events. These authors also noted that the range of bed angles that permit non-accelerating flows may also depend on the particular granular material, for example, the range for polystyrene beads was about 10 degrees.

Finally, for the flow of sand and water, the equilibrium slope (or bed slope where no deposition or erosion of grains occurred) for uniform flow was dependent on the solid volume concentration, the submerged weight of the solid particles within the flow, but independent of the flow rate [Winterwerp et al (1990)]. These experimental equilibrium slopes compared well with theoretical predictions, using the dynamic stress ratio (equation 2.14) and the momentum equation, when the angle of friction was set equal to the angle of repose [Winterwerp et al (1990)].

2.73 FLUID TURBULENCE

Bagnold (1956) stated that the total load of grains transported by the fluid may consist of bed load and suspended load during turbulent flow. The bed load was defined as that part of the load whose normal immersed weight component was in normal equilibrium with the grain stress, P . This stress was transmitted downwards via the dispersed grains to the stationary grains of the bed. The suspended load was defined as that part of the load whose immersed weight component was in equilibrium with a normal fluid stress originating in impulses by turbulent eddies. This stress was supposed to be transmitted not to the bed grains, but between them as an excess static fluid pressure. Neither the absolute nor the relative

distributions of the two load elements above the bed are known.

For analysis of a sand and water mixture during turbulent flow, Winterwerp et al (1990) ignored the grains transported as bed load and stated that the grains were entirely supported by the turbulent water movements. During steady flow, it was proposed a balance existed between the effects of settling of grains and the damping of turbulent exchange. This could be described by:

$$W_s C + \epsilon_{z,a} \frac{\partial C}{\partial z} = 0 \quad (2.15)$$

W_s = settling velocity of the grains

$\epsilon_{z,a}$ = apparent vertical diffusivity, affected by turbulence damping

At high concentrations, the settling velocity of the grains was strongly affected by interference with neighbouring grains. This was called hindered settling [Winterwerp et al (1990)]. This resulted in a decrease in the settling velocity, which could be described by the formula of Richardson/Zaki [(1965): cited Winterwerp et al (1990)], approximated by

$$W_s = W_{s0} (1 - C)^m \quad (2.16)$$

W_{s0} = settling velocity of a single grain in still water

m = exponent that is a function of the Reynolds number

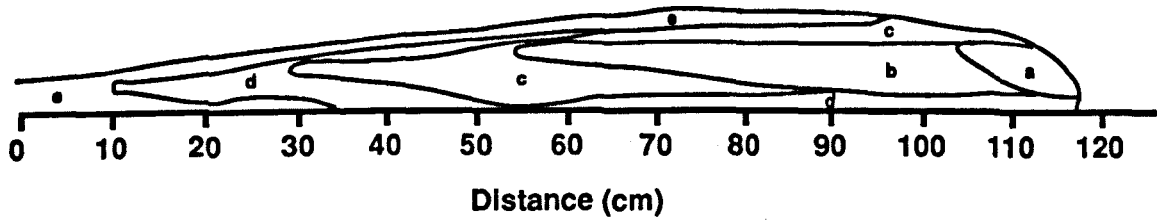
Winterwerp et al (1990) found that $m = 4$ (for grains where $120 \text{ microns} < D_{50} < 300 \text{ microns}$) and showed that the solid volume concentration profiles could be reasonably predicted with the 'well known' Rouse distribution (based on equation

2.15). Deviations from the expected and computed profiles were due to deviation of the apparent von Karman constant from its clear water value and assumptions concerning the profile of the experimental sand and water mixture. Experimental results showed that the apparent von Karman constant first decreased then increased from its clear water value with increasing concentration [Winterwerp et al (1990)].

Bagnold (1955) found that as the mean solid volume concentration was increased, the grains became uniformly dispersed from the bed up to a clearly defined level below the water surface at a solid volume concentration of about 0.3. The results of Winterwerp et al (1990) showed the sand grains ($D_{50} = 120$ microns) to be uniformly dispersed at a mean solid volume concentration of 0.4. Bagnold (1955) found that once a uniform dispersion had been attained, the mean solid volume concentration could be increased up to a mobile limit of about $C = 0.5$, with no change in the uniformity of the vertical solid volume concentration distribution.

Winterwerp et al (1990) found that an increase in the mean solid volume concentration from 0.1 to 0.3 did not affect the concentration near the bed, which was about 0.35 and 0.4 for the sands used ($D_{50} = 120$ and 225 microns, respectively). It was postulated that the concentration should have been even higher at the bed. Davies (1988) observed consistently low volume concentrations in the vicinity of the bed for a granular fluid wave (fig 2.12). A 'core' of higher volume concentration existed at mid-depth, decreasing from the head to the tail of the wave and a low concentration was present at the flow surface. Davies (1988) acknowledged that the volume concentration measured at the channel wall may not be representative of the interior of the flow because of the tendency of the cylindrical grains in contact with the wall to align themselves with their major axis either parallel or perpendicular to the wall. The low concentration observed at the bed by Davies (1988) was in contrast to the results of Winterwerp et al (1990).

FIG 2.12 CONCENTRATION DISTRIBUTION IN A GRANULAR FLUID WAVE
[Davles (1988)]



Bed speed = 0.39 m/s
Bed slope = 12.5 degrees

Zone	Solid volume concentration
a	> 1.2 C'
b	1.1 - 1.2 C'
c	1.0 - 1.1 C'
d	0.9 - 1.0 C'
e	0.8 - 0.9 C'

C' = mean solid volume concentration

Therefore, the solid volume concentration at the bed may also be dependent on the frictional nature of the boundary and whether it is composed of fixed or movable grains.

In the open channel experiments conducted by Bagnold (1955), it was found that the turbulence within the flow was gradually suppressed as the concentration of the grains increased. At a mean volume concentration of 0.3, the turbulence appeared to be markedly weaker and at a mean volume concentration of 0.35, the turbulence had entirely disappeared and with it all signs of secondary circulation. Laminar flow of the grains then occurred. The suppression of turbulence was also confirmed by the moving bed open channel experiments conducted by Davies (1988). The pathlines of individual grains showed only weak or no perturbations (fig 2.13). This also indicated that turbulence was damped out by the viscosity of the grain fluid mixture. Even in cases where a grain underwent a major transverse excursion, the grain path rapidly became linear again. Despite the suppression of turbulence by the presence of the grains, Davies (1988) obtained vertical velocity profiles in the body of the granular fluid wave whose shape was typical of turbulent flow (fig 2.14). Bagnold (1955) and Winterwerp et al (1990) also obtained vertical velocity profiles that indicated logarithmic behaviour. Due to the suppression of turbulence, Bagnold (1955) stated that fluid turbulence clearly cannot be regarded as an essential requisite in grain transport by fluids. Winterwerp et al (1990) also noted that at high concentrations, dispersive grain pressures may become increasingly important, but this effect could not be quantified. Little is known about the relations and interactions between the various phenomena [Winterwerp et al (1990)].

FIG 2.13

GRAIN PATHLINES IN A GRANULAR FLUID WAVE
[Davies (1988)]

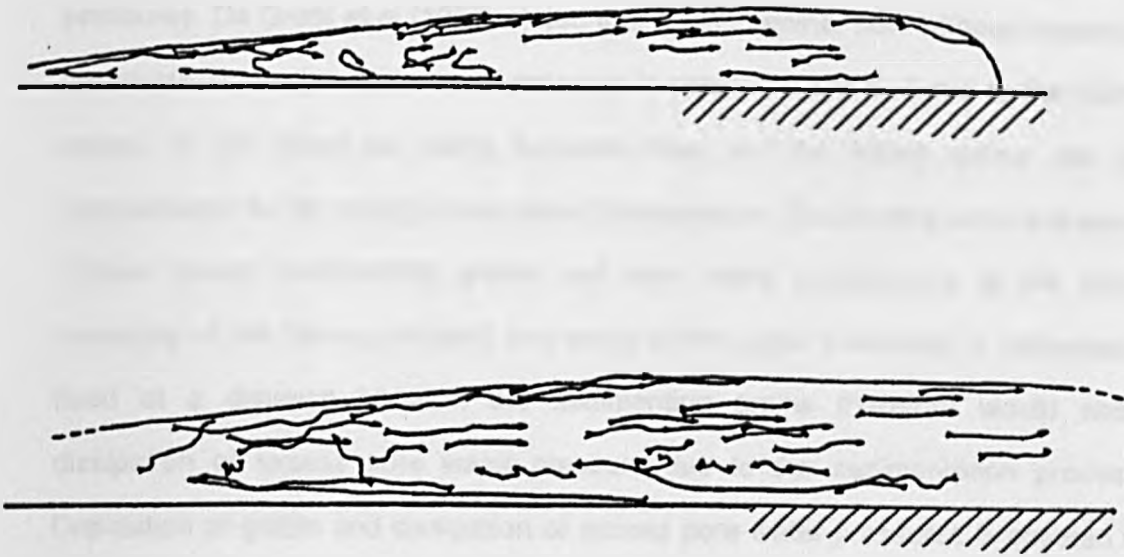
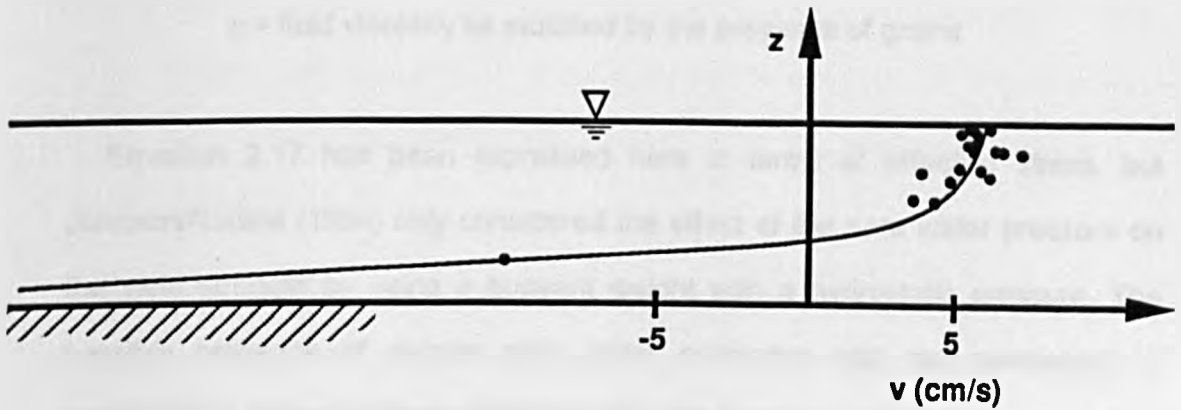


FIG 2.14

VERTICAL VELOCITY DISTRIBUTION IN THE BODY OF A
GRANULAR FLUID WAVE
[Davies (1988)]



2.74 LAMINAR FLOW WITHOUT DISPERSIVE PRESSURES

Silvis et al (1988) considered that the soil of a flowslide was changed into a heavy or thick liquid following liquefaction, due to the presence of excess pore pressures. De Groot et al (1987) stated that during laminar flow without dispersive pressures, an excess pore water pressure is present at the bed due to the falling grains, in the same as during turbulent flow, but the falling grains are not compensated for by mixing or any other phenomenon. The flowing sand and water mixture looses sedimenting grains and pore water continuously at the lower boundary of the flowing material and water at the upper boundary. A peizometer fixed at a distance beneath the sedimenting grains therefore would show dissipation of excess pore water pressure due to the sedimentation process. Deposition of grains and dissipation of excess pore water pressures is covered in section 2.85. De Groot et al (1987) gave no expression for the material's shear strength when laminar flow without dispersive pressures occurred. Debris flows have been analysed with the shear strength of flowing material described by the Coulomb-viscous model [Johnson/Rodine (1984)], where:

$$\tau = \sigma'_n \tan \phi + \eta \frac{dv}{dz} \quad (2.17)$$

η = fluid viscosity as modified by the presence of grains

Equation 2.17 has been expressed here in terms of effective stress, but Johnson/Rodine (1984) only considered the effect of the pore water pressure on the yield strength by using a buoyant weight with a hydrostatic pressure. The possible presence of excess pore water pressures was not mentioned. A simplification of the Coulomb-viscous model, the Bingham plastic fluid model, has also been used to describe the motion of debris flows [Johnson/Rodine (1984)]

and flowslides [Jeyapalan (1980)]:

$$\tau = \tau_B + \eta \frac{dv}{dz} \quad (2.18)$$

where τ_B = Bingham yield strength

The viscosity of the flowing material in Coulomb-viscous and the Bingham plastic fluid model is that of the interstitial fluid modified by the presence of the grains. Davies (1988) stated that this was a function of the solid volume concentration and the shear rate for the Bingham model.

Unfortunately, Jeyapalan (1980) calibrated his mathematical model for flowslides using oil, which is not a granular fluid. In addition, a rigid plug bounded laterally by shearing material is a characteristic of a Bingham plastic fluid. Support for the presence of a rigid plug was provided from observations of transverse surface velocity distributions [Johnson/Rodine (1984)]. These consisted of a uniform central region flowing at a constant velocity, bounded on each side by shearing material. Davies (1988) also observed that the grains at the surface of the flow body revealed no variation of grain velocity with position across the channel. The complete lack of variation in the transverse velocity distribution was due to the nature of his moving bed apparatus, as the mean flow velocity relative to the channel walls was zero. The complete lack of any cross channel variations in the surface layer gave the body the 'appearance' of a solid, non-shearing plug when viewed from above.

Despite the appearance of a rigid plug, Davies (1988) stated that in his experiments, adjacent grains in the 'plug' zone slid past each other, remaining in contact for substantial lengths of time (approximately 1 second). Iwamoto/Hirano [1981: cited Davies (1988)] also concluded that slow shear occurred throughout

the body region and no rigid plug was present. Davies (1988) therefore stated that the Bingham model is strictly inapplicable. In addition, the experimental vertical velocity distributions obtained by Davies (1988) showed that the whilst the upper part of the body had a relatively uniform velocity, slow shearing of grains here occurred (figs 2.11 and 2.14). A region of very high shear occurred at the base of the head and the body, in which the grain velocities relative to the bed increased rapidly (and decreased rapidly relative to the channel walls) with height above the bed. The measured velocity distributions (fig 2.14) showed this region to be deeper than was apparent to the eye and was about 5 to 6 grain diameters deep. Hanes/Inman (1985) suggested that the thickness of the shearing layer in ring shear experiments was governed by the weight of the grains, with larger thickness being observed for grains being sheared in water as compared to air.

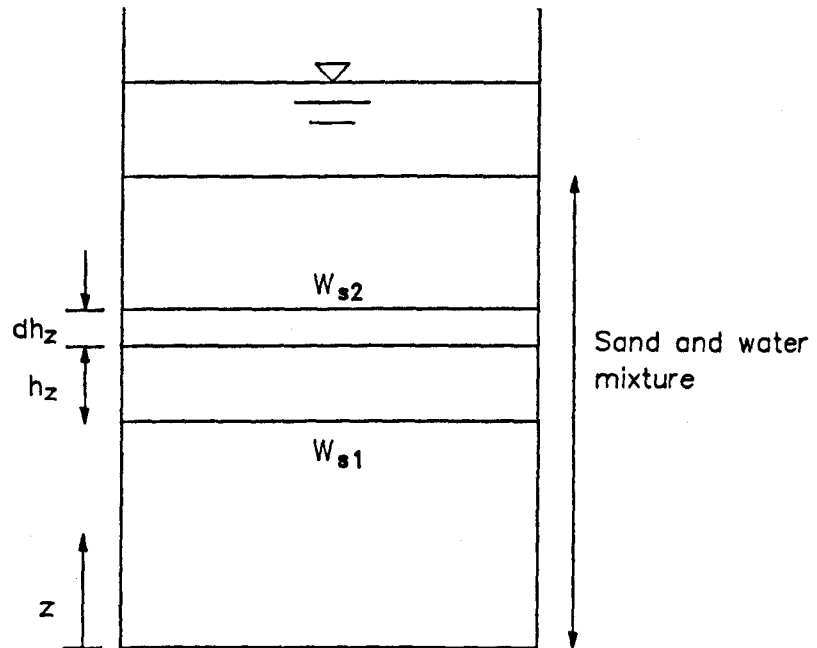
Bezuijen/Mastbergen (1988) conducted a series of experiments in which sub aqueous flowslides were observed. These authors suggested that sedimentation of a hyper-concentrated (high concentration) sand and water mixture in a flowslide is comparable with sedimentation of other sand and water mixtures. It was expected that no mixing of grains between the various layers occurred as only laminar type flow was observed. The resedimentation surface was expected to rise at a velocity, v_s , through the sand and water mixture, given by:

$$v_s = \frac{C}{C_{res} - C} W_s \quad (2.19)$$

C_{res} = resedimented concentration

W_s was calculated using equation 2.16, and the decrease in height, dh_s , of a thin layer of the sand and water mixture, h_s , (fig 2.15) could be described by:

FIG 2.15 DEFINITION SKETCH FOR RESEDIMENTATION NUMERICAL MODEL
[FROM BEZUIJEN/MASTBERGEN (1988)]



$$dh_z = -\frac{dW_s}{dz} h_z dt \quad (2.20)$$

If C was known as a function of z , then dW_s/dh_z could be calculated. The sand and water mixture was divided into N layers in the numerical scheme. Resedimentation occurred in the lowest layer. The model predicted that, during resedimentation, the major increase in concentration occurred at the transition between the sand and water mixture and the deposited sand. When the concentration was independent of depth (at high solid volume concentrations), it was predicted that no increase in concentration occurred except at the transition between the sand and water mixture and the bed during resedimentation or deposition. It was noted that the experimental decrease in porosity was not observed to be constant for different flowslides, but the maximum decrease was of the order of 3% [Bezuijen/Mastbergen (1988)]. The excess pore water pressure at the base of the flowing material was calculated using:

$$u = \sum_{i=n_i}^N (\rho_s - \rho_w) g h_z C_i \quad (2.21)$$

n_i = lowest not sedimented layer

N = total number of layers

As the z direction was taken as vertical, this analysis implies that the vertical effective stress at the base of the flowing material was zero. From measurements taken at the channel wall, Bezuijen/Mastbergen (1988) noted that the excess pore water pressure decreased linearly with height above the bed. It was found that the model over predicted the rate of resedimentation and dissipation of excess pore water pressures obtained during laboratory experiments. Improved accuracy was obtained when the reduced fall velocity, W_s , was calculated considering the

permeability, k , of the sand [Mastbergen/Bezuijen (1988): cited Bezuijen/Mastbergen (1988)]:

$$W_s = kC(G_s - 1) \quad (2.22)$$

In a similar way to hindered settling, Heidari/James (1982) proposed that the velocity of a compaction front travelling up through a static column of liquefied sand provided an explanation for the dissipation of excess pore water pressures. The velocity was assumed to be constant and dependent on the permeability, buoyant weight of the material, and initial and final porosities. Despite some experimental scatter, good agreement was obtained for the velocity of the compaction front and dissipation of excess pore water pressures.

Other alternative behaviour has been proposed. Hutchinson (1986) suggested that the flowslide debris would move by basal sliding, under the influence of the excess pore water pressures generated from undrained loading during failure. It was proposed that, during motion, the material would consolidate by single upward drainage, in accordance with 1-D consolidation theory for static soils. As a result, the pore pressure at the base of a flow element eventually decays to a value that brings the element to rest.

2.75 FLOW CLASSIFICATION

It was noted that the shear strength due to dispersive pressures in the macroviscous zone was similar to the Coulomb-viscous and Bingham models, but no yield strength term was present in the former. This may mean that a clear subdivision of laminar flow without dispersive pressures in granular fluids [De Groot et al (1987)] may not be correct. It may also not be possible to consider fluid

turbulence in isolation from dispersive pressures, as it has been shown that turbulence is modified by the presence of grains.

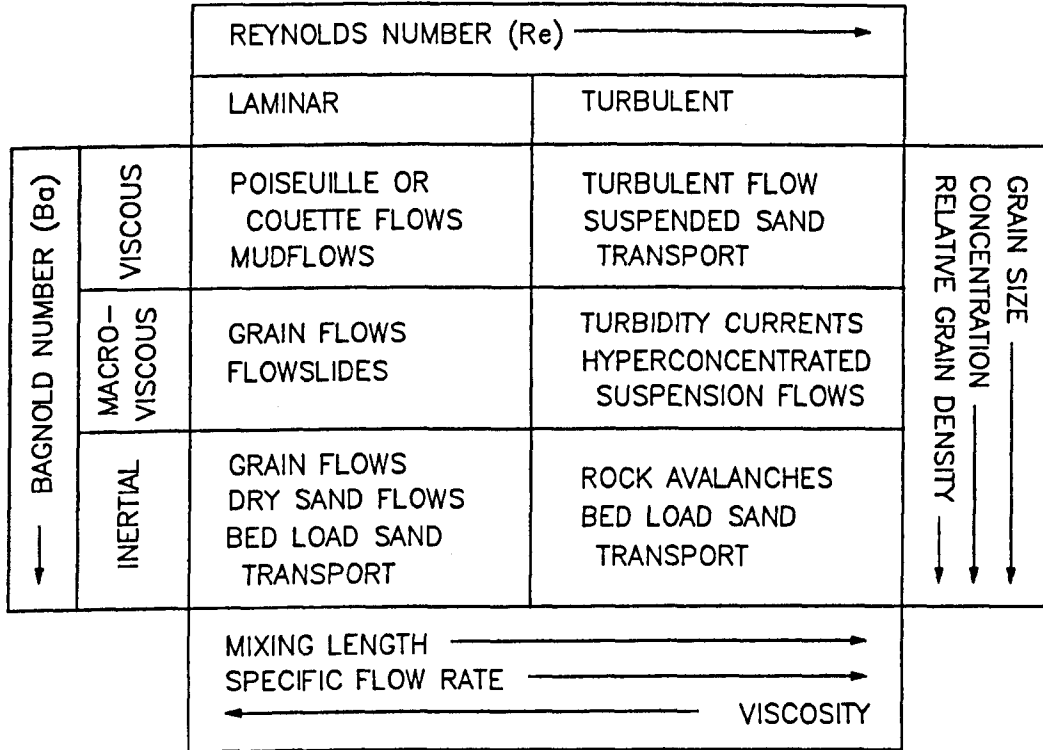
Mastbergen et al (1988) suggested that the *shear strength of a flowslide* was the sum of viscous, turbulent and inertial components. Which of these terms is dominant during flow can be determined using a Reynold's number (ratio of the turbulent to the viscous shear stress), which can be approximated by the ratio of the specific mixture flow rate (volume discharge of sand and water mixture per unit width) to the viscosity of the mixture, and the Bagnold number. Mastbergen et al (1988) provided a classification matrix into which all granular fluids could be located (fig 2.16).

De Groot et al (1987) also expected turbulent flow to occur if the viscosity of the sand and water mixture, as caused by water viscosity and grain collisions, was small compared to the product of velocity and layer thickness. Winterwerp et al (1990) stated that at full scale, the flow of a hyperconcentrated sand and water mixture was turbulent and turbulence was the dominant agent, whilst flow in a small laboratory flume was laminar and the grains supported by dispersive pressures. Laminar effects were also expected to become important for sand and water mixture flows at a solid volume concentration of 0.3 if the specific flow rate was less than or equal to $0.01 \text{ m}^2/\text{s}$ [De Groot et al (1988)]. The model scale effects of laboratory flowslides have not been fully determined.

Davies (1988) also suggested that the flow was assumed to be laminar or turbulent depending on whether the Reynold's number (Newtonian fluid) was less than or greater than 500. The flow was also expected to be Newtonian or non-Newtonian depending on whether the fine grains' (< 1 mm) solid volume concentration was greater than or less than 0.3 and the linear grain concentration of coarse grains (> 60 mm) was less than or greater than 14 respectively. Coarse

FIG 2.16

CLASSIFICATION MATRIX OF GRANULAR FLUIDS
[FROM MASTBERGEN ET AL (1988)]



$$\text{Relative grain density} = \frac{(\text{grain density} - \text{interstitial fluid density})}{\text{interstitial fluid density}}$$

grains of this size would not be expected in the material retained by mine tailings' dams.

Despite the location of flowslide in the macroviscous zone (fig 2.16), De Groot et al (1987) suggested that the results of flowslides tests indicated that the flow was probably somewhere between one controlled by dispersive pressures and one involving excess pore water pressures.

2.8 CONCLUSIONS

During the motion of a granular fluid, several mechanisms of particle support have been identified. These include dispersive pressures, turbulence and excess pore water pressures. Very little is known about the interactions between the various phenomena. It has been established that excess pore water pressures are generated during the initiation of a flowslide. This causes a reduction in the shear strength of the material, but questions concerning the presence of excess pore water pressures in a flowing material and their significance with respect to the material's shear strength remain.

Davies (1988) criticised the concept of excess pore water pressures enabling flow to occur, by virtue of the reduction in shear strength, and stated that it was unrealistic. He questioned whether the legitimate principle of excess pore water dissipation that applies to a stationary slurry or soil can be applied to the flowing body of a granular fluid. His argument was based on the fact that the interconnections between voids in a stationary body will be small, and only allow slow excess pore water pressure dissipation. It was proposed that the voids in a shearing body of material, however, will be continuously changing in location and geometry as the solid grains move, thus enabling the excess pore water pressure

to dissipate in the order of seconds, or less. This criticism may be applicable to those authors who have applied static behaviour to a dynamic situation [Pierson (1981), Hutchinson (1986)], but it is not supported by measurements of excess pore water pressures that have been recorded from moving flowslides in the laboratory [Bezuijen/Mastbergen (1988), Eckersley (1990)]. It is not known whether the theory for consolidation of static soils or the motion of hindered settling or a compaction front can be legitimately applied to a moving flowslide where particles are in constant motion. Further investigation into the magnitude of pore water pressures during flowslide motion and its effect on the shear strength of the material is therefore justified.

Attempts at sophisticated analysis [eg Cannon/Savage (1988), Sousa/Voight (1991)] may be inappropriate at present due to the lack of experimental data with which to check analytical results. It was therefore proposed to expand the flowslide experimental data base by conducting a series of small scale laboratory flowslides. This would allow the physical behaviour of flowslides to be observed. In particular, the presence of excess pore water pressures during flowslide motion was to be investigated, in order to provide more insight into the importance of this parameter to the fundamental characteristics of flowslides. It was realised that *uncertainty exists concerning model scale effects, but this could not be avoided.*

CHAPTER 3:

PRELIMINARY EXPERIMENTS

3.1 INTRODUCTION

This laboratory investigation into flowslide motion began with selection of an appropriate test material and construction of the experimental apparatus. This apparatus was designed to allow preparation and failure of the test material. The objectives of the preliminary tests were qualitative study of the laboratory flowslides and assessment of the suitability of the experimental apparatus.

3.2 SELECTION OF THE TEST MATERIAL

A variety of materials have been used previously to represent the behaviour of flowslides. Some of these have not been of a granular fluid nature. Oil, which is a Bingham plastic fluid, was used by Jeyapalan (1980). This fluid may possibly represent a flowslide during motion, but there is no similarity between liquefied tailings and oil in the mechanism whereby motion ceases. Oil is different in the respect that its resistance to shear is determined by its viscosity. Thus oil will continue to flow if the bed slope has only a slight gradient. It is not possible to bring flowing oil to a permanent halt, a phenomenon particular to flowslides and other granular materials. Bentonite has also been used during model investigations into landslides and debris flows [Hsu (1975), Johnson/Rodine (1984)]. Unfortunately, the thixotropic behaviour of bentonite is affected by

chemical bonding between the clay particles. No such bonding occurs during the flow of tailings with sand sized particles. The mechanics of flow are different and the usefulness of bentonite as a predictive tool would be limited. It was felt that these fluids could not accurately represent flowslides due to their inherently different material properties. A material that was present in field flowslide events was therefore chosen to avoid this uncertainty.

Tailings' dams contain both solid particles and water. The chemical nature of the latter may vary according to the mined ore and the mineral extraction process. In these laboratory tests, the pore fluid was tap water. The possible influence of the mill effluent's chemical nature on flowslide mobility was beyond the scope of this research project.

The particle size of material retained by tailings' dams may vary from coarse to medium sands down to silts or clays, but it is often found to be in the fine sand category (section 2.1). The particle size distribution may also vary from uniformly graded to well graded. As the choice of particle size to be used during the preliminary experiments was large, the material was selected in order to maximise the probability of being able to create and sustain a laboratory flowslide.

The presence and dissipation of excess pore water pressures have been established as possible controlling factors in flowslide mobility; the faster excess pore water pressures are dissipated, the less mobile the flowslide. Dissipation of excess pore water pressures in a static material is inhibited by a decrease in the permeability of the material. As permeability decreases with decrease in particle size, a very fine sand was selected [Leighton Buzzard sand, < 90 μm]. The use of finer material was precluded due to the potential influence of electrostatic forces between particles and problems associated with test sample preparation with material of a silty or clayey nature.

Tests were performed according to B.S. 1377: 1975 to determine the specific gravity and the particle size distribution. The sand had a specific gravity, $G_s = 2.71$, and was uniformly graded with $D_{50} = 80 \mu\text{m}$ and $D_{10} = 50 \mu\text{m}$ (fig 3.1). The material's angle of repose was determined by pouring a known mass of oven dried sand into one end of a small perspex container. Some experimental error in measurement of the void ratio may exist as it was assumed that the void ratio was constant throughout the sample and the shape of the sand poured into the container formed a perfect triangular based prism. The results obtained were as follows:

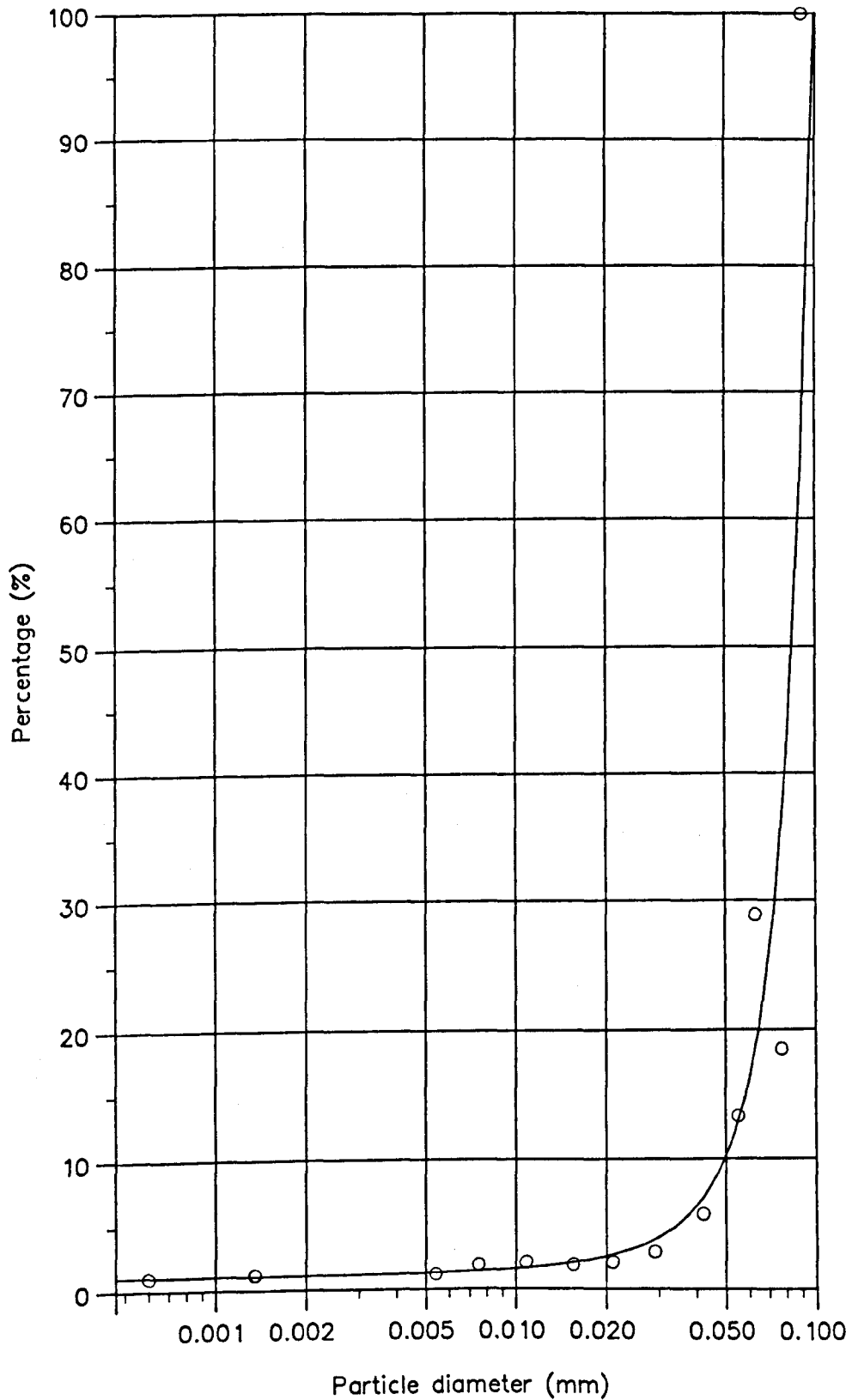
TABLE 3.1: Test material's angle of repose

Leighton Buzzard sand ($< 90 \mu\text{m}$)	mean value (degrees)	void ratio
mean value	33.37	1.07
σ_{n-1} (sample size = 6)	0.27	0.0210

3.3 EXPERIMENTAL APPARATUS

Although a field flowslide event will involve motion in three dimensions, knowledge of the propagation of liquefaction, failure mechanisms and flowslide behaviour is not yet sufficiently advanced for two dimensional analysis of failure. Therefore, the influence of three dimensional phenomena, such as dam breach characteristics and lateral spreading, cannot be considered at present. The study of flowslide motion was therefore restricted to two dimensions. It was hoped that

FIG 3.1 PARTICLE SIZE DISTRIBUTION CURVE OF LABORATORY TEST MATERIAL
(Leighton Buzzard sand < 90 microns, tested to B.S. 1377:1975)



this type of movement could be achieved by making the perspex channel width narrow (0.1 m) with respect to its overall length (2 m), and by making the channel of uniform width over its entire length. It was anticipated that this would enable the internal motion of the particles to be viewed at the channel wall. This would not be possible if lateral spreading was allowed or if the flowslide created its own boundaries of static material (section 2.7). The width of the channel was several orders of magnitude greater than the test material's D_{50} particle size, in order to minimise the potential effect of side friction on the forward motion of the laboratory flowslide.

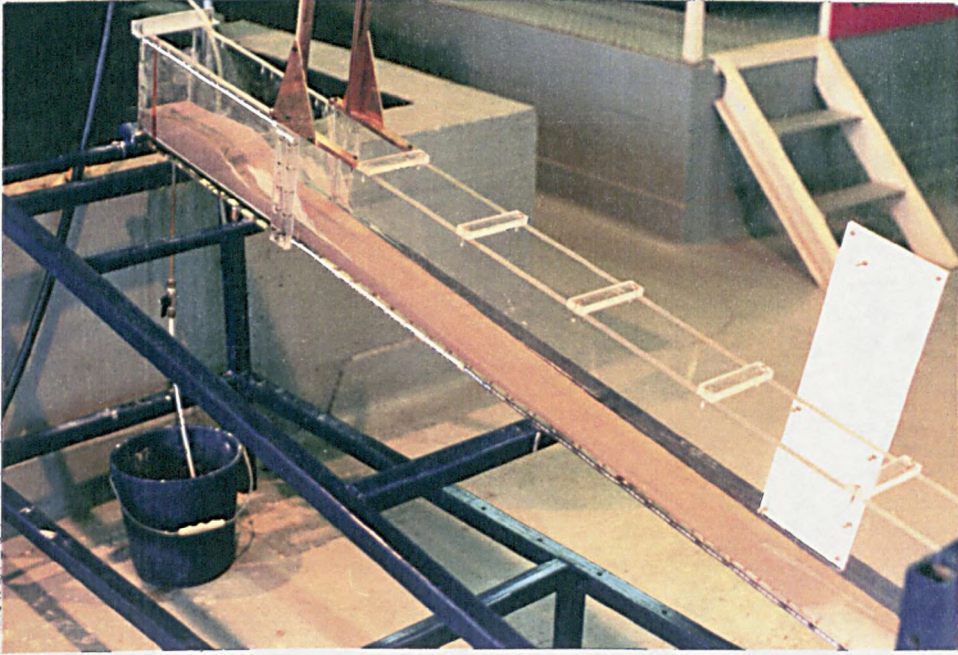
The 0.5 m channel section upstream of the sluice gate site, referred to hereafter as the upstream section, was designed to enable preparation of the test sample. The 1.5 m length of channel downstream of the sluice gate site allowed unimpeded movement of a flowslide. The channel was constructed in such a way so that it could be lengthened in both the upstream and downstream directions, if the results of the preliminary tests indicated that this was necessary. A general view of the perspex channel is shown (fig 3.2).

A review of flowslide field data indicated that the majority of events have occurred over bed slopes ranging from 0° [eg Gypsum tailings dam, S.E.Texas: Kleiner (1976)] to 12° [Colliery spoil tip No 7, Aberfan 1966: Bishop (1973)]. The perspex channel was therefore supported by a frame, the upstream end of which pivoted on a base frame, whilst the downstream end could be positioned by hand and bolted to the base frame to give a range of slopes from 0° to 14° . Both the channel support frame and base frame were made from steel box sections (cross-section = 40×40 mm).

The sides and base of the channel were constructed entirely from clear perspex. A Panasonic VHS HQ NV-M5 video camera was used to assist visual

FIG 3.2

GENERAL VIEW OF PRELIMINARY APPARATUS



observation. Large sections of the flowslide event could be viewed to capture information regarding the failure of the test sample and the forward motion of the flowslide. The flow of the sand and water mixture at close range could also be recorded using the macro facility of the video camera. The advantage of filming the transient nature of the flowslide was that it gave a permanent record of the event that could be replayed, enabling features to be observed that might otherwise have been missed.

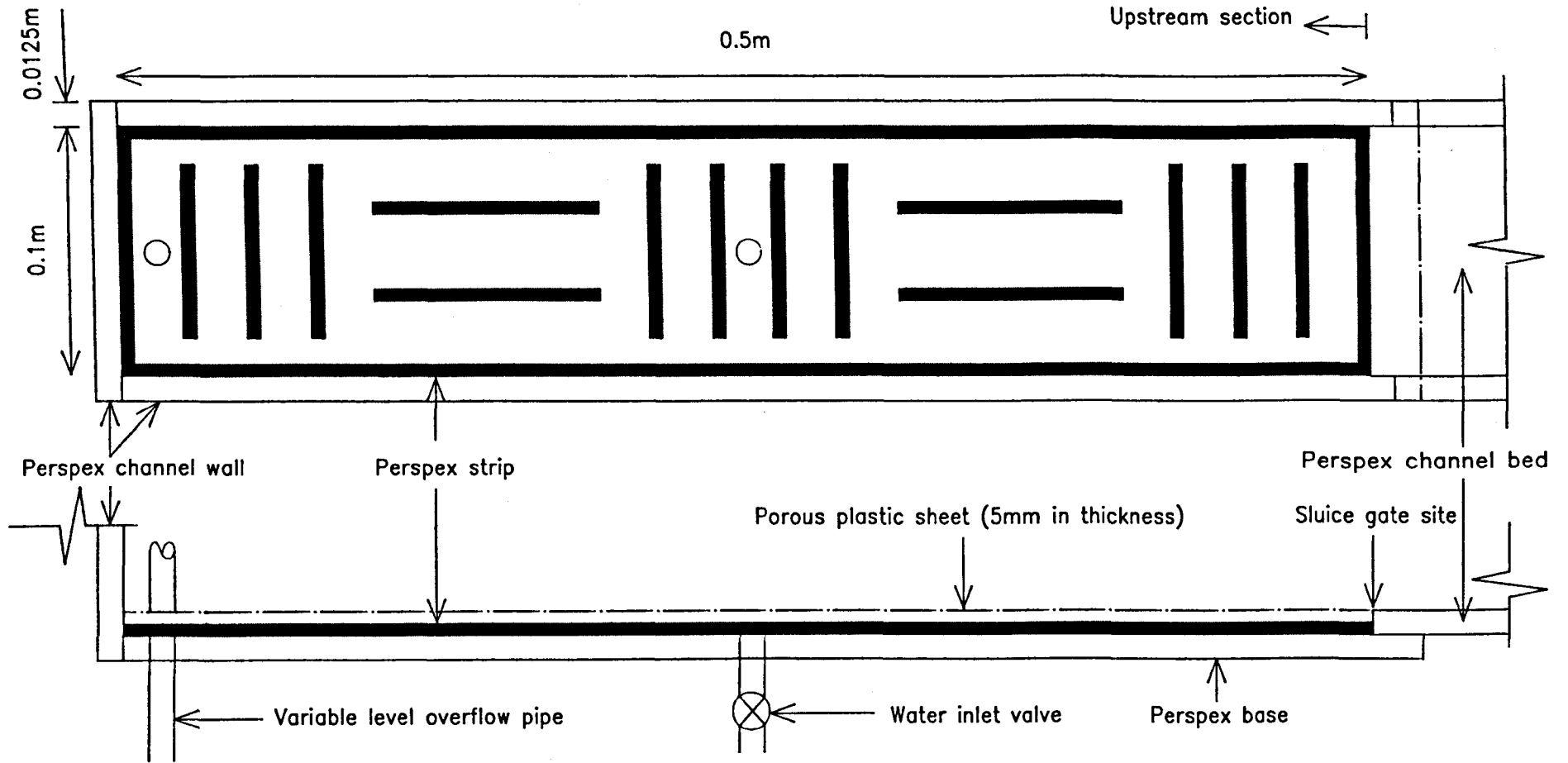
For liquefaction to be observed in the laboratory at the low stress levels associated with model testing at a small scale under atmospheric pressure, a soil sample should be prepared at the highest void ratio (or lowest bulk density) attainable so that contractive (strain softening) behaviour is achieved. Poulos (1981) stated that the initial structure of the sand is completely remoulded into a new flow structure at the steady state of deformation, therefore the method of preparing the initial structure of the test sample does not seem to be critical to flowslide behaviour.

To achieve a high initial void ratio, a known mass of sand was to be fluidised and then allowed to settle. A header tank, mounted on a length of steel box section (40*40 mm) bolted vertically to the side of the base frame, provided water from the mains' system to fluidise the sand. A constant head of water (about 2 m) was maintained using a variable level overflow within the tank. Water from the header tank was piped to an inlet valve at the base of the upstream section. A grid of perspex strips was mounted on the channel bed to support a porous plastic sheet (fig 3.3). The perspex strips allowed free movement of water from the centre of the channel underneath the porous plastic. An evenly distributed flow of water through the porous plastic into the upstream section of the channel was obtained. The porous plastic was fixed in position by a series of screws and the edges sealed against the inside of the channel with silicon sealer. The channel base in

FIG 3.3

SCHMATIC DIAGRAM SHOWING UPSTREAM SECTION OF CHANNEL;
DESIGNED FOR TEST SAMPLE PREPARATION

Plan view, with porous plastic sheet removed



Side elevation, with channel sidewalls removed

the upstream section was recessed so that the surface of the porous plastic was level with the channel bed of the downstream section. A sluice gate was used to retain the sand and water during test sample preparation and to initiate the flowslide. It was constructed from a brass sheet that was 2 mm thick and 0.23 m high, with the width being slightly narrower than that of the channel. It was sealed into position in the channel using a thin smear of silicon sealer. A variable level overflow of a constant section (internal diameter = 5 mm) was positioned at the rear of the upstream section to control the height of water. The fitting for the overflow contained a rubber O-ring seal to prevent leakage. The height of the channel's sides (0.2 m) allowed a variety of sand depths to be prepared.

3.4 RESULTS OF THE PRELIMINARY EXPERIMENTS

3.4.1 TEST SAMPLE PREPARATION

A known mass of dry sand was placed in the channel. The inlet valve from the header tank was opened and the sand fluidised for a sufficient time such that the height of the fluidised bed reached a constant value. This value was dictated by the head conditions upstream and downstream of the sand bed. The fluidised material was often stirred to ensure that no static material remained and to release any entrained air bubbles. The water inlet valve was closed and the sand allowed to settle to a static mass in the water. The overflow was carefully lowered to remove the surplus water that remained above the static sand mass. During this process, the disturbance to the sand sometimes resulted in a small amount of further settlement in the area of the overflow pipe.

When the fluidised sand was allowed to settle at a bed slope equal to 0

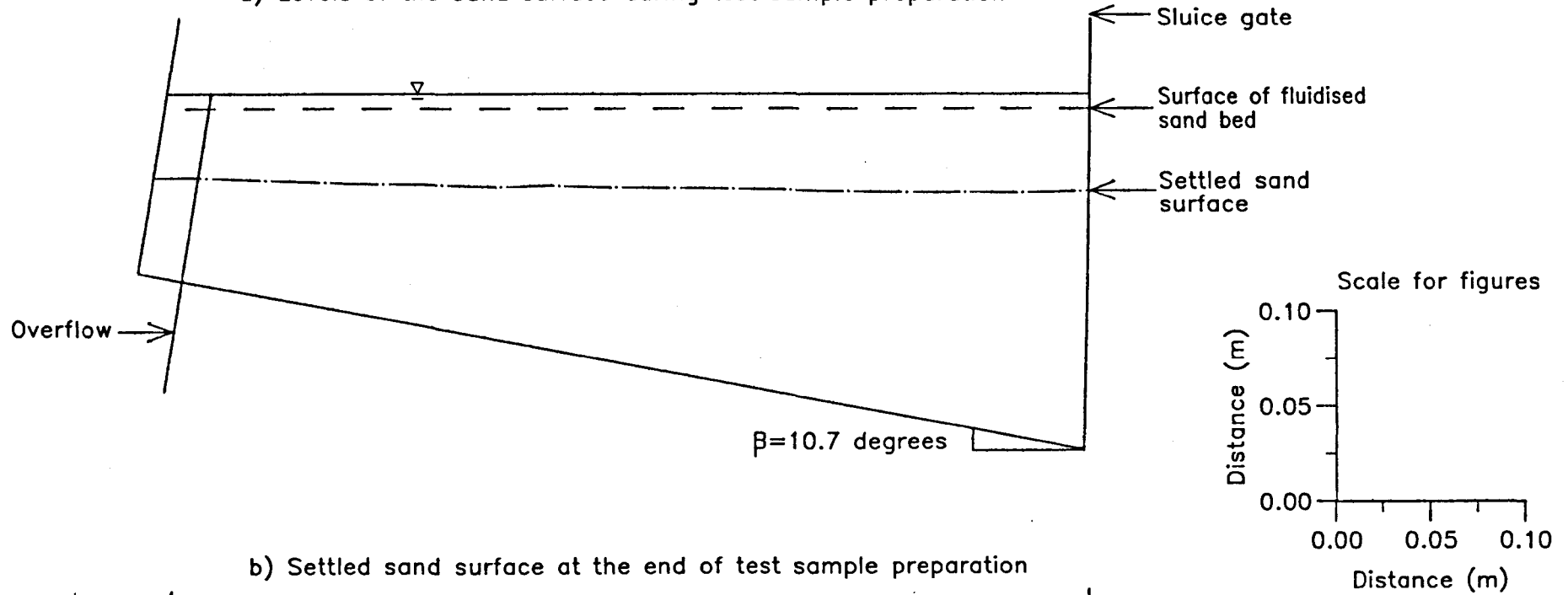
degrees, the surface of the settled sand was parallel to the bed. Any deviation from this was caused by the disturbance caused to the test sample when the overflow was lowered to remove the surplus water. When the test sample was prepared at a bed slope greater than 0 degrees, the surface of the fluidised sand bed was horizontal, but a greater depth of fluidised material was of course present at the downstream end [fig 3.4(a)]. It was assumed that the same degree of consolidation occurred throughout the sand during settlement, therefore, the greater depth at the downstream end resulted in a greater decrease in height. The surface of the settled sand therefore sloped towards the sluice gate, causing problems with removal of all the water above the sand through the overflow pipe. This was resolved by preparing the test sample at approximately 2 degrees (found by trial and error) above the bed slope at which the test was to be performed. After the sand had settled, the bed slope was then reduced to the bed slope at which the flowslide was to be initiated [fig 3.4(b)]. A flat sand surface, or a small negative surface slope, was then obtained. This method proved satisfactory and the surplus water could be easily removed. A variety of different experimental procedures were examined to determine which method enabled the lowest density to be obtained. It was found that the optimum procedure was to allow the sand to settle completely before any surplus water was removed.

The configuration of a tailings' dam in the field consists of a sloping downstream face with an upstream area of a very low slope (for example 0.5 degrees). Efforts were made initially to reproduce both these features in the test sample. This could be accomplished by sealing the sluice gate in the channel at an angle and preparing the test sample at a higher angle than that at which the flowslide test was to be performed. This method of angling the downstream face was abandoned, due to difficulty in removing the sluice gate, and subsequently the sluice gate was positioned vertically irrespective of the channel bed slope.

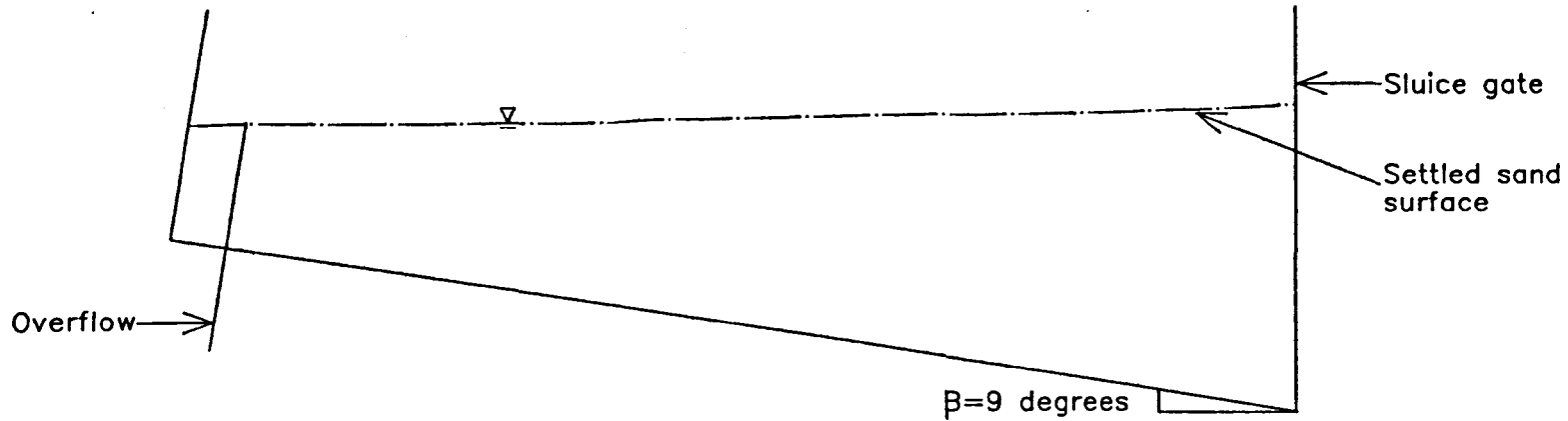
FIG 3.4

SIDE ELEVATIONS OF CHANNEL SHOWING PREPARATION OF TEST SAMPLE

a) Levels of the sand surface during test sample preparation



b) Settled sand surface at the end of test sample preparation



The saturated bulk density of the test sample was calculated in the following way. The mass of sand (M_s) was determined by weighing the dry sand used for sample preparation and subtracting from this any sand mass that was lost down the overflow pipe during the sample preparation procedure. The volume of solid grains (V_s) could then be calculated:

$$\rho_g = G_s \rho_w \quad (3.1)$$

$$V_s = \frac{M_s}{\rho_g} \quad (3.2)$$

ρ_g = density of solid grains

ρ_w = density of water = 1000 kg/m³

The total volume of the settled test sample (V) was calculated by first marking the height of the settled sand on the channel wall at 50 mm longitudinal intervals. These data were used to determine the surface slope of the settled sand. After the flowslide test, when the laboratory channel had been cleaned, the channel was set to this angle and the sluice gate was reinserted in the same position. The volume of water required to fill the upstream section of the channel to the marked level was determined using measuring cylinders. The surface slope of the settled sand was usually greater at the upstream end of the channel. This additional volume was calculated and added to the measured water volume. It was estimated that the total volume could be measured with an accuracy of at least +/-15 ml of water. The saturated bulk density (ρ_{sat}) could now be calculated:

$$\begin{aligned} \rho_{sat} &= \rho_w(1-C) + \rho_g C \\ &= \rho_w [1 + C(G_s - 1)] \end{aligned} \quad (3.3)$$

The ability to achieve the same initial saturated bulk density of the test sample was important in connection with obtaining repeatable experimental conditions. It was noticed that some silt was lost down the channel overflow during the flowslide sample preparation procedure. Repetition of the test to determine the particle size distribution on a sample of the sand that had been used for 20 tests revealed that only 13.2% of the particles passed the 63 μm sieve size, compared to 20% for a soil sample that had not been used for flowslide tests. The specific gravity of the sand was unaltered. The effect of silt content loss on the ease of obtaining a low density was also to be determined.

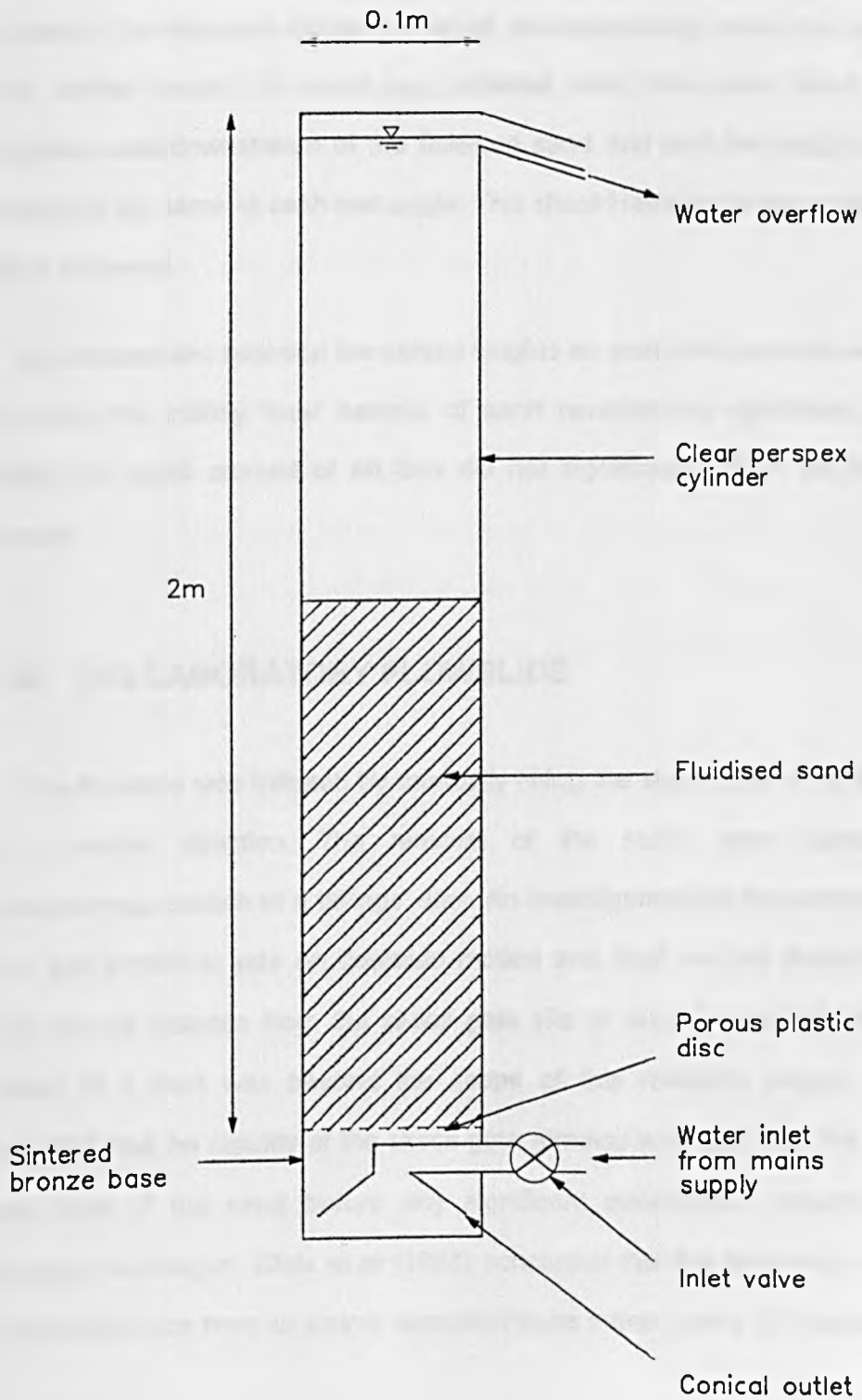
As the vertical dimensions of the laboratory channel were small, experimental investigations of this phenomenon were performed in a completely separate fluidisation system that incorporated a 2 m high perspex cylinder of 0.1 m diameter (fig 3.5). In the channel's fluidisation system, the height to which the fluidised sand was raised was approximately 1.3 times greater than the final settled height, whereas in the perspex cylinder, the fluidised sand was raised to a maximum of 3 times the final settled height. This improved the measurement accuracy with respect to comparison of the fluidised and final settled heights. The results of these separate fluidisation tests indicated that:

a) The fluidised sand bed height should be observed to be constant for a period of time (at least 10 minutes), otherwise the sand bed may not have reached its minimum density under the prevailing head conditions. Failure to do so may lead to a higher final density of the settled sand.

b) Once the sand had settled to its final height, which occurred in a relatively short period of time (eg 5 minutes), any further time period for settling (eg 30 minutes) did not lead to any further significant consolidation.

c) For a constant depth of water in the column, an increase in the height to

FIG 3.5 SCHEMATIC DIAGRAM OF APPARATUS USED FOR COLUMN OF SAND EXPERIMENTS



which the fluidised sand bed was raised decreased the final density of the settled sand. For example, when the sand bed was raised to 2 m the settled height was 0.842 m and when the sand bed was raised to 1.5 m the settled height was 0.836 m. It was assumed that the range of fluidised heights used in the upstream section of the flowslide apparatus would not significantly affect the value of the final settled height. To avoid any potential error, the water head conditions upstream and downstream of the fluidised sand bed and the height of the bed should be the same at each test angle. This should lead to the same initial density being achieved.

d) Comparisons between the settled heights as more and more silt was washed out from the initially 'new' sample of sand revealed no significant difference. Hence the small amount of silt loss did not significantly affect the test sample density.

3.42 THE LABORATORY FLOWSLIDE

The flowslide was initiated by manually lifting the sluice gate from the channel in a vertical direction. The removal of the sluice gate represented an instantaneous breach of a tailings' dam. An investigation into the effects of breach size and formation rate on flowslide motion and final run out distance (defined here as the distance from the sluice gate site or breach at which the flowslide comes to a halt) was beyond the scope of this research project. Video film indicated that the rapidity of the sluice gate removal was such that the sluice gate was clear of the sand before any significant downstream movement of the flowslide had begun. Silvis et al (1988) concluded that the behaviour of the sand at some distance from its source appeared to be independent of initiation method.

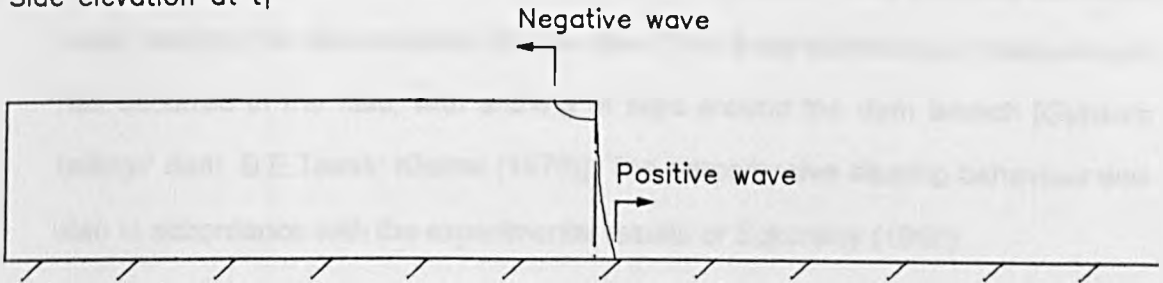
Experiments on the initial structure of sand whilst the sluice gate was still in position revealed that the sand could easily be liquefied by a dynamic shock, intentional or otherwise, to the side of the channel. Video film of the sand at the sluice gate site revealed that the sand immediately next to the sluice gate was pulled upwards to a small extent as the sluice was removed. Thus these laboratory flowslides were probably initiated by a combination of the shearing action on the vertical face of the sand sample by the sluice gate, the shock imparted to the channel as the sluice was removed and collapse of the sample as a result of the downstream face being left laterally unrestrained.

The top of this laterally unrestrained vertical wall of sand and water moved down under the influence of gravity. This caused a negative wave that travelled upstream into the material that had not yet failed (fig 3.6). Negative wave behaviour has also been noticed immediately after failure during the course of subaqueous flowslide experiments [Silvis et al (1988)]. The lower part of this vertical wall deformed and moved down the channel, becoming the leading edge of the flowslide (fig 3.6).

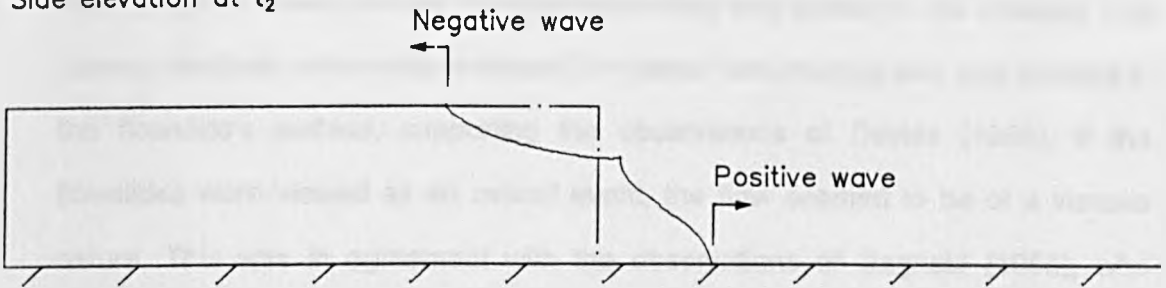
After a period of time, the negative wave ceased to travel backwards and further material then joined the flowslide by the progress of retrogressive non-circular slipping. The time of transition from negative wave behaviour to slipping and the conditions that influenced this were not identified, but the distance that the negative wave progressed into the upstream area increased with increase in channel bed slope. At high channel bed slopes (12-14 degrees), some tests were performed where all the material became involved in the flowslide as a result of the movement of the negative wave, with only one slip surface being formed as the last of the material joined the flowslide. In these cases, the flowslide moved at a high velocity (about 120 mm/s) down the channel. In addition, it was noticed in another test at a similar angle, the flowslide even became separated from its

FIG 3.6 SCHEMATIC DIAGRAM SHOWING THE FAILURE OF THE TEST SAMPLE AT VARIOUS TIME INTERVALS AFTER SLUICE GATE REMOVAL

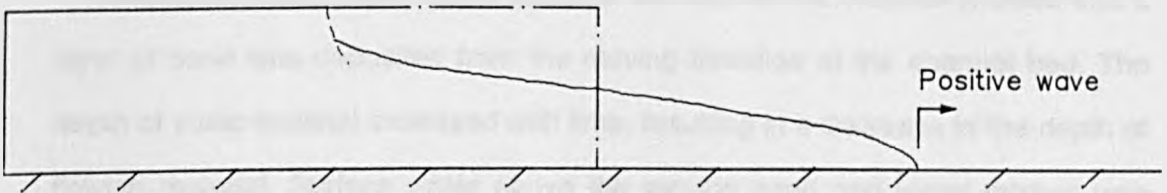
Side elevation at t_1



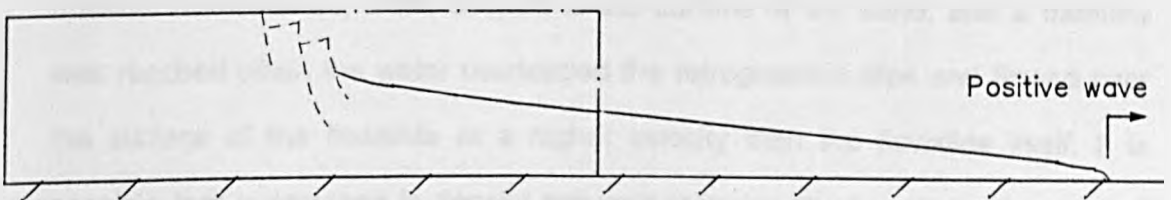
Side elevation at t_2



Side elevation at t_3 : end of negative wave behaviour, non-circular slip forming



Side elevation at t_4 : material joins flowslide through non-circular slips



————— Initial profile of test sample prior to sluice gate removal

- - - - - Non-circular slip surface

t = time, where $t_1 < t_2 < t_3 < t_4$

source material. The material from the non-circular slips was not in a rigid state as it joined the flowslide. The slips had a thickness varying between 4–8 mm. The retrogressive slip surfaces were three dimensional, with arching between the flume walls, making the slips concave in plan view. This three dimensional phenomenon has occurred in the field, with arching of slips around the dam breach [Gypsum tailings' dam, S.E.Texas: Kleiner (1976)]. The retrogressive slipping behaviour was also in accordance with the experimental results of Eckersley (1990).

Visual observation of the flowslide indicated fluid-like behaviour; the sand and water mixture flowed around any obstruction that was placed in the channel. The flowing sand and water mixture moved 'en masse' and no rigid plug was present at the flowslide's surface, supporting the observations of Davies (1988). If the flowslides were viewed as an overall event, the flow seemed to be of a viscous nature. This was in agreement with the observations of Bagnold (1956), who expected turbulence within a granular fluid to be suppressed by the presence of grains at high solid volume concentrations.

Visual and video observations made at the side of the channel showed that a layer of sand was deposited from the moving flowslide at the channel bed. The depth of static material increased with time, resulting in a decrease in the depth of flowing material. Surface water above the moving sand and water mixture was present at a later stage during flowslide motion. This seemed to be derived from material in the upstream area that was not involved in the flowslide. As this material consolidated, water seeped to the surface of the sand, and a moment was reached when the water overtopped the retrogressive slips and flowed over the surface of the flowslide at a higher velocity than the flowslide itself. It is possible that a decrease in density occurred following the transition of sand and water from a fluid to a static state as it was deposited at the channel bed, with the water expelled contributing to the volume of surface water. This surface water,

which was usually less than 1 mm in depth, moved some sand grains over the surface of flowslide through bed transport mechanisms and saltation, in a manner described by Bagnold (1956). The flow of surface water continued at a very slow rate after the flowslide had ceased moving, as the water seeped out of the static sand under the influence of gravity.

Some experiments were also performed where a small depth of water was left over the upstream area of the test sample, to simulate the pond water of a tailings' dam. This water flowed over the flowslide surface, in the manner described previously. This pond water only increased both the depth of water flowing over the flowslide and the uncertainty concerning the influence of bed transport mechanisms on grain movement at the flowslide's surface. This procedure was therefore not continued.

After all movement had ceased, a slight camber of the flowslide surface was visible (convex in plan view). This camber may have existed during flowslide motion, or may have been caused by erosion of sand from the continued slow flow of surface water along the channel walls after flowslide motion had ceased. A cambered nature of the flow surface was observed by Davies (1988) during granular fluid motion. At the sluice gate site in one flowslide test, the flowslide surface was concave in section after all motion had ceased.

The difference between the surface angle of the final settled flowslide, α , after all motion had ceased and the channel bed slope, β , was observed to increase with decrease in the channel bed slope. For example, when β was equal to 0 degrees, α was between 6 and 9 degrees, whereas α was sometimes equal or almost equal to the channel bed slope at higher values of β such as 12-14°.

3.43 LIMITATIONS OF THE PRELIMINARY APPARATUS

During the course of the preliminary experiments, it became apparent that certain components of the laboratory apparatus required modification. These have been listed below. Some parts required substantial alteration, and these modifications have been described in the following chapter, whilst others only required minor alterations and these have been covered here:

a) The stability of the base frame was not satisfactory as the welded construction of the base frame caused a slight distortion of the steel members, causing the frame to stand unevenly on the floor.

b) After the test sample had been prepared, the bed slope was decreased to the angle at which the flowslide was to be initiated. This involved lowering of the channel support frame by hand, followed by bolting it into position. This method was soon found to be unsatisfactory, as the jolting and vibration caused during this process often disturbed the sand, requiring the test sample preparation procedure to be repeated.

c) The design of the channel support frame was unsatisfactory, as the video equipment could not be placed close enough to the channel wall to make full use of the macro facility available.

d) It was found that the length of the channel in the upstream direction was sufficient for the progressive failure of the sample, but the downstream length of 1.5 m was not sufficient to allow full movement of the flowslide at bed slopes in excess of 9 degrees.

e) The diameter of the channel's overflow pipe was too narrow for adequate drainage of water during test sample preparation. The performance of the overflow

was improved by increasing the internal diameter of the overflow pipe from 5 mm to 12 mm.

f) The sluice gate design was sufficient for the purposes of the preliminary experiments, but sections of silicon sealer remained in the channel. A new method of sealing the sluice gate in the channel was therefore necessary to avoid this. The manual method of the sluice gate removal was also adequate, but mechanical removal of the sluice gate would ease the difficulty and improve the repeatability of this operation.

3.5 CONCLUSIONS

The observations of these laboratory flowslides were consistent with expected behaviour from reported field and laboratory data. The qualitative conclusions made on the test sample failure were drawn from visual and video film observation of the upstream area. The negative wave behaviour, the transition to retrogressive slipping, the rate of slipping and the conditions that affect these must influence the mass inflow rate to the flowslide. Possible variations in the time sequence of the failure mechanisms between flowslide tests will have an effect of the degree of repeatability of tests. If a complete investigation of a flowslide event is to be performed, attention should be paid to this area. Unfortunately, the lack of availability of instrumentation made this topic beyond the scope of this research project. The next step in the laboratory investigation was to modify the experimental apparatus and to provide instrumentation in order that flowslide motion could be studied in more detail.

CHAPTER 4:

DEVELOPMENT OF THE EXPERIMENTAL APPARATUS

4.1 PERSPEX CHANNEL

The downstream section of the perspex channel of the experimental apparatus was extended from 1.5 m to 3.5 m. This was achieved with the addition of two 1 m channel sections. The height of these sections was reduced to 0.1 m, but the width remained constant at 0.1 m. The channel sections were bolted together by means of flanged joints. This initial method resulted in increased resistance to flow at the junctions, causing a local variation in the final depth of static material at these points. This problem was solved by the use of 'plastic padding' at the flanged joints, which provided a smooth transition between the sections of the channel.

A new support beam for the perspex channel was designed to allow closer positioning of the video camera to the channel wall. This was constructed from two lengths of 40*40 mm steel box section to provide adequate stiffness against deflections. The two lengths were bolted together to avoid any distortion that might be caused by welding, which was a problem in the original design. The width of the support beam was no greater than that of the channel. The perspex channel was securely bolted to the channel support beam.

The base frame was structurally altered to accommodate the change in method

by which the new channel support beam was raised and lowered. The stability of the frame was increased by the addition of concrete blocks on two angle sections running the length of the base frame (fig 4.1). The channel support beam was pivoted near its centre point at the downstream end of the base frame (fig 4.1). A tapped bush was mounted at the upstream end of the channel support beam and threaded onto a screwed rod. The lower end of the screwed rod was machined smooth and supported by a bush bolted to the base frame (figs 4.1 & 4.2). This allowed rotation of the channel in a vertical plane that was coincident with its longitudinal axis. The upper end was also machined smooth and inserted into a bush bolted to the screwed rod frame (fig 4.2). The purpose of the latter was to prevent lateral movement of the upstream end of the channel. The lower ends of this frame were pinned to the base frame. A change in bed slope was achieved by rotation of a wheel firmly bolted to the top of the screwed rod.

The change in bed slope was monitored using a wooden metre rule and a brass pointer mounted at the centre of the bush on the channel support beam. This pointer reached across the front of the rule and allowed direct observation of the scale value (fig 4.2). The base of the rule was pinned at the centre line of the lower bush. The upper end was attached using a collar to the smooth upper end of the screwed rod (below the screwed rod frame). This arrangement meant that the rule was always fixed in the same position with respect to the screwed rod.

In order to calculate the bed slope from the scale value, this complicated arrangement was reduced to a single triangle (fig 4.1). The lengths AB and BC remained constant at all times and the bed slope could therefore be altered by changing the length AC. Calculation of the value of AC required for any bed slope between 0° and 13° enabled the channel to be set to any angle required within this range. This distance was set by recording the position of the pointer on the scale of the rule. The accuracy of measurement of this length and the repeatability in

FIG 4.1

SCHEMATIC DIAGRAM OF EXPERIMENTAL APPARATUS

(Screwed rod frame and sluice gate frame not shown)

Side elevation

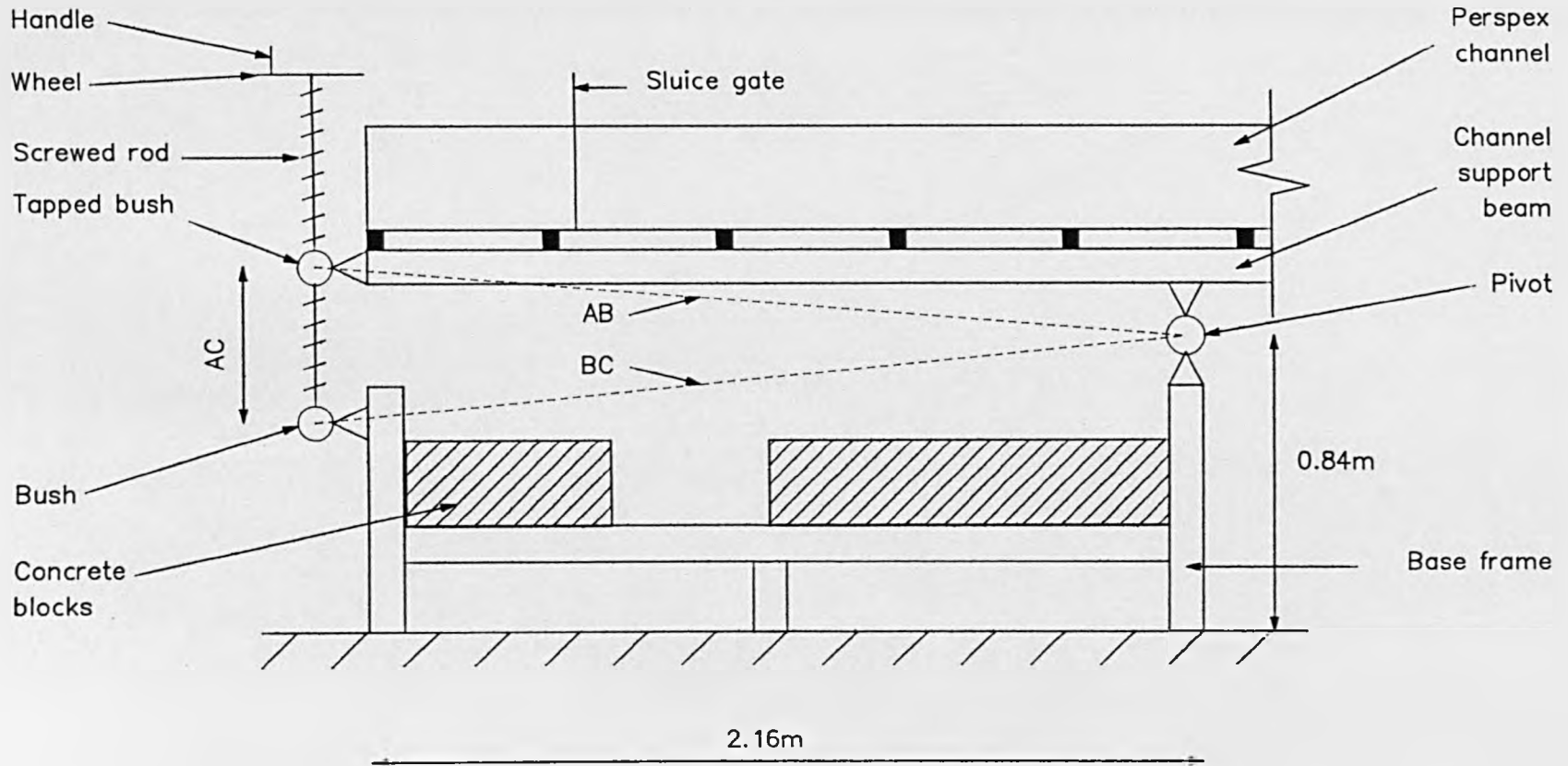
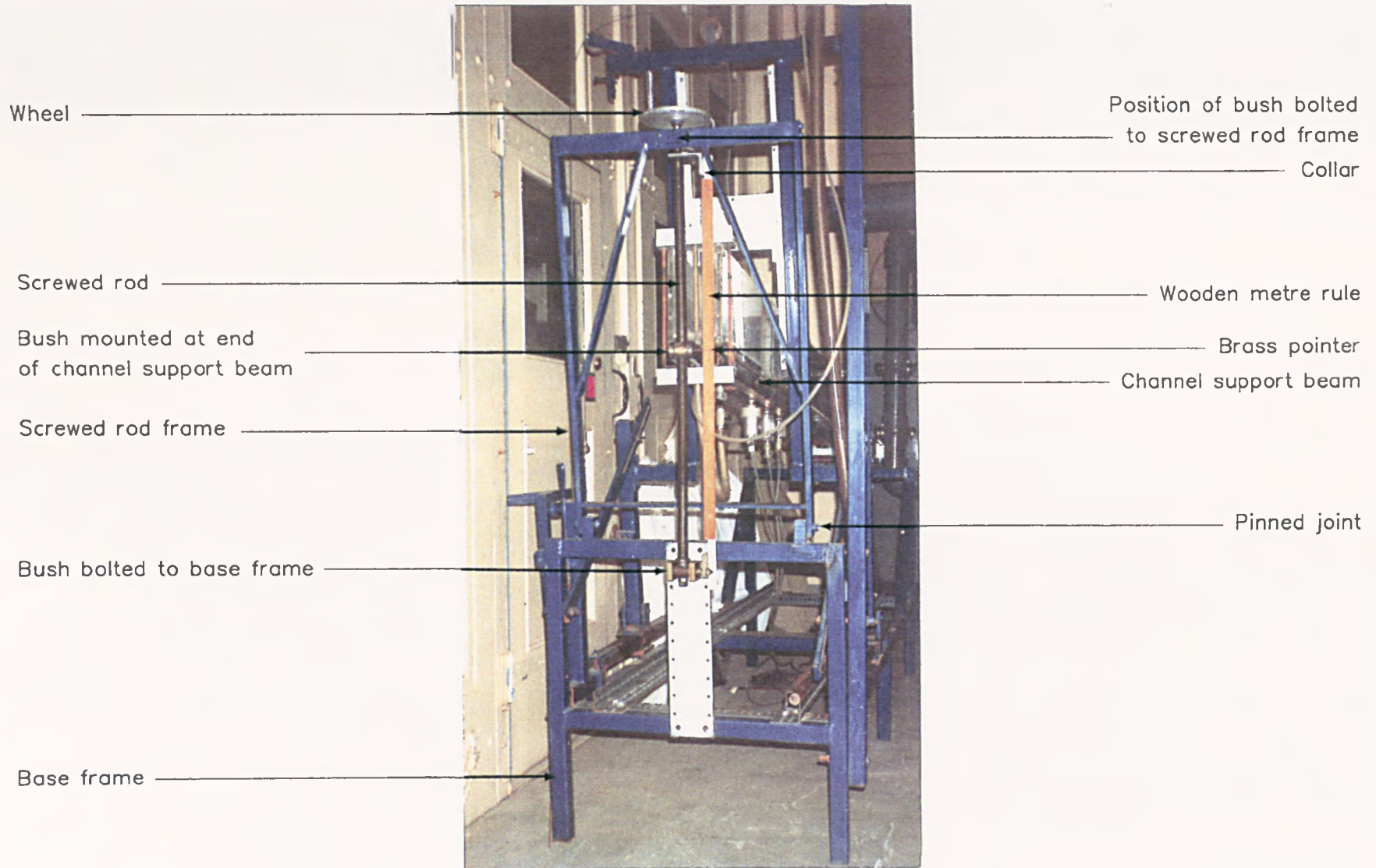


FIG 4.2

GENERAL VIEW OF RAISING AND LOWERING MECHANISM FOR LABORATORY CHANNEL



setting up the corresponding angle was improved by having the edge of the rotating wheel graduated in 30 divisions. A pointer mounted on the top of the wooden metre rule indicated the position of the wheel.

The channel bed was set horizontal using a steel rule and a level. The scale and wheel positions were noted. The scale lengths for all the other angles were taken from this datum point. Independent checks of each bed slope were made using the distances obtained with a level and staff positioned at various intervals along the channel bed. Due to irregularities in the perspex of the channel bed, the bed slope was estimated to be accurate within ± 0.15 degrees.

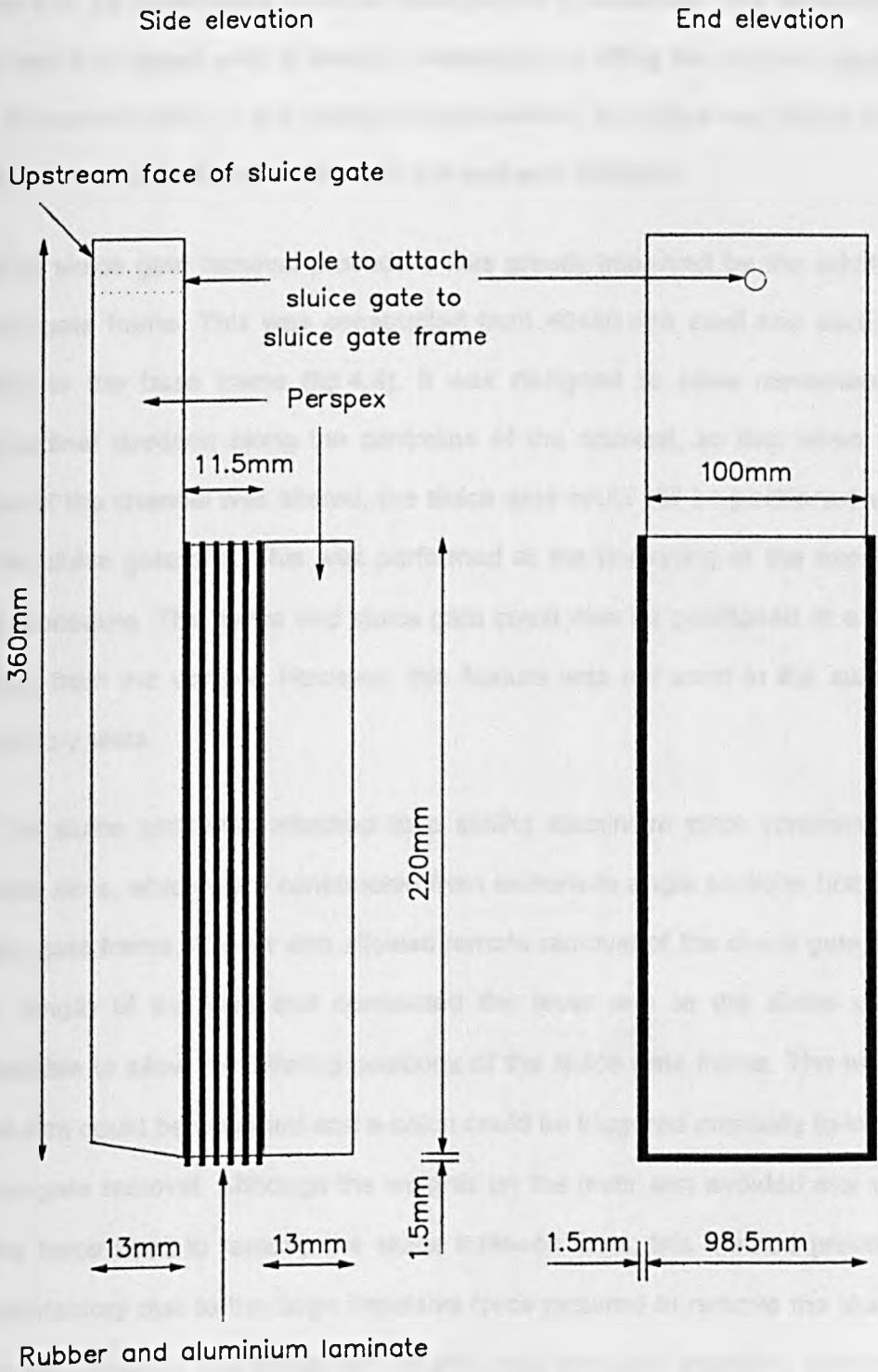
4.2 SLUICE GATE

A new sluice gate was designed (fig 4.3) which avoided the use of silicon sealer to provide a watertight seal. The width of the perspex of the sluice gate was 1.5 mm smaller than the internal dimensions of the channel. The bottom edge of the upstream section of perspex was sloped at a 12° angle (fig 4.3) to allow close contact with the channel floor when the bed slope was greater than 0° . To provide a watertight seal, a rubber and aluminium sheet laminate was clamped between the two sections of perspex.

The main difficulty in providing a watertight seal in a rectangular channel was in the corners. The presence of the laminate was found to be inadequate. The small amount of leakage observed was overcome by filling the spaces between the rubber sheets, provided by the aluminium sheeting, with silicon grease. The sluice gate was clamped in position in the channel using a G-clamp on the outside of the channel at the sluice gate site, before the test sample was prepared. This decreased the width of the channel slightly and provided a better seal.

FIG 4.3

SCHEMATIC DIAGRAM OF SLUICE GATE



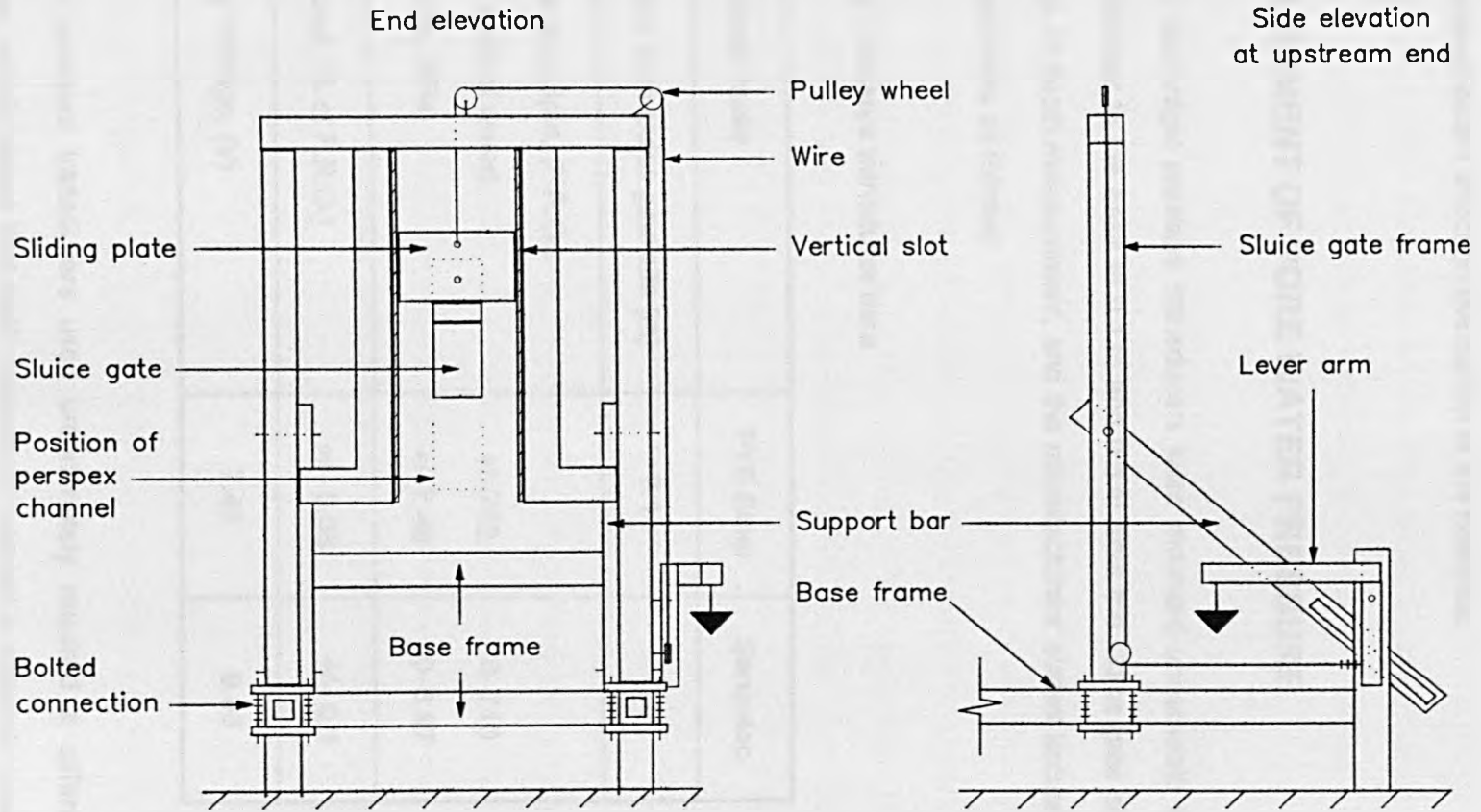
Immediately prior to initiation of the flowslide, the tension on the clamp was reduced slightly to facilitate sluice gate removal. The final sluice gate design proved to be satisfactory, with no leakage being observed. The effectiveness of the seal was tested prior to sample preparation by filling the channel upstream of the sluice with water. If any leakage was observed, the sluice was simply removed, regreased, replaced and tested until the seal was effective.

The sluice gate removal procedure was greatly improved by the addition of a sluice gate frame. This was constructed from 40*40 mm steel box sections and bolted to the base frame (fig 4.4). It was designed to allow movement in the longitudinal direction along the centreline of the channel, so that when the bed slope of the channel was altered, the sluice gate could still be positioned vertically at the sluice gate site. This was performed at the beginning of the experimental test procedure. The frame and sluice gate could also be positioned at a range of angles from the vertical. However, this feature was not used in the subsequent laboratory tests.

The sluice gate was attached to a sliding aluminium plate contained in two vertical slots, which were constructed from aluminium angle sections bolted to the sluice gate frame. A lever arm allowed remote removal of the sluice gate (fig 4.4). The length of the wire that connected the lever arm to the sluice gate was adjustable to allow for differing positions of the sluice gate frame. The end of the lever arm could be weighted and a catch could be triggered manually to initiate the sluice gate removal. Although the weights on the lever arm avoided any variation in the force used to remove the sluice between tests, this method proved to be unsatisfactory due to the large impulsive force required to remove the sluice gate from the channel. The movement of the lever arm was therefore performed by hand. Video film of the flowslide event at the sluice site during sluice removal indicated that hand operation of the lever arm was satisfactory. It is acknowledged

FIG 4.4

SCHEMATIC DIAGRAM OF SLUICE GATE FRAME



that this procedure varied slightly between tests, but the rapidity of the sluice gate removal meant that any slight variation in the hand operation of the device was likely to have an insignificant effect on the motion of the flowslide.

4.3 MEASUREMENT OF PORE WATER PRESSURE

Strain gauge diaphragm pressure transducers were mounted underneath the channel, perpendicular to the base at 0.1 m and 0.5 m from the sluice gate site. The make, range of depth measurement, and the manufacturers' stated accuracy of each transducer were as follows:

TABLE 4.1: Pressure transducer data

Transducer make	PYE Ether	Sensotec
Distance from sluice gate site (m)	0.1	0.5
Full range output, (F.R.O.):		
Head, (mm of water)	+/-762	0-710
Pressure, (kPa)	+/-7.48	0-6.97
Accuracy, (% of F.R.O.)	+/- 0.08	+/- 0.1
Supply Voltage, (V)	7.45	9.95

Each of the pressure transducers used unfortunately required a different excitation voltage, which meant that each transducer needed a separate power supply. Each power supply was tested for the stability of its voltage output .This

was performed over both short and long periods of time. The voltage output from a transducer was dependent on its excitation voltage. The stability of the voltage output of the supplies was therefore important, as any voltage drift would adversely affect the pressure transducer output. After much testing of available power supplies, two were selected whose voltage output remained constant over both long and short periods of time.

The initial voltage output of each power supply was set using a digital volt meter (DVM), which had been calibrated against a national reference standard. A slight difference in the values recorded by the DVM and the computer was observed. This was caused by the averaging of voltage values by the DVM, and also by the computer being slightly incorrectly calibrated. This was not a problem provided that the voltage output of the supplies was set to the same value each time with the same DVM prior to any calibration or flowslide testing. The voltage could not be set using the computer, as a continual slight variation in the monitor display made observation difficult.

As an additional precaution, the voltage outputs of the selected power supplies were monitored at the same rate as the voltage output from the pressure transducers during flowslide testing. This was to determine whether variations in the output of the pressure transducers could be correlated to possible variation in the voltage supply output. No correlation could be found as the supplies' voltage output remained constant. For example, the following results were obtained during the course of Test 12S:

TABLE 4.2: Stability of transducers' power supplies

Make of transducer:	PYE Ether	Sensotec
DVM voltage, (V):	7.450	9.950
Mean computer voltage, (V):	7.4482	9.9497
Standard deviation (σ_{n-1}):	0.00127	0.00174

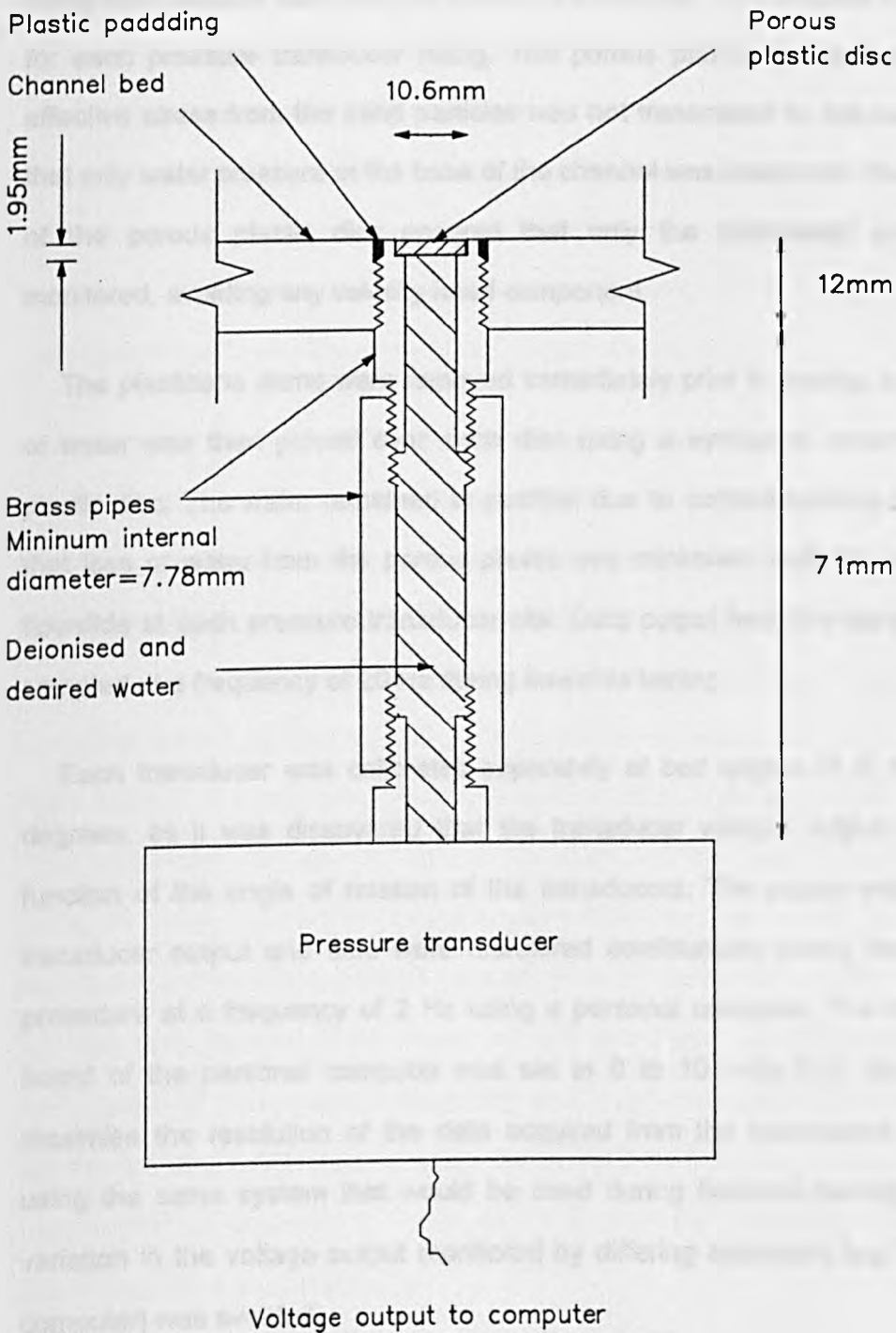
It was discovered that the voltage output of the transducers was affected by a 'warm up' period, therefore, the transducers were continuously powered to avoid this effect.

Although the water pressure measured during the tests was much smaller than the available full range output, financial restrictions prevented use of transducers with the optimum range. The PYE Ether transducer, having the largest range of measurement and the lowest accuracy, was placed nearest the sluice gate site where the depth of the flowslide was greater than further downstream. The error as a percentage of the whole measured depth would therefore be minimised.

A typical fitting used for connection of the pressure transducer to the channel base is illustrated (fig 4.5). Prior to any flowslide tests, a small plasticene dam was inserted in the channel about 50 mm downstream of each fitting. The fitting was then flushed out and subsequently filled with deionised and deaired water using a syringe, to ensure that no air bubbles remained inside. The top of the fitting was completely submerged by the deaired water retained by the plasticene dam. The length of the fitting was dictated by the construction of the channel support frame. This was slightly longer than the length of the hypodermic needle used, in order to avoid puncturing the diaphragm of the transducer.

FIG 4.5

SCHMATIC DIAGRAM OF
A PRESSURE TRANSDUCER FITTING



(all fitting connections sealed using PTFE tape)

A porous plastic disc, having been deaired by boiling in water for several hours, was carefully inserted into the recess of the top of the fitting. The top of the whole fitting then became flush with the base of the channel. This process was repeated for each pressure transducer fitting. The porous plastic disc ensured that any effective stress from the sand particles was not transmitted to the transducer, so that only water pressure at the base of the channel was measured. The orientation of the porous plastic disc ensured that only the hydrostatic pressure was monitored, avoiding any velocity head component.

The plasticene dams were removed immediately prior to testing, and a droplet of water was then placed over each disc using a syringe to cover the porous plastic disc. The water remained in position due to surface tension and ensured that loss of water from the porous plastic was minimised until the arrival of the flowslide at each pressure transducer site. Data output from the transducers was sampled at a frequency of 20 Hz during flowslide testing.

Each transducer was calibrated separately at bed angles of 0, 6, 9 and 12 degrees, as it was discovered that the transducer voltage output varied as a function of the angle of rotation of the transducers. The supply voltage output, transducer output and time were monitored continuously during the calibration procedure at a frequency of 2 Hz using a personal computer. The input voltage board of the personal computer was set to 0 to 10 volts D.C. input range to maximise the resolution of the data acquired from the transducers. Calibration using the same system that would be used during flowslide testing meant any variation in the voltage output monitored by differing apparatus (eg DVM versus computer) was avoided.

Calibration was performed in the following way. Firstly, the excitation voltage supplied to each transducer was monitored and set at its correct value using a

DVM. Scale rules (perpendicular to the bed) were carefully located at each transducer site on the outside of the channel using a theodolite. This was to measure the water level above the porous plastic discs. When the water level was monitored, parallax error in the longitudinal direction was avoided by aligning the scale with a line drawn perpendicular to the bed on the other channel wall, at the same longitudinal distance. A watertight barrier was placed in the channel just downstream of the furthest transducer, to reduce the overall length of the channel and hence the volume of water required during the calibration procedure. Manual variation of the depth of water was controlled using a syphon.

For each transducer, calibration data was obtained by lowering the water level above the porous plastic disc from 60 mm to 5 mm, in 5 mm increments of depth. Parallax error in the vertical direction was avoided using an electric lamp light directed onto the underside of the water. The underside of the water was viewed and then, by slowly raising one's eye level until the underside disappeared from view, the lamp light that had been reflecting on the underside of the water was then reduced to a very thin light streak at the bottom of the meniscus at this point. This light contrasted sharply against the scale on the channel. The water level could be slowly lowered by releasing water from the syphon until the light streak was in the centre of the desired graduation of the scale. Once this was achieved, the time from the start of the procedure was noted and the depth was maintained for a period of 30 seconds. The setting up of each calibration depth proved to be repeatable; the same mean voltage output (to 5 sf) from the pressure transducer could often be achieved for each depth. The whole procedure was conducted three times for each transducer.

This calibration procedure gave three separate sets of data for each transducer, per bed angle. For each data set, the relevant voltage output for each depth was obtained using the time record. This voltage output was checked to

determine whether it was steady. The depths of water measured perpendicular to the bed were converted into pressure. Linear least squared regression analysis was then performed on each set of data, using all the data points for each depth to give the calibration gradient and constant. All the data from the three separate sets was also combined and least squared regression analysis again performed.

Comparison of the data obtained for each separate calibration revealed that a maximum variation of 3 Pa (approximately 0.3 mm) occurred for the PYE Ether transducer, which was much smaller than the stated accuracy of the transducer. A smaller variation was recorded for the Sensotec transducer. Therefore, the calibration results obtained for a transducer at each angle were combined. The measure of fit of the regression line to the calibration data points can be expressed in terms of the coefficient of correlation r , or r^2 , where $r^2 = 1$ for perfect correlation. Regression analysis indicated that r^2 was greater than 0.9999 for each of the transducer calibrations. It was therefore concluded that very good fits to the data were obtained.

Efforts were also made to obtain calibration data with a rising water level, but observation of the water level from the side of the channel proved too difficult. Surface tension produced an irregular water level as the depth increased, making it very difficult to take repeatable and accurate observations. From those observations that were possible, it seemed that some hysteresis may have occurred between unloading and loading of the transducers, although it was not possible to determine whether this was due to the more inaccurate measurement system in the latter. Thus the data acquired from raising the water level over the transducer were disregarded as being of inferior quality. It was also fortunate that the maximum height of sand and water over a transducer was achieved rapidly when the flowslide arrived at a transducer site during a test and afterwards the height decreased. Thus calibration data obtained with the reduction of water level

were of most relevance. The voltage output of the pressure transducers under a constant load was also monitored over a period of one hour. The results indicated no drift in the output over this time.

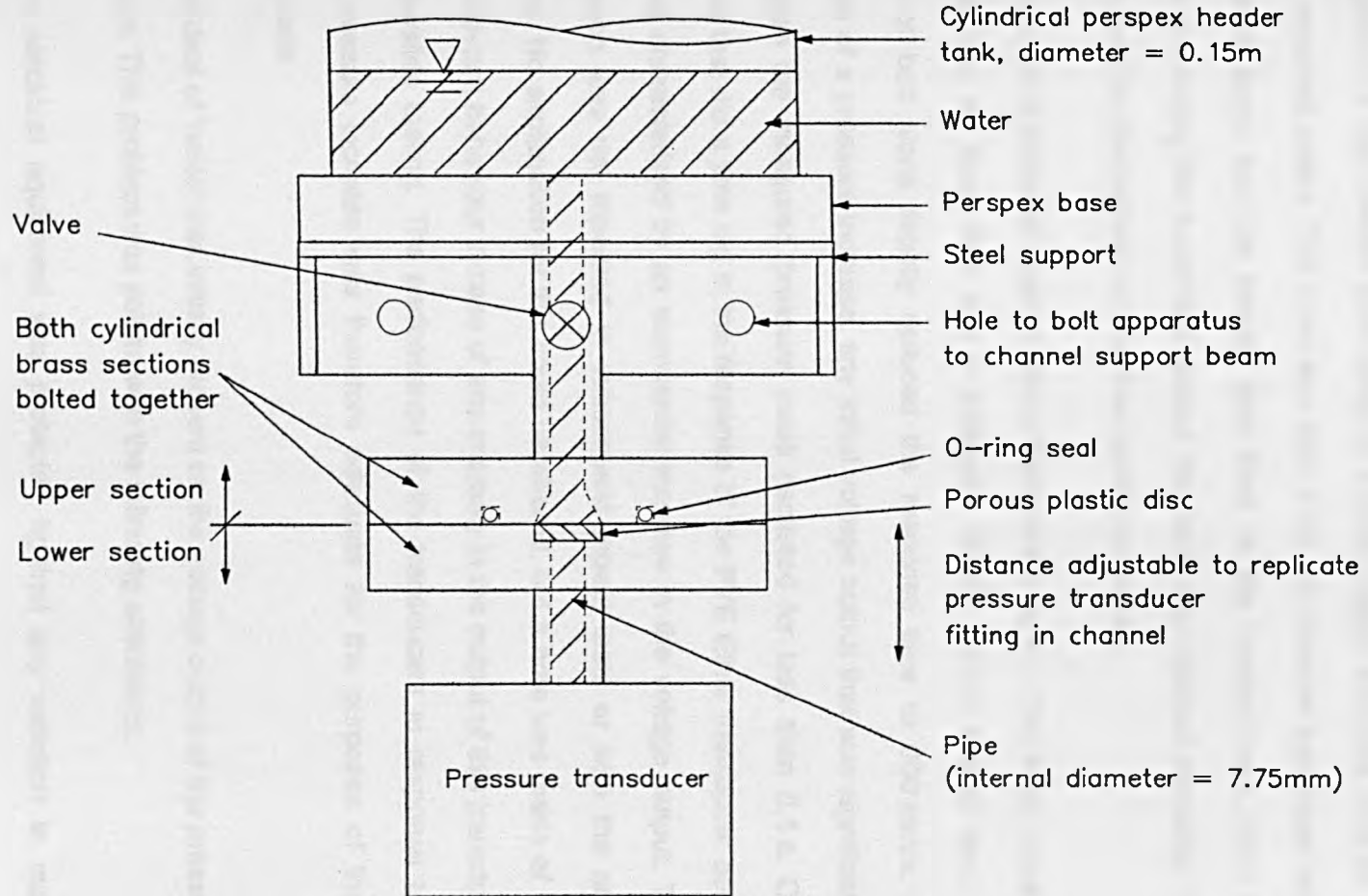
The air temperature of the room and that of the water used were noted during calibration and flowslide testing to verify that they were the same as the room air temperature. The air temperature of the laboratory varied from 13°C to 24°C during the course of the experimental work. It is well known that the density of water varies with temperature. For this range of temperature differences encountered, the density change of water could result in a 0.2% variation in measured pressure. The additional complications in apparatus required to measure any water temperature variation between that of the transducer fitting and the test sample during testing and calibration were not justified as this error was deemed to be insignificant. Thus no alteration of the calibration data due to the change in water density with temperature was performed.

The potential effect of the presence of the porous plastic disc on the transducers' response time was unknown. Test apparatus was designed to allow investigation of this effect (fig 4.6). This apparatus consisted of two sections. The lower section containing the porous plastic disc and the transducer was constructed so that the distance from the top face of the porous plastic to the transducer could be adjusted to duplicate the fittings in the channel. The same thickness and diameter of the porous plastic disc were used. This section was bolted to an upper part which contained a valve and a header tank. An O-ring was used to provide a watertight seal between the two sections. The apparatus was mounted on the side of the channel support beam of the main test apparatus to allow investigation of any possible influence of bed slope.

The porous plastic disc was deaired and the lower section filled with deionised

FIG 4.6

SCHEMATIC DIAGRAM SHOWING SIDE ELEVATION OF APPARATUS USED TO TEST PERFORMANCE OF PRESSURE TRANSDUCERS UNDER A SUDDEN HEAD INCREASE



and deaired water in the same way as described in section 4.71. After the porous plastic was inserted in the lower section, the two sections were bolted together. With the valve in the open position, the top section was filled with deaired water up to the bottom of the header tank using a syringe, again ensuring that no air bubbles remained inside. The valve was then shut, the channel bed slope set to the required angle and the header tank filled to the desired level. With the computer monitoring the transducer output, the valve was opened manually. The pressure head on the transducer was thus rapidly increased.

A typical plot of pressure against time is illustrated in fig 4.7. The tests indicated that there was no head loss due to presence of the porous plastic disc. An increase of bed slope slightly reduced the response time to 600 mm/s. On application of a pressure increase, any initial voltage output that was significantly greater than the measured pressure value persisted for less than 0.1 s. Only during one test did a time lag in the response of the PYE Ether transducer occur, which was characterised by an exponential increase in the voltage output. This phenomenon was not repeated in subsequent repeat tests or with the other transducer. No explanation for this could be offered, but a note was made of this potential deviant behaviour in case of any anomaly in the output of this transducer during flowslide testing. The performance of the transducers in response to a sudden pressure increase was therefore adequate for the purposes of these flowslide tests.

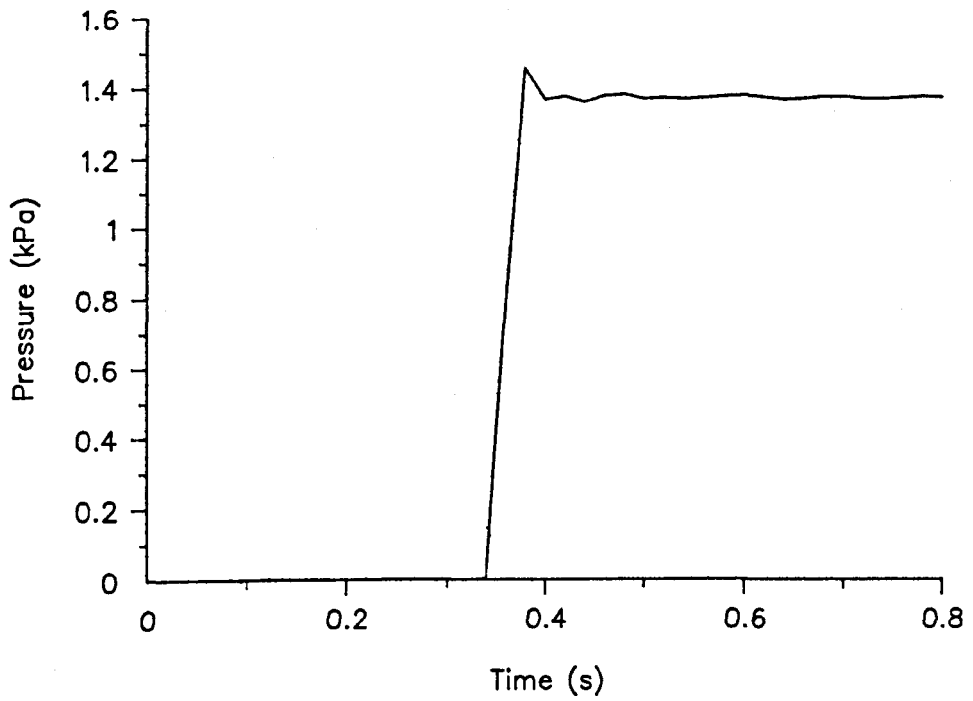
A great deal of 'noise' was initially present on the voltage output of the pressure transducers. This problem was solved with the following alterations:

- a) The electrical equipment was protected against any variation in mains voltage by the use of a mains filter.
- b) All electrical wires, where not protected by screened cable, were twisted

FIG 4.7

PRESSURE TRANSDUCER RESPONSE TIME
TO A SUDDEN PRESSURE INCREASE

Pressure transducer = Sensotec
Bed slope = 12 degrees



together to prevent any RF (radio frequency) pick up.

c) The voltage output wires from all electrical measurement devices were hardwired directly to the interface box of the computer to minimise the number of connections. Screwed contacts reduce the possibility of resistance build up that may occur with 'banana clip' friction type connections.

d) Care also had to be taken with earth connections to reference them to the same point. This avoids any difference in earth potential, or 'earth loop' effects, which can cause a variation or instability in the voltage output of electrical measurement apparatus.

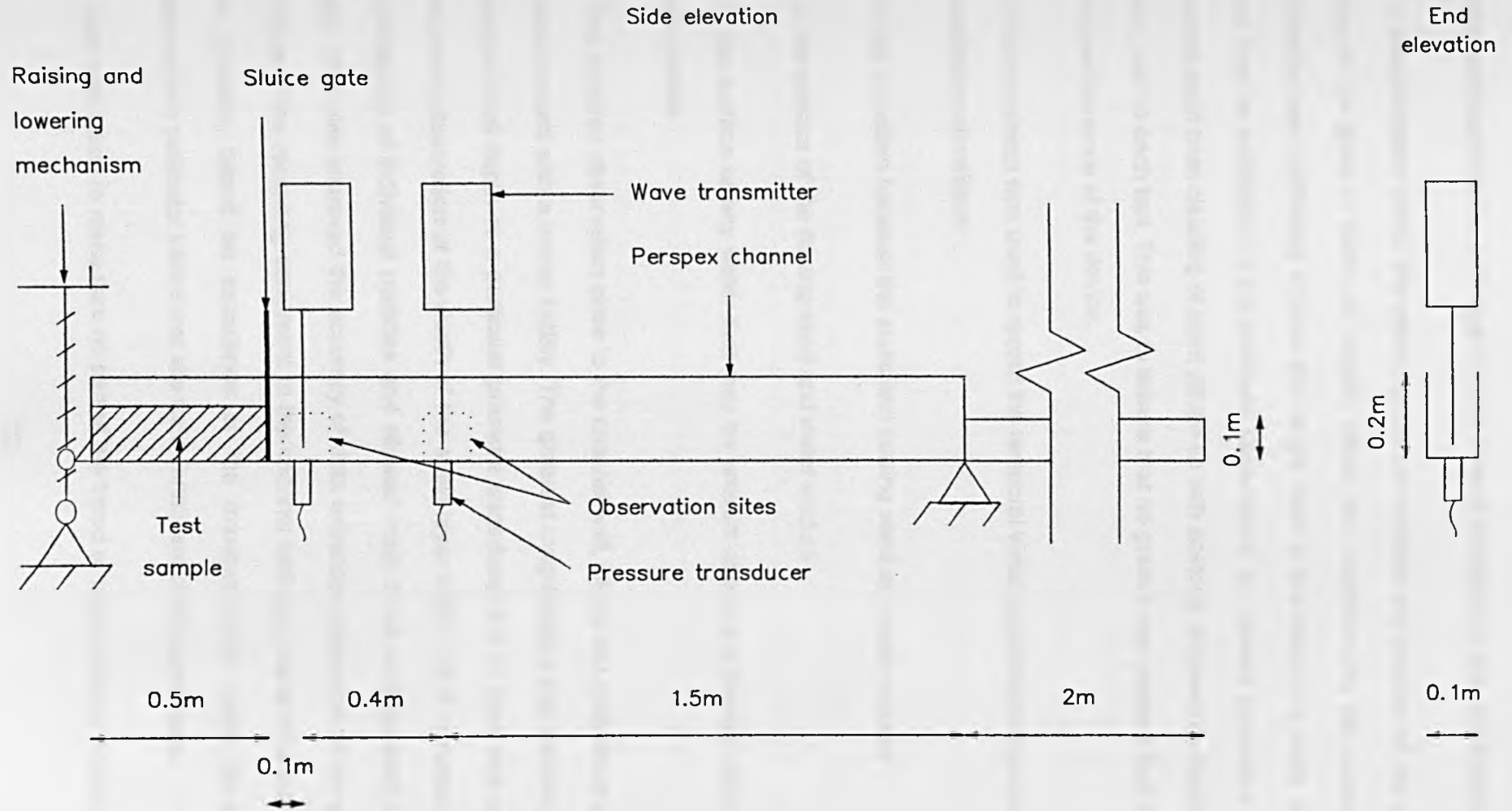
In addition, all electrical equipment that derived its power from the mains supply, directly or indirectly, was protected by electrical trip switches from any potential electric shock that could be caused by water spillage.

4.4 EQUIPMENT USED FOR DEPTH MEASUREMENTS

Two motorised point gauges, or wave transmitters were mounted perpendicular to the bed above each pressure transducer site (fig 4.8). This meant that the wave transmitters did not require repositioning as the channel bed slope was changed. The wave transmitters monitored the overall depth of the flowslide continuously. It was able to follow the surface of the flowslide by completing an electrical circuit between the end of point gauge and the water, which was earthed to the wave transmitter from the base of the channel. The instrument was set up to immerse the end of the point gauge to a depth of 0.5 mm. If the water level rose, a slightly greater depth was immersed in the water and the point gauge rose to maintain its original immersion depth. The opposite occurred if the water level fell. The

FIG 4.8

SCHMATIC DIAGRAM OF LABORATORY APPARATUS
SHOWING POSITIONS OF PRESSURE TRANSDUCERS AND WAVE TRANSMITTERS



instrument responded to a change in water level at a maximum rate of 18 mm/s.

A potentiometer within the wave transmitter enabled the position of the point gauge to be given in terms of voltage, which was monitored by the computer. Calibration was performed at each bed angle used in the laboratory tests at the same time as calibration of the pressure transducers. No special procedure was required apart from cleaning of point gauge tip with acetone, followed by deionised water, prior to each test. This was to ensure that no grease was present that might affect performance of the device.

A video camera was used to record the temporal variation at the channel wall of the following elevations:

- a) the transition between the static and flowing sand and water mixture
- b) the surface of the flowing sand and water mixture
- c) the surface of any water that may be present above the flowing sand and water mixture

This required observation close to the channel wall, which was performed using a video camera with a macro facility. The greatest magnification that retained the maximum total depth at a particular pressure transducer site in view was used. This made observation of the depth of the static layer easier, as it increased the magnification of individual particles and allowed them to be distinguished more easily. This also improved the accuracy of data extraction. Selection of the exact distance of the recording equipment to the channel wall was made on a trial and error process, based on experience of the maximum flow depth generally observed at a particular transducer site for a certain set of test conditions.

Care was taken to make sure no part of the tripod or video camera touched the

test apparatus. This avoided any vibration or movement to the viewing apparatus that might occur when the sluice gate was removed. Focusing of the camera lens was helped by placing a sheet of log-log graph paper directly against the inside of the channel wall. The lens was manually adjusted to obtain a sharp picture. This was performed after the test sample preparation procedure had been completed. Artificial lighting was occasionally required, depending on the intensity of the natural background light present and the proximity of the video camera lens to the channel wall. Correct focusing of the equipment was extremely important to enable data extraction from the video tape records. On occasion, data could not be obtained from video records because of incorrect focusing, probably as result of slight accidental jarring of the video apparatus. For this reason, absolutely no vibration or movement of the camera should be allowed.

The main disadvantage of the video system was the extremely laborious process of data extraction that required considerable care and patience. Initially, all depths were measured normal to the bed, as is standard practice in hydraulics. This also allowed comparison of the depths obtained from the video film to the data obtained from the wave transmitters.

It was necessary to incorporate a scale within the video image to allow quantitative measurements of the various depths. Initial experiments incorporated a ruler on the outside of the channel, so that the flow would not be disturbed. It was found that with this method, the video camera distorted the actual depths due to the thickness of the perspex channel wall. This was overcome by drawing a grid of lines, spaced apart 10 mm vertically and 5 mm horizontally, on an acetate sheet with an indelible pen. This sheet was placed on the inside of the channel and was sufficiently long to cause no disturbance to the flow at the site of measurement.

Data extraction from video tape records required two observers. Whilst the

surface of the flowing sand and water mixture varied slowly after the initial rapid increase in depth, the surface of the static material increased erratically, increasing the difficulty of measurement. For a certain depth of static material, an identifiable sand particle coming to a halt at the observation site was sought. Having identified an appropriate particle and determined the exact depth at which its motion ceased, the film was rewound to the beginning of the event and the tape started.

Time measurements were taken using a stop watch, which was started at the moment of sluice gate removal (a sharp distinctive noise on the sound track). When the static sand layer reached the predetermined level, measurements of the time, the surface level of the flowing sand and water mixture and the level of any surface water were taken simultaneously. The extraction of the level of the surface water was given a lower priority owing to its small depth, but could be checked by pausing the video tape at the appropriate time value. The procedure was repeated until the measurements of time agreed to within ± 0.1 s and an average of these time values was then taken. This sometimes involved more than 10 runs of the film to obtain a set of results for one time value. Where agreement to this degree of accuracy could not be obtained, the results were disregarded. The whole procedure was then repeated until the depth of the flowing material was reduced to the order of 1 mm. The accuracy of the measurement of the position of any layer is dependent on the quality of the video film and the degree of magnification, but is estimated to be within maximum bounds of ± 0.25 mm.

Errors in obtaining time values for the static and flowing sand data were difficult to avoid. Due to the close proximity of the camera to the channel wall, efforts to incorporate a stop watch into the picture were not successful because of focusing problems and physical distance limitations. Attempts at incorporating a time base on the video film after the event resulted in a video tape copy of poorer quality.

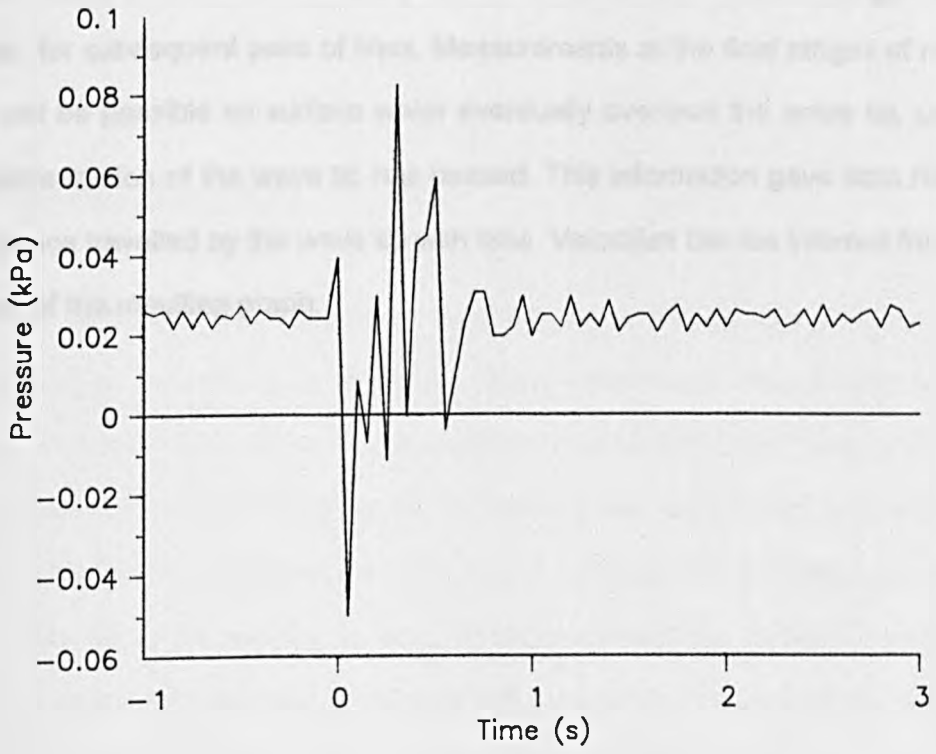
The different flowslide layers could not be distinguished from these copies. It was also found that stopwatches with a positive click mechanism for starting and stopping found on older analogue-type stopwatches gave more repeatable results than those obtained using modern digital stopwatches with push button control.

The time and depth measurements taken from the video film were sequenced with the appropriate pressure transducer record. This was achieved easily as the point of sluice gate removal was also registered on both pressure transducer traces as noise (fig 4.9). The duration of the variation in output due to this effect was of the order of 1–1.5 seconds. For each transducer mounted in the channel, the appearance of the noise on the voltage output occurred at exactly the same time. During flowslide testing, each transducer voltage output should be checked for any possible increase in voltage that occurs as a result of the shock imparted to the channel during sluice gate removal. This can be achieved by comparing the average voltage output before and after the noise. This may not always be possible for the *PYE Ether* transducer mounted at 0.1 m from the sluice gate site, as the arrival of the flowslide may occur before the noise has fully dissipated. Therefore, the pressure transducer output for a duration of 1.5 s from sluice gate removal should not be used for the purposes of analysis. This is due to the possible superposition of noise on any recorded pressure from the flowslide.

4.5 MEASUREMENT OF FLOWSLIDE WAVE TIP VELOCITY

Each channel wall was marked with lines at 0.1 m intervals, perpendicular to the bed. A push button switch, that supplied a small voltage pulse when depressed, was wired to the interface board of the computer. This voltage was registered on one of the channels of the data acquisition program to record the

FIG 4.9 NOISE REGISTERED ON PRESSURE TRANSDUCER DUE TO SLUICE GATE REMOVAL



time at which the button was pressed. As a flowslide began to move, the switch operator lined up the first pair of lines, to avoid parallax error, and pressed the push button when the wave tip, defined as the leading edge of the flowslide, first reached these lines. This procedure was then repeated along the length of the channel, for subsequent pairs of lines. Measurements at the final stages of motion would not be possible as surface water eventually overtook the wave tip, usually just before motion of the wave tip has ceased. This information gave data relating the distance travelled by the wave tip with time. Velocities can be inferred from the gradient of the resulting graph.

CHAPTER 5:

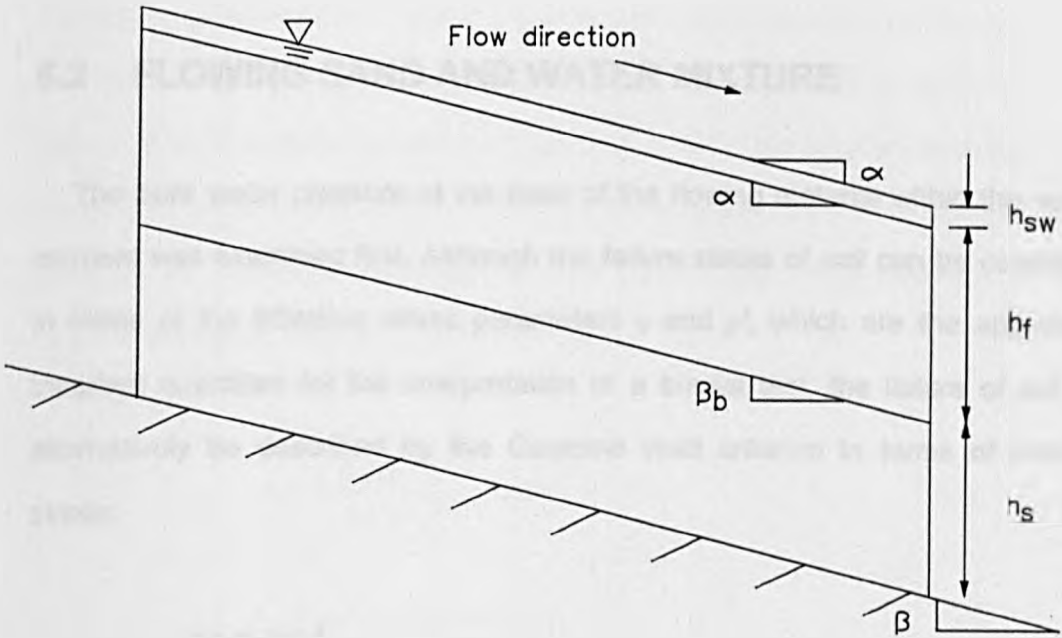
ANALYSIS OF PORE WATER PRESSURE

5.1 INTRODUCTION

Several possible shear resistance mechanisms during flowslide motion have been identified (section 2.8). Although shear strains are responsible for the collapse of a loose soil structure and generation of excess pore water pressures during liquefaction, uncertainty exists concerning the importance and effect of excess pore water pressures on the shear strength of the material during subsequent flowslide motion. It was considered that the easiest method of investigating this problem was to monitor the pore water pressure at the channel bed and then compare these experimental data to theoretical values calculated for the vertical element of the flowslide above the pressure measurement site. From the results of the preliminary experiments, it was known that this vertical element could be composed of up to three layers; a flowing sand and water mixture, static material beneath the flowing material and surface water above it. Not all of these layers may of course have been present at any one time (fig 5.1).

A slight camber of the upper surface of the sand was noticed during the preliminary experiments after motion had ceased, but it was assumed that no transverse variation of this and the surface elevations of other layers occurred. In addition, the slope of the flowslide surface, α , after motion had ceased was observed to increase with decrease in channel bed slope. This feature was ignored for the present. It was assumed that the surface slopes of each of the

FIG 5.1 SCHEMATIC DIAGRAM OF A VERTICAL ELEMENT OF A FLOWSLIDE



- α = slope of flowslide surface
- β_b = slope of surface of static material
- β = channel bed slope
- h_{sw} = vertical height of surface water
- h_f = vertical height of flowing sand and water mixture
- h_s = vertical height of static material

layers were parallel to the channel bed slope, such that $\alpha = \beta_b = \beta$ (fig 5.1). In order to calculate the pore water pressure at the channel bed, the pore water pressure at the base of each layer of material was considered.

5.2 FLOWING SAND AND WATER MIXTURE

The pore water pressure at the base of the flowing material within the vertical element was examined first. Although the failure states of soil can be considered in terms of the effective stress parameters q and p' , which are the appropriate invariant quantities for the interpretation of a triaxial test, the failure of soil can alternatively be described by the Coulomb yield criterion in terms of effective stress:

$$\tau = \sigma'_n \tan \phi' \quad (5.1)$$

σ'_n = effective stress normal to a failure plane

ϕ' = effective angle of friction

Cohesion did not need to be considered due to the granular nature of sand. It is assumed during use of the Coulomb yield criterion that the intermediate principal stress has no effect on the failure of the soil [Atkinson/Bransby (1978)]. This value would indeed be difficult to measure in a laboratory channel. The stresses at the interface, or slip surface between static and yielding material, are considered and hence no assumption concerning the pore water pressure distribution within the flowing material was necessary. It was proposed that the pore water pressure at the slip surface at the base of the flowing material (or basal pore water pressure) must be of sufficient magnitude to reduce the intergranular friction in order that

sliding of the grains could occur. This basal pore water pressure was calculated by resolving forces parallel and perpendicular at the slip surface. Possible contributions to the resisting shear stress from dynamic effects, such as viscosity, were ignored, as was the possible influence of the presence of surface water on the driving shear stress. A similar procedure has been used during the 'analysis of an infinite landslide' [eg Bolton (1984), Scott (1980): section A.1], where a factor of safety against landsliding was obtained. As a first approach to analysis, it was assumed that the driving and resisting forces were just in balance during flowslide motion. The factor of safety was therefore equal to one. This gave the predicted value of the basal pore water pressure as:

$$u_{b,pred} = \left[1 - \frac{\tan \beta_b}{\tan \phi'} \right] \rho_{sat} g h_f \cos^2 \beta_b \quad (5.2)$$

ρ_{sat} = saturated bulk density

h_f = vertical height of flowing material

This expression is therefore only strictly applicable during uniform flow, when the momentum equation is reduced to a simple body force component parallel to the bed. It was hoped that any change in momentum that might occur during flowslide motion would have a small effect and not cause a significant error. To consider material strength following liquefaction after its peak strength has been attained, the effective angle of friction was set equal to the critical state angle of friction, and hence to the angle of repose [Bolton (1986)]. The steady and critical state angles of friction were expected to be the same, given the similarity between the steady and critical states [Hird/Hassona (1986, 1990)]. In addition, the angle of friction measured in ring shear experiments has been found to be close to the angle of repose (section 2.72).

Ideally, the saturated bulk density of the flowing material should be measured, which can be achieved using conductivity probes [Bezuijen/Mastbergen (1988), pers comm Bezuijen (1990)]. Unfortunately, lack of availability precluded the use of such equipment. According to steady state theory, the void ratio (or density) should remain at its pre-failure value during flow, if no drainage occurs. Thus the saturated bulk density of the flowing material was assumed to be equal to that of the settled test sample. The presence of small air bubbles was thought to be negligible and both the initial test sample and flowing sand and water mixture were assumed to be fully saturated.

From the results of the preliminary experiments, the solid volume concentration, C , of the test sample was found to be greater than 0.4. Therefore, following other experimental observations [Bagnold (1955), Winterwerp et al (1990)], the sand grains were expected to be uniformly dispersed within the flowslide and hence the density was assumed to be uniform within the flowing sand and water mixture. As the solid volume concentration was high, the presence of turbulence was expected to be 'damped out' [Bagnold (1955)] and, as the flowslide tests were also conducted at a small scale, turbulence was not anticipated to be an important mechanism in the generation of shear stress [Winterwerp et al (1990)]. Therefore, the presence of excess pore water pressures due to suspended load was not expected.

In the analysis of granular fluids, it has been proposed that the shear strength of a granular fluid is governed by dispersive pressures [Bagnold (1956)]. In the absence of grain support by eddies of fluid turbulence, no excess pore water pressures are present and a hydrostatic pressure distribution exists within the flowing material [Bagnold (1956), Davies (1988)]. A smaller pore water pressure could not exist if flowslides are fully saturated. A lower bound to the predicted basal value was therefore proposed by assuming that hydrostatic pressure

distribution existed within the flowing material. This minimum basal pore water pressure can be expressed by:

$$u_{b,\min} = \rho_w g h_f \cos^2 \beta_b \quad (5.3)$$

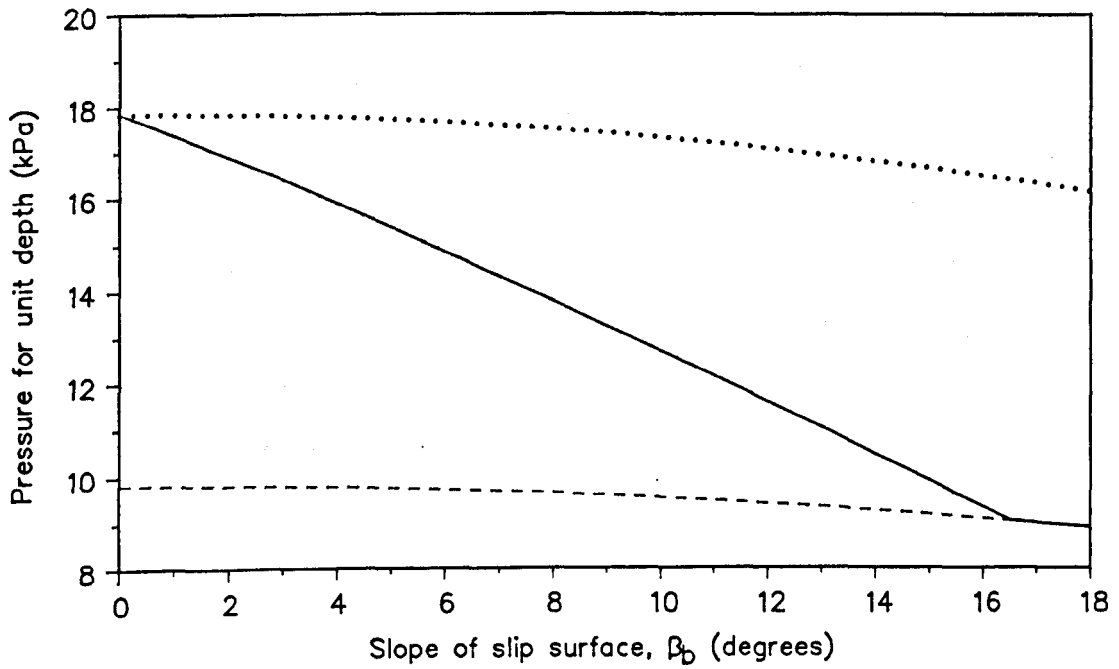
An upper bound value of the basal pore water pressure, $u_{b,\max}$, was at first calculated by assuming that the vertical effective stress was zero [Hird/Spence (1991)], following the method used by Bezuijen/Mastbergen [(1988): section 2.74]. It was decided that a more realistic upper bound to the basal pore water pressure would be obtained if the normal effective stress at the base of the flowing material was zero. This implied that the flowing sand had no shear strength, causing the factor of safety in the landslide model to be equal to zero, giving:

$$u_{b,\max} = \rho_{sat} g h_f \cos^2 \beta_b \quad (5.4)$$

Consideration of the influence of the slip surface slope, β_b , on the magnitude of each of these three pore water pressure expressions illustrated relationships between them. Using specimen data values obtained during the preliminary experiments ($\phi' = 33.37$ degrees, $\rho_{sat} = 1820 \text{ kg/m}^3$), it could be seen that at a slip surface slope of 0 degrees, the maximum and predicted basal pore water pressures were equal (fig 5.2). As the slope was increased from 0 to 16.5 degrees, the value of the predicted basal pore water pressure decreased. Flow or sliding with no excess pore water pressures would be possible at a slip surface slope of 16.5 degrees, where the predicted and minimum basal pore water pressure values were equal. The value of this slope can be calculated from:

$$\beta_b = \tan^{-1} \left[\left(1 - \frac{\rho_w}{\rho_{sat}} \right) \tan \phi \right] \quad (5.5)$$

FIG 5.2 VARIATION IN BASAL PORE WATER PRESSURES WITH SLIP SURFACE SLOPE



Legend

- Maximum basal pore water pressure, $u_{b,max}$
- Predicted basal pore water pressure, $u_{b,pred}$
- Minimum basal pore water pressure, $u_{b,min}$

Assume unit depth, $h_f = 1\text{m}$

$\phi' = 33.37^\circ$

$\rho_s = 1820 \text{ kg/m}^3$

The uniform flow of a sand and water mixture at various solid volume concentrations (or saturated bulk densities) has been studied [Winterwerp et al (1990)]. By relating the momentum equation and the dispersive shear stress [$\tau = P \tan \phi_d$ (equation 2.13)], it was found that theoretical predictions of the slope at which uniform flow occurred agreed well with experimental data when the dynamic angle of friction, ϕ_d , was set equal to the angle of repose. This gave an expression for the slope at which uniform flow occurred that was identical to that shown above (equation 5.5). It could therefore be seen that this expression for the dispersive shear stress was then identical to Coulomb's yield criterion, when no excess pore water pressures were present and if the angles of friction were the same. Further evidence of the dynamic angle of friction being close to that obtained in static or quasi-static experiments has been recorded (section 2.72). Experimental validation of $u_{b,pred}$ when $u_{b,pred} = u_{b,min}$ has therefore been obtained.

5.3 SURFACE WATER AND STATIC MATERIAL

The pressure at the base of a layer of flowing water is dependent on the slope over which it is moving. The surface slope of the water, α , was assumed to be equal to the channel bed slope, β . The pore water pressure contribution from this layer was calculated using:

$$u_{sw} = \rho_{sat} g h_{sw} \cos^2 \alpha \quad (5.6)$$

It was initially assumed that the pore water pressure at the base of the static material, u_s , was equal to a vertical hydrostatic distribution [Hird/Spence (1990)]:

$$u_s = \rho_w g h_s \quad (5.7)$$

It was thought subsequently that it would be more realistic to presume that some seepage of water within the static material occurred. In this case, calculation of the pore water pressure at a position within a static body of soil would usually require construction of a flownet. As temporal variation of the elevation of the static material at a particular longitudinal position happened during the flowslide event, it was unrealistic to construct flownets when instrumentation was not available to determine spatial and temporal variations in the elevations of static material. It was therefore assumed that seepage parallel to the channel bed occurred, with the pore water pressure within the static sand, u_s , calculated using:

$$u_s = \rho_w g h_s \cos^2 \beta \quad (5.8)$$

An upper and lower bound to the pore water pressure at the base of the static material was not obtained as it was felt that this would not assist in resolving the investigation into the pore water pressure at the base of the flowing sand and water mixture.

5.4 TOTAL PORE WATER PRESSURE

The total pore water pressure at the channel bed was composed of the sum of the pore water pressure in each of static, flowing and surface water layers. As it was assumed that $\alpha = \beta_s = \beta$, the measured pore water pressure was therefore to be compared to the following maximum, $u_{t,max}$, predicted, $u_{t,pred}$, and minimum, $u_{t,min}$, total pore water pressures:

$$u_{t,max} = \rho_w g \cos^2 \beta \left[h_s + h_f \frac{\rho_{sat}}{\rho_w} + h_{sw} \right] \quad (5.9)$$

$$u_{i, pred} = \rho_w g \cos^2 \beta \left[h_s + \left(1 - \frac{\tan \beta}{\tan \phi'} \right) \frac{\rho_{sat}}{\rho_w} h_f + h_{sw} \right] \quad (5.10)$$

$$u_{i, min} = \rho_w g \cos^2 \beta [h_s + h_f + h_{sw}] \quad (5.11)$$

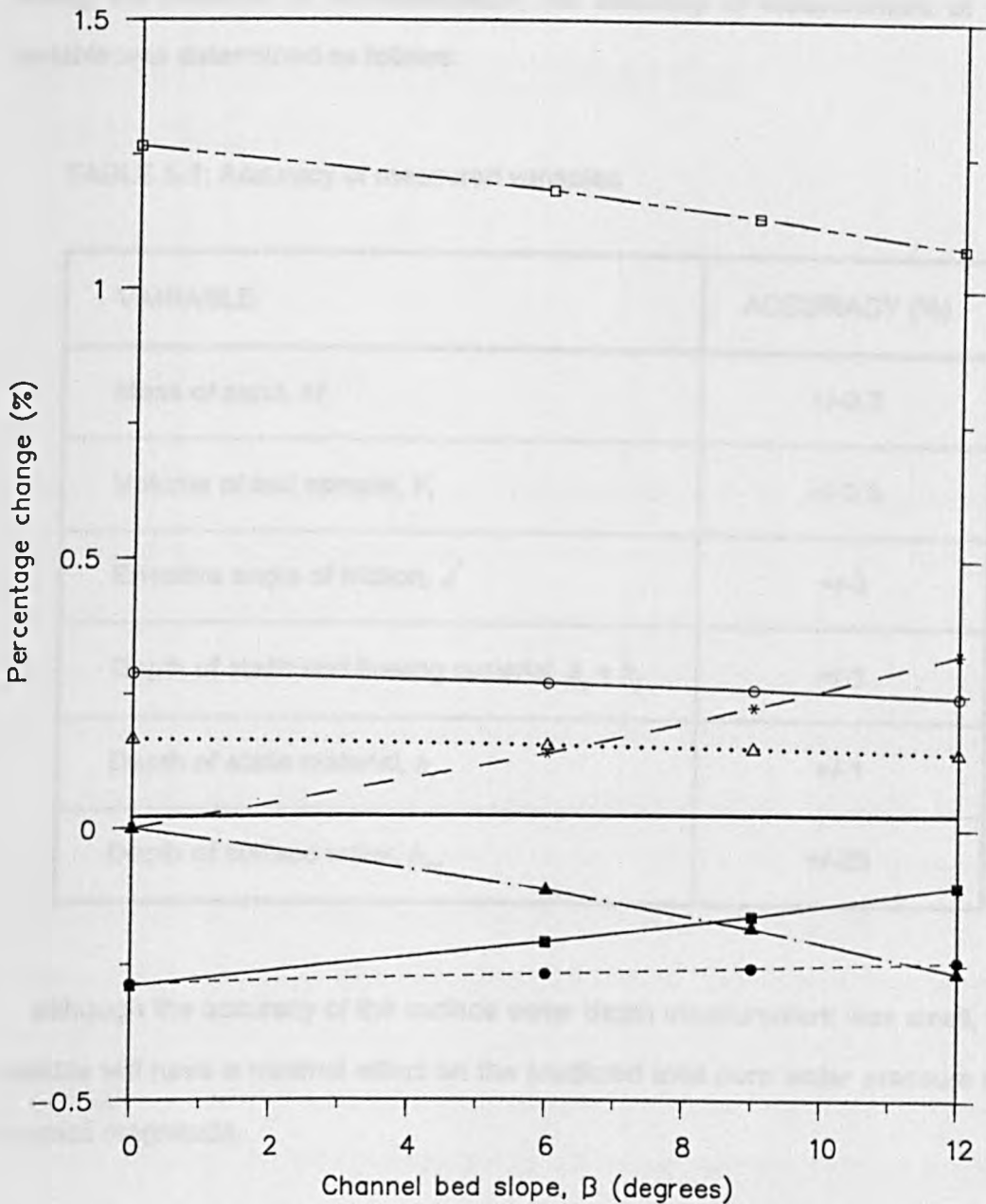
It should be noted that this analysis does not predict any temporal variation of the depth of the flowing material which may occur. It only provides three values for the magnitude of the pore water pressure in order that the importance of the pore water pressure could be investigated.

5.6 SENSITIVITY CALCULATIONS

The sensitivity of the predicted total pore water pressure (equation 5.10) with change in channel bed slope to a percentage change in each of the laboratory measured variables was assessed. This was performed by both increasing and decreasing the magnitude of each variable in turn by 1% and observing the resulting percentage change of the predicted total pore water pressure. The initial value of each variable was taken from data obtained during the preliminary experiments. Although temporal variations of the depths of both the static and flowing material occurred during the course of a flowslide event, these depths were set equal to 15 mm for the purposes of this investigation.

The results for a 1% increase in each variable (fig 5.3) showed that the total predicted pore water pressure was most sensitive to the depth of static and flowing material, $h_s + h_f$. The results for a 1% decrease in each variable were almost a reflection of results obtained for a 1% increase in the x-z co-ordinate plane.

FIG 5.3 VARIATION OF PERCENTAGE CHANGE IN TOTAL PREDICTED PORE WATER PRESSURE ($u_{t, pred}$) WITH CHANNEL BED SLOPE FOR A 1% INCREASE IN EACH MEASURED VARIABLE



Initial value of variables	Legend
Mass of sand = 5.975kg	○
Volume of test sample = 0.004502m ³	●
Specific gravity, $G_s = 2.71$	△
Effective angle of friction, $\phi' = 33.37$	*
Channel bed slope, $\beta = x$ axis value	▲
Depth of static and flowing material, $h_s + h_f = 30\text{mm}$	□
Depth of static material, $h_s = 15\text{mm}$	■
Depth of surface water, $h_{sw} = 1\text{mm}$	—

From the preliminary experimental results and laboratory work conducted during the provision of instrumentation, the accuracy of measurement of each variable was determined as follows:

TABLE 5.1: Accuracy of measured variables

VARIABLE	ACCURACY (%)
Mass of sand, M_s	+/-0.3
Volume of test sample, V_t	+/-0.5
Effective angle of friction, ϕ'	+/-3
Depth of static and flowing material, $h_s + h_f$	+/-1
Depth of static material, h_s	+/-1
Depth of surface water, h_{sw}	+/-25

Although the accuracy of the surface water depth measurement was small, this variable will have a minimal effect on the predicted total pore water pressure due its small magnitude.

CHAPTER 6:

SECOND SERIES OF FLOWSLIDE EXPERIMENTS

6.1 INTRODUCTION

This series of flowslide tests were conducted principally to obtain experimental data concerning the pore water pressures at the channel bed over the duration of the flowslide. Although two pressure transducers were mounted at the channel bed, the availability of one video camera only allowed a record of the passage of the flowslide at one pressure transducer observation site per test. Comparison of the measured and calculated pore water pressures could therefore only be performed at one longitudinal distance for each flowslide event. From observations of the flowslide surface angle, α , during the preliminary tests, it was established that the surface elevation after movement had ceased decreased with increase in longitudinal distance for channel bed slopes less than or equal to 9 degrees. The rate of this decrease increased with decrease in channel bed slope. Data were therefore obtained at the 0.1 m pressure transducer site for tests at 0 and 6 degrees, to maximise the depth of material observed and the length of time over which observations could be taken.

The influence of the distance downstream at which measurements were taken on the magnitude of the pore water pressures was investigated by collecting experimental data at the 0.5 m observation site for tests at 9 and 12 degrees. Due to the increase in channel bed slope, it was expected that the flowslide would

persist at this site for a sufficient period of time for an adequate amount of data to be extracted. Flowslide tests were not performed at higher bed slopes due to the small difference between the total expected and minimum pore water pressure values.

6.2 FLOWSLIDE MOTION

The leading edge of the flowslide was defined as the wave tip [fig 6.1(a)]. Immediately behind the wave tip, the flowslide material was composed of collapsing material from the failure of the test sample and was defined as the wave front [fig 6.1(a-f)]. Davies (1988) defined this region as the 'head'. The wave front began at the wave tip and ended when all the collapsing material had passed the transducer site [fig 6.1(a & f)]. Over this region, the surface elevation of the flowslide increased very rapidly with time and the depth in the centre of the channel was greater than that observed at the channel wall [fig 6.1(a-f)], making accurate observation of the surface elevation of the flowslide extremely difficult.

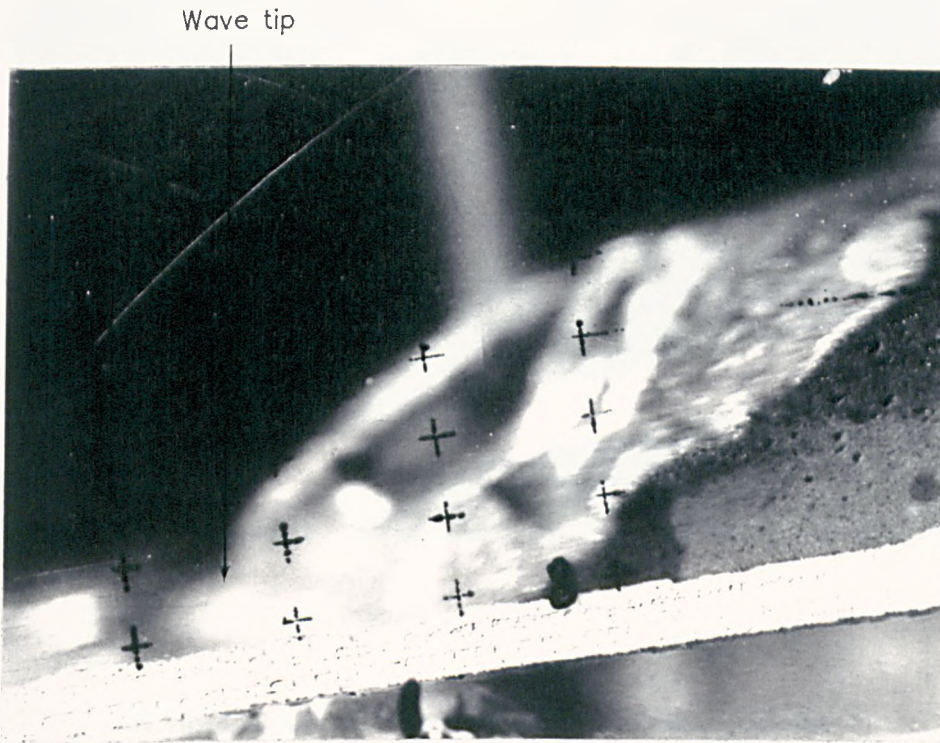
At the end of the wave front, the surface of the flowing layer was much smoother [fig 6.1(f)] and the surface elevation at the centre and the side of the channel after the end of the wave front were assumed to be equal and any potential transverse camber of the flow surface was neglected. Figs 6.3–6.10 show the length of time the wave front took to pass the observation site for each test. This time seemed to be random, depending on how the material collapsed as the sluice gate was removed.

With reference to figs 6.3–6.10, the surface elevation of the flowing sand and water mixture, $h_s + h_f$, was observed to increase in all cases initially and generally remained at this maximum value when the channel bed slope was equal to 0

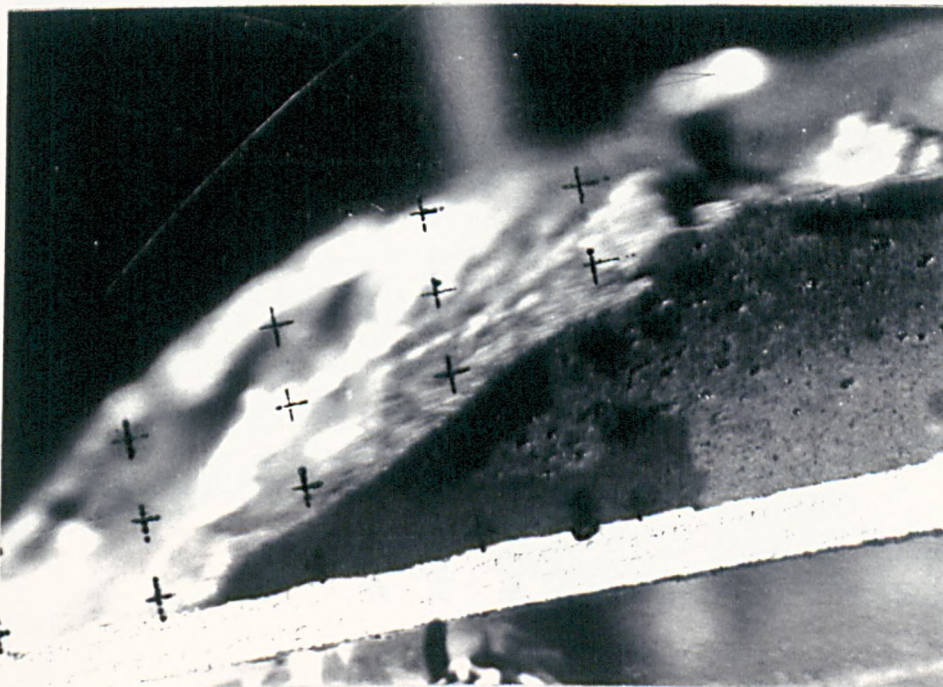
FIG 6.1 MOVEMENT OF A FLOWSLIDE WAVE FRONT PAST AN OBSERVATION SITE
0.3m FROM THE SLUICE GATE SITE (TEST 4M, BED SLOPE = 9 DEGREES)

Grid crosses spaced 10mm apart along the longitudinal axis of the channel
and 5mm apart perpendicular to the channel bed

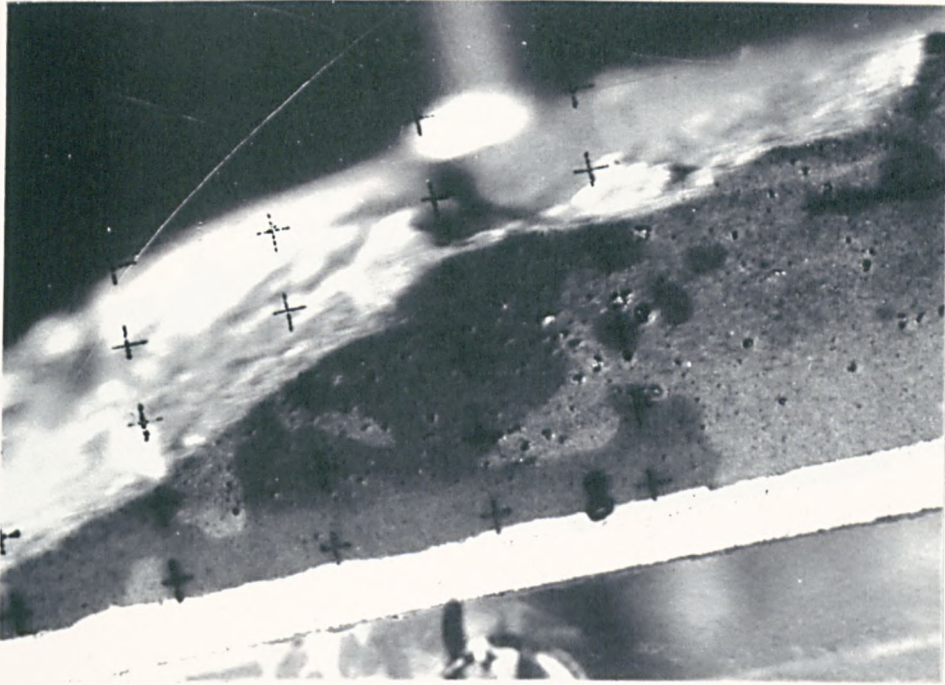
a) Time = 10 seconds from sluice gate removal



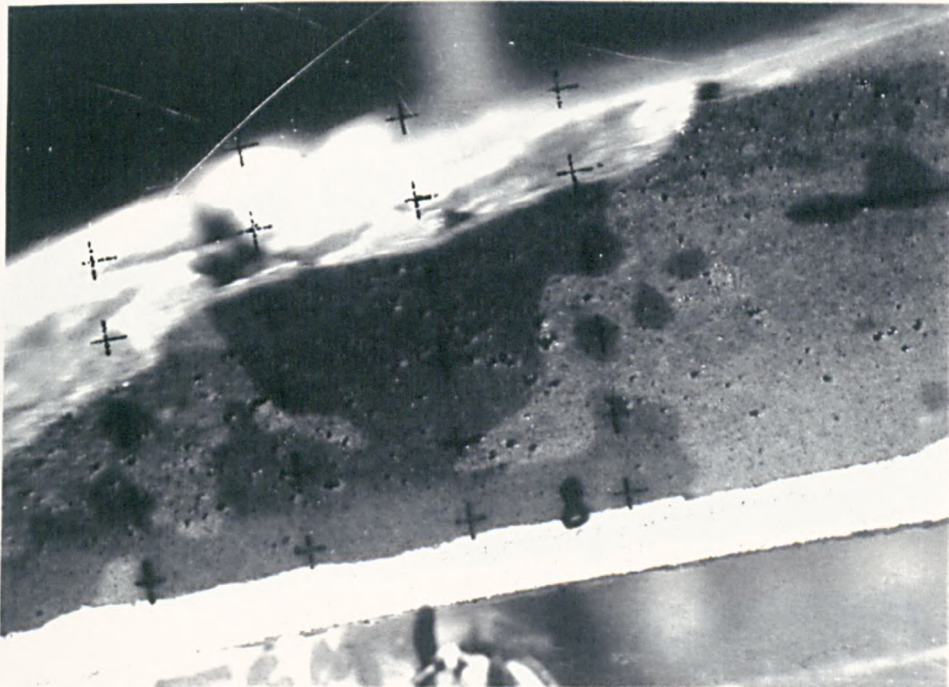
b) Time = 10.55 seconds from sluice gate removal



c) Time = 11.05 seconds from sluice gate removal



d) Time = 11.5 seconds from sluice gate removal



e) Time = 11.95 seconds from sluice gate removal







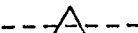
f) Time = 12.45 seconds from sluice gate removal

End of wave front



FIG 6.2

LEGEND FOR FIGURES 6.3-6.10

	Surface level of water, $h_s + h_f + h_{sw}$ (mm)
	Approximate surface level of flowing sand and water during passage of wave front, $h_s + h_f$ (mm)
	Surface level of flowing sand and water mixture $h_s + h_f$ (mm)
	Surface level of static material, h_s (mm)
	Elevation of secondary shear surface, h_{s2} (mm)

(All distances measured perpendicular to channel bed)

FIG 6.3 TEMPORAL VARIATION OF DEPTHS OF FLOWSLIDE MATERIAL (TEST 8S)
 AT 0.1m FROM THE SLUICE GATE SITE, CHANNEL BED SLOPE = 0 DEGREES

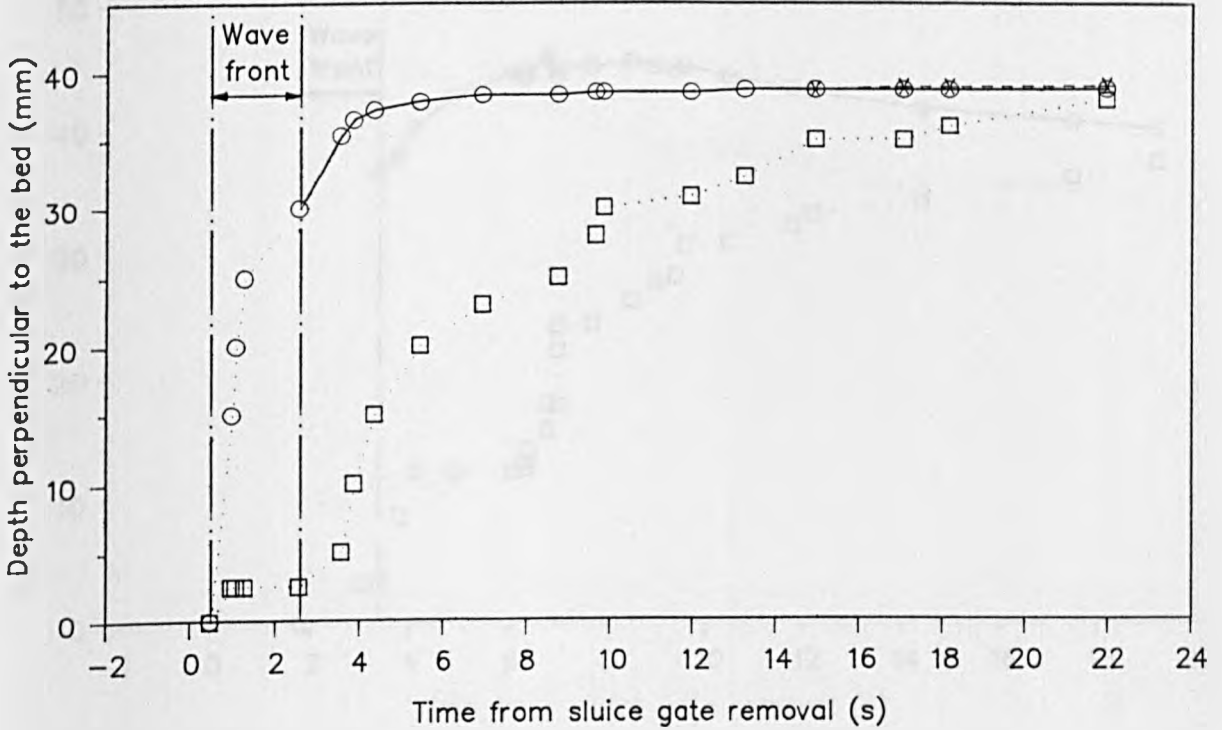


FIG 6.4 TEMPORAL VARIATION OF DEPTHS OF FLOWSLIDE MATERIAL (TEST 15S)
 AT 0.1m FROM THE SLUICE GATE SITE, CHANNEL BED SLOPE = 0 DEGREES

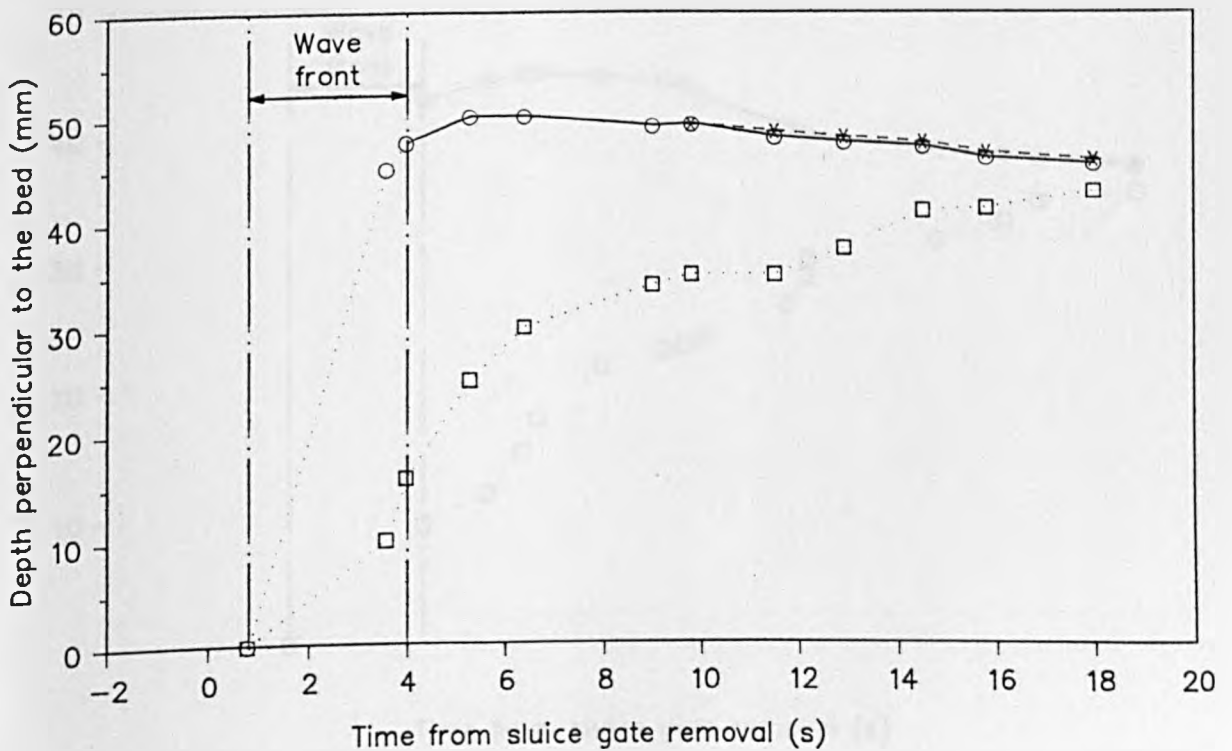


FIG 6.5 TEMPORAL VARIATION OF DEPTHS OF FLOWSLIDE MATERIAL (TEST 12S)
 AT 0.1m FROM THE SLUICE GATE SITE, CHANNEL BED SLOPE = 6 DEGREES

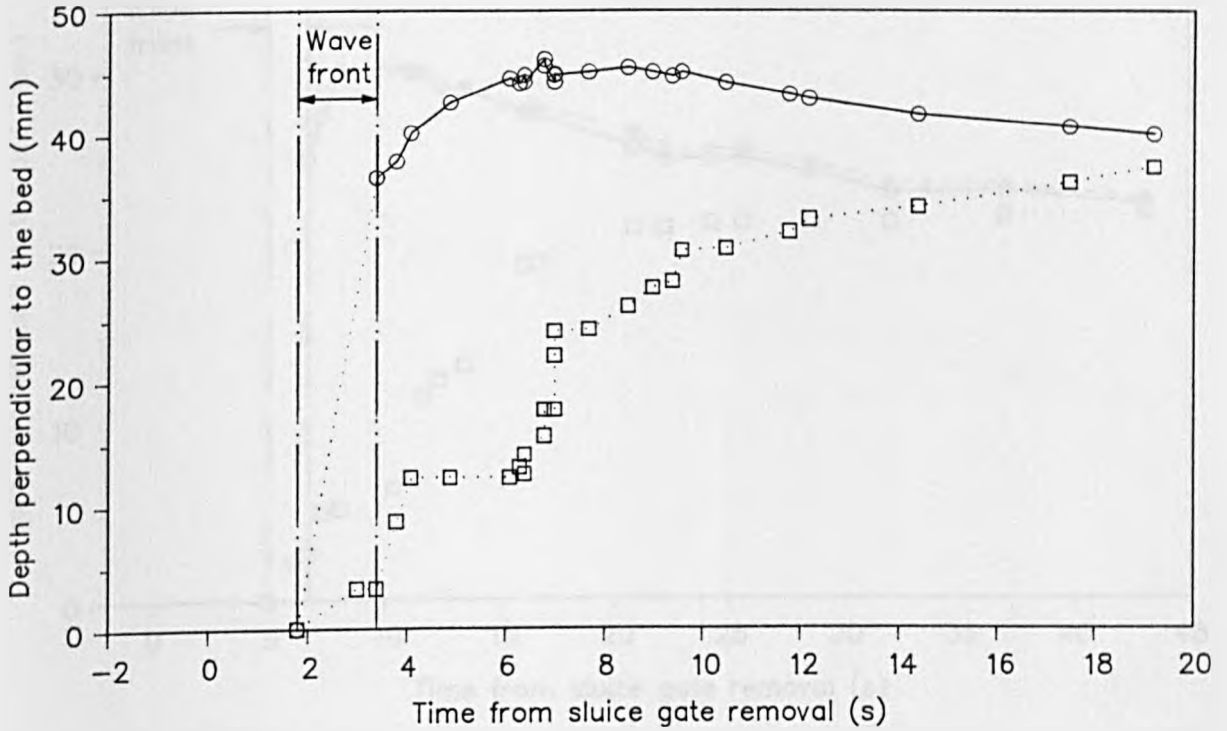


FIG 6.6 TEMPORAL VARIATION OF DEPTHS OF FLOWSLIDE MATERIAL (TEST 13S)
 AT 0.1m FROM THE SLUICE GATE SITE, CHANNEL BED SLOPE = 6 DEGREES

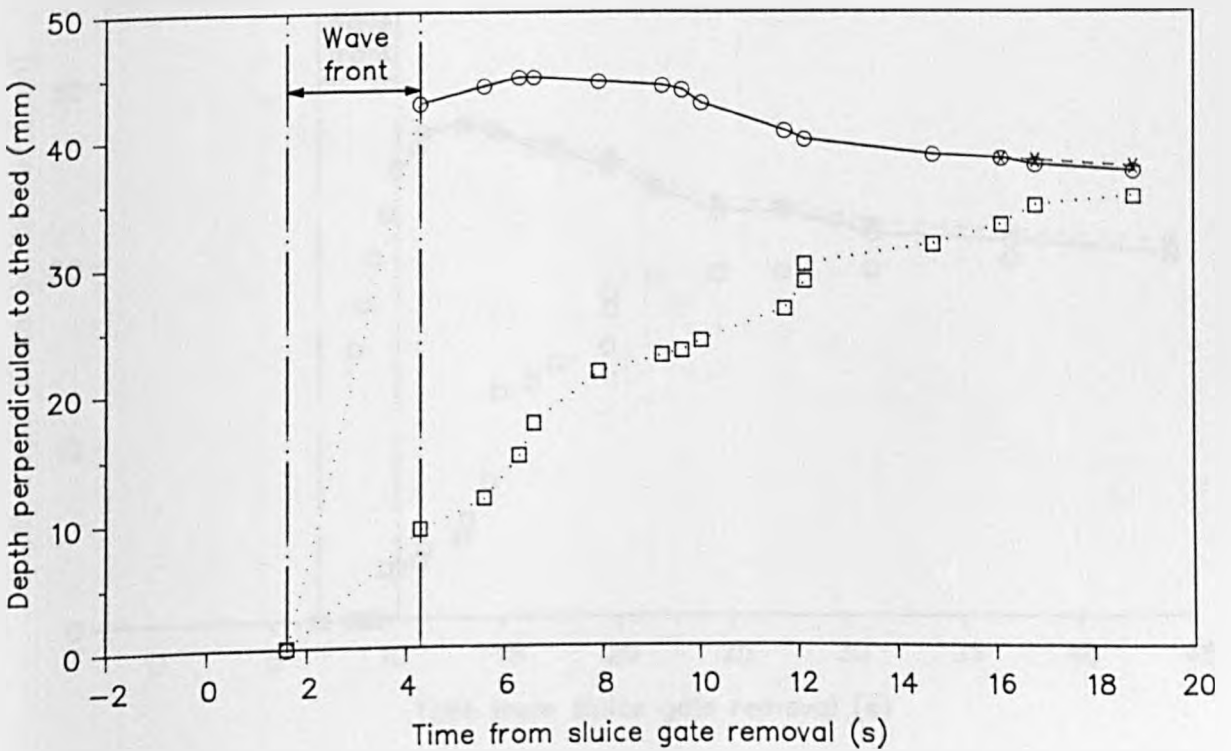


FIG 6.7 TEMPORAL VARIATION OF DEPTHS OF FLOWSLIDE MATERIAL (TEST 16S)
AT 0.5m FROM THE SLUICE GATE SITE, CHANNEL BED SLOPE = 9 DEGREES

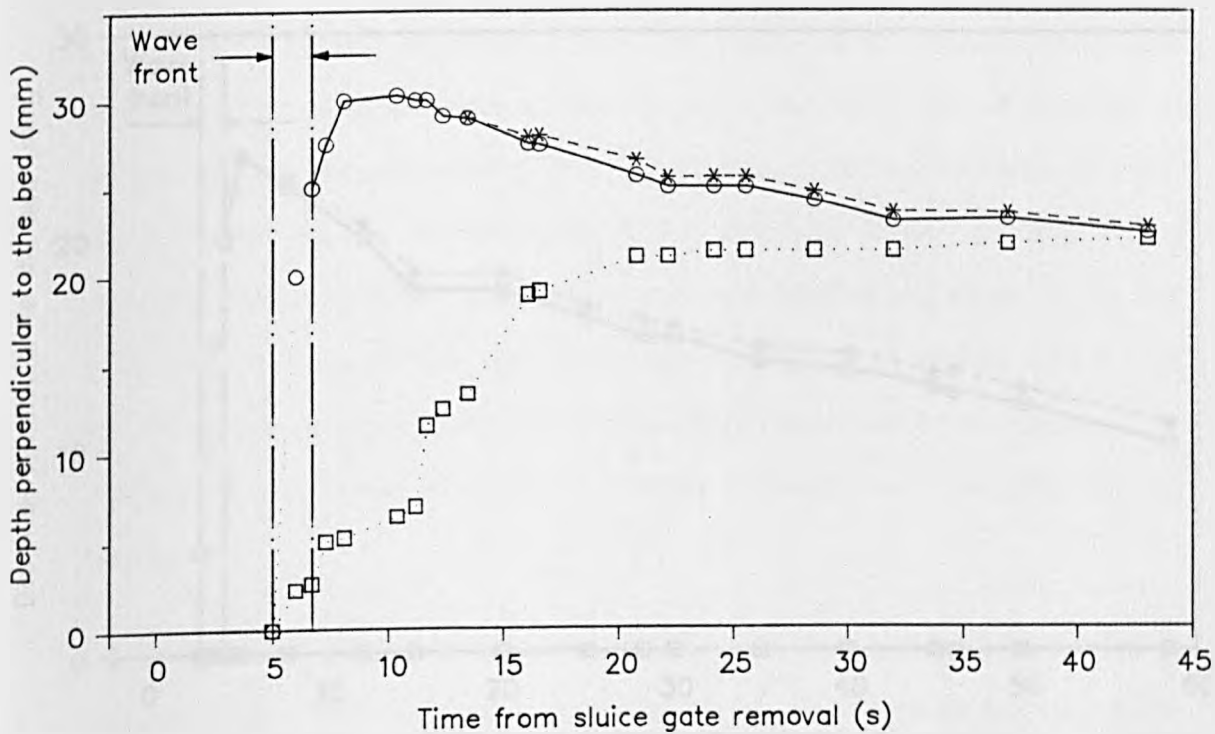


FIG 6.8 TEMPORAL VARIATION OF DEPTHS OF FLOWSLIDE MATERIAL (TEST 19S)
AT 0.5m FROM THE SLUICE GATE SITE, CHANNEL BED SLOPE = 9 DEGREES

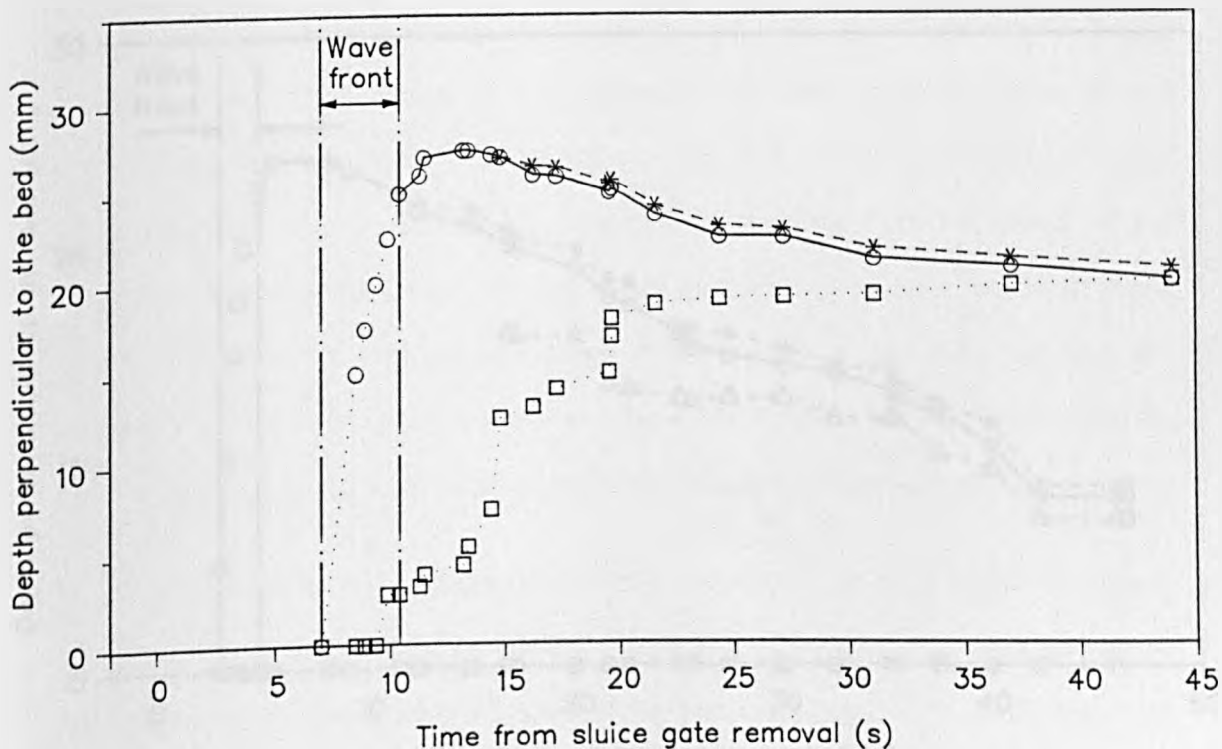


FIG 6.9 TEMPORAL VARIATION OF DEPTHS OF FLOWSLIDE MATERIAL (TEST 9S)
 AT 0.5m FROM THE SLUICE GATE SITE, CHANNEL BED SLOPE = 12 DEGREES

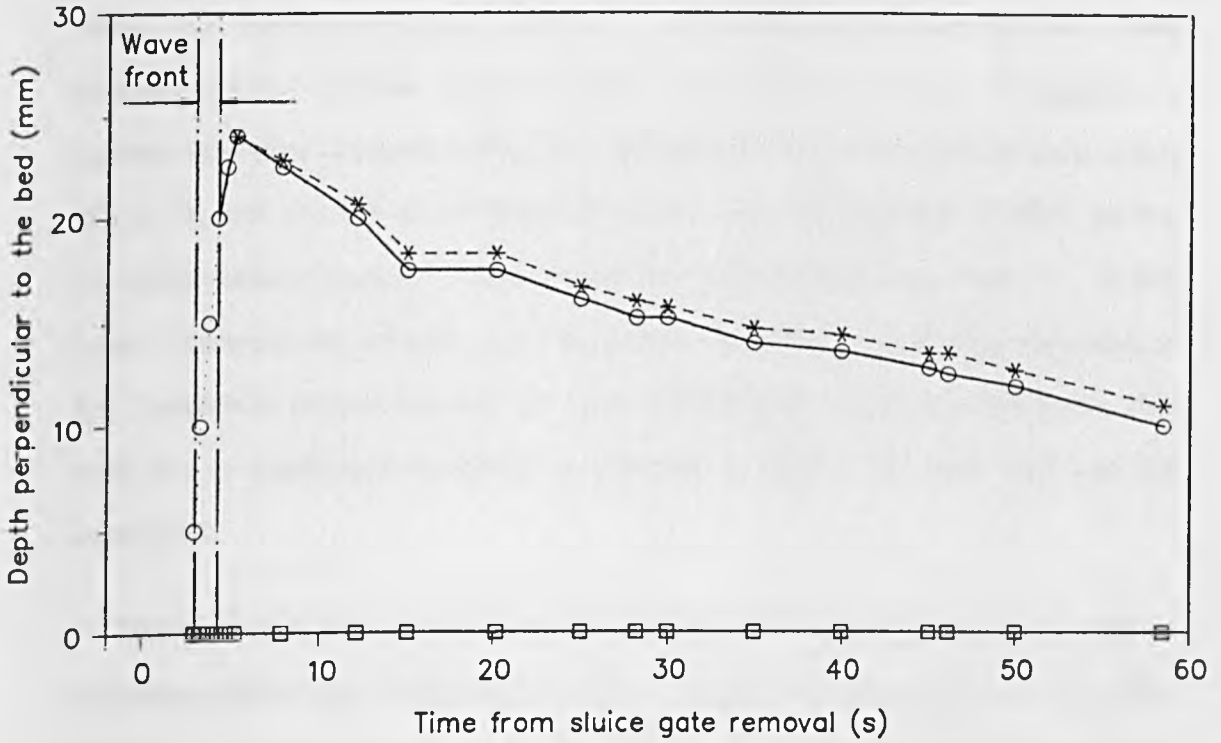
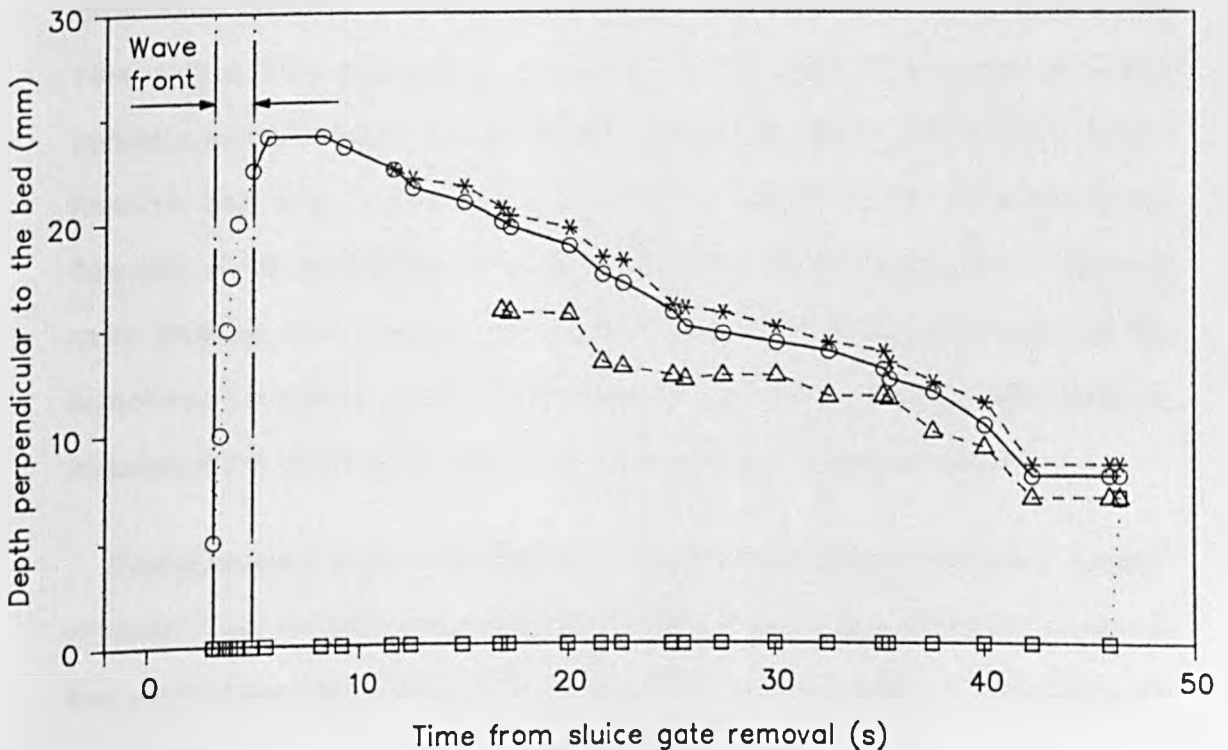


FIG 6.10 TEMPORAL VARIATION OF DEPTHS OF FLOWSLIDE MATERIAL (TEST 10S)
 AT 0.5m FROM THE SLUICE GATE SITE, CHANNEL BED SLOPE = 12 DEGREES



degrees. When the channel bed slope was equal to 6 degrees, the surface elevation of the flowing sand and water mixture remained close to its maximum value, but decreased slightly with time. This decrease in elevation was more pronounced for flowslide tests at channel bed slopes of 9 and 12 degrees. A further rapid drop occurred during Test 10S just before the flowslide came to a halt (fig 6.10), but this did not correspond to any 'tail' zone [Davies (1988)], as the flowslide surface slope, α , was greater than the channel bed slope, β , at this point. The wave transmitters used to monitor this change in surface elevation of the flowslide in conjunction with the video cameras proved to be inadequate. This was due to insufficient sensitivity to changes in depths and their use was not continued.

The temporal increase in the depth of static material at the various bed slopes and observation sites is also shown (figs 6.3–6.10). The transition from the static to the flowing layer was observed to be distinct. For channel bed slopes of 0 and 6 degrees, it was observed that a small depth of static material (approximately 2 mm) was rapidly deposited at the bed as the wave front passed. Afterwards, the static sand exhibited a variable increase in depth with time, for example, during Test 12S a 30% increase in the depth of the static layer occurred almost instantaneously at about 7 seconds after sluice gate removal [fig 6.5(a)]. For this flowslide test, after a time period of about 14 seconds from the arrival of the flowslide at the observation site, the depth of the static material then increased more steadily. At a channel bed slope of 9 degrees, it was observed that slip sometimes occurred at the channel bed for a short period initially, followed by an increase in the depth of the static layer in the manner already described.

During flowslide tests conducted at a channel bed slope of 12 degrees, a depth of about 5 mm of sand was rapidly deposited at the bed after the wave tip passed the observation site during Test 4S (data not included due to difficulties with

scaling of the elevations), whilst during Test 10S (fig 6.10) slip at the bed was observed to occur for a period of about 45 seconds.

As the flowslide passed an observation site, no water could be seen at the surface initially until a small water wave of 0.3–1 mm in depth arrived and travelled over the surface of the moving flowslide material. The velocity of the surface water seemed to be only slightly greater than that of the flowslide itself. The presence of surface water was observed in each of the tests performed, apart from a negligible depth during Test 12S (fig 6.5). The conclusions concerning the source of this surface water remained unchanged from those made previously (section 3.42). If the velocity of the surface water was greater than the velocity of particles at the top of the flowing sand and water mixture of the flowslide, it was presumed that the surface water would exert an additional shear force on the top of this flowing layer, as in the 'stream case' mode described by Bagnold (1956). This would cause an increase in velocity of the upper part of the flowing sand and water mixture. The depth affected and the velocity increase would be expected to be dependent on the shear force exerted and the shear strength of the sand and water mixture.

For the majority of flowslide tests, the influence of the surface water on the flowing sand and water mixture could not be quantified, apart from during Test 10S (fig 6.10). This was due to a large increase in the velocity of the upper part of the flowing sand and water mixture that was visually apparent. The approximate depth affected during this flowslide test was indicated by the line marked secondary shear surface, and resulted in two layers of flowing the sand and water mixture travelling at different mean velocities (fig 6.10). The slower layer gradually decelerated and came to a halt, with the depth of static material increasing rapidly after about 45 seconds from sluice gate removal. The faster layer continued to move above this static material, gradually decreasing in depth until no flow was

observed.



In flowslide tests at lower bed slopes, this phenomenon was not obvious. It was possible that in the later stages of the flowslide movement, when the surface elevation of the static material only increased slowly (generally after 15–18 seconds from the arrival of the flowslide at the observation site), the flowing sand and water mixture could have been affected by the shear force imparted by the flow of surface water. This was because the flowing sand and water mixture seemed to be travelling at a greater velocity than before. Temporal variation in vertical velocity distributions would identify the time and depth of the flowing sand and water layer affected by the shearing action of the surface water. It was not possible to gain this information using the video apparatus as attempts at measuring particle velocities were unsuccessful due to difficulty in maintaining any selected grain under visual observation.

A decrease in the depth of the static layer with time, indicating erosion of the static material by the moving material was not observed in any of these experiments. Data should generally not be inferred between the elevations of static material illustrated (figs 6.3–6.10), especially when the surface elevations of the static material are widely spaced temporally and rapid increases are observed. The increase in depth of static material (or the reduction in flow depth) with time in all these flowslide tests disprove the simplified analysis of Lucia (1981), who assumed that a flowslide was a liquefied wedge as it came to a halt.

The final run out distance of any flowslide is important with regard to the hazard it poses to both people and property downstream. Examples of the final run out distances obtained at various bed slopes are shown (figs 6.11, 6.12 & 6.13). This was observed to be dependent on several factors. An increase in the vertical height of the test sample generally resulted in a longer final run out distance (fig

FIG 6.11

SIDE ELEVATION OF SETTLED TEST SAMPLE AND CORRESPONDING FLOWSLIDE
 AFTER ALL MOVEMENT HAS CEASED, BED SLOPE = 0 DEGREES

Settled test sample	Flowslide	Surface slope of flowslide over 0.2–0.4m from sluice gate site
Test 8S		$\alpha = 5.1$ degrees
Test 15S		$\alpha = 3.9$ degrees

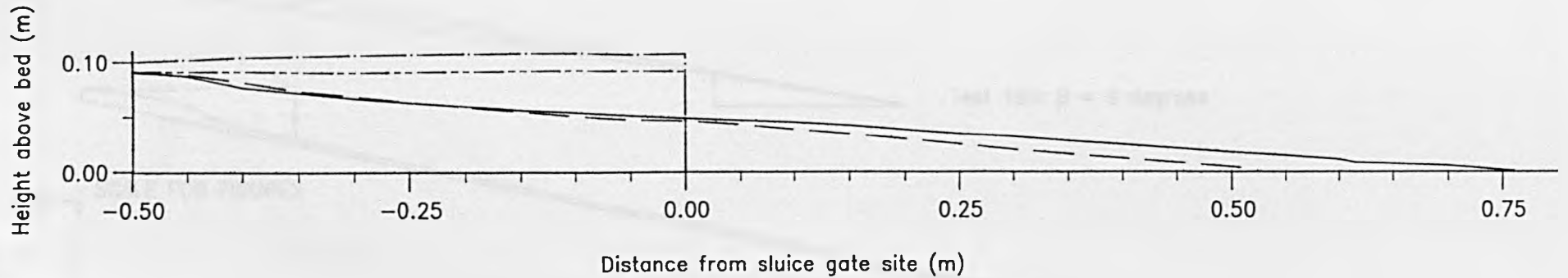


FIG 6.12

SIDE ELEVATIONS OF SETTLED TEST SAMPLE AND CORRESPONDING FLOWSLIDE
AFTER ALL MOVEMENT HAS CEASED, AT VARIOUS CHANNEL BED SLOPES

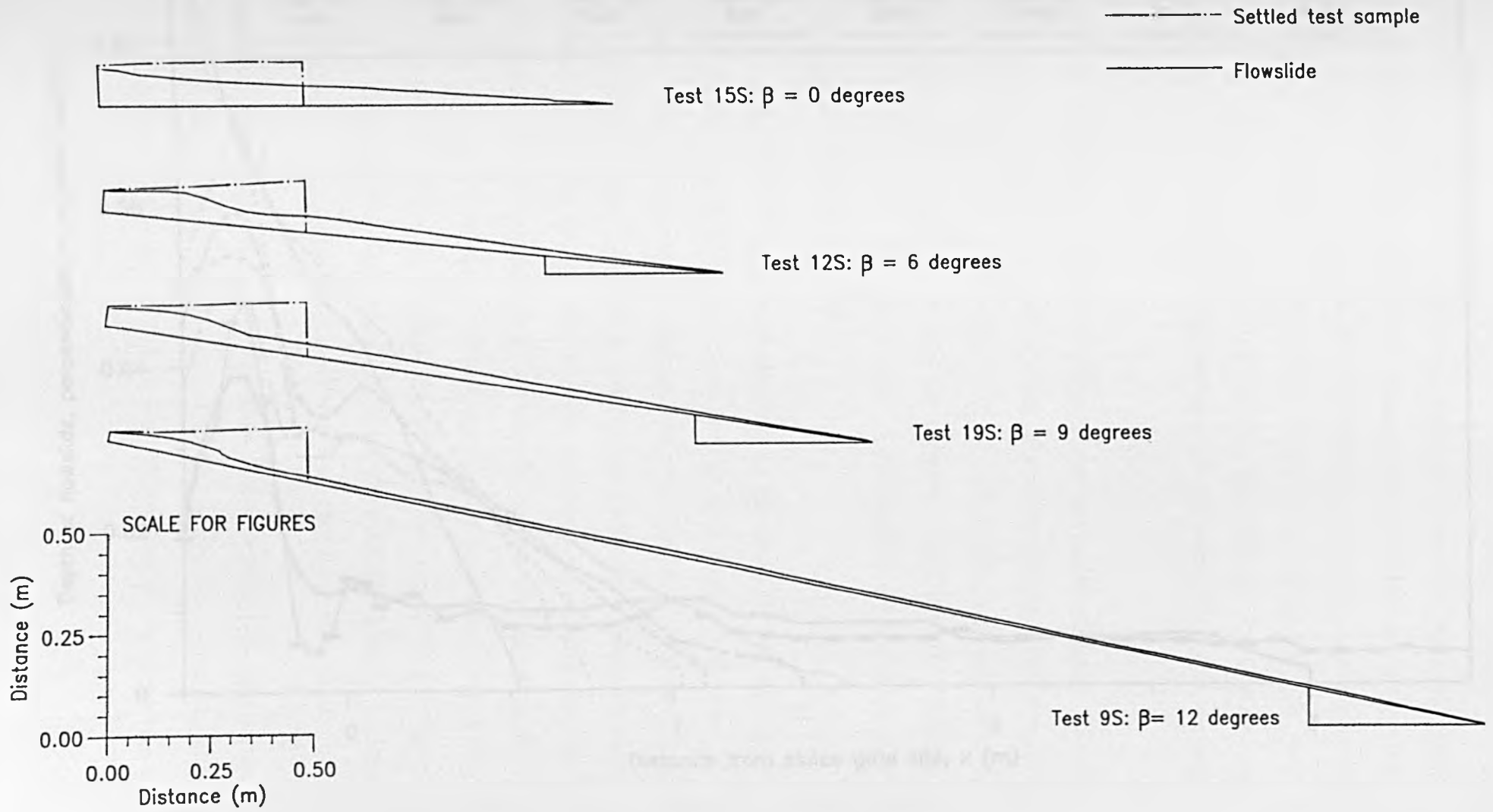
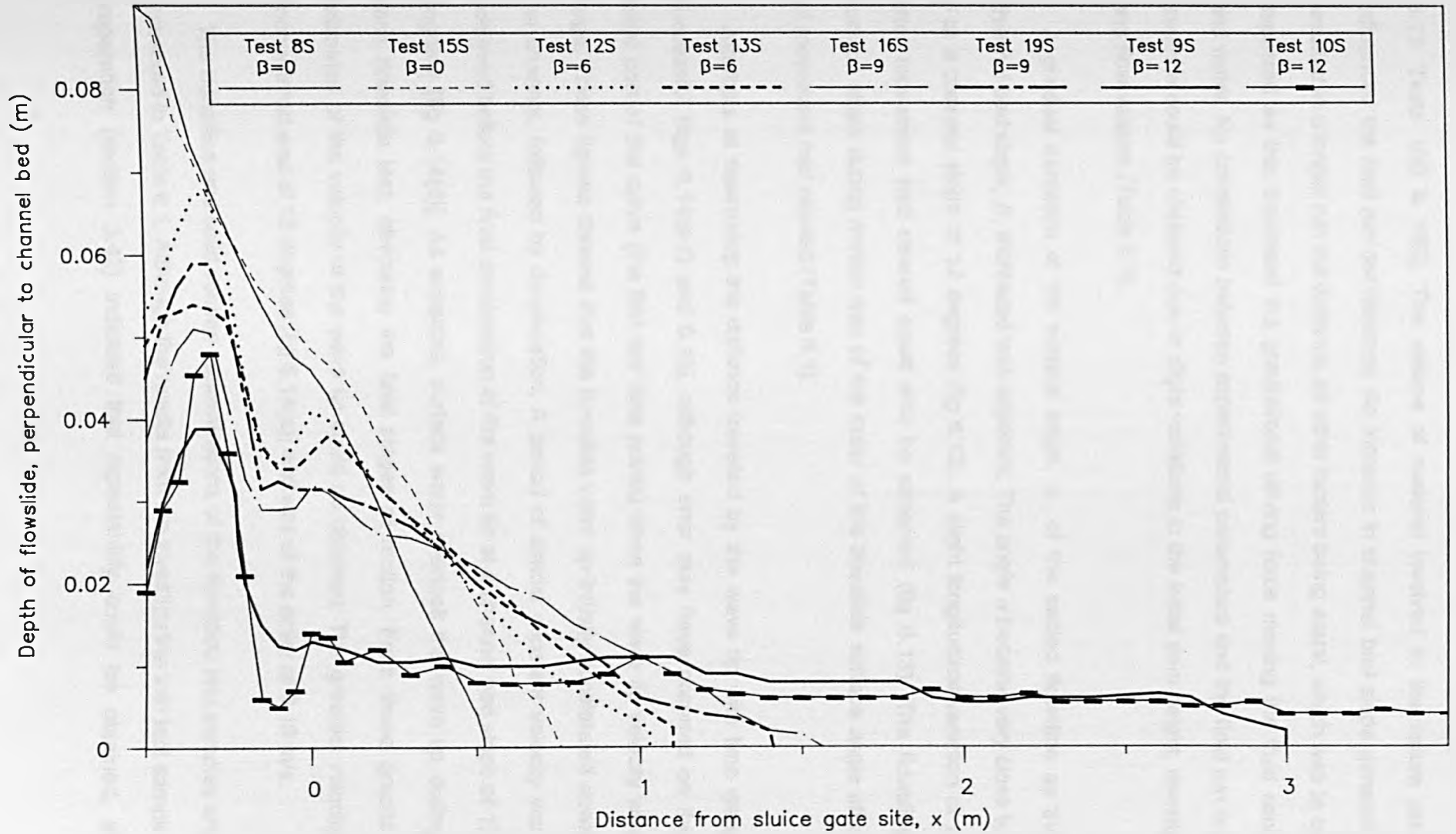


FIG 6.13

SIDE ELEVATIONS OF FLOWSLIDES AFTER ALL MOVEMENT HAS CEASED



6.13: Tests 16S & 19S). The volume of material involved in the failure also influenced the final run out distance. An increase in channel bed slope generally resulted in a longer run out distance, all other factors being equal, which was to be expected as this increased the gravitational driving force moving the fluid sand and water. No correlations between experimental parameters and the final run out distance could be obtained due to slight variations in the initial dam height, density and flow volume (Table 6.1).

A gradual decrease of the surface angle, α , of the settled flowslide as the channel bed slope, β , increased was apparent. The angle α became very close to β at a channel slope of 12 degrees (fig 6.13). A slight longitudinal variation of α after movement had ceased could also be observed (fig 6.13). The flowslide surface slope during motion was of the order of the flowslide surface angle after all movement had ceased (Table 6.1).

Attempts at measuring the distance travelled by the wave tip with time were successful [figs 6.14(a-d) and 6.15], although error may have occurred on the initial part of the curve (the first few data points) when the wave tip velocity was large. These figures showed that the flowslide wave tip initially accelerated down the channel, followed by deceleration. A period of almost constant velocity was achieved before the final deceleration of the wave tip at a channel bed slope of 12 degrees [fig 6.14(d)]. As expected, surface water overtook the wave tip during each flowslide test, obscuring the final stages of motion. From these graphs, estimates of the velocity of the wave tip could be obtained. The greatest velocity encountered was at 12 degrees [fig 6.14(e)] and was of the order of 0.16 m/s.

The densities and solid volume concentrations of the flowslide test samples are presented in Table 6.1. Although the results from the investigation into test sample preparation (section 3.42) indicated that repeatability could be obtained, in

TABLE 6.1

EXPERIMENTAL DATA FROM THE SECOND SERIES OF FLOWSLIDE TESTS

Flowslide test	8S	15S	12S	13S	16S	19S	9S	10S
H_d (m)	0.091	0.107	0.126	0.126	0.140	0.135	0.133	0.137
V_t ($\times 10^{-6} \text{ m}^3$)	4580	5320	4502	4524	4534	4544	3827	3793
Initial C	0.479	0.481	0.490	0.486	0.485	0.485	0.487	0.481
Initial ρ_{sat} (kg/m^3)	1819	1824	1837	1830	1829	1829	1818	1823
Final C x (m) % change	—	—	—	0.475 0.1 → 1 -2.2%	0.497 0.1 → 0.8 2.5%	0.472 0.2 → 0.9 -2.7%	—	0.480 0.5 → 2.5 -0.2%
Final ρ_{sat} x (m) % change	—	—	—	1812 0.1 → 1 -1.0%	1849 0.1 → 0.8 1.1%	1807 0.2 → 0.9 -1.2%	—	1821 0.5 → 2.5 -0.1%
Channel bed slope, β (degrees)	0	0	6	6	9	9	12	12
Slope of flowslide surface, α (degrees) x (m)	4.5 0.3 → 0.5	4.1 0.3 → 0.5	9.9 0.3 → 0.5	7.9 0.3 → 0.5	9.6 0.3 → 0.5	11.0 0.3 → 0.5	12.1 0.3 → 0.5	12.3 0.3 → 0.5
Run out distance, x (m)	0.52	0.76	1.03	1.10	1.56	1.41	3.00	> 3.5

H_d = vertical height of test sample at sluice gate site

V_t = volume of test sample

x = longitudinal distance from sluice gate site

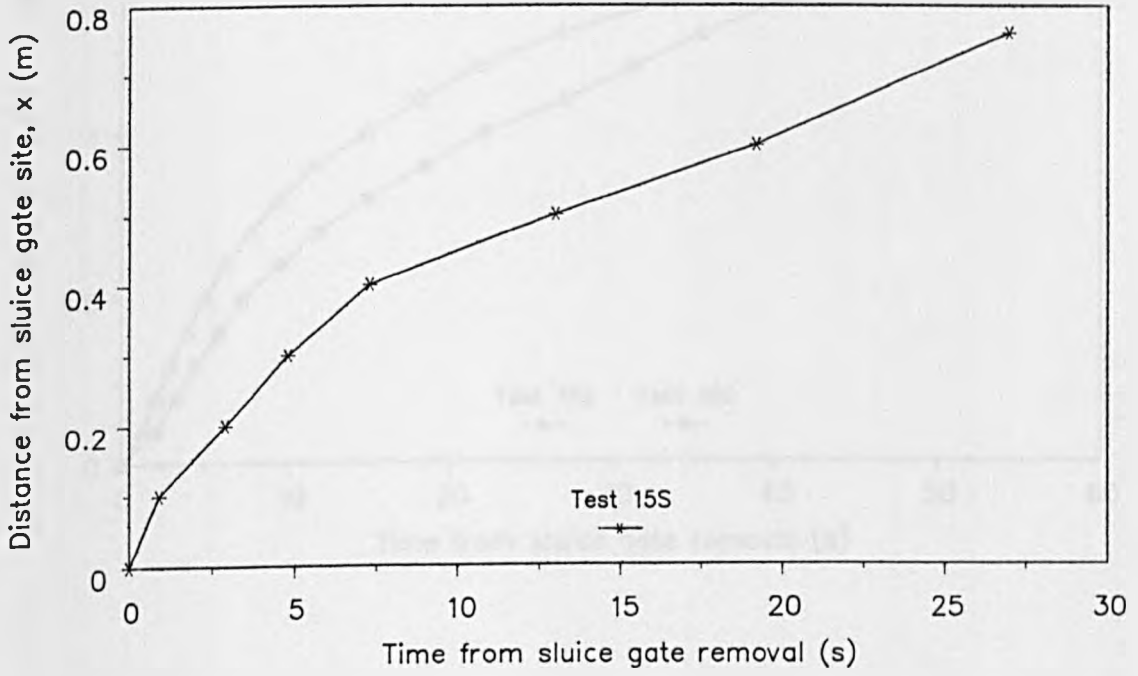
C = solid volume concentration

ρ_{sat} = saturated bulk density of sand

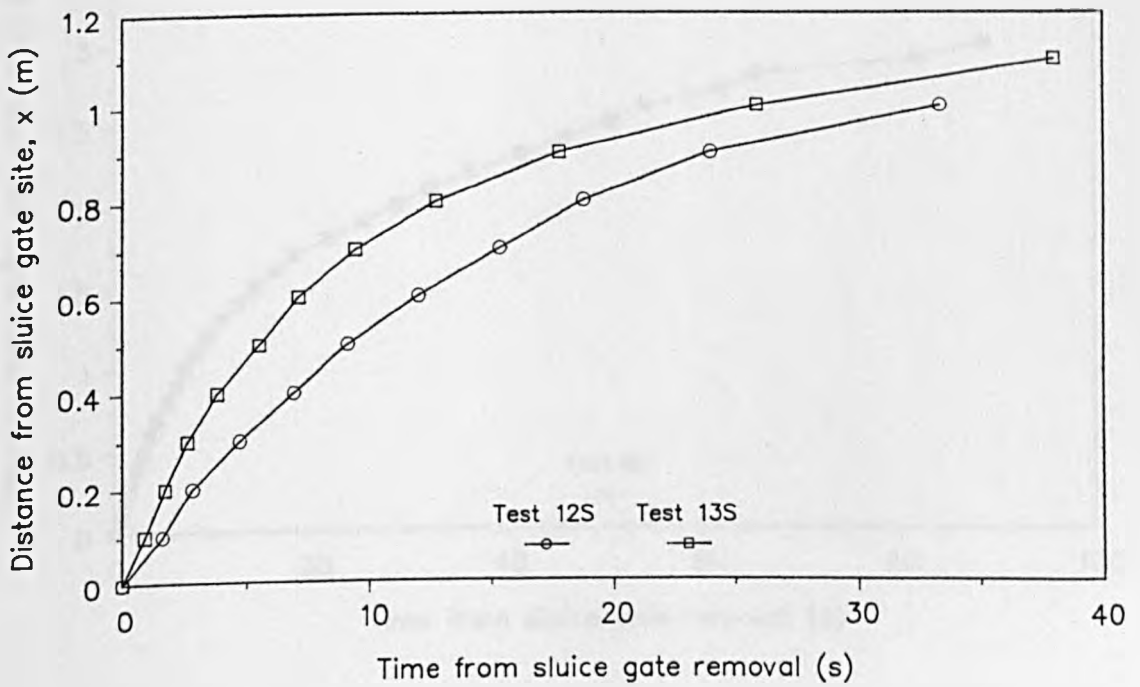
FIG 6.14

LONGITUDINAL VARIATION OF FLOWSLIDE WAVE TIP WITH TIME FOR TESTS AT DIFFERENT CHANNEL BED SLOPES

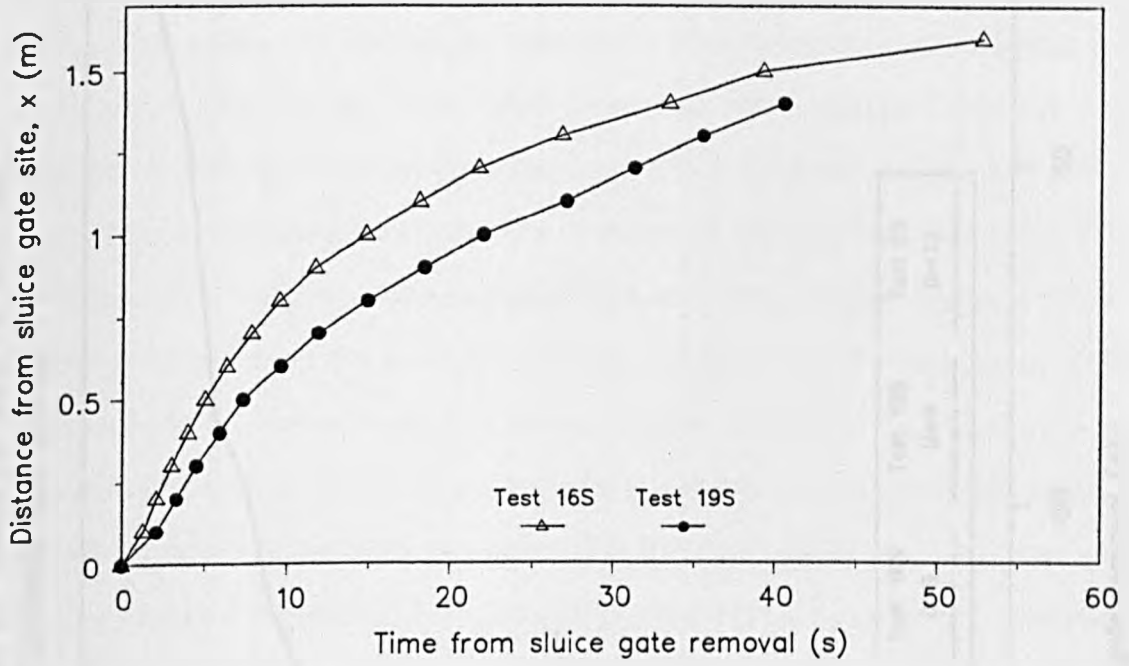
a) Channel bed slope = 0 degrees



b) Channel bed slope = 6 degrees



c) Channel bed slope = 9 degrees



d) Channel bed slope = 12 degrees

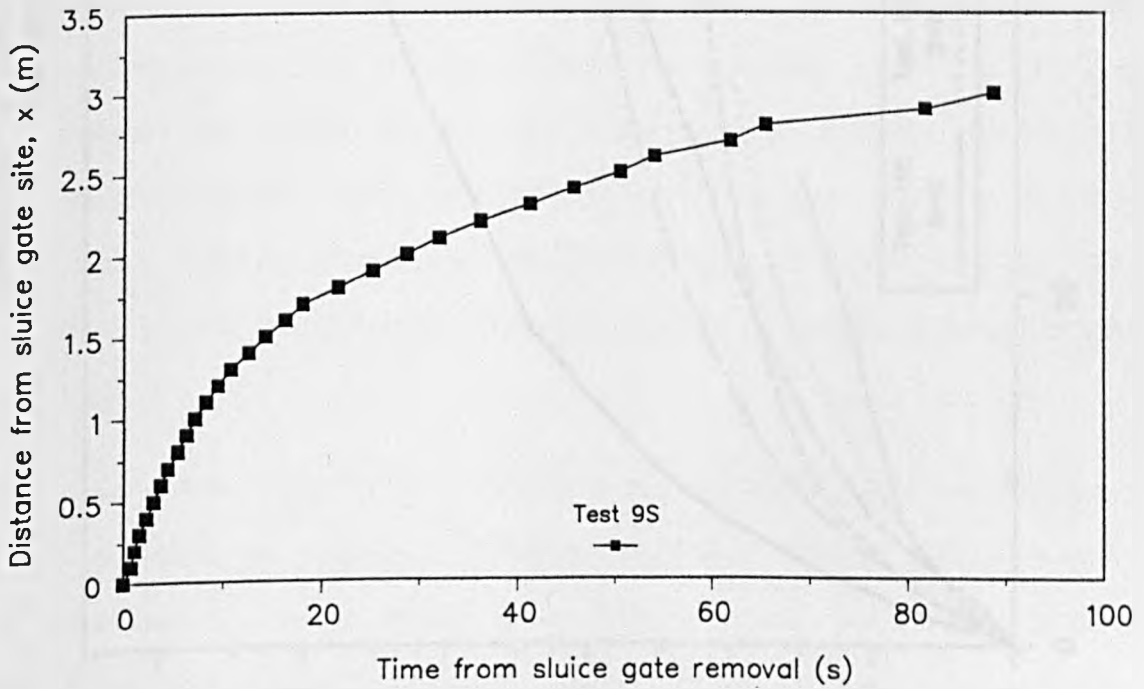
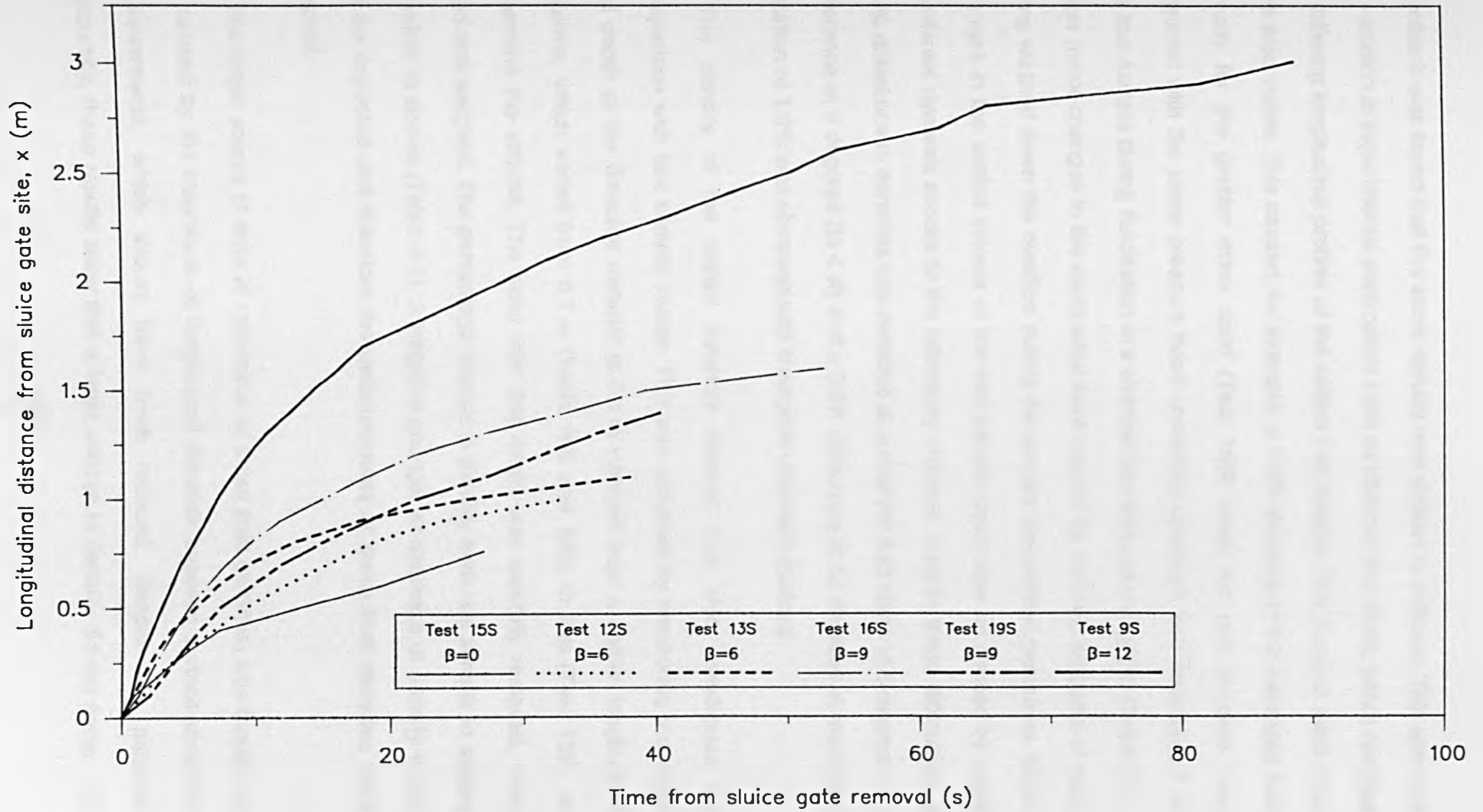


FIG 6.15

COMPARISON OF LONGITUDINAL VARIATION OF FLOWSLIDE WAVE TIP WITH TIME
FOR TESTS AT DIFFERENT CHANNEL BED SLOPES



practice it was found that the same density was difficult to achieve. This was due to variation in experimental parameters such as channel bed slope, which resulted in differing longitudinal profiles of the settled test sample. The mass of sand used was also varied. This caused, for example, a 0.3% increase in the saturated bulk density for the greater mass used (Test 15S) when the test samples were prepared with the same pressure head conditions upstream and downstream of the test sample during fluidisation at a channel bed slope of 0 degrees (Table 6.1). Other minor changes in the mass used were caused by differing amounts of sand being washed down the overflow during the sample preparation procedure. Minor changes in the settled volume of the test sample could also be caused by small accidental dynamic shocks to the laboratory channel. Despite these difficulties, a 0.4% difference in densities was detected at a channel bed slope of 6 degrees, no difference at 9 degrees (to 4 sf) and a 0.3% difference at 12 degrees. A maximum variation of 1.0% was observed with change in channel bed slope.

The density of the settled flowslide material was also investigated for comparison with test sample values. This was achieved by measuring the width and depth of the flowslide material at 0.1 m intervals over a certain longitudinal distance, which varied from 0.7 m (Tests 16S and 19S) to 2 m (Test 13S), to determine the volume. The sand over this length was carefully removed, oven dried and weighed. The percentage change in density from test sample to settled flowslide is shown (Table 6.1). A negative change, or decrease in density would not be expected and therefore the measurements of these final densities were suspect.

The major source of error in calculation of these final densities was thought to be caused by the magnitude of longitudinal distance between surface elevation measurements, which should have been reduced. Despite the potential inaccuracy, these results show that a large change in density did not occur. The

1.1% increase in density (Test 16S) or 2.3% decrease in porosity was within the maximum decrease in porosity of 3% that has occurred during subaqueous flowslide experiments when the sand and water mixture changed from a fluid to a static state [Bezuijen/Mastbergen (1988)].

The small difference between the initial and the approximate final bulk densities meant that the assumption of the saturated bulk density of the test sample being equal to that of the flowing material remained sensible. Bagnold (1954) suggested that dilatation of the grains, or a decrease in the bulk density of the flowing material may occur during shear, or more specifically during accelerations. Some dilatation of the grains may have occurred when the surface water was observed to have a marked influence on the velocity of the flowing layer (section 5.42), but this could not be quantified.

The sand was in a very loose state prior to failure in soil mechanics terms. In the context of the granular fluids, the bulk densities or solid volume concentrations were high (Table 6.1) and close to that value at which the flow would be expected to 'freeze' [$C = 0.5$: Bagnold (1955)]. At this solid volume concentration, further motion was only observed to continue by the process of sliding rather than flow, with the granular material being pushed bodily along the channel [Bagnold (1955)].

Although the sand and water mixture was taken to be fully saturated, a number of small air bubbles were detected at the channel wall from the video records. These bubbles were not dislodged from within the sand mass during test sample preparation, even though the fluidised sand was stirred repeatedly. Due to their small number, it was assumed that these air bubbles were of negligible importance to the value of the bulk density. Their presence did not seem to affect flowslide motion and they remained trapped within the flowing sand and water mixture, with some very slight upward motion with time sometimes being observed.

6.3 COMPARISON OF MEASURED AND CALCULATED PORE WATER PRESSURES

Comparison of the measured and calculated pore water pressure was restricted until after the passage of the wave front. This was due to the uncertainty regarding the position of the flowing layer's surface in this region (section 6.2). The possibility of noise from the sluice gate removal (fig 4.9) adversely affecting the pressure transducer output was considered, but the time at which the end of the wave front occurred was the dominant factor.

For the flowslide tests at a channel bed slope of 0 degrees, only three calculated pore water pressures were shown (figs 6.17 and 6.18) as the predicted and maximum total pore water pressures were equal at this bed slope. It can be seen that the measured pore water pressure was less than the predicted total value for approximately 4 seconds after sluice gate removal. After this point, the measured pore water pressure was greater than the predicted total value until the flow ceased in both tests. The measured pore water pressure was much greater than the minimum total pore water pressure, indicating that excess pore water pressures were definitely present during the motion of the flowslide.

For Test 12S, performed at a channel bed slope of 6 degrees, the predicted total pore water pressure was greater than the measured pore water pressure for a period of about 5 seconds after the arrival of the flowslide at the observation site (fig 6.19). After this time, the predicted total pore water pressure was close to the measured value. The difference in magnitude between each of the calculated total pore water pressures decreased with increase in time due to the reduction in depth of flowing material (fig 6.5). The results for Test 13S (fig 6.20) showed similar trends to the those discussed for Test 12S (fig 6.19). These tests also provided positive evidence that the excess pore water pressures were present

FIG 6.16

LEGEND FOR FIGURES 6.17-6.24


	Measured pore water pressure, u_{expt} (kPa)
∇	Maximum total pore water pressure, $u_{t,\text{max}}$ (kPa)
\diamond	Predicted total pore water pressure, $u_{t,\text{pred}}$ (kPa)
Δ	Minimum total pore water pressure, $u_{t,\text{min}}$ (kPa)
+	Pore water pressure contribution to total pore water pressure from the static material, u_s (kPa)

FIG 6.17 MEASURED AND CALCULATED PORE WATER PRESSURES (TEST 8S)
 AT 0.1m FROM THE SLUICE GATE SITE, CHANNEL BED SLOPE = 0 DEGREES

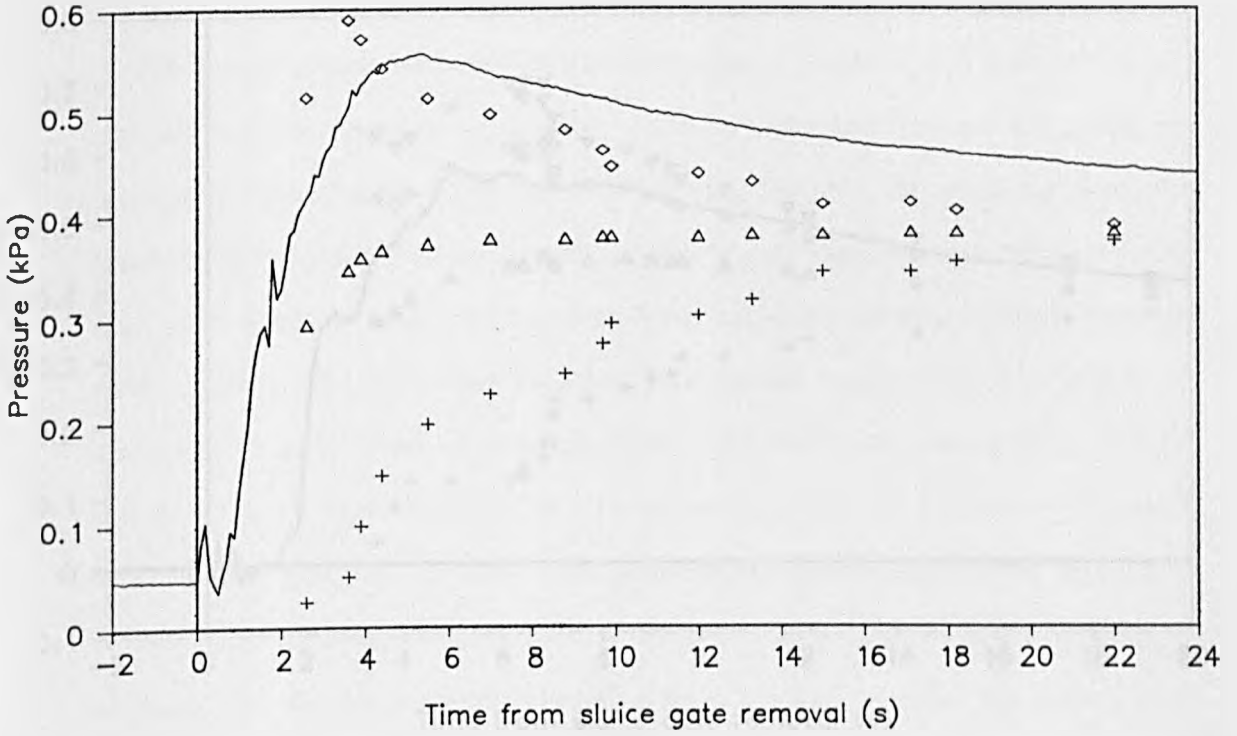


FIG 6.18 MEASURED AND CALCULATED PORE WATER PRESSURES (TEST 15S)
 AT 0.1m FROM THE SLUICE GATE SITE, CHANNEL BED SLOPE = 0 DEGREES

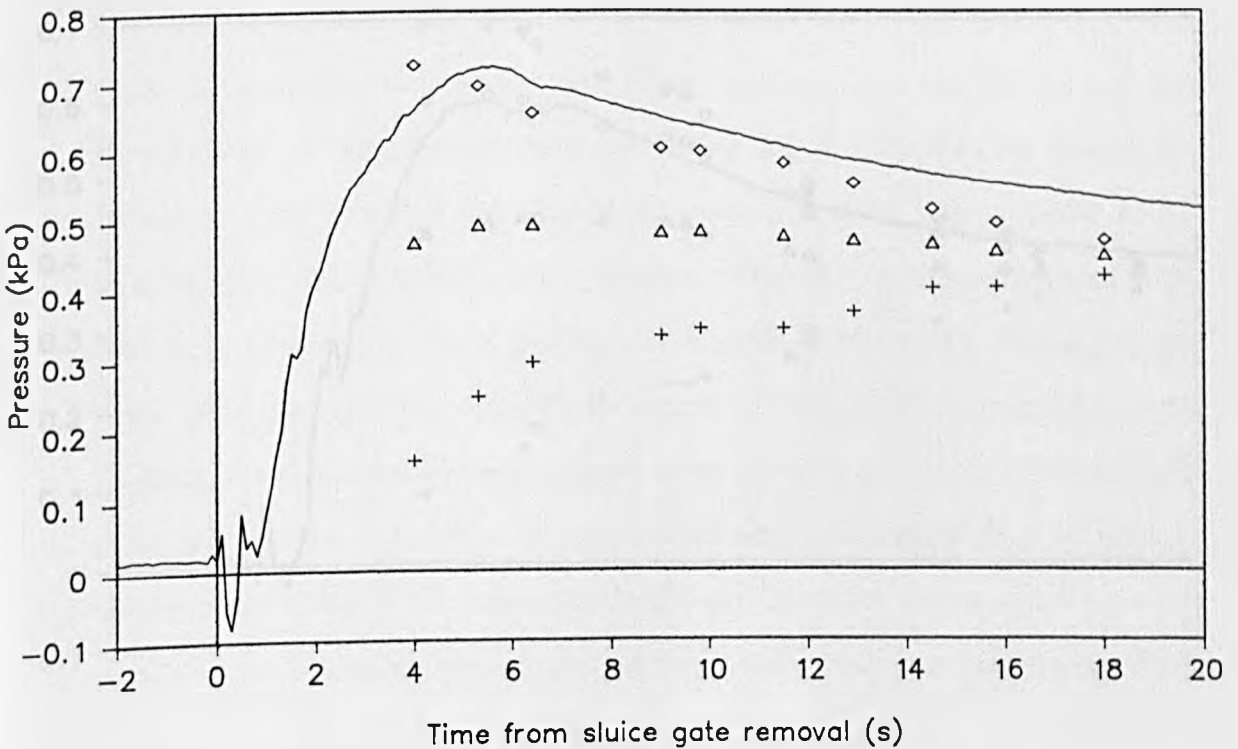


FIG 6.19 MEASURED AND CALCULATED PORE WATER PRESSURES (TEST 12S)
 AT 0.1m FROM THE SLUICE GATE SITE, CHANNEL BED SLOPE = 6 DEGREES

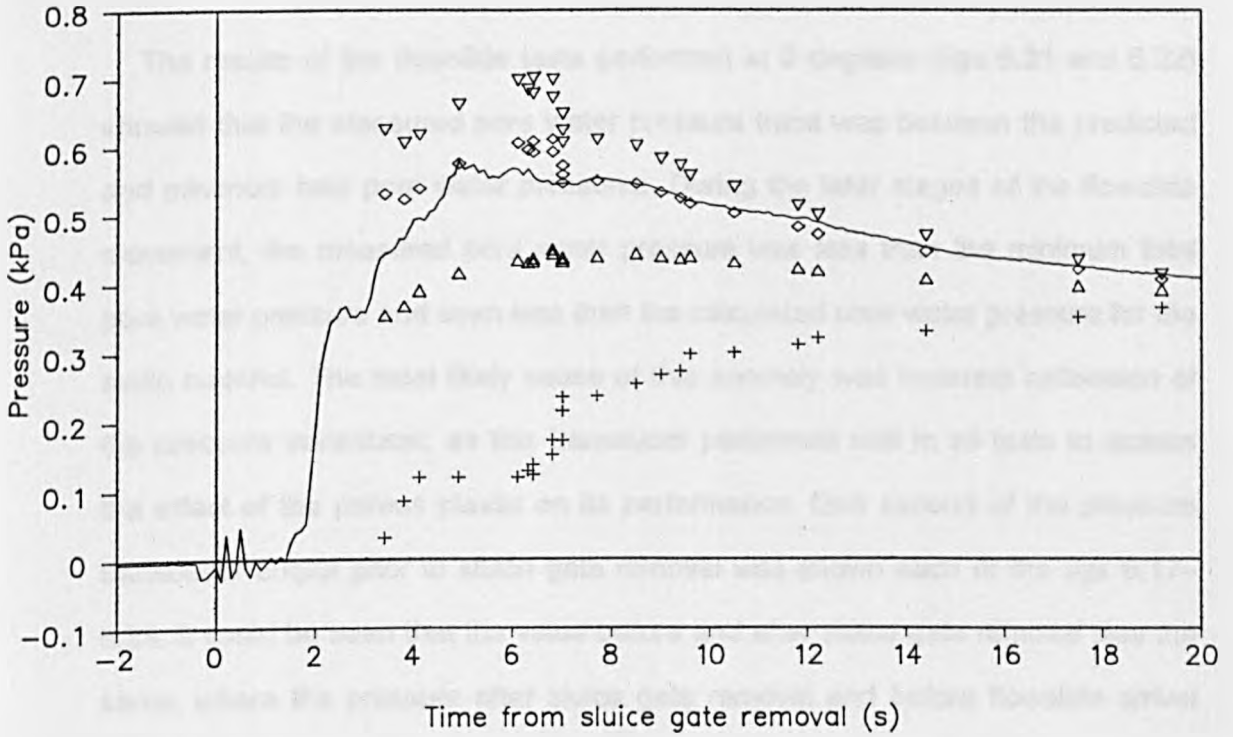
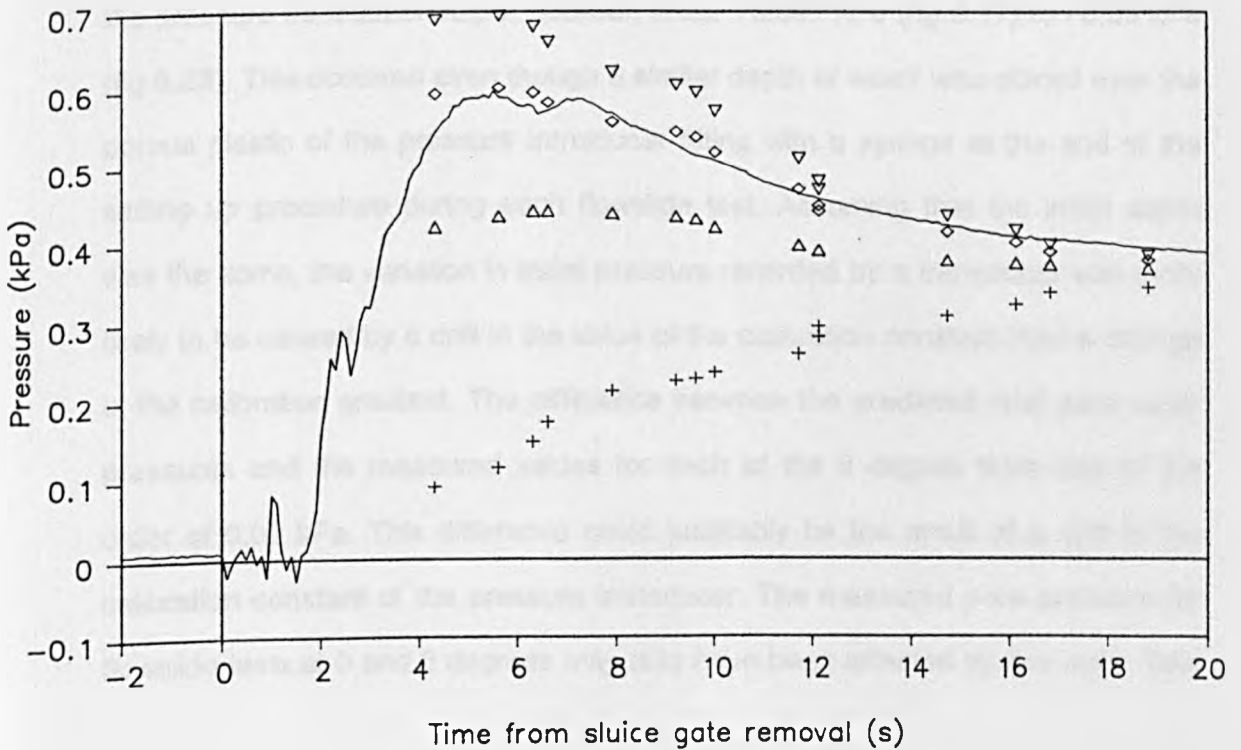


FIG 6.20 MEASURED AND CALCULATED PORE WATER PRESSURES (TEST 13S)
 AT 0.1m FROM THE SLUICE GATE SITE, CHANNEL BED SLOPE = 6 DEGREES



during the motion of the flowslide. The predicted total pore water pressures were closer to the measured values at 6 degrees than at 0 degrees.

The results of the flowslide tests performed at 9 degrees (figs 6.21 and 6.22) showed that the measured pore water pressure trace was between the predicted and minimum total pore water pressures. During the later stages of the flowslide movement, the measured pore water pressure was less than the minimum total pore water pressure and even less than the calculated pore water pressure for the static material. The most likely cause of this anomaly was incorrect calibration of the pressure transducer, as this transducer performed well in all tests to assess the effect of the porous plastic on its performance. One second of the pressure transducer output prior to sluice gate removal was shown each of the figs 6.17–6.24. It could be seen that the value before and after sluice gate removal was the same, where the pressure after sluice gate removal and before flowslide arrival could be determined (figs 6.21-6.24). The effect of the shock of the sluice gate removal on the pressure transducers could therefore be excluded in these cases. What was revealed was that there was a substantial variation in the initial value of the pressure transducer output between tests, +0.047 kPa (fig 6.17) to –0.05 kPa (fig 6.23). This occurred even though a similar depth of water was placed over the porous plastic of the pressure transducer fitting with a syringe at the end of the setting up procedure during each flowslide test. Assuming that the initial depth was the same, the variation in initial pressure recorded by a transducer was more likely to be caused by a drift in the value of the calibration constant than a change in the calibration gradient. The difference between the predicted total pore water pressures and the measured values for each of the 9 degree tests was of the order of 0.02 kPa. This difference could justifiably be the result of a drift in the calibration constant of the pressure transducer. The measured pore pressure for flowslide tests at 0 and 6 degrees may also have been affected by this error. Test

FIG 6.21 MEASURED AND CALCULATED PORE WATER PRESSURES (TEST 16S)
 AT 0.5m FROM THE SLUICE GATE SITE, CHANNEL BED SLOPE = 9 DEGREES

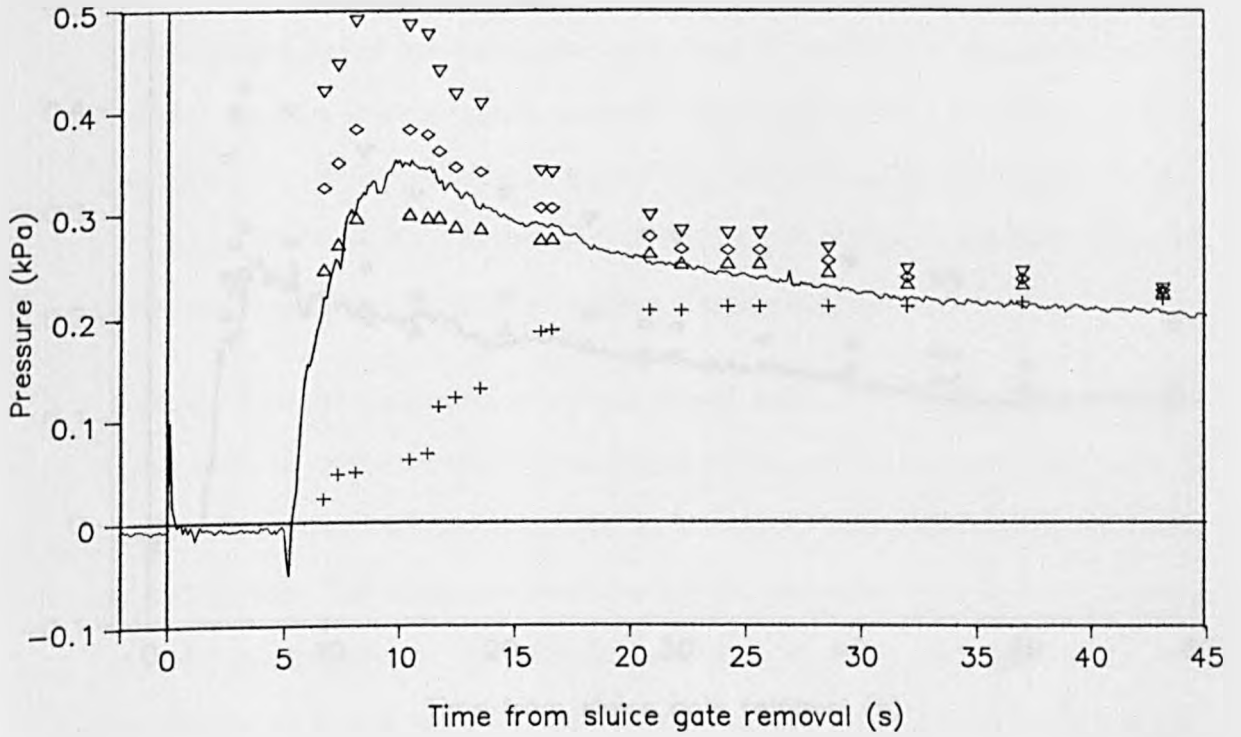


FIG 6.22 MEASURED AND CALCULATED PORE WATER PRESSURES (TEST 19S)
 AT 0.5m FROM THE SLUICE GATE SITE, CHANNEL BED SLOPE = 9 DEGREES

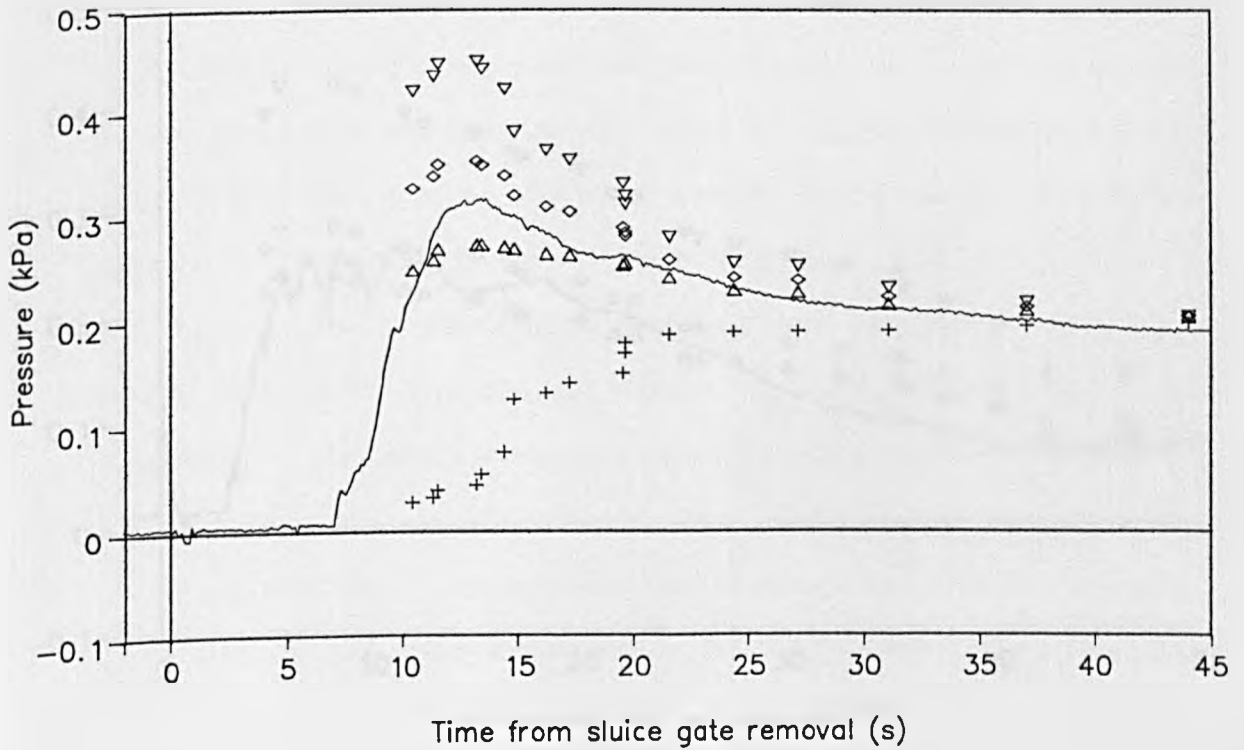


FIG 6.23 MEASURED AND CALCULATED PORE WATER PRESSURES (TEST 9S)
 AT 0.5m FROM THE SLUICE GATE SITE, CHANNEL BED SLOPE = 12 DEGREES

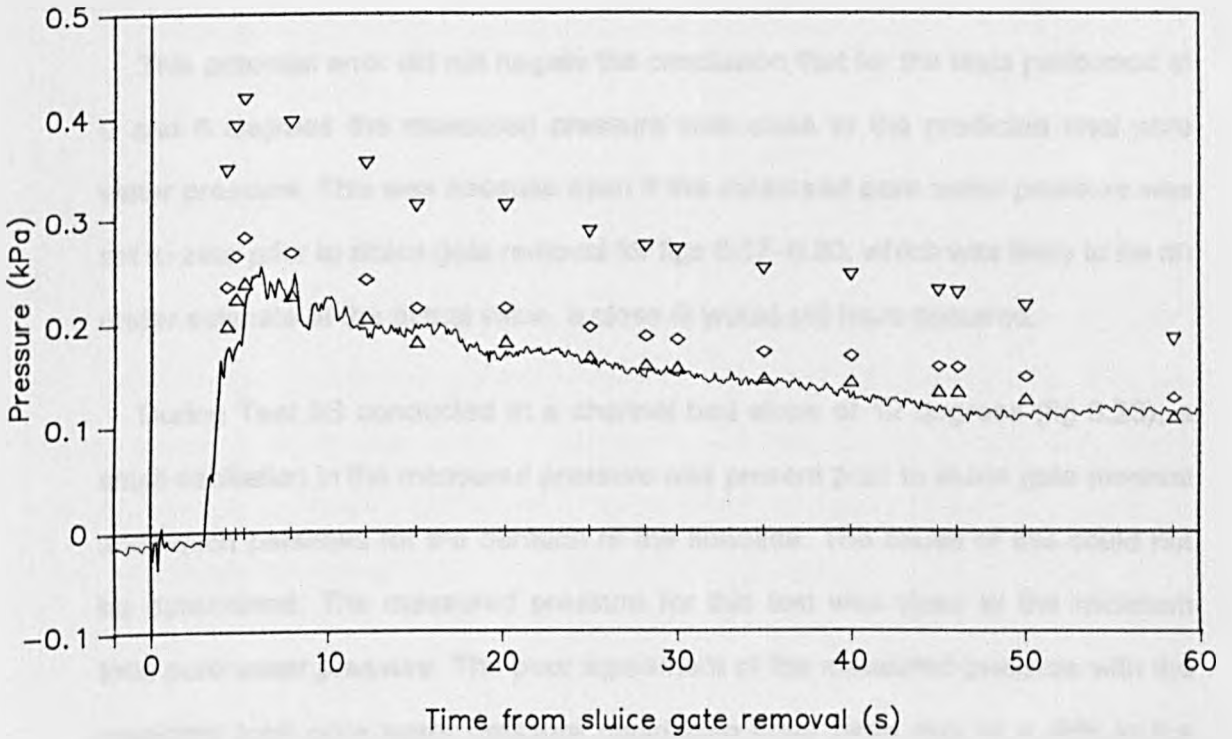
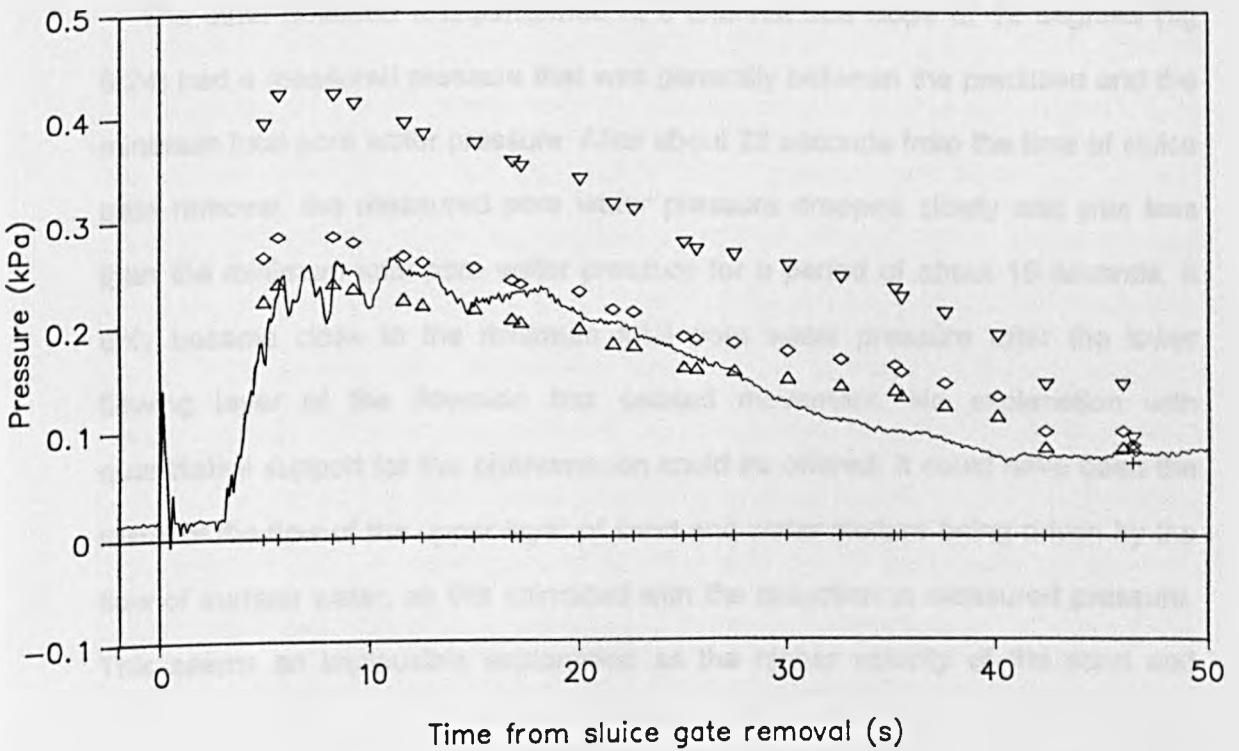


FIG 6.24 MEASURED AND CALCULATED PORE WATER PRESSURES (TEST 10S)
 AT 0.5m FROM THE SLUICE GATE SITE, CHANNEL BED SLOPE = 12 DEGREES



8S (fig 6.17) was particularly suspect as the measured pore water pressure was relatively high prior to sluice gate removal.

This potential error did not negate the conclusion that for the tests performed at 0 and 6 degrees the measured pressure was close to the predicted total pore water pressure. This was because even if the measured pore water pressure was set to zero prior to sluice gate removal for figs 6.17–6.20, which was likely to be an under estimate of the actual value, a close fit would still have occurred.

During Test 9S conducted at a channel bed slope of 12 degrees (fig 6.23), a small oscillation in the measured pressure was present prior to sluice gate removal and which persisted for the duration of the flowslide. The cause of this could not be determined. The measured pressure for this test was close to the minimum total pore water pressure. The poor agreement of the measured pressure with the predicted total pore water pressure could also have been due to a drift in the calibration constant, as a negative value of the measured pore water pressure was observed prior to sluice gate removal.

The other flowslide test performed at a channel bed slope of 12 degrees (fig 6.24) had a measured pressure that was generally between the predicted and the minimum total pore water pressure. After about 23 seconds from the time of sluice gate removal, the measured pore water pressure dropped slowly and was less than the minimum total pore water pressure for a period of about 15 seconds. It only became close to the minimum total pore water pressure after the lower flowing layer of the flowslide has ceased movement. No explanation with quantitative support for this phenomenon could be offered. It could have been the result of the flow of the upper layer of sand and water mixture being driven by the flow of surface water, as this coincided with the reduction in measured pressure. This seems an implausible explanation as the higher velocity of the sand and

water mixture would have been extremely unlikely to reduce the measured pore water pressure below that of the minimum total pore water pressure. Instability or incorrect calibration of the pressure transducer may also have been causes.

A further point that may have had some influence was that when sliding or flow directly over the channel bed occurred, the effective angle of friction used in calculation of the total pore water pressures should have been altered from the steady or critical state value to an angle of friction that represented the roughness between the sand grains and the perspex bed [Augenstein/Hogg (1974)]. This was not performed for this series of flowslide tests due to the general uncertainty concerning the correct calibration of the pressure transducers and the difficulty in obtaining a correct value for this angle of friction [Augenstein/Hogg (1978)].

Further errors in analysis may have been resulted from the fact that two stipulations in calculation of the predicted basal pore water pressure (equation 5.2) were that the forces on either side of the slice of the vertical element of flowing material under consideration were equal and that the mean flow velocity was constant. Equal forces on either side of the slice would occur if the slope of the flowing sand surface, α , was the same as the slip surface slope, β . Measurement of the latter was not practicable with the equipment available and therefore it was still assumed that this value was equal to the channel bed slope, β_b . For low channel bed slopes it has already been established that the flowslide surface slope, α , was greater than the bed slope and the difference between these two values decreased with increasing bed slope (section 6.2). In addition, measurements of the various depths of the flowslide were made normal to the bed and the influence of α being greater than β may have caused under estimation of the vertical height. Accelerations of the flowslide would be impossible to avoid completely in this type of flowslide test, but records of the temporal variation of the flowslide wave tip's position [figs 6.14(a)–(d)] showed that the time period at which

accelerations were small increased with increase in channel bed slope.

6.4 CONCLUSIONS

The results of this series of flowslide tests were encouraging as the measured pore water pressures were close to the predicted values at channel bed slopes of 0 and 6 degrees. This was despite potential errors due to calibration of the transducers, measurement of normal rather than vertical depths of flowslide material, accelerations and the flowslide surface slope. A third series of flowslide tests was therefore proposed to validate these initially promising results. The flowslide depths were subsequently to be measured vertically. As additional laboratory equipment became available for further instrumentation of the experimental apparatus it was possible to investigate:

a) the calibration of the pressure transducers and its effect on the comparison of the measured and calculated pore water pressures

b) whether any horizontal and vertical velocity profile could be obtained by the introduction of tracer particles into the flowslide to obtain more information concerning the acceleration of the flowslide

c) the temporal variation in the surface angle, α , of the moving flowslide

d) the correlation between comparisons of the measured and calculated pore water pressures at three longitudinal distances during one flowslide experiment.

CHAPTER 7:

FURTHER INSTRUMENTATION

7.1 PRESSURE TRANSDUCERS AND PRE-TEST CALIBRATION

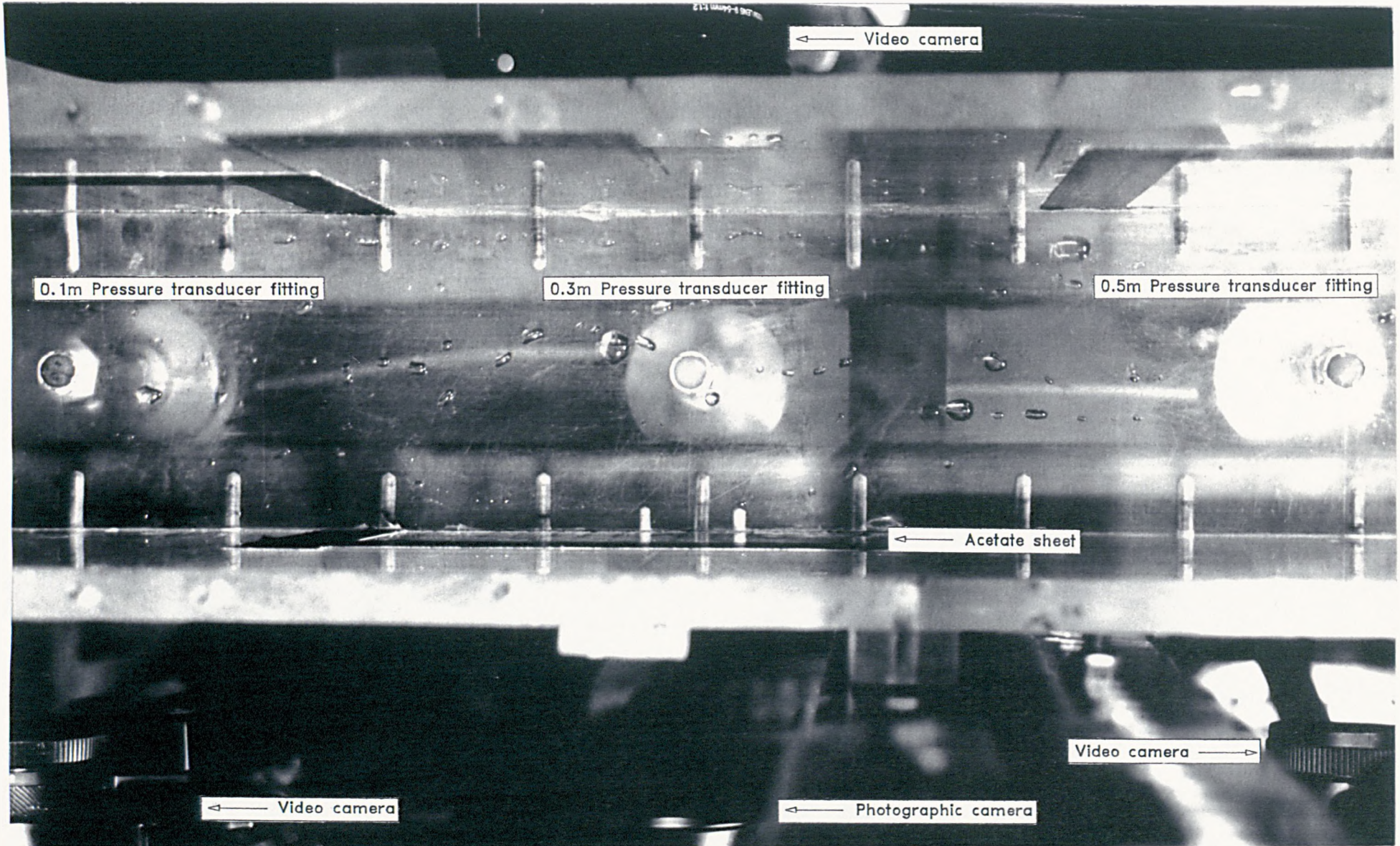
An additional strain gauge diaphragm pressure transducer was mounted in the centre of the channel at a longitudinal distance of 0.3 m from the sluice gate site (fig 7.1):

TABLE 7.1: Pressure transducer data

Make of transducer	Sensotec
Full range output, (F.R.O): Head, (mm of water) Pressure, (kPa)	0-710 0.697
Accuracy, (% of F.R.O.)	+/- 0.1
Supply Voltage (V)	27.99

The pressure transducer fitting and the preparation procedure prior to testing was the same as that described previously for the other pressure transducers (section 4.3). An alternative power supply was provided for this transducer. It was

FIG 7.1 PLAN PHOTOGRAPH SHOWING POSITIONS OF PRESSURE TRANSDUCER FITTINGS, PHOTOGRAPHIC AND VIDEO CAMERAS



checked for stability of output and found to be satisfactory (section 4.3). The pressure transducer calibration procedure remained unaltered (section 4.3).

It was apparent that a drift in the calibration constant of the pressure transducers may have occurred in the time between initial transducer calibration and performance of flowslide tests (section 6.3). This problem needed to be resolved in order that the transducers' voltage outputs obtained during subsequent flowslide tests could then be interpreted with more confidence.

This was achieved by evaluating a new calibration constant for each transducer immediately prior to flowslide testing. A Mitutoyo digital vernier scale was converted into a point gauge and mounted on a section of aluminium angle that could be positioned on top of the channel at each transducer site, perpendicular to the bed. A series of point gauges could not be permanently positioned above each pressure transducer site, due to interference with plan photography of the flowslide event. This would have avoided any possible errors in repositioning the single gauge at each transducer site between flowslide tests. In order that the point gauge did not damage the porous plastic, the gauge was slightly offset to one side, but its tip remained at distances of 0.1 m, 0.3 m and 0.5 m from the sluice gate site for the respective transducers. Small crosses were scribed on the channel bed so that the point gauge tip could be located in the same place each time.

Calibration of one pressure transducer at each channel bed slope using the method described in section 4.3 was performed with simultaneous measurements taken with the point gauge, giving two sets of calibration data. The calibration gradients were compared by setting the values of the calibration constants to zero and observing the difference between the calculated pressures obtained for an arbitrary voltage corresponding to a pressure of 0.74 kPa. This pressure was

greater than the maximum value recorded during the second series of flowslide tests. It was found that a maximum difference of 0.0026 kPa or 0.26 mm was obtained for this pressure. This difference was only slightly greater than the maximum variation encountered between the calibration gradients obtained with the previous method (section 4.3) for a transducer at a particular bed slope (0.0025 kPa). It was felt that the pre-test calibration constant of the pressure transducers could therefore be satisfactorily evaluated using the point gauge.

The pre-test calibration was performed after the test sample preparation had been completed and before the video cameras were set running. Three depth measurements were taken above each transducer, with the magnitude of the difference between each depth being limited by the height of the plasticene dam. The setting up of the point gauge at the water surface during calibration was facilitated by shining a light source on the water surface. The reflection of the point gauge tip on the water surface could be observed and aligned with the point gauge tip. The distance between the point gauge tip and the water surface as the point gauge was slowly lowered could then be more easily judged than when no light source was used. The voltage output of the pressure transducer corresponding to each of the three depths was recorded using the computer. A calibration constant for each depth was calculated by recording the transducer voltage output and subtracting from this the measured depth multiplied by the combined calibration gradient (section 4.3). These three calibration constants obtained for each transducer were then averaged. This averaged value, together with the combined calibration gradient was used for conversion of the voltage data collected during a flowslide test into pressures.

7.2 VIDEO CAMERAS

A further two video cameras, a Panasonic VHS HQ NV-M7B and a Sony TR 60, were used during the late stages of the third series of flowslide tests. The addition of these cameras enabled the elevations of the static and flowing material to be recorded at all three pressure transducer sites during a flowslide test. The small size of the Sony video camera made positioning of this camera at the channel wall much easier than the other types.

The setting up procedure and the method of data extraction for these new cameras remained the same as described previously (section 4.4). One modification involved the removal of the perspex sheet with the grid of crosses for scaling. After a video camera had been set running and the lens focused, a scale rule was placed on the inside of the channel directly against the channel wall at the observation site where the camera was located. This process was repeated for other video cameras. The scale was recorded on the video tape for each camera so that when the tapes were analysed, a scale could be marked on the television screen from this image. During data extraction, all depth measurements were made vertically rather than perpendicular to the bed. In conjunction with these data, the angle of the flowslide surface, α , at a particular observation site was measured vertically above each transducer site at the channel wall over a 5 mm to 10 mm longitudinal distance. The curvature of the monitor screen used for video data extraction restricted the magnitude of this distance. The angle was measured by pausing the video tape recorder at certain time intervals from the removal of the sluice gate. The resulting image of the flowslide on the television screen tended to flicker, making data difficult to obtain. The accuracy of the measured angle was estimated to be within +/-1 degree.

7.3 STILL PHOTOGRAPHY (35 mm)

7.31 PLAN PHOTOGRAPHY

Timed exposure photography was used with light reflective particles to record the surface velocity at all three pressure transducer sites during the course of a flowslide test. A Canon T90 camera, incorporating a data back, was used with a Canon 35–70 mm zoom lens. The data back was very versatile, enabling both the shutter speed and the rate of exposure to be selected. A time delay before the first exposure was taken could also be specified and this feature proved to be very useful. Black and white ASA 50 film was used, which is a fine grained film that enables good quality enlargements to be obtained. The camera was mounted on a cantilever projecting from a column bolted to the channel support beam. There were some initial problems associated with vibration of the camera due to the shock imparted to it when the sluice gate was removed. This was solved by making the column much stiffer. The camera was positioned at a sufficient height above the channel so that all three pressure transducer sites were photographed in a single exposure.

The tracer particles used during these flowslide tests were small square 'glitter' particles of 0.5–1 mm in length, with a thickness of about 0.2 mm. These were carefully sprinkled over the surface of the test sample after sample preparation had been completed. A studio lamp was arranged so that it illuminated the channel bed. The lens was focused on the channel bed at the central pressure transducer site. Although the surface of the flowslide would not be exactly in focus, this was not found to be critical. When the sluice gate was removed, the flowslide proceeded down the channel and timed exposure photographs with a duration of 0.25 seconds were taken of the surface of the flowslide at 1 second

intervals. The tracer particles then appeared as light streaks in the resulting photographs (fig 7.2), as in the manner described by Johnson/Rodine (1984). Despite the increased stiffness of the camera support column, it was found that some slight oscillation of the light streaks occurred, caused by vibration of the camera following sluice gate removal and by the shutter release mechanism.

The reflection of light on the flowslide surface caused 'flare' on the photographs. This was caused by reflection of light from the studio lamps on the water of the flowing sand and water mixture. The light sources used to illuminate the side of flowslide caused the majority of this flare, rather than being caused by the overhead lamp used specifically for the plan photographs (fig 7.2).

The time sequence of the photographs was related to the other measuring devices by using the sound track of one of the video cameras, where the sound of the first exposure could be heard. The average surface velocity in the centre of the channel above each pressure transducer site was determined from the length of the light streaks. The method of obtaining these surface velocities proved to be successful and not complicated. Transverse surface velocity distributions were not required for the purposes of this research. During the late stages of flowslide motion, it was found that the number of tracer particles was insufficient for complete distributions to be obtained. If this information is desired, it is advised that regular introduction of tracer particles upstream of the measurement site is performed.

7.32 SIDE ELEVATION PHOTOGRAPHY

Attempts were made initially to record the side elevation of the flowslide using the plan photographic camera. This was performed using mirrors mounted along

FIG 7.2

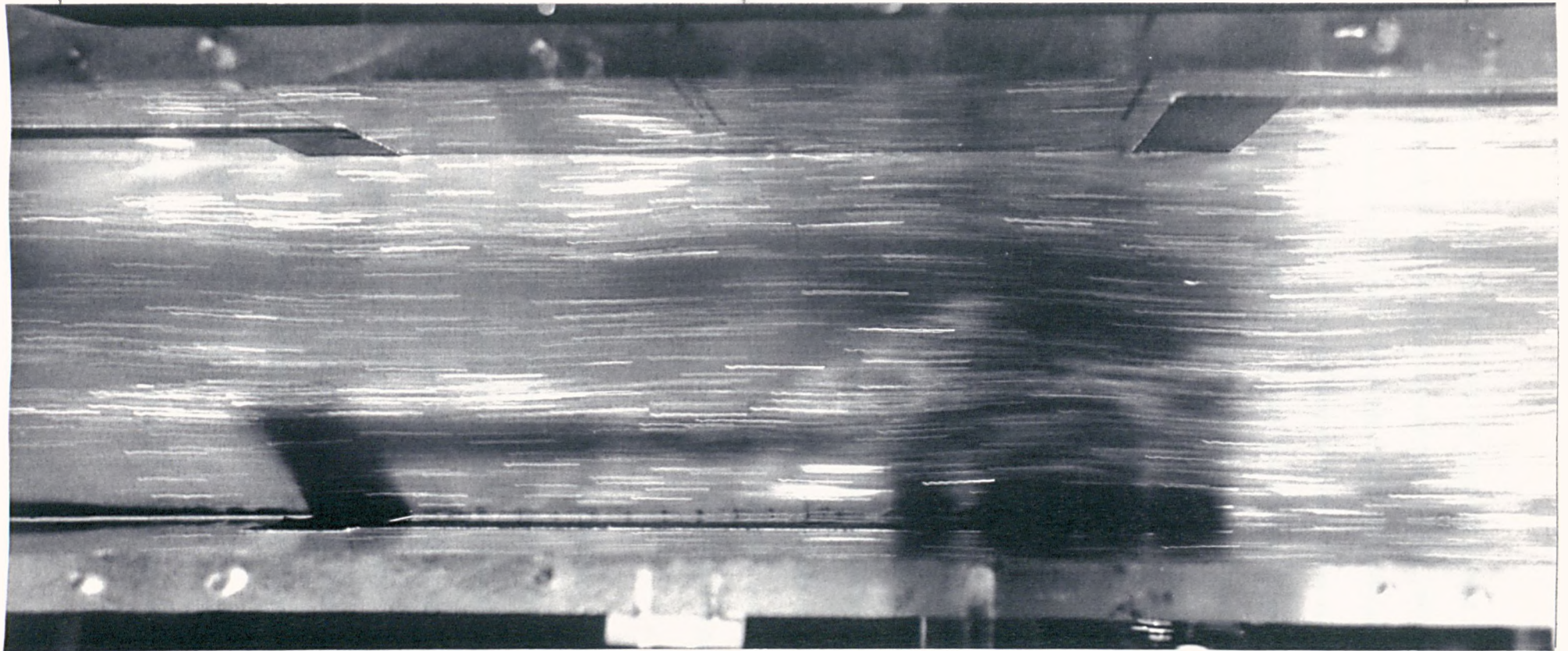
PLAN PHOTOGRAPH SHOWING LIGHT STREAKS OBTAINED FROM TIMED EXPOSURE PHOTOGRAPHY
(TEST 7M, CHANNEL BED SLOPE = 9 DEGREES)

Negative exposed 6.8 seconds after sluice gate removal
Length of exposure = 0.25 seconds

Distance = 0.1 m from sluice gate site

Distance = 0.3m from sluice gate site

Distance = 0.5m from sluice gate site



the side of the channel support beam and set at about 45 degrees above the horizontal in the manner described by Hungr/Morgenstern (1984). Whilst photographs of both elevations could be obtained, the detail on the side elevation photographs was not sufficient for extraction of the surface elevation of the static material. This was probably due to the inability to obtain the degree of focus required for photography of individual sand grains from a camera mounted about a metre above the channel bed. This method was therefore abandoned and the side elevation photographs were taken separately to plan photographs.

A Nikon F-301 camera with a 55 mm AF Micro Nikkor macro lens was positioned at the channel wall at a pressure transducer position to photograph the side elevation of the flowslide. The same type of film was used. No facility existed to control the rate of exposures on the camera. Efforts were made to control this electronically using the analogue output mode of the personal computer software. This enabled a voltage pulse to be generated at a specified rate, which could be used to trigger the camera shutter via the remote shutter release socket. Unfortunately, malfunction of this aspect of the software forced this method to be abandoned due to time limitations.

This problem was solved by using a hand held double pole single throw push button switch connected to the remote shutter release socket and a voltage supply. When the button was depressed, two electrical circuits were completed simultaneously; one activated release of the shutter, the other allowing a voltage to be registered on one of the channels of the data acquisition software. This meant that the exact time that the button was pressed and the negative exposed was recorded. The time assigned to each negative was obtained from this record with the addition of half the exposure time to each value.

The photographic camera was placed as close as possible to the channel wall

whilst still being able to record the maximum depth likely to occur at that site during the flowslide. This was to maximise the detail on the negatives. Manual focusing of the lens on the fine grid present on log-log graph paper, placed directly against the interior of the channel wall for this purpose, was sufficient to give the definition on the photographs required. The camera body or tripod was not touched after this setting up procedure had been completed, to avoid altering the focus of the lens.

The presence of flare on the photographs was initially encountered. In extreme cases, the flowslide appeared white on the resulting photographs. This problem was minimised by using the maximum lens aperture size and the minimum amount of artificial light from a studio lamp that satisfied the camera light meter. The degree of light required also depended on the shutter speed. A light brown card, simulating the flowslide, was placed inside the channel during this process, as it was discovered that a different amount of light was required if the channel was left empty. In addition, tracing paper was mounted in front of the studio lamp to diffuse the light source. The degree of light from the studio lamp was controlled using a variable resistor. Minimising the amount of light required reduced interference with plan photography.

In order that the static layer may appear different to the flowing layer in a photograph, selection of the length of exposure had to be determined by trial and error. If it was too short, the whole of the flow depth appeared to be static [fig 6.1(a-f)]. If the length of exposure was too long, difficulty occurred with identification of the position of the surface of both the static layer and the flowing sand and water mixture. It was found that a length of exposure of 0.25 seconds was satisfactory.

A permanent record of a scale was required on each exposure. This was

achieved by drawing a series of crosses forming a grid on a sheet of acetate, as described under the scaling of depth measurements for the video camera (section 4.4) and was placed in the channel in the same way (fig 7.1).

Specific sections of the resulting negatives were enlarged at a scale of about 9:1, which depended on the maximum total depth at the observation site. The grid crosses were used to mark a line representing the vertical distance above a pressure transducer on each photograph. Any distance measured from the photographs was converted using a scaling factor calculated from the position of the grid crosses.

If no surface water was present, the surface of the flowslide was of a light appearance on both video tape and photographic records, extending downwards for a real depth of about 0.5 mm. This light zone appeared as flare on the photographs and was due to the use of the studio lamp for the plan photographs. The surface of this light zone defined a clear line, with no or a very small water meniscus being present (fig 7.3). This elevation could be extracted confidently. If a change in this level occurred during the period in which the negative was exposed, a more blurred white line occurred (fig 7.4) and the true depth had to be estimated.

When the surface water arrived at the observation site, distinctions had to be made between the top and bottom of the meniscus from the surface water and the surface of the flowing sand and water mixture (fig 7.5). This was achieved by observing variations in shades of the photographs in this region. The elevations could be determined on the original photograph shown in fig 7.5, but unfortunately some clarity has been lost during reproduction. For this reason, the levels of the surface water and sand and water mixture have been illustrated with dashed lines. Assessment of the depth of the water meniscus could also be assisted by examining the irregularity of the top of the meniscus. The amount of detail at the

FIG 7.3 SIDE ELEVATION OF THE SURFACE OF THE FLOWING SAND AND WATER MIXTURE OF A FLOWSLIDE, BEFORE THE ARRIVAL OF SURFACE WATER

(Grid crosses spaced 10mm along longitudinal axis of channel and 5mm apart perpendicular to the channel bed)

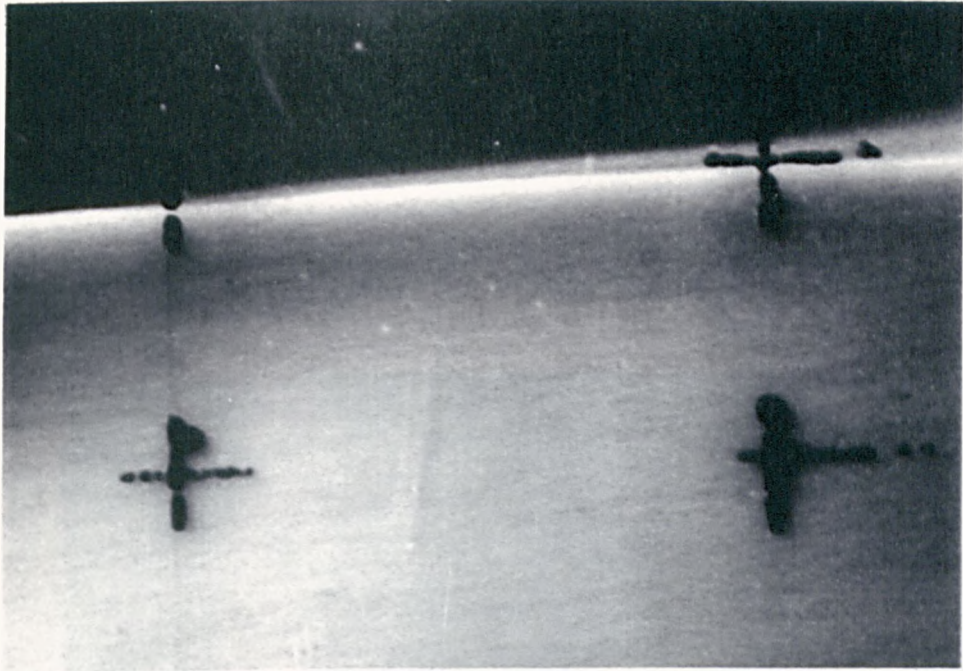


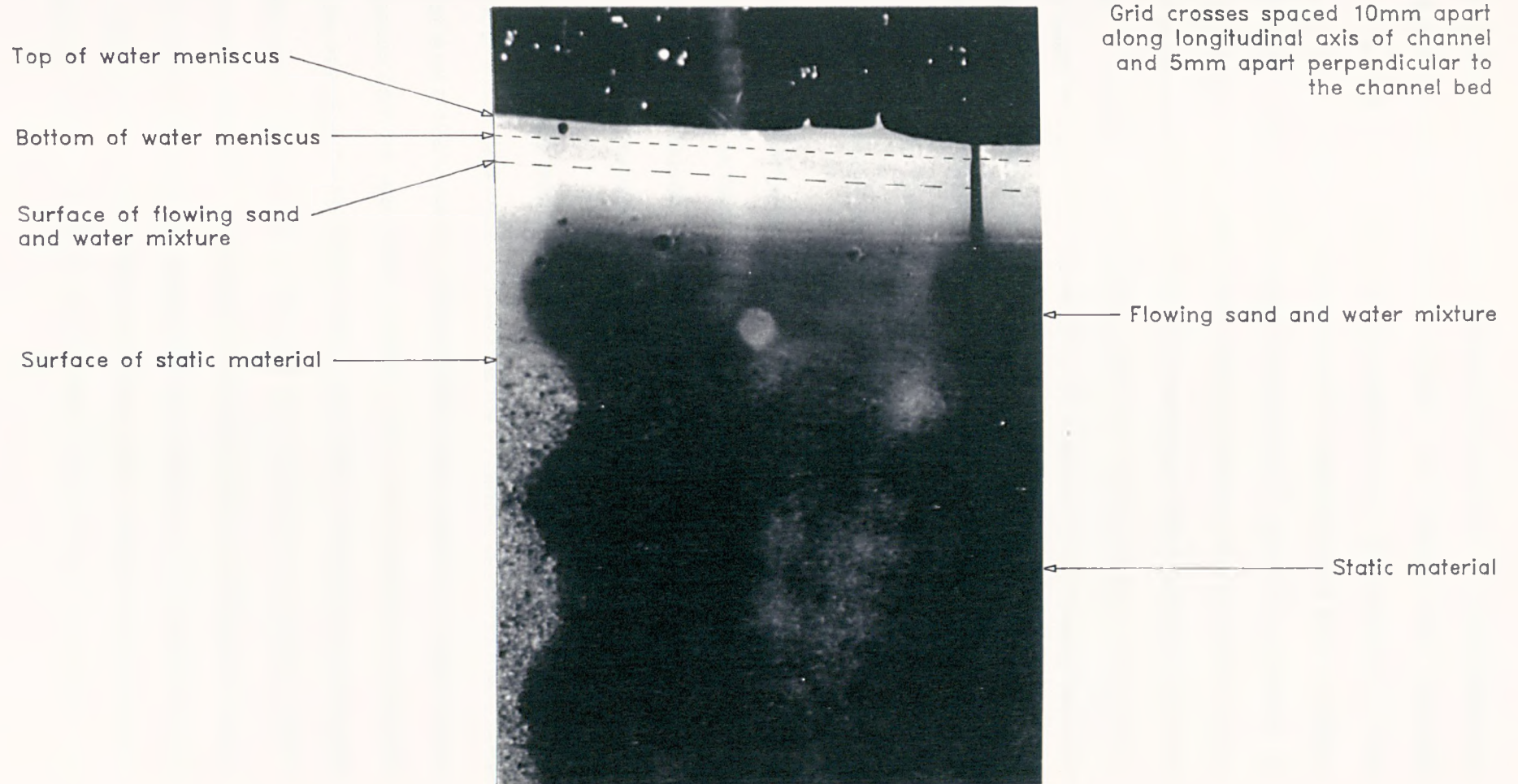
FIG 7.4 SIDE ELEVATION OF THE SURFACE OF THE FLOWING SAND AND WATER MIXTURE OF A FLOWSLIDE, BEFORE THE ARRIVAL OF SURFACE WATER



FIG 7.5

SIDE ELEVATION OF A FLOWSLIDE AT THE 0.3m OBSERVATION SITE AFTER THE ARRIVAL OF SURFACE WATER (TEST 7M AT A BED SLOPE OF 9 DEGREES)

Photograph taken 13 seconds after sluice gate removal



surface of the flowslide could be maximised during exposure of the photograph by masking the flowslide material below the flare zone when it was adequately exposed. The flare zone could then be exposed for a longer period of time. Occasionally, the presence of flare obscured the surface level of both the flowing sand and water mixture and the water flowing above it. When this occurred, the values of the depth of the surface water and its meniscus were calculated from an average of each respective depth from the photographs taken before and after the photograph in question. These depths were then subtracted from the maximum measured depth to obtain the elevation of the surface of the flowing sand and water mixture. The accuracy of the surface water level was estimated to be within ± 0.5 mm when the presence of flare from the plan photography studio lamps hindered measurement. The accuracy of extraction of this level from the video records was also affected to a similar degree.

In most cases, determining the position of the top of the static layer was relatively simple. The particles that were static were in focus and those that were moving were slightly blurred. The interface between these layers was judged by eye. The accuracy of this layer was estimated to be greater than ± 0.2 mm.

The accuracy of the time value assigned to each photograph was only limited by the rate at which data were collected by the computer (20 Hz in these tests). This was at least a 100% more accurate than the time measurements taken during data extraction from the video tape records. It was also possible to estimate the angle of the interface between the flowing and static material from photographs. These data could certainly not be obtained from the video tape records with the available analysis facilities. It was easier to extract data from photographic records than from video tape records, especially with respect to the flowslide surface angle, α . This method was therefore preferred. The accuracy of this angle was estimated to be within ± 0.25 to 0.5 degrees. The surface slope of the static

material could also be obtained, with its accuracy being similar to that of the flowslide's surface slope. These data could not be determined from the video records.

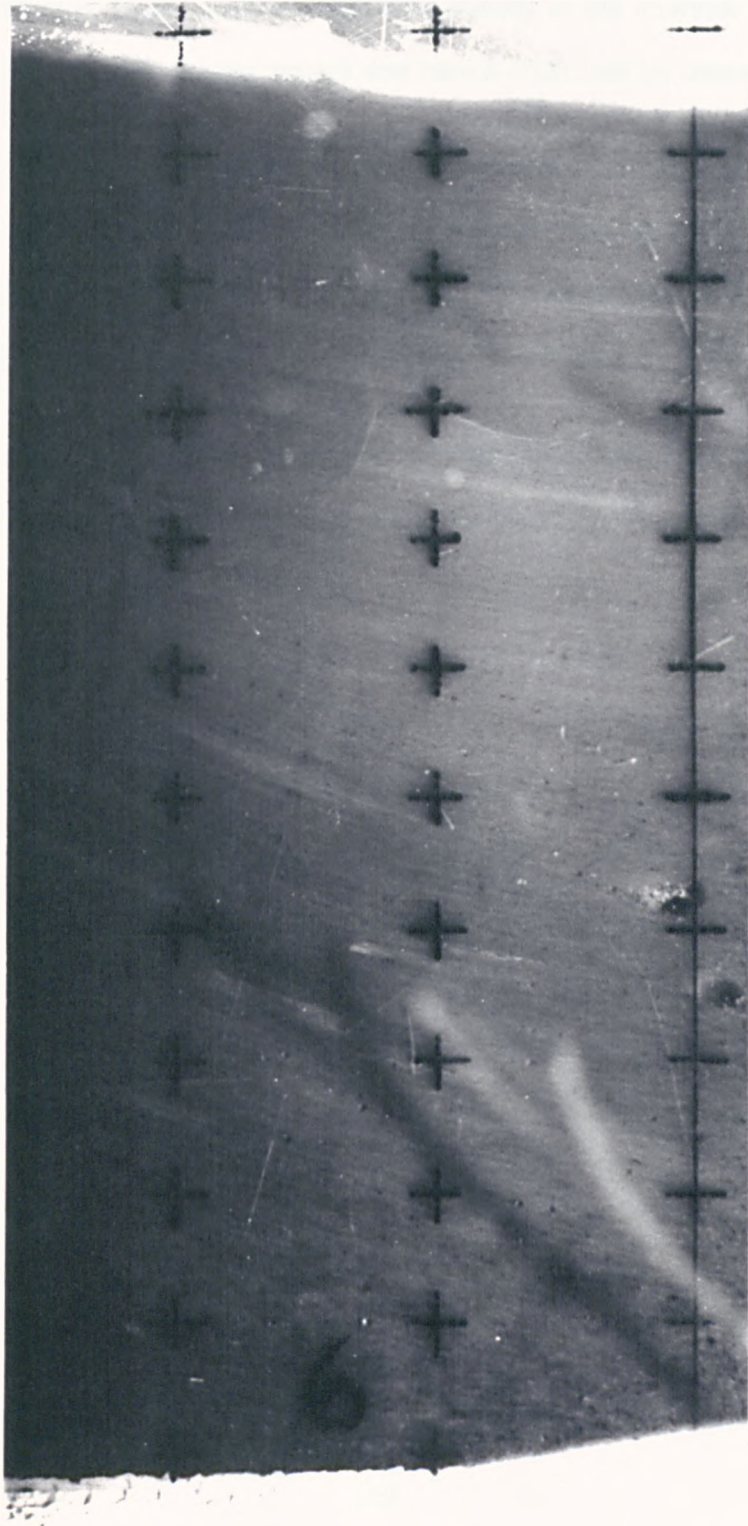
In an attempt to obtain vertical velocity distributions, the same type of light reflective tracers obtained for the plan photographs was used. These were incorporated into the test material at the channel wall, as the sand was placed in the upstream section of the channel. The specific gravity of the tracer particles should be similar to that of the sand grains to avoid settling of the particles at the bottom of the channel, or particles moving to the top of the sand during fluidisation of the test sample. The total mass of tracer particles used was noted for calculations of the bulk density of the test sample and was less than 1.4% of the total mass of test material. About 0.7% of the total mass consisted of tracer particles incorporated into the body of the test sample. The tracer particles on the surface of the flowslide were assumed to have no effect and those within the flowslide were assumed to have an insignificant effect on the dynamics of the flowslide.

Some success was achieved with obtaining light streaks on side elevation photographs at the end of the third series of flowslide tests (fig 7.6). On this figure the light streaks are curving upwards as the flowslide moves from right to left because the plasticene dam used during the pressure transducer preparation procedure (section 4.3) was unfortunately left in place during the flowslide test. Even so, an insufficient number of tracer particles was present for a vertical velocity distribution to be obtained and in subsequent photographs taken during this test no light streaks were present. This was surprising when the number of tracer particles introduced into the test sample at the channel wall was considered. Although only a small number of light streaks were observed on the photographs, more tracer particles were apparent on the video tape records for this flowslide

FIG 7.6 SIDE ELEVATION OF A FLOWSLIDE AT THE 0.1m OBSERVATION SITE SHOWING LIGHT STREAKS OBTAINED FROM PHOTOGRAPHY OF LIGHT REFLECTIVE TRACER PARTICLES (TEST 8M AT A BED SLOPE OF 9 DEGREES)

Photograph taken approximately 2 seconds after sluice gate removal

Grid crosses spaced 10mm apart along longitudinal axis of channel and 5mm apart perpendicular to the channel bed



test. This phenomenon also occurred during Test 7M. The probable reasons for this were:

a) an insufficient number of tracer particles present initially. This was not increased due to the possible influence on flowslide motion.

b) incorporation of tracer particles that were initially at the channel wall into the main body of the flowslide during motion and hence could not be viewed.

c) orientation of the tracer particles The position of the light source meant that light reflected from a glitter particle would only be registered by the camera when the glitter particle was angled in a particular direction. The introduction of additional light sources may cause further problems with flare on the photographs.

Due to time restrictions, these problems could not be satisfactorily resolved and vertical velocity distributions could not be obtained.

CHAPTER 8:

THIRD SERIES OF FLOWSLIDE EXPERIMENTS

8.1 INTRODUCTION

The flowslide tests conducted during this series of experiments were restricted to channel bed slopes of 6 and 9 degrees. Further tests at 0 degrees were not performed. This was because both the depth and duration of flow at the 0.3 m and, in particular, the 0.5 m observation sites were too small for a sufficient amount of data to be obtained for comparison with the 0.1 m site. Flowslide tests at a channel bed slope of 12 degrees were not conducted as flow directly over the channel bed had been observed. This caused uncertainty in the value of the effective friction angle required for pore water pressure calculations. In addition, the difference between the predicted and minimum basal pore water pressures was small compared to that obtained at lower slopes (fig 5.2). This difference required maximising to make comparisons with the measured pore water pressure easier. The difference between the flowslide's surface slope after all movement had ceased and the channel bed slope decreased with increase in channel bed slope. The majority of the third series of experiments were performed at a channel bed slope of 9 degrees to minimise this uncertainty.

8.2 ADDITIONAL EXPERIMENTAL DATA

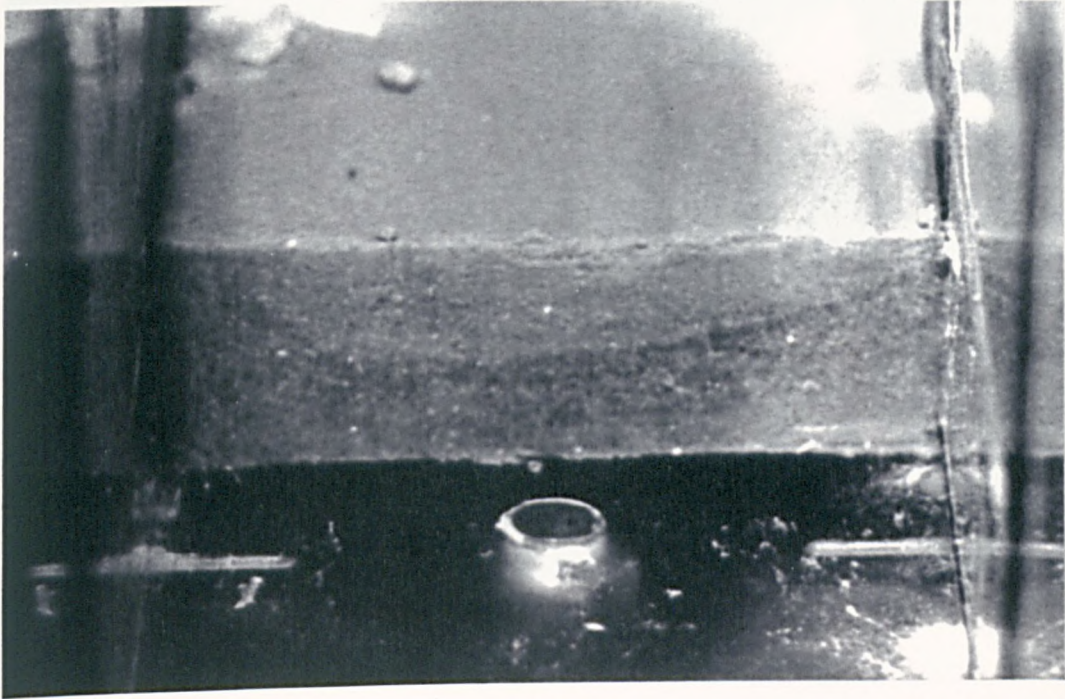
8.21 THREE-DIMENSIONAL FLOW

Evidence was obtained at the end of the third series of experiments that indicated that three-dimensional flowslide motion occurred within the laboratory channel. When flowslide material was being removed from the laboratory channel near the sluice gate site after Test 7M, a striking curved line of dark sand grains was seen in a transverse section through the flowslide material [fig 8.1(a)]. The patterns of light and dark material were caused by the presence of black sand grains within the usual buff coloured sand grains of the test material. As these grains were often found at the base of the upstream section of the channel following test sample preparation, it was presumed that these grains were slightly denser than the buff coloured grains. Upon discovery of this phenomenon, further flowslide material was carefully removed and the presence of further curves of dark material was found. Examination of the photographs of these further transverse sections revealed a series of curved lines in each of the exposures [fig 8.1(b-d)].

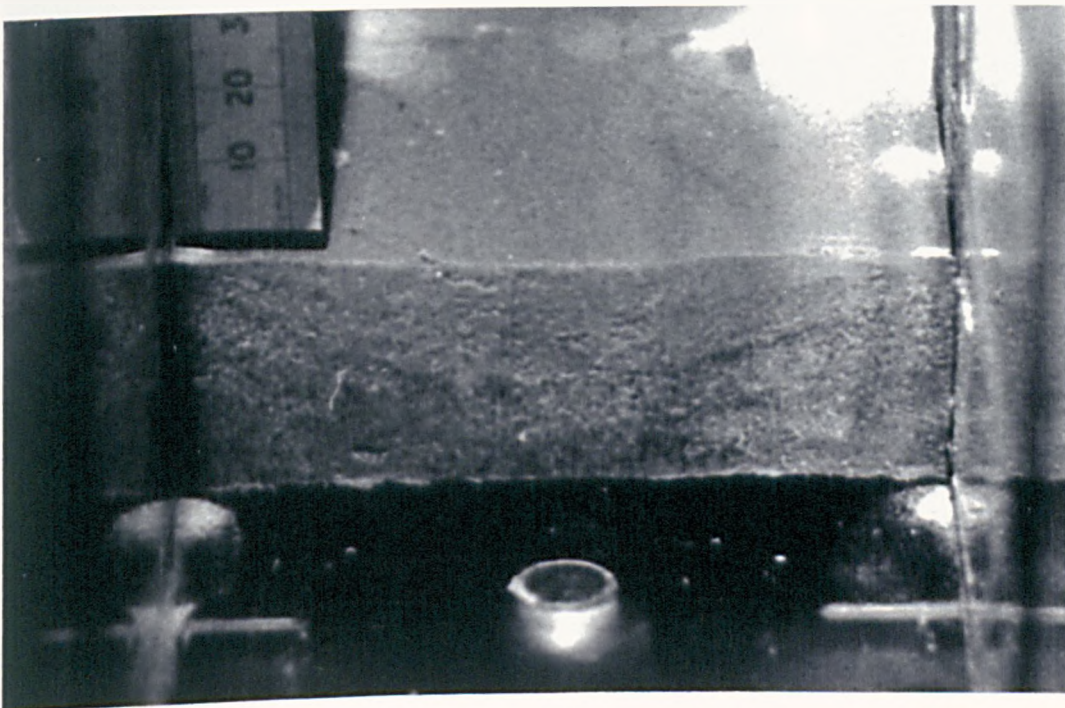
The number, shape and the fact that these curves often extended from one side of the channel to the other indicated that this phenomenon was not the result of some random occurrence. It was felt that this was caused by dark sand grains being deposited at the base of the flowing sand and water mixture during flowslide motion. Thus, where different curves could be seen in a single exposure, these indicated the position of the interface between the flowing and the static material at different time intervals during flowslide motion, at that particular longitudinal distance. At a high channel bed slope ($\beta = 12$ degrees), a concave surface of the flowslide (in plan view) was also observed near the sluice gate site after all motion

FIG 8.1 TRANSVERSE SECTION PHOTOGRAPHS OF FLOWSLIDE MATERIAL
AFTER ALL MOVEMENT HAS CEASED (TEST 7M, BED SLOPE = 9 DEGREES)

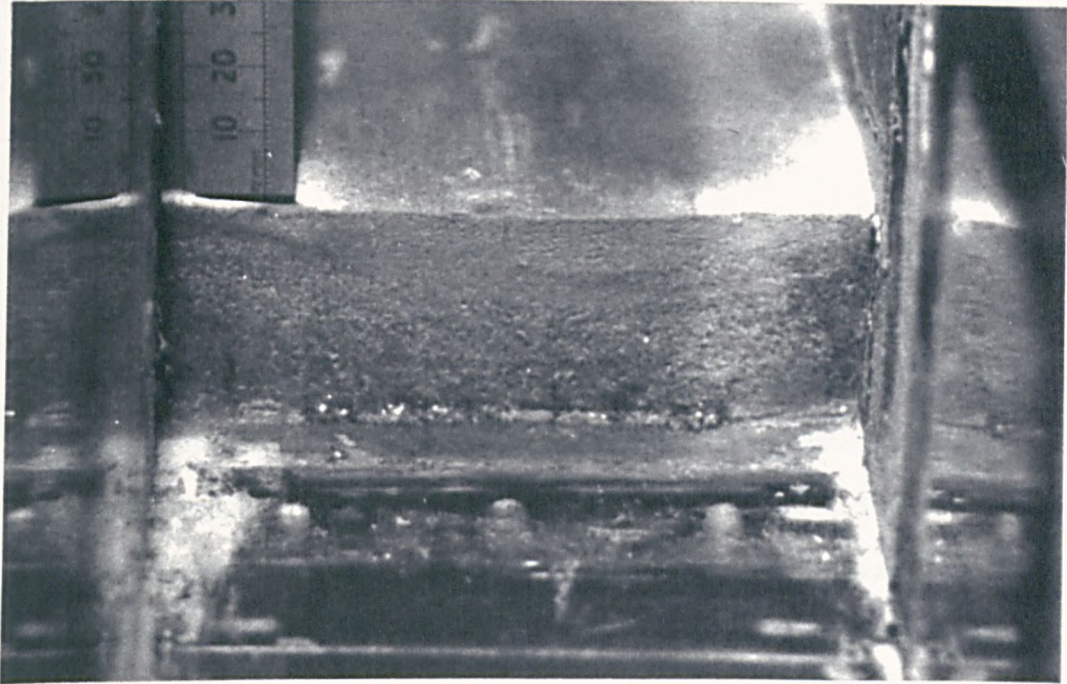
a) Longitudinal distance = 0.08m from the sluice gate site



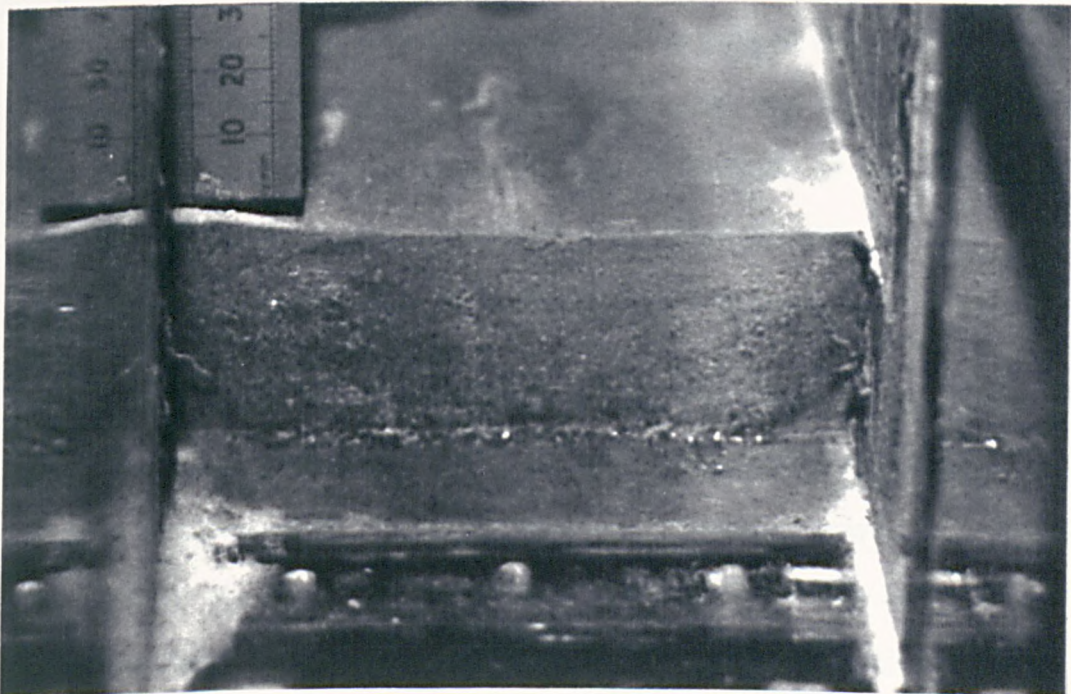
b) Longitudinal distance = 0.07m from the sluice gate site



c) Longitudinal distance = -0.014m from the sluice gate site



d) Longitudinal distance = -0.03m from the sluice gate site



had ceased during a preliminary flowslide test. This was a lower flow boundary that remained after flowing material moved over it and then continued down the channel without further deposition at this longitudinal position. This material was therefore similar to the levées formed in field flowslide and debris flow events [Bishop (1973), Johnson/Rodine (1984)].

The curvature of the lines illustrated was not always symmetrical about the centreline of the channel's longitudinal axis [fig 8.1(a)]. This suggested that some meandering of the flowing sand and water mixture within the confines of the channel occurred. This assumption was supported by flowslide elevation data collected during the same flowslide experiment at each channel wall, at a longitudinal distance of 0.3 m (fig 8.2). It can be seen that temporal variation of the difference between the static material's surface elevation, h_s , at each channel wall occurred. Although in the time period from 8.2 to 12.3 seconds a maximum difference of 2 mm occurred between the flowing sand and water mixture's elevations ($h_s + h_f$) at each channel wall, for the rest of flowslide motion, this difference was very small. A maximum difference of 0.3 mm was observed. This agreement indicated that the data obtained at each channel wall could be compared. The difference in the elevations of the surface water ($h_s + h_f + h_{sw}$) was within the degree of accuracy expected (± 0.5 mm). The plan photographs taken of the moving flowslide showed longitudinal variation of the magnitude and direction of the light streaks obtained from tracer particles (fig 8.3). This also indicated that meandering of the flowing material took place.

Although it can be seen in one photograph that the curvature of each of the lower flow boundaries was similar [fig 8.1(b)], other photographs indicated that the degree of curvature decreased with increase in elevation above the channel bed [figs 8.1(c & d)]. The maximum elevation of flowslide's surface occurred when the depth of static material was small [figs 6.3-6.10 & 8.8(a)-8.13(a)]. Therefore, each

FIG 8.2

COMPARISON OF DEPTHS OF FLOWSLIDE MATERIAL OBSERVED AT EACH CHANNEL WALL
AT THE 0.3M OBSERVATION SITE (TEST 7M, CHANNEL BED SLOPE = 9 DEGREES)

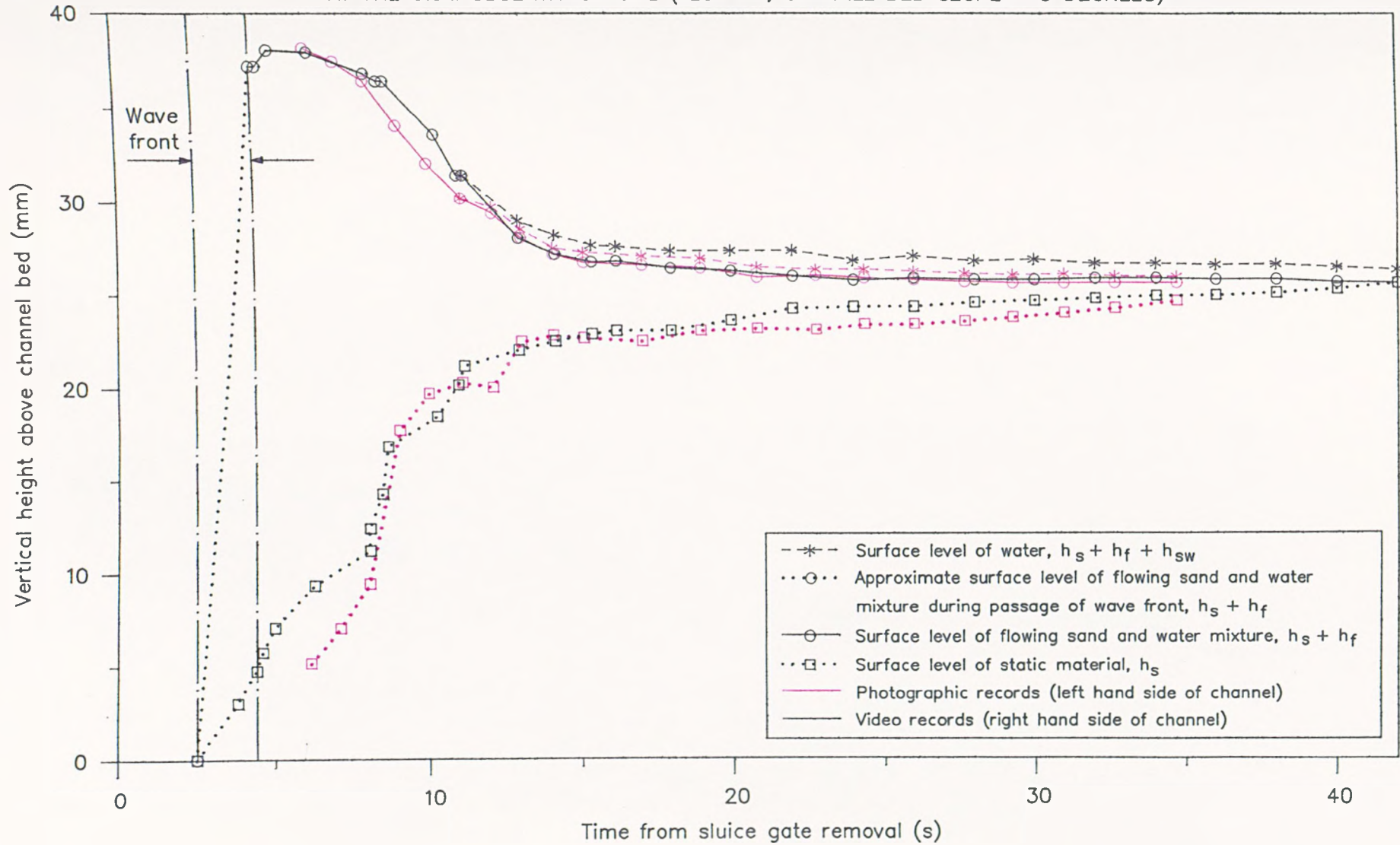


FIG 3.3

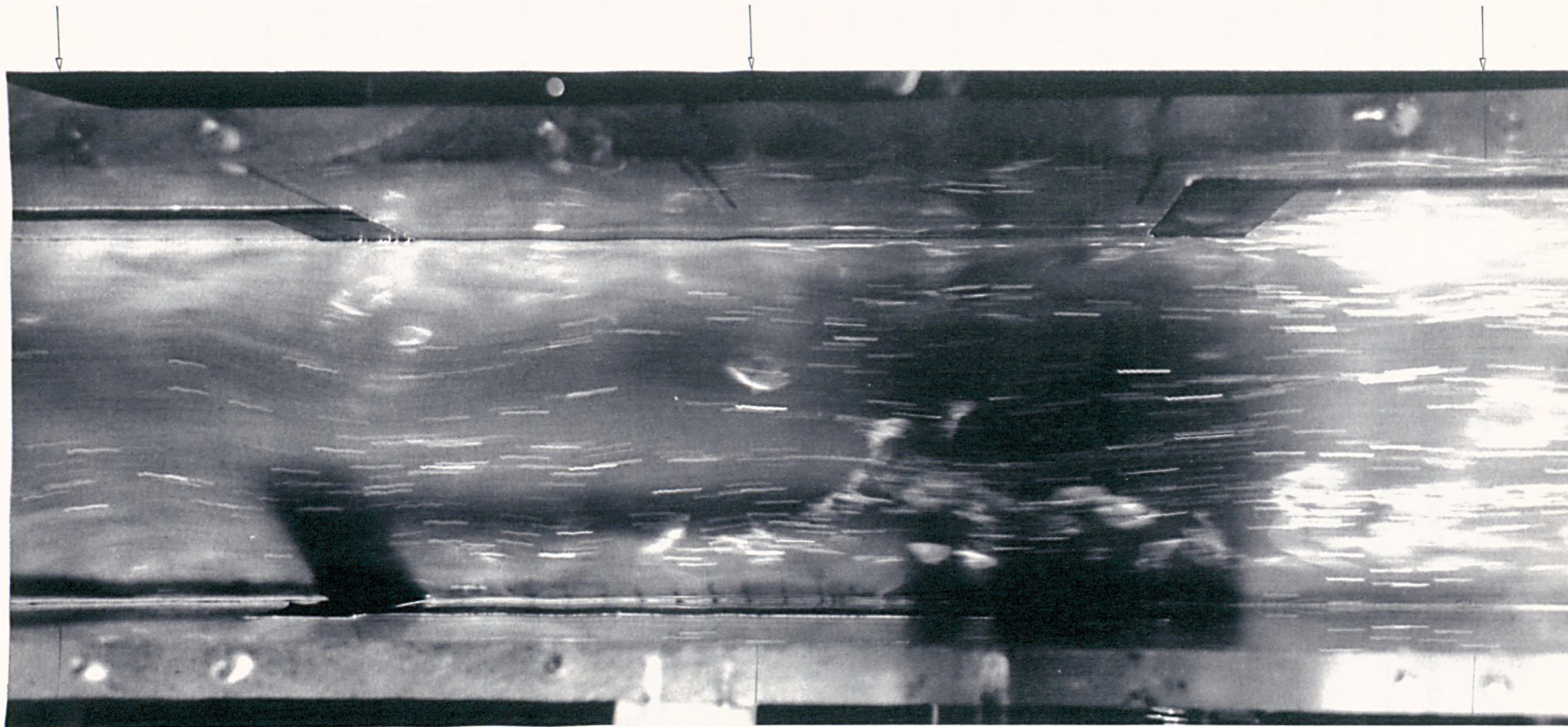
PLAN PHOTOGRAPH SHOWING LIGHT STREAKS OBTAINED FROM TIMED EXPOSURE PHOTOGRAPHY
(TEST 7M, CHANNEL BED SLOPE = 9 DEGREES)

Negative exposed 11.8 seconds after sluice gate removal
Length of exposure = 0.25 seconds

Distance = 0.1 m from sluice gate site

Distance = 0.3m from sluice gate site

Distance = 0.5m from sluice gate site



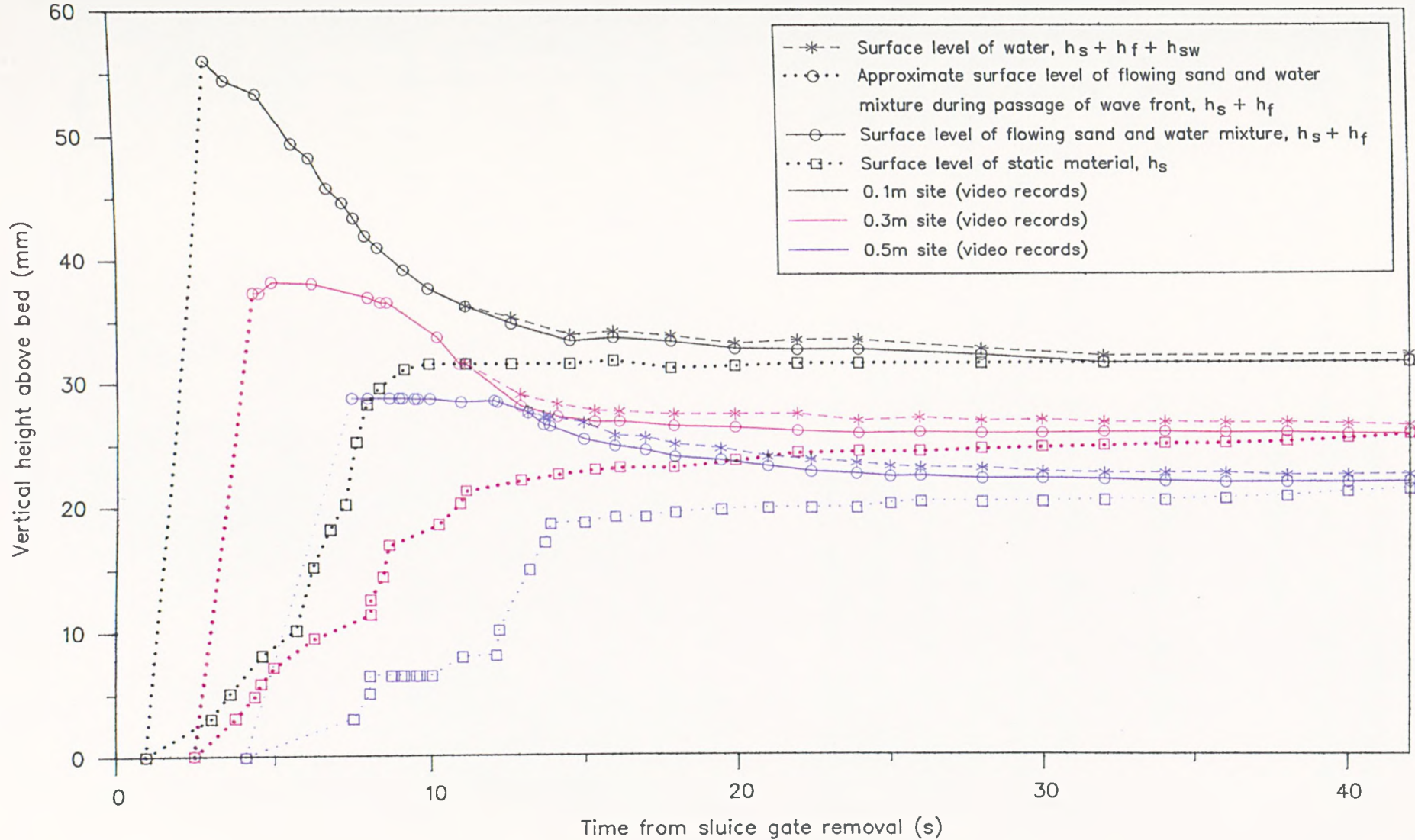
curved line in the progression of lines from the channel bed would have had a progressively decreasing flow depth above it. Although flowslide surface elevation data were not available for these transverse sections, it was expected that the degree of curvature would generally increase with increase in flow depth. It was also expected that the flowslide's solid volume concentration and the width to depth ratio of the channel would be influencing factors.

A curved line at the right hand side of the channel can be seen in fig 8.1(b). This indicated that at this longitudinal distance, a depth of about 12 mm of static material would have been observed at the channel wall at some stage during flowslide motion, but no static material would have been present in the centre of the channel, as this curved line coincided with the perspex bed before the centre of the channel was reached. The gradient of the temporal increase in static material's surface elevation at the observation sites was often unsteady below an elevation of about 10 mm (depending on the quantity of data obtained), whilst above this elevation, an increase in the deposition rate occurred [figs 8.4 & 8.8(a)-8.13(a)]. The similarity of this 10 mm elevation to the 12 mm elevation observed in fig 8.1(b) suggested that this increase in deposition rate corresponded to the moment when the flowslide was no longer travelling over the channel bed.

The presence of these curved lower flow boundaries obviously has important implications concerning the accuracy of the flow depth in the centre of the channel determined from channel wall flowslide elevations. This error could not be quantified as the temporal variation of the flowing sand and water mixture's surface elevation were not available at the longitudinal distances at which the photographs were taken. The meandering of the flowslide within the channel would cause additional problems in predicting the flow depth in the centre of the channel from measurements taken at the channel wall. The positive aspect of these photographs was that they provide further evidence for the fluid behaviour

FIG 8.4

VARIATION IN DEPTHS OF FLOWSLIDE MATERIAL WITH TIME AT THE THREE OBSERVATION SITES DURING TEST 7M, BED SLOPE = 9 DEGREES



of flowslides. The curved lower flow boundaries show that a minimal amount of boundary frictional contact was obtained by maximising of the hydraulic radius (cross sectional area of flow divided by the wetted perimeter).

8.22 SURFACE SLOPES OF THE FLOWSLIDE'S LAYERS

Both the flowslide's surface slope and the surface slope of the static material were measured during flowslide motion. This was important as an assumption had been made in the calculation of the pore water pressures that the interslice forces either side of an element of the flowslide were equal (section 5.1). Flowslide surface angles were obtained during each flowslide test, but only the results from flowslide Test 7M are presented graphically here (figs 8.5-8.6). Other results are tabulated in appendix A 2.3.

At the 0.1 m site, the flowslide's surface slope was 6 degrees greater than the channel bed slope initially (fig 8.5). This high angle is associated with the flowslide material that immediately followed the end of the wave front (see fig 6.1). As the wave front progressed downstream, the surface slope at the end of the wave front point diminished in magnitude until it was close to the channel bed slope at the 0.5 m observation site. The surface slopes at the different longitudinal distances obtained from the video records for the rest of flowslide motion were often within two degrees.

Test 4M, which was also performed at a bed slope of 9 degrees, had higher flowslide surface slopes at the 0.5m pressure transducer site (see appendix) than were observed at the same site during Test 7M. The flowslide velocity of Test 4M was seen to be much smaller (although no quantitative measurements were taken during this experiment) and the final run out distance was smaller in comparison to

FIG 8.5

COMPARISON OF FLOWSLIDE SURFACE SLOPES AT THE THREE OBSERVATION SITES (TEST 7M, CHANNEL BED SLOPE = 9 DEGREES)

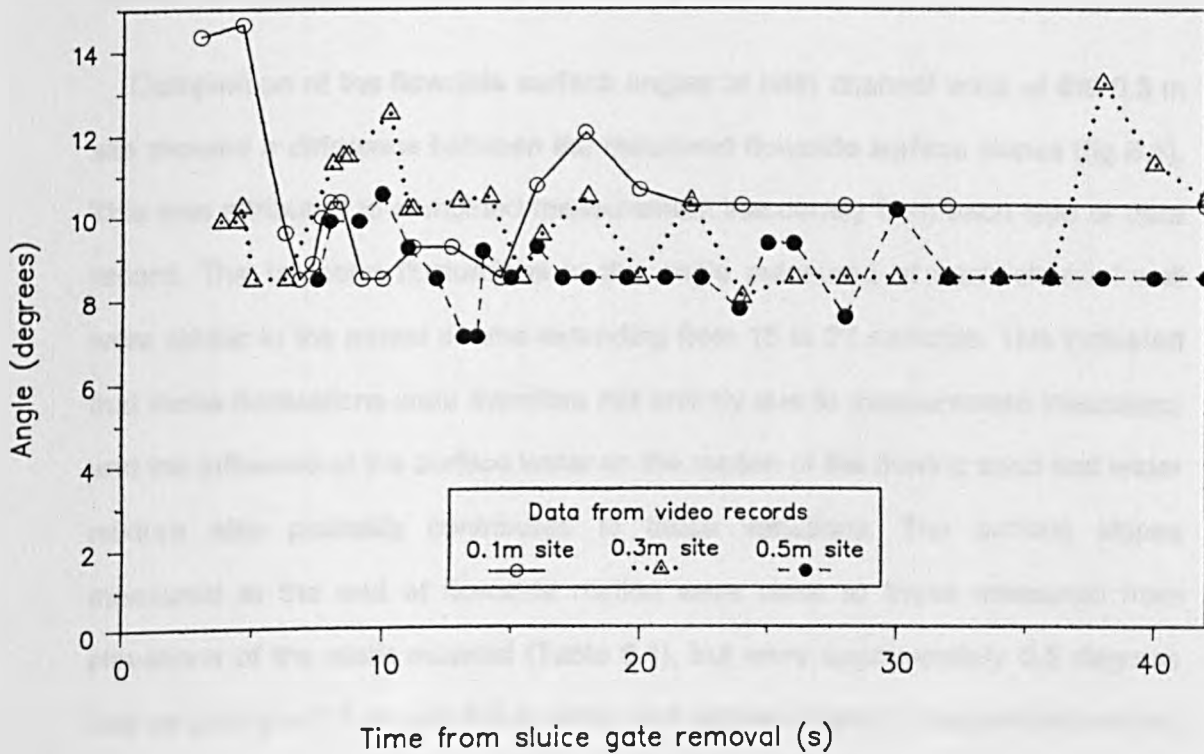
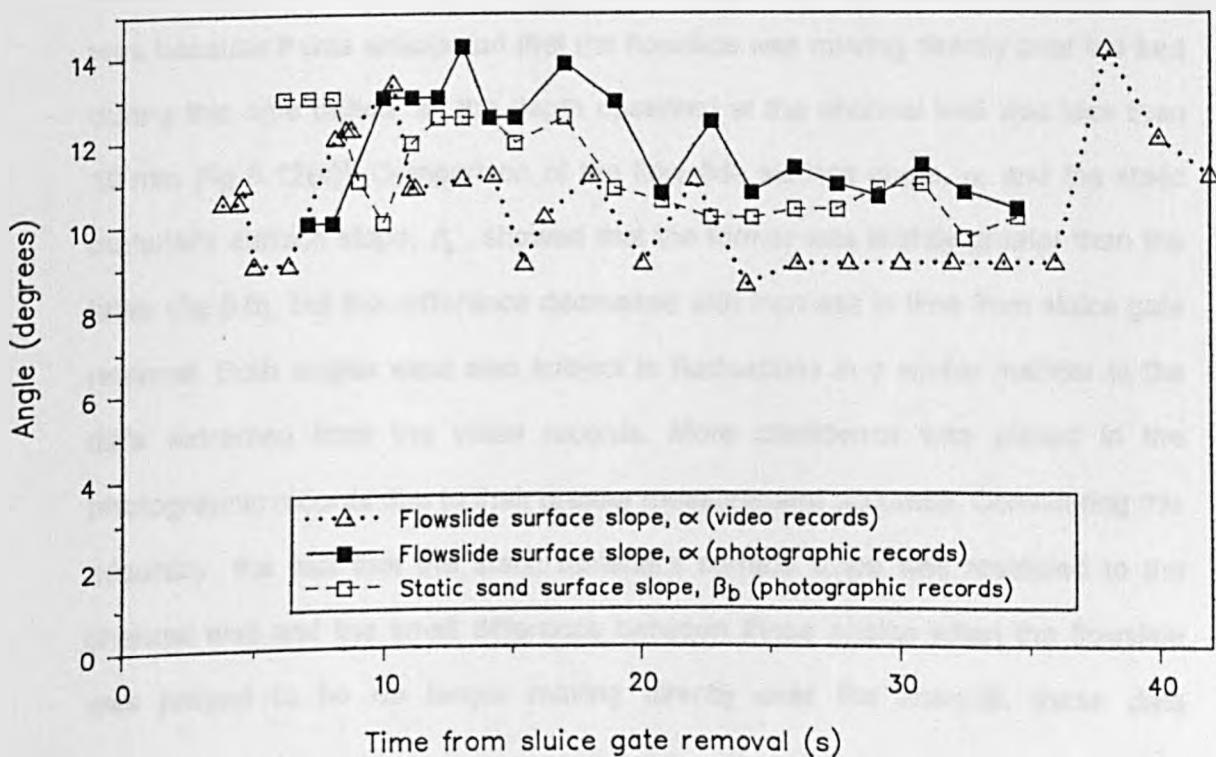


FIG 8.6

COMPARISON OF FLOWSLIDE AND STATIC MATERIAL SURFACE SLOPES AT THE 0.3M OBSERVATION SITE (TEST 7M, CHANNEL BED SLOPE = 9 DEGREES)



Test 7M. Thus the higher surface angles were expected as the flowslide did not 'spread out' along the channel to the same degree.

Comparison of the flowslide surface angles at both channel walls at the 0.3 m site showed a difference between the measured flowslide surface slopes (fig 8.6). This was attributed to combined measurement inaccuracy from each type of data record. The temporal fluctuations in the angle measured at each channel wall were similar in the period of time extending from 15 to 27 seconds. This indicated that these fluctuations were therefore not entirely due to measurement inaccuracy and the influence of the surface water on the motion of the flowing sand and water mixture also probably contributed to these variations. The surface slopes measured at the end of flowslide motion were close to those measured from elevations of the static material (Table 8.1), but were approximately 0.5 degrees less at both the 0.1 m and 0.3 m sites, and approximately 2 degrees less at the 0.5 m site.

The initial measurements of the static material's surface slope, or slip surface slope, were not relevant (up to about 8 seconds after sluice gate removal). This was because it was anticipated that the flowslide was moving directly over the bed during this time period, as the depth observed at the channel wall was less than 10 mm [fig 8.12(a)]. Comparison of the flowslide surface angle, α , and the static material's surface slope, β_s , showed that the former was slightly greater than the latter (fig 8.6), but this difference decreased with increase in time from sluice gate removal. Both angles were also subject to fluctuations in a similar manner to the data extracted from the video records. More confidence was placed in the photographic records due to their greater measurement accuracy. Considering this accuracy, the fact that the static material's surface slope was restricted to the channel wall and the small difference between these angles when the flowslide was judged to be no longer moving directly over the channel, these data

TABLE 8.1

EXPERIMENTAL DATA FROM THE THIRD SERIES OF FLOWSLIDE TESTS

Flowslide test	3M	4M	6M	7M			
H_d (m)	0.122	0.133	0.134	0.135			
V_t ($\times 10^{-6} \text{ m}^3$)	4446	4134	4400	4520			
Initial C	0.495	0.532	0.503	0.494			
Initial ρ_{sat} (kg/m^3)	1846	1909	1861	1845			
Final C x (m) % change	—	0.499 0.58 \rightarrow 0.64 -6.0%	0.506 0.08 \rightarrow 0.18 0.5%	0.498 0.08 \rightarrow 0.18 0.8%	0.499 0.22 \rightarrow 0.32 1.0%	0.501 0.45 \rightarrow 0.6 1.4%	
Final ρ_{sat} x (m) % change	—	1853 0.58 \rightarrow 0.64 -2.9%	1865 0.08 \rightarrow 0.18 0.2%	1852 0.08 \rightarrow 0.18 0.4%	1853 0.22 \rightarrow 0.32 0.4%	1856 0.45 \rightarrow 0.6 0.6%	
Channel bed slope, β (degrees)	6	9	9	9			
Slope of flowslide surface, α (degrees) x (m)	9.4 0.3 \rightarrow 0.5	12 0.3 \rightarrow 0.5 12.8 0.58 \rightarrow 0.64	11.8 0.08 \rightarrow 0.18 10.7 0.3 \rightarrow 0.5	10.8 0.08 \rightarrow 0.18	11 0.22 \rightarrow 0.32	10.2 0.3 \rightarrow 0.5	10.4 0.45 \rightarrow 0.6
Run out distance (m)	0.64	0.84	1.51	1.66			

H_d = vertical height of test sample at sluice gate site

V_t = volume of test sample

x = longitudinal distance from sluice gate site

C = solid volume concentration

ρ_{sat} = saturated bulk density of sand

supported the assumption that there was no difference between the slopes of the surface and base of the flowing material. Therefore, the effect of interslice forces on the element of the flowslide considered for pore water pressure calculations was not expected to be significant.

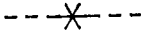



The trend of these photographic data suggested that the slip surface slope was greater than that of the channel bed slope (fig 8.6). This was supported by the elevation data gained at the three longitudinal sites during Test 7M (fig 8.4), as a difference in the static material's surface elevation at each observation site occurred at any particular time interval after sluice gate removal. Whilst the interior of the flow could not be seen, it could be deduced that this increase in slip surface slope was caused by deposition of material beginning at the 0.1 m site, followed by deposition at the other sites in sequence of increasing longitudinal distance.

8.3 COMPARISON OF MEASURED AND CALCULATED PORE WATER PRESSURES

The results of the second series of flowslide experiments indicated that improvement in the calibration of the pressure transducers was required. This would increase confidence in the measured pore water pressures. This was achieved by providing an additional transducer calibration immediately prior to testing, in the manner described in section 7.1. The value of the pressure recorded by each pressure transducer prior to sluice gate removal was positive in each flowslide test [figs 8.8(b)-8.13(b)], compared to the initially negative values obtained in three flowslide tests during the second series of experiments (figs 6.19, 6.21 & 6.23). The initial pressure recorded in each flowslide test during the third series of experiments compared favourably to pressure recorded after sluice

FIG 8.7

LEGEND FOR FIGURES 8.8(a)–8.13(a)

	Surface level of water, $h_s + h_f + h_{sw}$ (mm)
	Approximate surface level of flowing sand and water during passage of wave front, $h_s + h_f$ (mm)
	Surface level of flowing sand and water mixture, $h_s + h_f$ (mm)
	Surface level of static material, h_s (mm)

(All distances measured vertically)

LEGEND FOR FIGURES 8.8(b)–8.13(b)






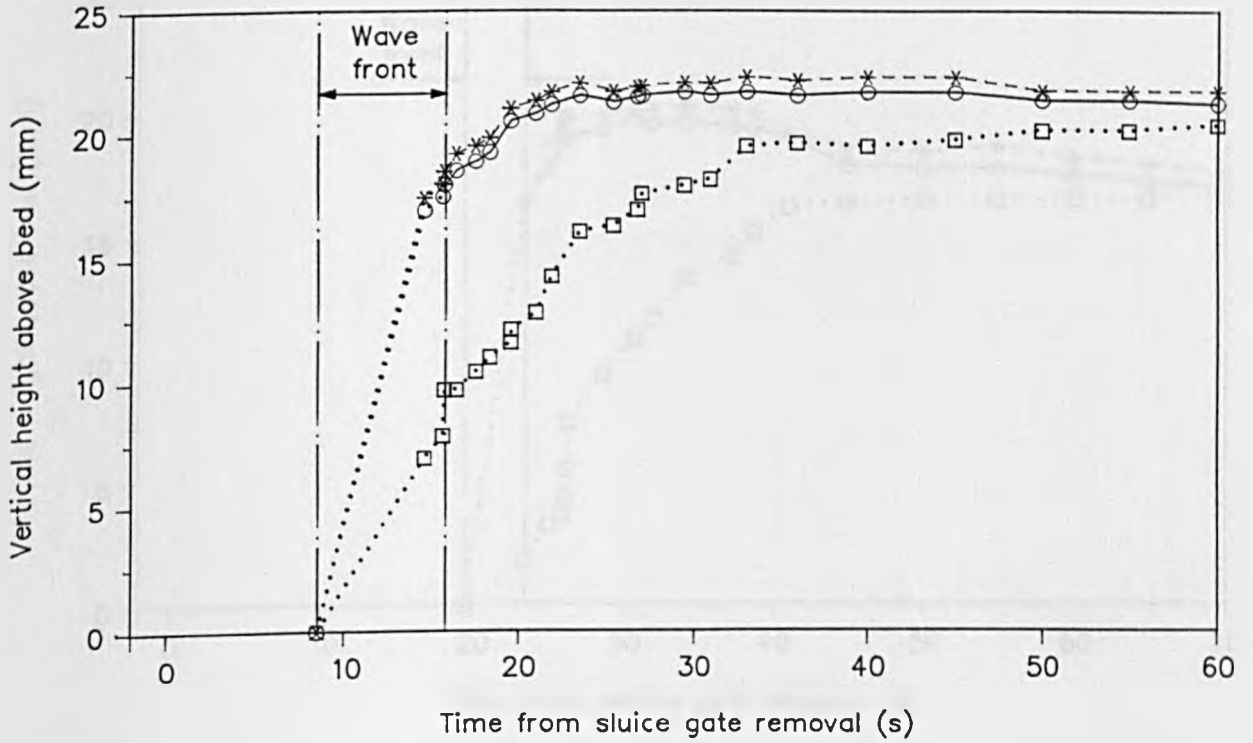
	Measured pore water pressure, u_{expt} (kPa)
	Maximum total pore water pressure, $u_{t,max}$ (kPa)
	Predicted total pore water pressure, $u_{t,pred}$ (kPa)
	Minimum total pore water pressure, $u_{t,min}$ (kPa)
	Pore water pressure contribution to total pore water pressure from the static material, u_s (kPa)

FIG 8.8

TEST 3M AT 0.3M FROM THE SLUICE GATE SITE
CHANNEL BED SLOPE = 6 DEGREES
(VIDEO RECORDS)

a) TEMPORAL VARIATION IN DEPTHS OF FLOWSLIDE MATERIAL



b) COMPARISON OF MEASURED AND CALCULATED PORE WATER PRESSURES

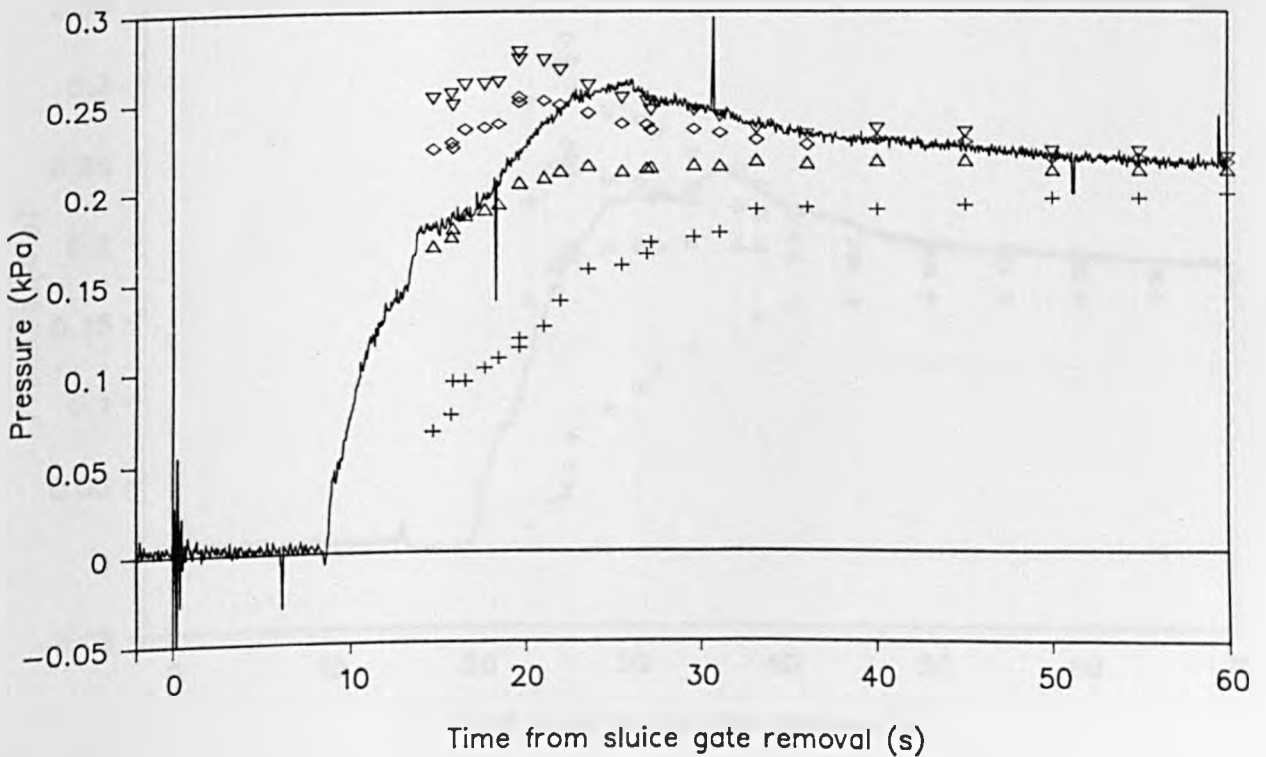
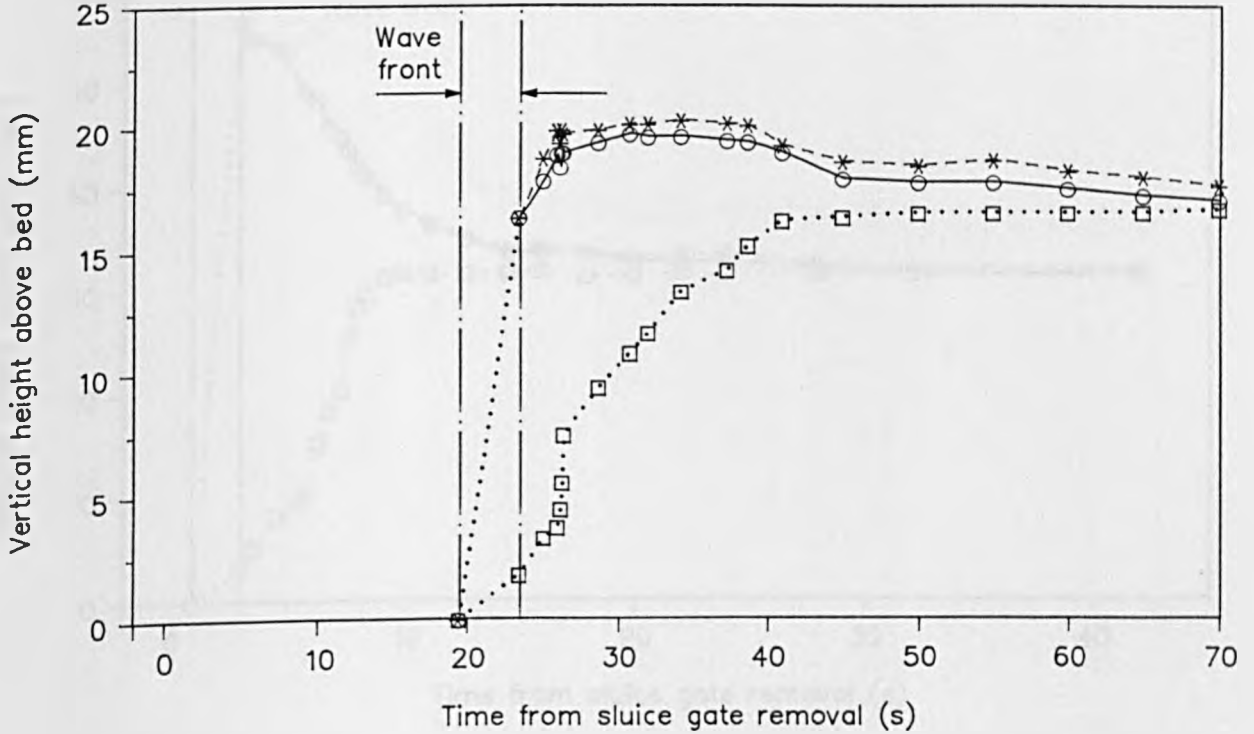


FIG 8.9

TEST 4M AT 0.5M FROM THE SLUICE GATE SITE
CHANNEL BED SLOPE = 9 DEGREES
(VIDEO RECORDS)

a) TEMPORAL VARIATION IN DEPTHS OF FLOWSLIDE MATERIAL



b) COMPARISON OF MEASURED AND CALCULATED PORE WATER PRESSURES

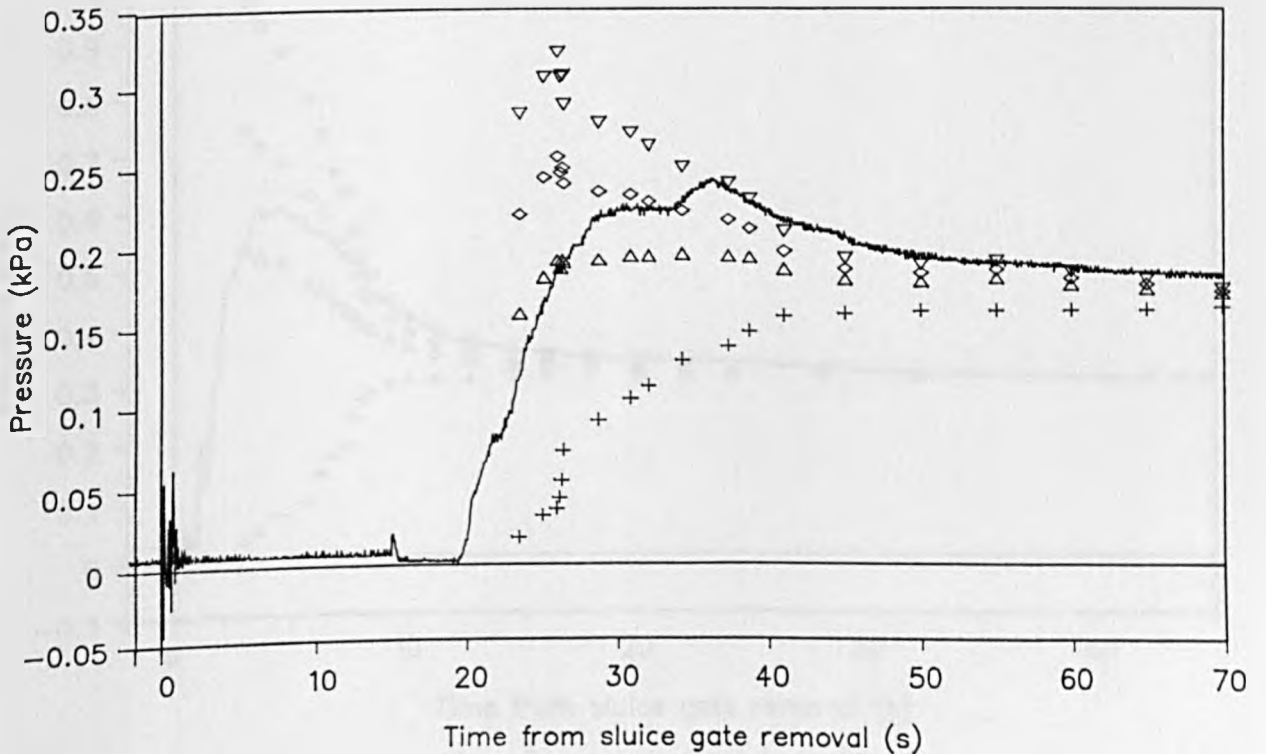
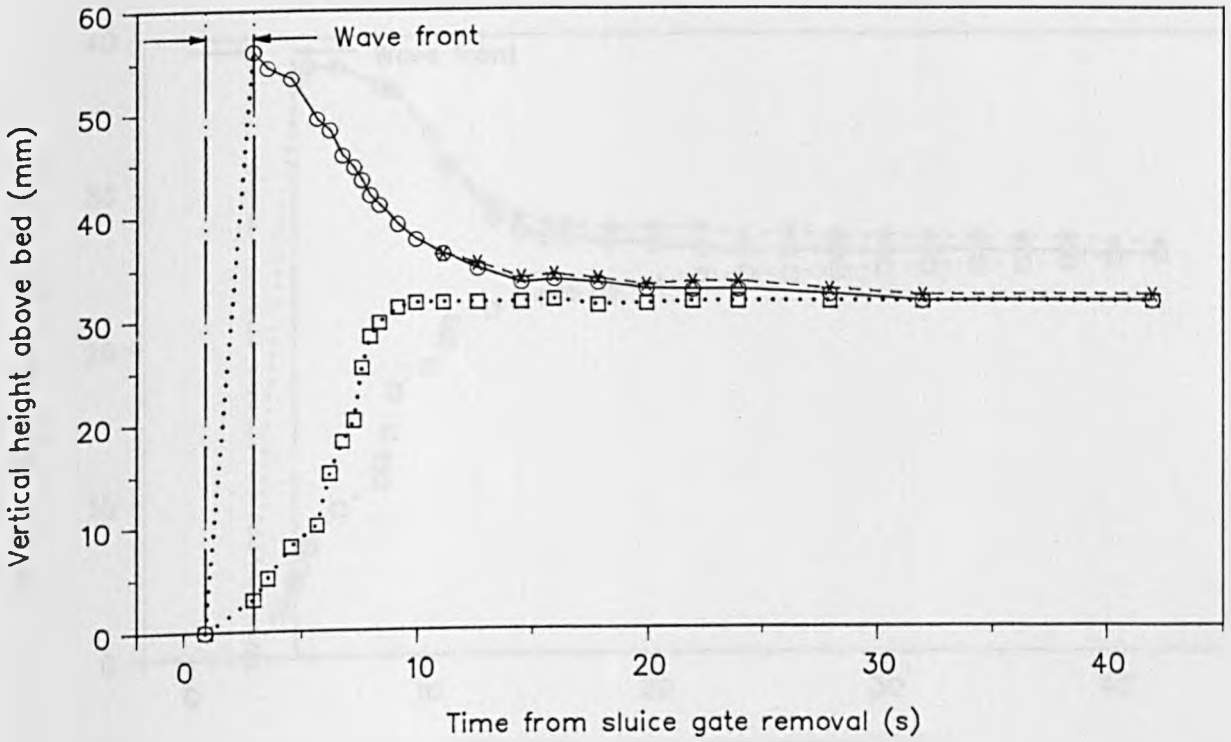


FIG 8.10

TEST 7M AT 0.1M FROM THE SLUICE GATE SITE
 CHANNEL BED SLOPE = 9 DEGREES
 (VIDEO RECORDS)

a) TEMPORAL VARIATION IN DEPTHS OF FLOWSLIDE MATERIAL



b) COMPARISON OF MEASURED AND CALCULATED PORE WATER PRESSURES

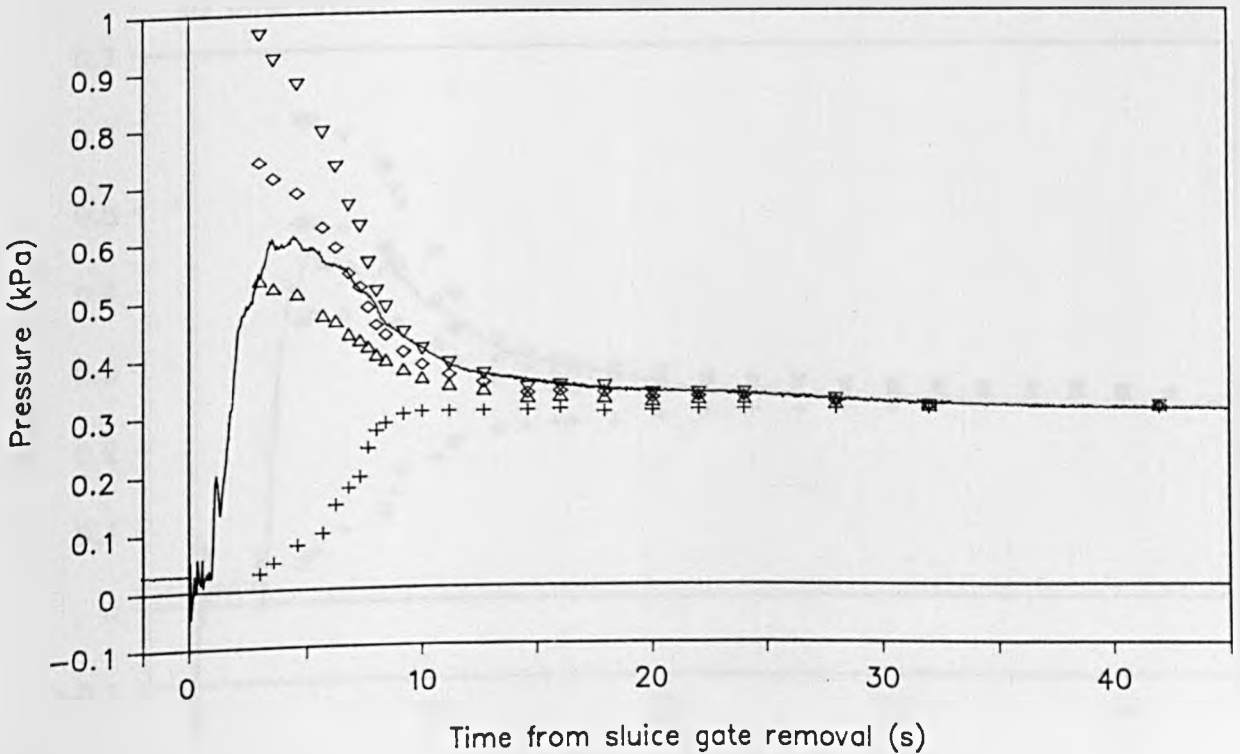
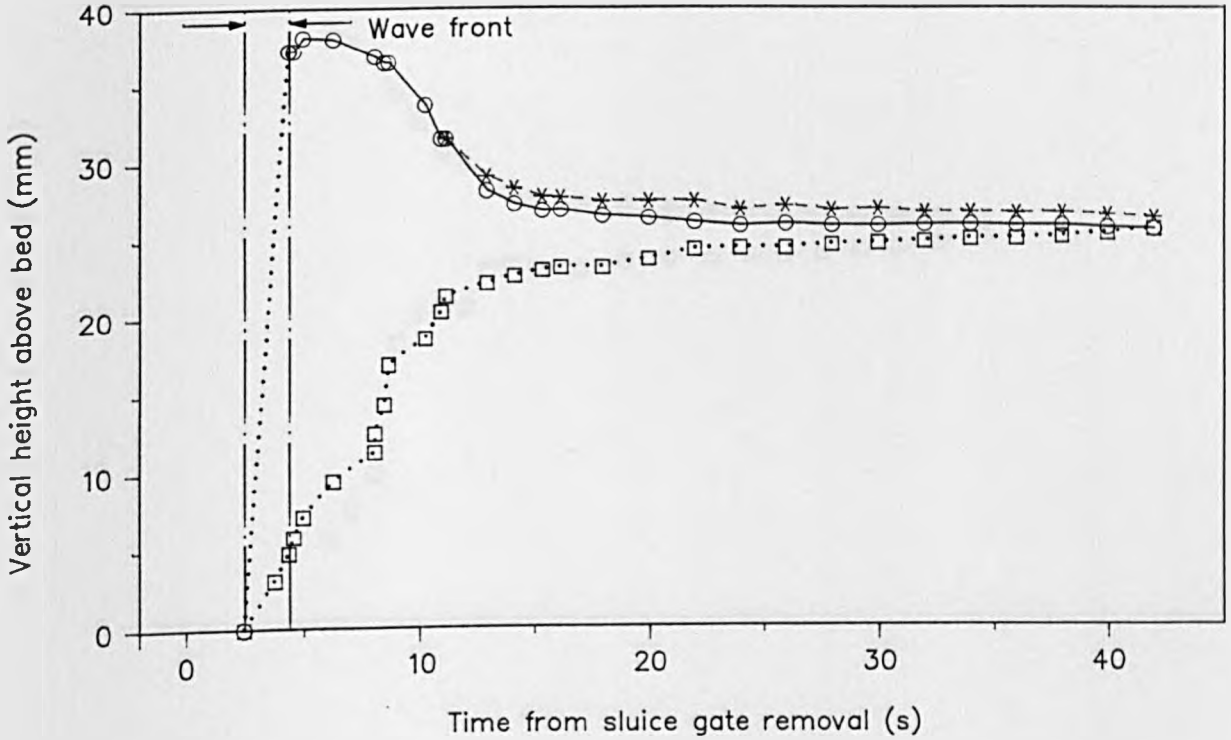


FIG 8.11

TEST 7M AT 0.3M FROM THE SLUICE GATE SITE
 CHANNEL BED SLOPE = 9 DEGREES
 (VIDEO RECORDS)

a) TEMPORAL VARIATION IN DEPTHS OF FLOWSLIDE MATERIAL



b) COMPARISON OF MEASURED AND CALCULATED PORE WATER PRESSURES

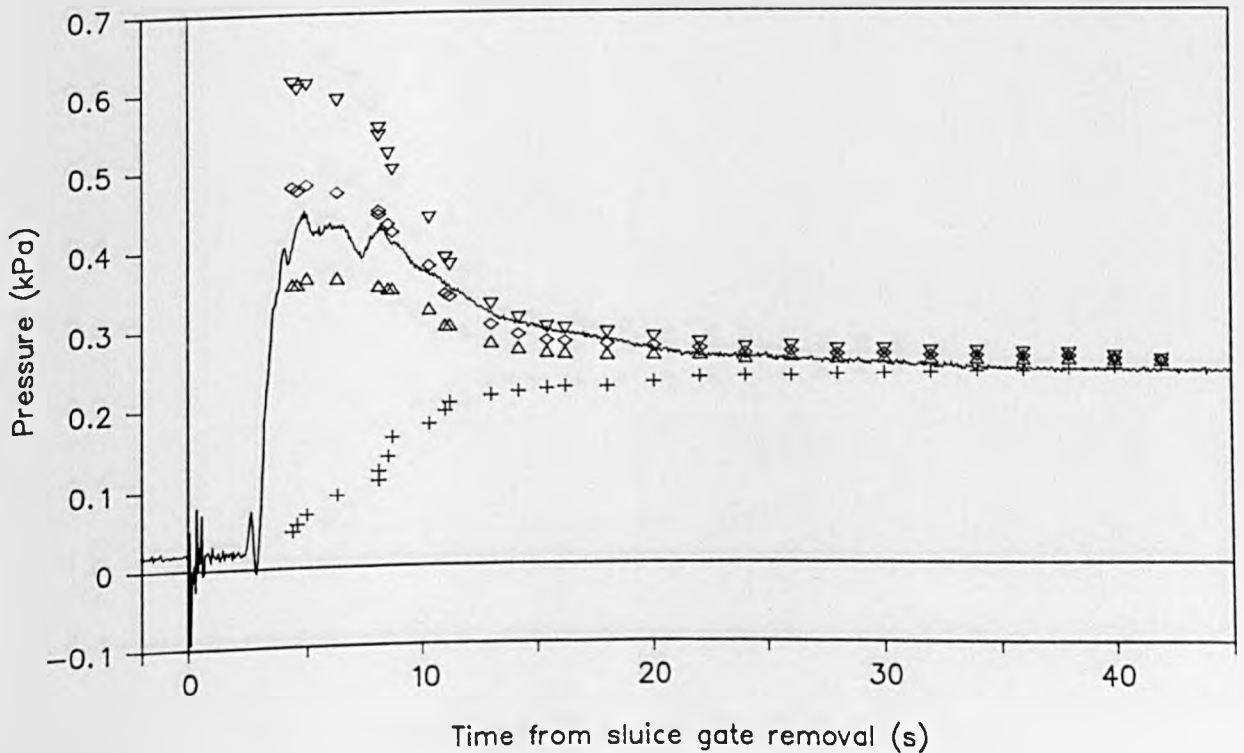
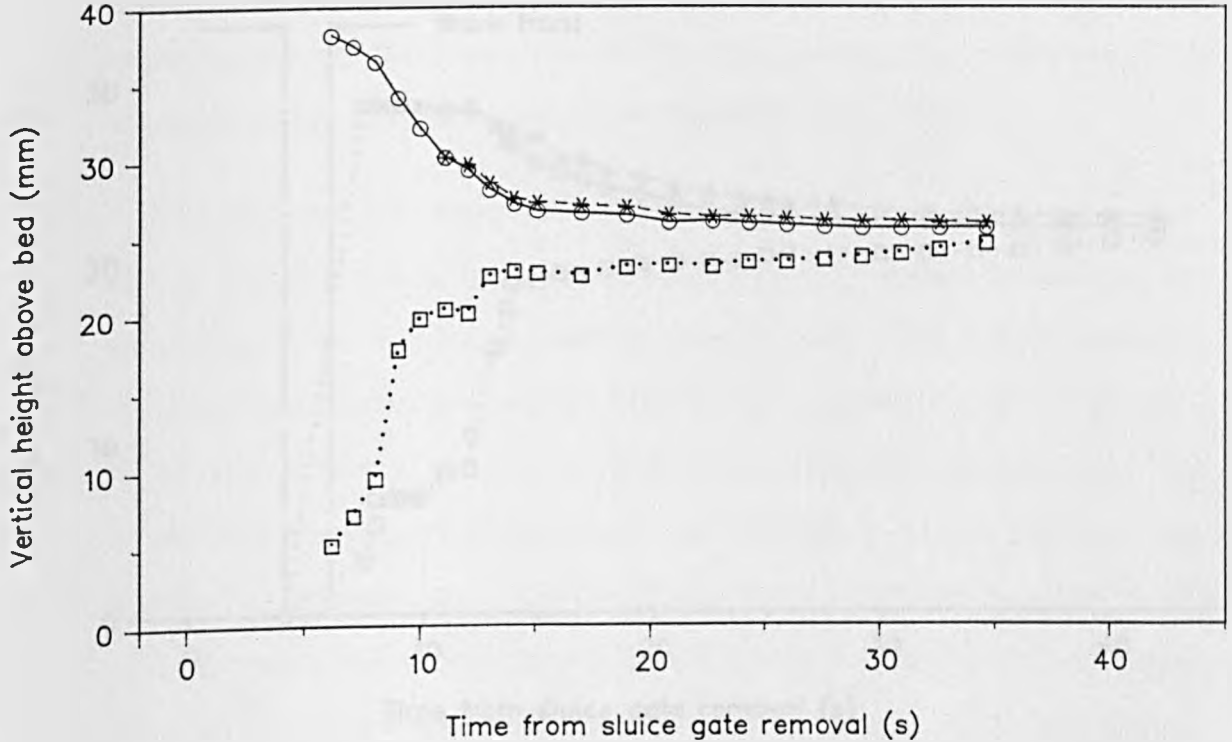


FIG 8.12

TEST 7M AT 0.3M FROM THE SLUICE GATE SITE
CHANNEL BED SLOPE = 9 DEGREES
(PHOTOGRAPHIC RECORDS)

a) TEMPORAL VARIATION IN DEPTHS OF FLOWSLIDE MATERIAL



b) COMPARISON OF MEASURED AND CALCULATED PORE WATER PRESSURES

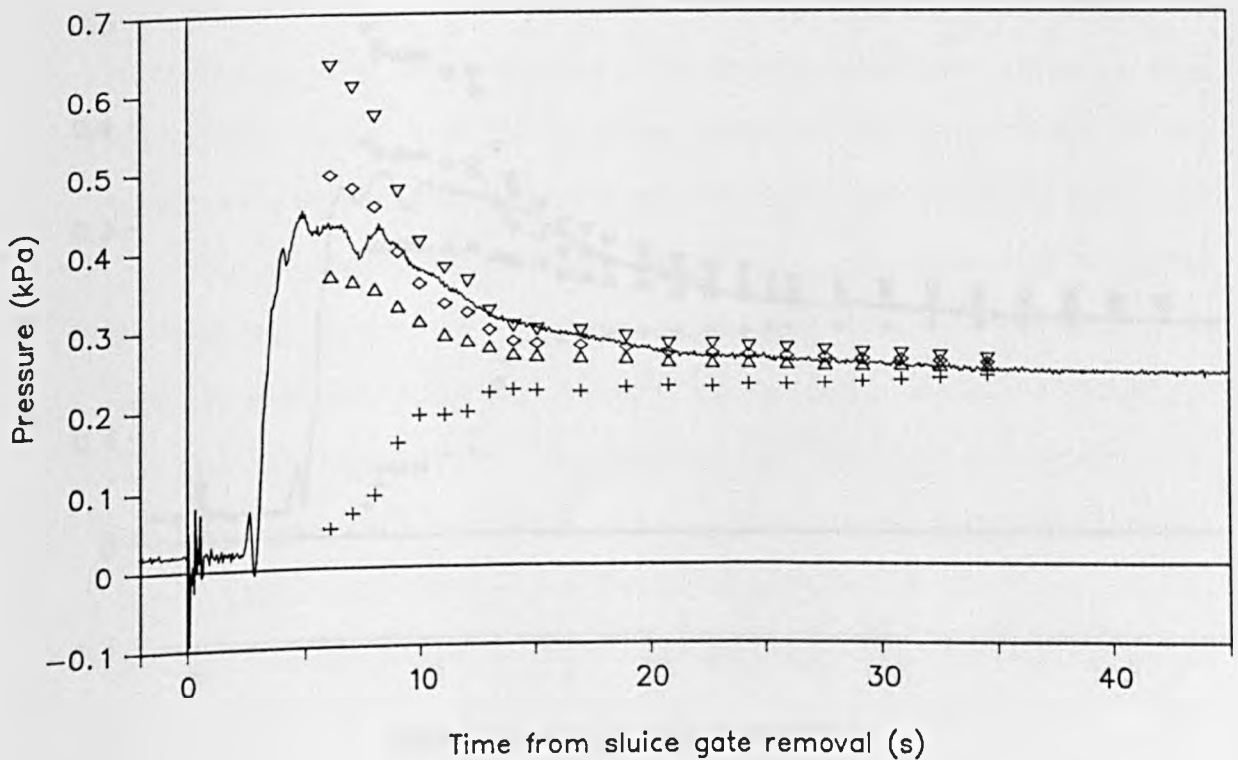
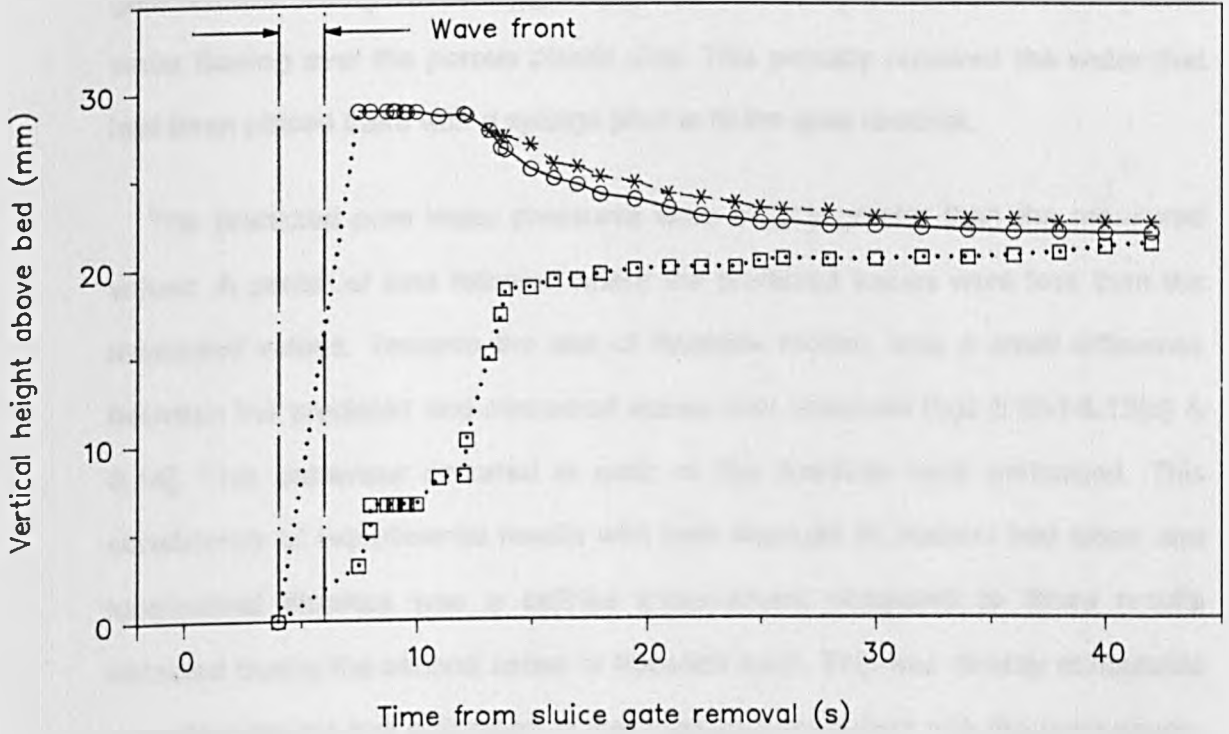


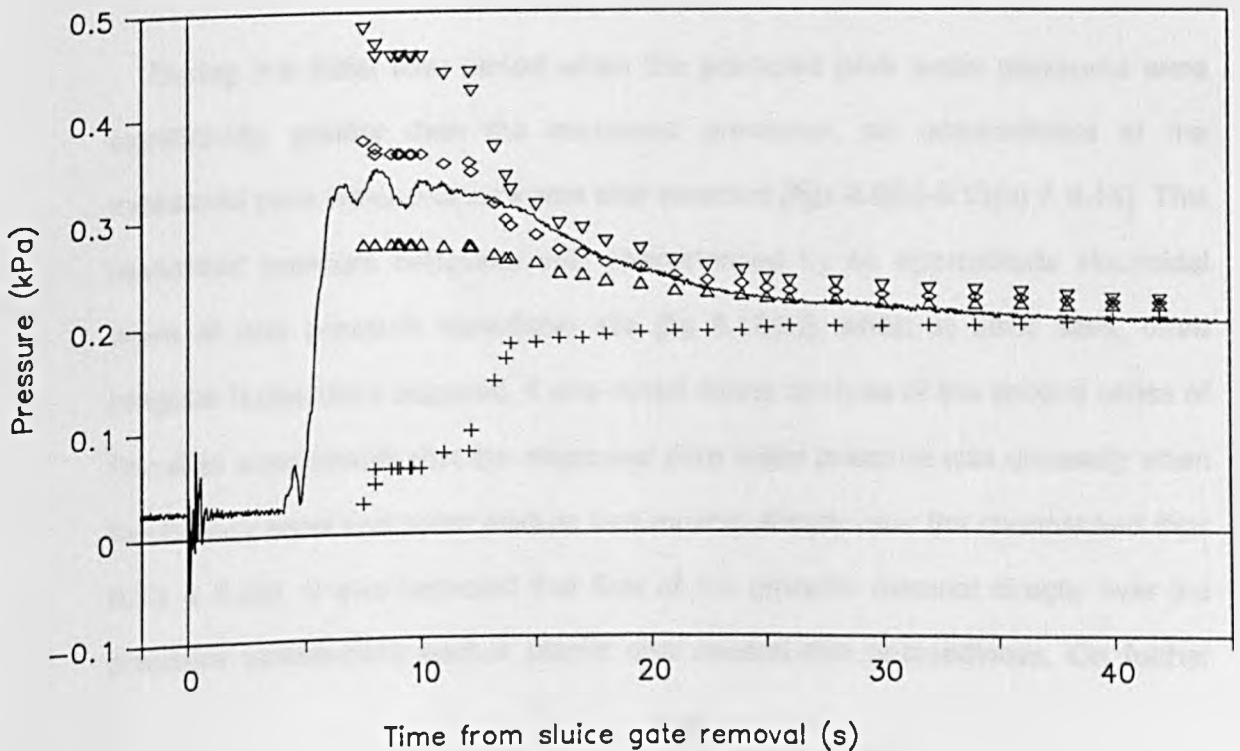
FIG 8.13

TEST 7M AT 0.5M FROM THE SLUICE GATE SITE
CHANNEL BED SLOPE = 9 DEGREES
(VIDEO RECORDS)

a) TEMPORAL VARIATION IN DEPTHS OF FLOWSLIDE MATERIAL



b) COMPARISON OF MEASURED AND CALCULATED PORE WATER PRESSURES



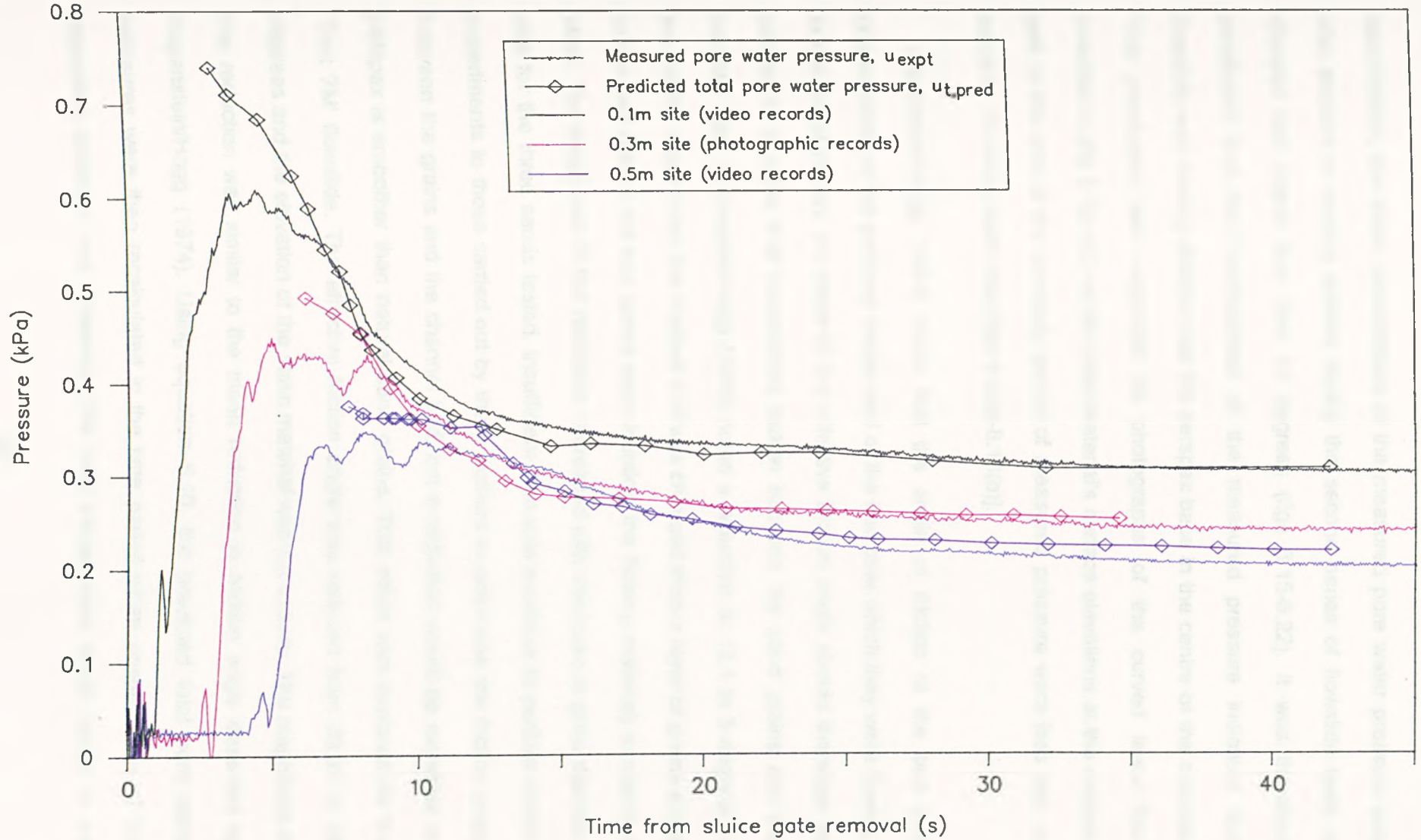
gate removal, prior to the arrival of the flowslide [figs 8.8(b)-8.13(b)]. Therefore, the removal of the sluice gate did not cause any drift in the pressure transducer output. The decrease in the pressure observed at about 15 seconds from sluice gate removal during Test 4M [fig 8.9(b)] was caused by a small isolated droplet of water flowing over the porous plastic disc. This partially removed the water that had been placed there with a syringe prior to sluice gate removal.

The predicted pore water pressures were initially greater than the measured values. A period of time followed where the predicted values were less than the measured values. Towards the end of flowslide motion, only a small difference between the predicted and measured values was observed [figs 8.8(b)-8.13(b) & 8.14]. This behaviour occurred in each of the flowslide tests performed. This consistency of experimental results with both changes in channel bed slope and longitudinal distance was a definite improvement compared to those results obtained during the second series of flowslide tests. This was directly attributable to performing pre-test calibration of the pressure transducers with the point gauge. The temporal variation of the difference between the predicted and measured pore water pressures is now discussed.

During the initial time period when the predicted pore water pressures were significantly greater than the measured pressures, an unsteadiness of the measured pore water pressure was also detected [figs 8.8(b)-8.13(b) & 8.14]. This measured pressure behaviour was characterised by an approximate sinusoidal wave at one pressure transducer site [fig 8.13(b)], whilst at other sites, more irregular fluctuations occurred. It was noted during analysis of the second series of flowslide experiments that the measured pore water pressure was unsteady when the flowing sand and water mixture was moving directly over the channel bed (figs 6.23 & 6.24). It was expected that flow of the granular material directly over the pressure transducer's porous plastic disc caused this unsteadiness. On further

FIG 8.14

COMPARISON OF THE MEASURED AND PREDICTED TOTAL PORE WATER PRESSURES AT THREE OBSERVATION SITES DURING FLOWSLIDE TEST 7M; CHANNEL BED SLOPE = 9 DEGREES



measured pressures at each longitudinal distance (fig 8.15). The initially high flowslide surface slope observed at the 0.1 m site may explain the poor agreement of the first two values of the altered predicted pore water pressure with the measured pressure. In addition, accelerations of the flowslide at each of the transducer sites occurred during this initial period, with the magnitude of the acceleration decreasing with increasing longitudinal distance (fig 8.16). The potential influence of flowslide acceleration was not incorporated into pore water pressure analysis, but it was noted that a change in shear strain rate would not affect the value of the effective friction angle, as strain rate does not affect the position of the steady state line in (p', q) stress space (section 2. 51).

Attention is now focused on the time period where the predicted total pore water pressure was less than the measured pressure. It was noted that for flowslide Test 7M, deceleration from the peak surface velocity at each pressure transducer site continued until about 17 seconds after sluice gate removal (fig 8.16). This was close to the end of this pressure period for each transducer position (fig 8.14). It was expected that an increase in the slip surface slope occurred during flowslide motion (section 8.22). The influence of this on the magnitudes of the predicted and minimum total pore water pressures was explored using the data collected at the 0.3 m site during Test 7M. This was performed by substitution of the flowslide surface slopes obtained from the photographic records in place of the channel bed slope (equations 5.10 & 5.11). This procedure affected all the contributions to the total pore water pressure. The photographic records were used due to their greater accuracy. The flowslide surface slopes were used as these were slightly greater than the surface slope of the static material, thereby maximising the potential error. As expected from fig 5.3, the increase in slope caused a reduction in the predicted pore water pressure and a smaller reduction in the minimum total pore water pressure (fig 8.17).

examination, this initial unsteadiness of the measured pore water pressure was also present to varying extents during the second series of flowslide tests at channel bed slopes less than 12 degrees (figs 6.15-6.22). It was therefore concluded that this unsteadiness of the measured pressure indicated that flowslide was moving directly over the perspex base in the centre of the channel. This conclusion was supported by photographs of the curved lower flow boundaries [fig 8.1(a-d)], as the static material's surface elevations at the channel wall at the end of the unsteady period of measured pressure were less than or equal to 10 mm in each case [figs 8.8(b)-8.13(b)].

Augenstein/Hogg (1974) found that the angle of friction at the bed was characteristic of the particles' nature and of the bed over which they were flowing. In this initial region, the value of the effective friction angle should therefore be altered to a value that represented friction between the sand grains and the perspex bed. Augenstein/Hogg (1974) noted a reduction of 12.1 to 5 degrees in the friction angle when the channel bed was changed from a layer of grains glued to the bed (where the bed grains were identical the flowing material) to stainless steel. The magnitude of this reduction decreased with decrease in grain diameter size for the three sands tested. Insufficient time was available to perform similar experiments to those carried out by these authors to determine the friction angle between the grains and the channel bed, but a reduction would be expected as perspex is smoother than natural sand grains. This effect was explored for the 'Test 7M' flowslide. The effective friction angle was reduced from 33.37 to 25 degrees and the elevation of the static material was set to zero. The magnitude of this reduction was similar to the mean reduction in friction angle observed by Augenstein/Hogg (1974). Using equation 5.10, the predicted total pore water pressures were then recalculated in the time period when unsteadiness of the measured pressure was observed. The new values were much closer to the

FIG 8.15 COMPARISON OF MEASURED AND PREDICTED TOTAL PORE WATER PRESSURES, ILLUSTRATING REDUCTION IN CALCULATED VALUES WHEN FLOW OVER CHANNEL BED WAS EXPECTED (TEST 7M, CHANNEL BED SLOPE = 9 DEGREES)

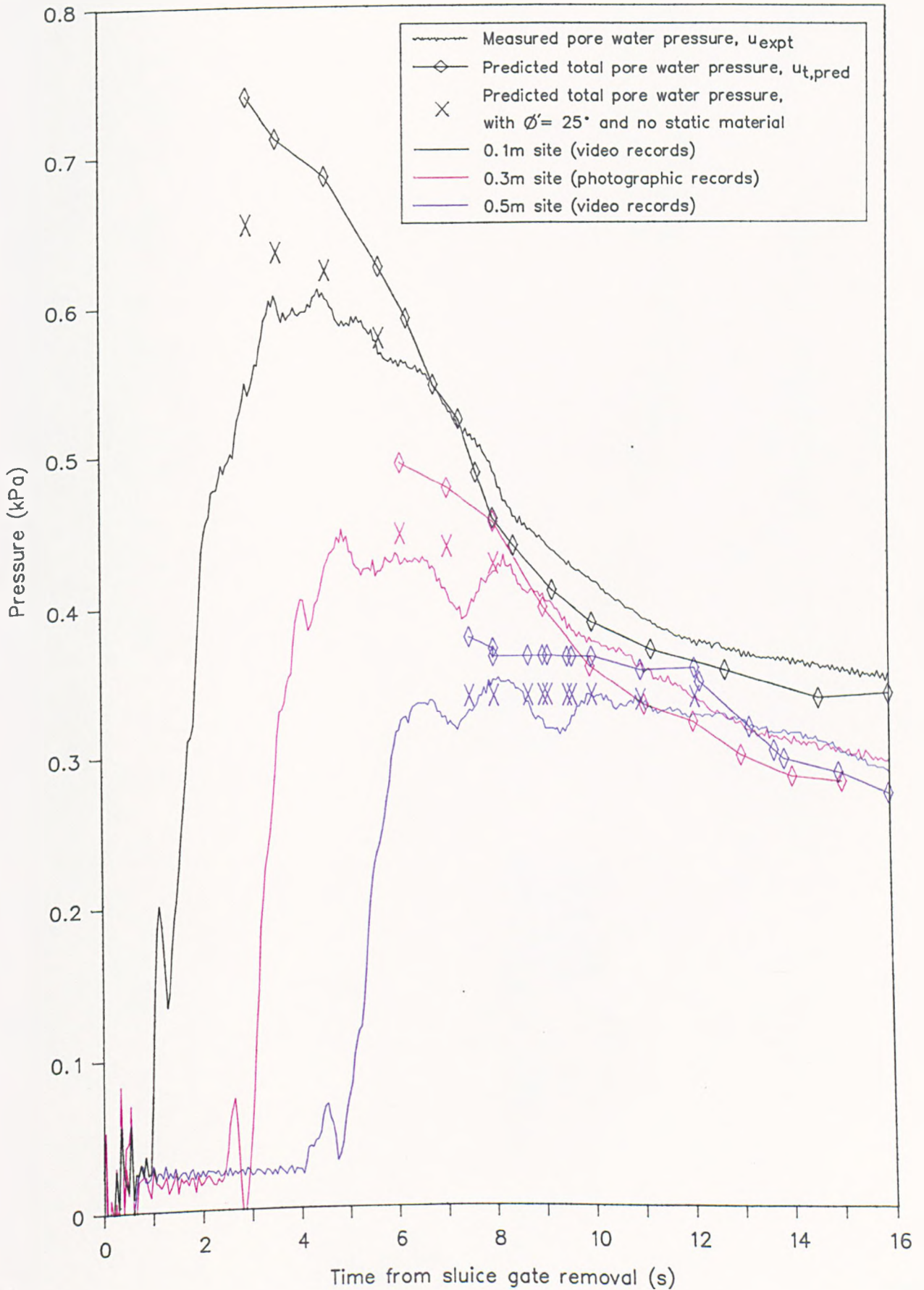


FIG 8.16

AVERAGE SURFACE VELOCITIES MEASURED ABOVE THE THREE OBSERVATION SITES
DURING FLOWSLIDE TEST 7M; CHANNEL BED SLOPE = 9 DEGREES

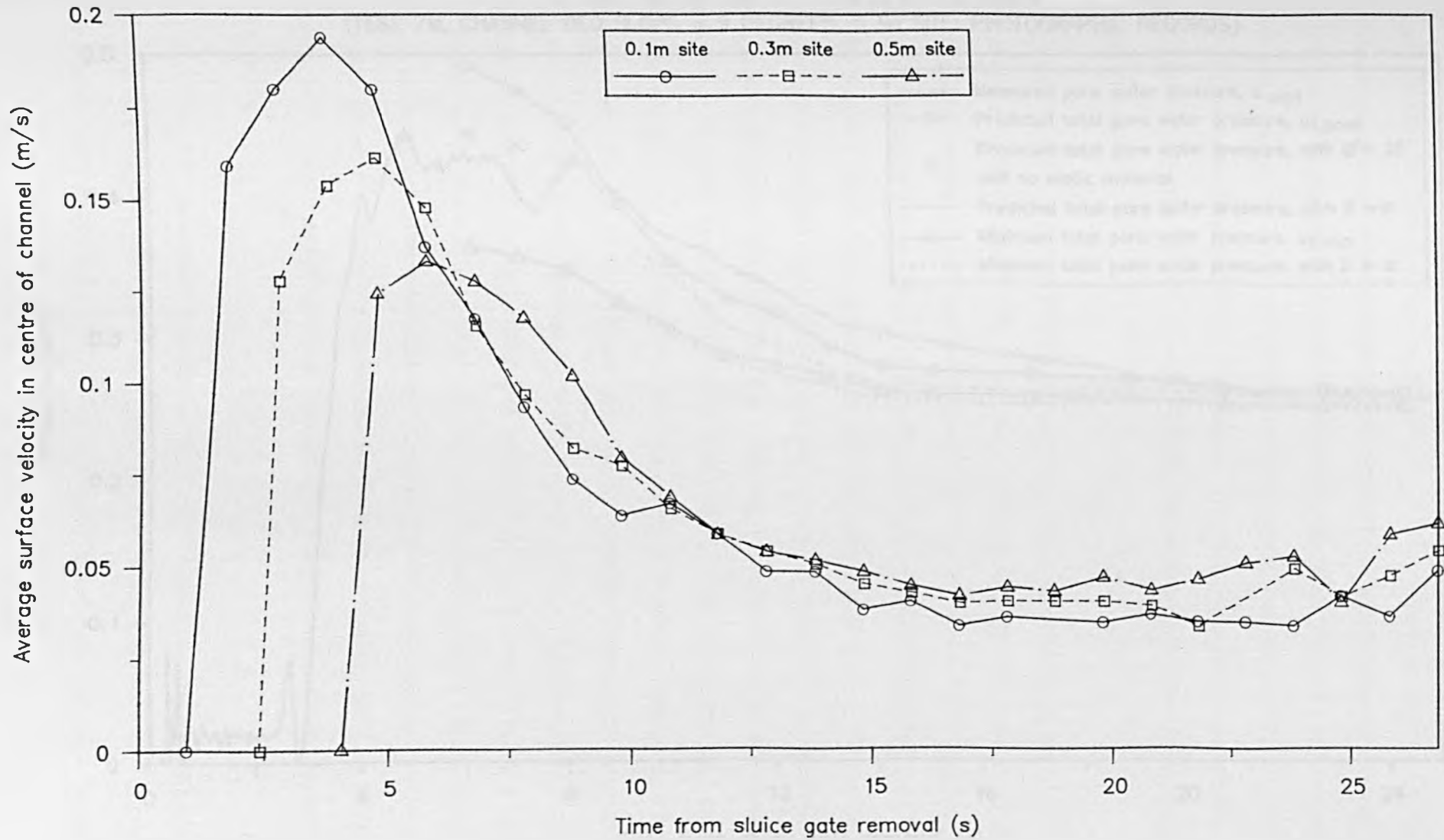
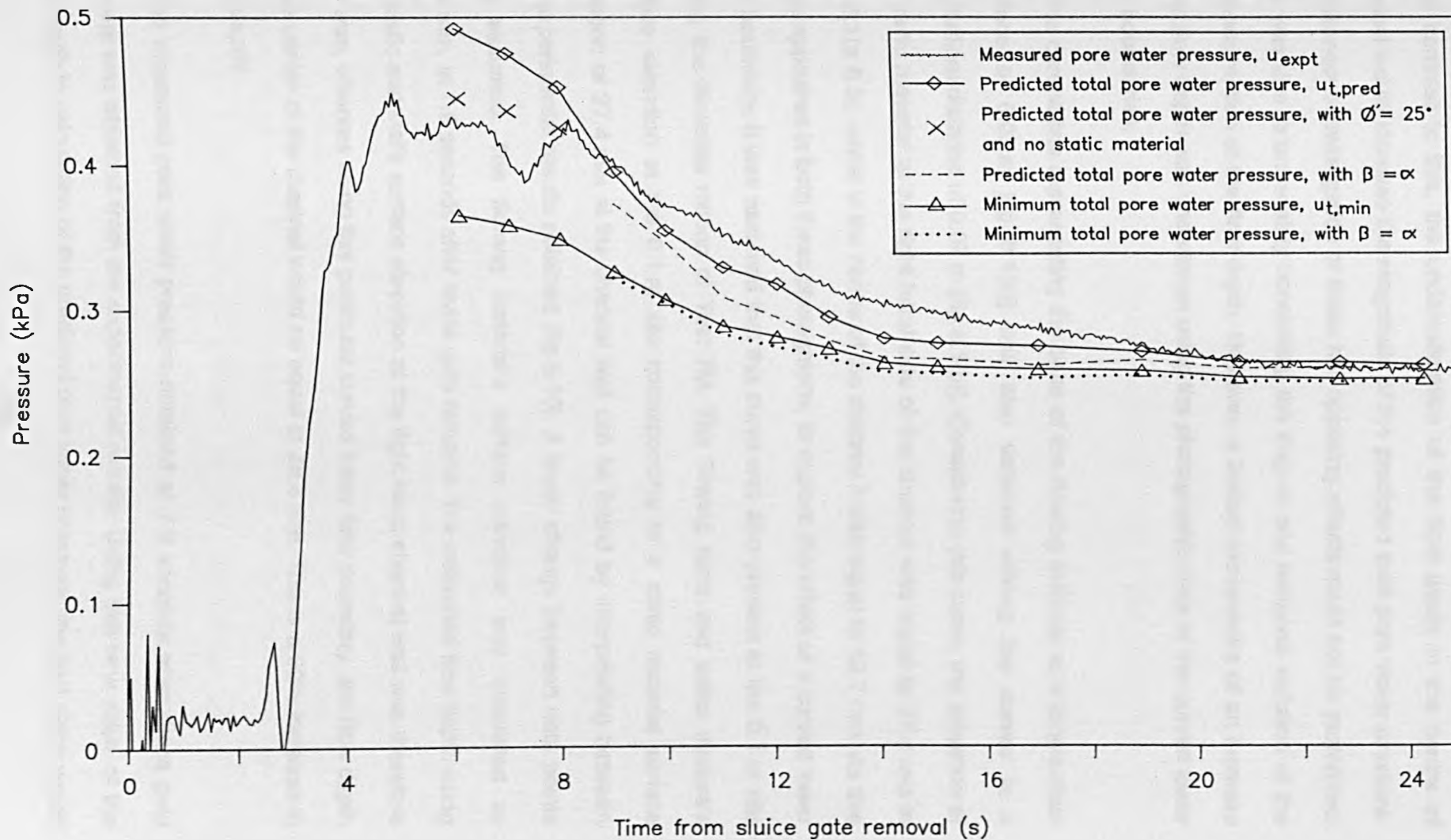


FIG 8.17

COMPARISON OF MEASURED AND CALCULATED PORE WATER PRESSURES,
 ILLUSTRATING EFFECT OF CHANGE IN BED SLOPE
 (TEST 7M, CHANNEL BED SLOPE = 9 DEGREES, 0.3M SITE: PHOTOGRAPHIC RECORDS)



In contrast to this, the underestimation of the flow depth in the centre of channel would increase the magnitude of the predicted total pore water pressure. Simultaneous investigation of these two opposing effects could not be performed. This was due to uncertainty concerning the degree and temporal variation of the underestimation of the flow depth. However, a limited assessment of an increase in the flow depth was undertaken using the photographic data of the curved lower flow boundaries.

The curved line representing the base of the flowing material at a longitudinal distance of 0.08 m [fig 8.1(a)] was also detected among the curves at a longitudinal distance of 0.07 m [fig 8.1(b)]. Considering this curve, the elevation of the static material at the right hand side of the channel was equal to 27.4 mm in figs 8.1(a & b), whilst in the centre of the channel it was equal to 13.7 mm. As this curve appeared in both these photographs, to explore the effect of a curved lower flow boundary, it was assumed that this curve was also present at the 0.1 m site during the flowslide motion of Test 7M. The flowing sand and water mixture's surface elevation at the 0.1 m site corresponding to a static material surface elevation of 27.4 mm at the channel wall can be found by interpolating between the experimental results obtained (fig 8.10). A linear change between data points was assumed. The flowing material's surface elevation was calculated as 42.5 mm, at 7.9 seconds after sluice gate removal. The estimated flow depth using the static material's surface elevation at the right hand channel wall was therefore 15.1 mm, whereas using this particular curved lower flow boundary, the flow depth in the centre of the channel would be equal to 28.8 mm. This is a 90% increase in flow depth!

The measured pore water pressure obtained at 7.9 seconds after sluice gate removal was obtained from the experimental results. Using this new value of the flow depth in calculation of the predicted pore water pressure, the bed slope would

have to be increased from 9 to 10.43 degrees to obtain agreement with the measured pressure. This increased bed slope was similar to the measured flowslide surface angle α of 10.6 and 11 degrees measured at 7.65 and 8 seconds respectively after sluice gate removal at the 0.1 m site (fig 8.5). Given that assumptions had to be made, the effect of an increase in both the bed slope and the flow depth seems to satisfactorily explain why the predicted total pore water pressure was less than the measured values [figs 8.8(b)-8.13(b) and 8.14].

The results of Test 4M [fig 8.9(b)] showed that an increase in the measured pore water pressure occurred at a time of about 34 seconds from sluice gate removal. The magnitude of the rise in measured pressure was just greater than the manufacturers' stated accuracy for the pressure transducer. The surface elevation of the static material was about 13 mm at this point. This behaviour may have been caused by the material moving over the channel bed. This rise resulted in a poorer fit with the predicted total pore water pressure than was achieved in the other flowslide tests in the third series of experiments. The quality of this test must therefore be regarded as poorer due to this anomaly.

Near the end of flowslide motion, the measured and predicted total pore water pressures were close for Test 3M [fig 8.8(b)], and for Test 7M at the 0.1 m and 0.3 m sites (fig 8.14). The measured pressure was greater than the predicted pore water pressure during Test 4M [fig 8.9(b)], whilst it was less than predicted and minimum pore water pressures for Test 7M at the 0.5 m position [fig 8.13(b)]. At the end of flowslide motion, it was even less than the pore water pressure calculated to be present at the surface of the static material at this site [fig 8.13(b)]. The major contribution to the calculated pore water pressures was from the static material, hence the similarity between the maximum, predicted and minimum values. It was assumed that seepage of water parallel to the channel bed occurred within the static material (section 5.3). If it is assumed that the water

was seeping parallel to the surface of the static material, this would for example only result in a 0.5% decrease in the calculated pore pressure for the last data point obtained at the 0.1 m site for Test 7M [fig 8.10(b)]. The variation in fit with the measured pore water pressure was therefore attributed to possible small combined errors in pressure transducer calibration, accuracy of the pressure transducers, data extraction from the video records and assumptions concerning the pore water pressure within the static material.

After all flowslide motion had ceased, the static material's saturated bulk density was again determined for comparison with the density of the test sample prior to failure. The accuracy of the volume calculations was increased by reducing the longitudinal distance between height measurements at the channel wall. The results are presented in Table 8.1. These show that only a small percentage increase in density from the test sample value was observed for Tests 6M and 7M. In particular, the percentage increase in density of the three longitudinal sections measured from the Test 7M flowslide were very similar. A high initial saturated bulk density or solid volume concentration was recorded for Test 4M, indicating that a 2.9% decrease in density had occurred. The effect of this change in density for the flowing material on the predicted total pore water pressure was explored by altering the volumes of the test sample in a sensitivity analysis, keeping the other variables the same as those reported in section 5.6. At a channel bed slope of 9 degrees, this resulted in a 1.7% decrease in pore water pressure, with a 2.1% decrease occurring when elevations of 10, 30 and 31 mm were used for the static material, flowing material and surface water respectively. This possible decrease in density would worsen the fit of the predicted total pore water pressure with the measured values. Bagnold (1955) observed a change in flow mechanism when the solid volume concentration was greater than 0.5, with grains being pushed bodily along the bed, rather than flow. An obvious difference in flow mechanism

was not observed in this test.

The shearing action of the surface water could also have caused a possible dilatation of the grains in the flowing sand and water mixture. The depth of material affected by the surface water could not be quantified, due to the failure to obtain vertical velocity profiles at the channel wall. The possible decrease in density was of minor importance, compared to uncertainty concerning the value of the slip surface slope and the position of the lower flow boundary in the centre of the channel. Due to the similarity of the initial and final bulk densities, it was concluded that there was little error in the use of the saturated bulk density obtained from the initial test sample for the density of the flowing material when $C < 0.5$.

Comparison of the measured pressure with the upper and lower bounds to the predicted total pore water pressure illustrated that the maximum total pore water pressure was significantly higher than the measured pore water pressure in all cases initially [figs 8.8(b)-8.13(b)]. Underestimations of both the flow depth and slip surface slope meant that an apparently better fit of the maximum total pore water pressure with the measured pressure was obtained at some stages during the flowslide motion. This was not significant and it can be taken that the upper bound values were a less realistic representation of the measured pore water pressures than the predicted values.

The influence of the error in bed slope or flowslide surface slope during motion on the minimum total pore water pressure has already investigated (fig 8.17). The results showed only a small lowering of the minimum total pore pressure values. The neglect of the surface slope of the flowslide in these calculations was justified because the minimum calculated pore pressure was used as a lower bound. The results of this operation further lowered its position relative to the measured pore

water pressure, hence the unaltered values were more conservative. The position of the base of the flowing layer did not have an influence on the magnitude of the minimum total pore water pressure. The results of the third series of flowslide tests [figs 8.8(b)-8.13(b)] showed that the minimum calculated pore water pressure was lower than the measured pore water for the duration of the flowslide at each observation site, except near the end of flowslide motion during Test 7M at the 0.5 m observation site. It can therefore be concluded that excess pore water pressures were definitely present during flowslide motion. This refutes the proposal that particle support by the presence of excess pore water pressures is not realistic [Davies (1988)].

The predicted total pore water pressure gave a good representation of the measured pore water pressure during these flowslide tests. Investigation of the effect of errors concerning the magnitudes of flow depth and slip surface slope has shown that the difference between predicted total pore water pressure and the measured pressure can be satisfactorily explained. The similarity of the data obtained at the three different longitudinal sites during one flowslide experiment [fig 8.10(b)-8.13(b) & 8.14] and at different bed slopes [fig 8.8(b) & 8.12(b)] suggested that change of these variables did not affect the agreement of the predicted and measured pore water pressures. The results of the third series of experiments can only be compared to those of the second with a degree of caution, due to potential errors in pressure transducer calibration in the latter. The extremely close agreements obtained at the 0.1 m position with a channel bed slope of 6 degrees (fig 6.19 & 6.20) during the second series of experiments were perhaps somewhat fortuitous. This close agreement was probably the result of the opposing effects of potential increases in slip surface slope and flow depth on the predicted total pore water pressure. No error bounds were presented on any of the figures illustrating experimental data. The accuracy to which the various elevations

were measured was high. Illustration of these would only have made the figures more confusing. The main reason for not including error bounds was that they would have been misleading, as the effect of flow depth underestimation could not be properly quantified and therefore could not be incorporated.

8.4 IMPLICATIONS OF THE OF THE LABORATORY RESULTS

It was proposed during this research that the pore water pressure present at the base of the flowing material must be of sufficient magnitude to reduce intergranular friction, such that the driving force and resisting force according to Coulomb's law were just in balance. This predicted basal pore water pressure, together with pore water pressure contributions from the static material and surface water, gave a good representation of the measured pore water pressure, within the errors of experimental measurement. The presence and magnitude of these excess pore water pressures are important because the reduction in intergranular friction explained why fluid-like behaviour of the flowslide was observed.

The required magnitude of these excess pore water pressures decreased with increase in slip surface slope, until flow with no excess pore water pressures would be possible. Uniform flow at this slope [or equilibrium slope: Winterwerp et al (1990)] has been observed. As the flowslides during this research were conducted at bed slopes less than their equilibrium slopes, deceleration and an eventual halt of the flowslide were observed. Thus, whilst excess pore water pressures were present at the base of the flowing material, it was apparent that these could not be maintained as sand grains were deposited at the base of the flowing material.

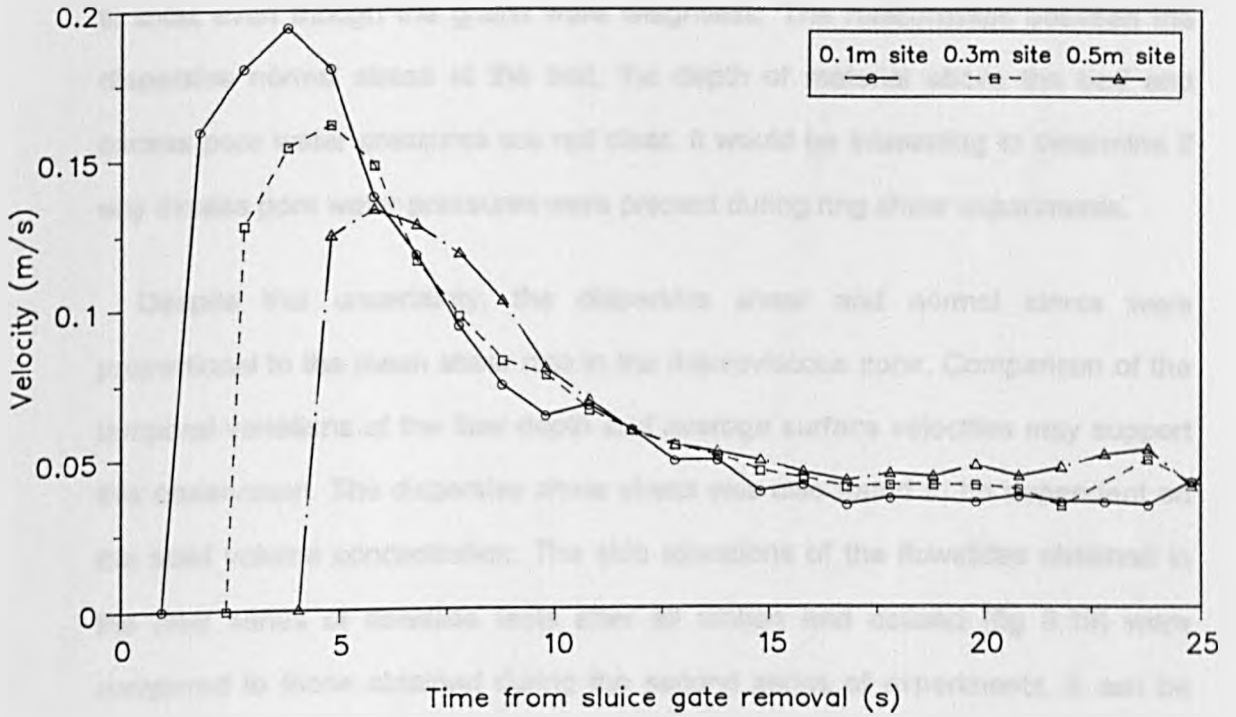
It was therefore interesting to compare the temporal variation of both the flow depth and the average surface velocity (fig 8.18). Despite uncertainty concerning the exact magnitude of the flow depth in the centre of the channel, similar trends were observed at the 0.1 m and 0.3 m sites, and less so at the 0.5 m site. Comparison of figs 8.4 and 8.16 also revealed that the peak flowslide surface elevation corresponded to the peak average surface velocity in the centre of the channel. The velocity, or shear strain rate, in addition to the driving force was therefore expected to influence grain deposition. This was supported by data obtained from moving bed experiments where the height of a granular fluid wave was found to be proportional to the bed speed [Davies (1988)]. In addition, it has been shown that a granular fluid wave can be maintained indefinitely in a moving bed apparatus [Davies (1988)]. Therefore, those theories that propose grain deposition in isolation from accelerations of the flowslide, such as 1-D consolidation [Hutchinson (1986)] and hindered settling [Bezuijen/Mastbergen (1988)] may not be correct.

Bagnold (1954) showed that a resistance to shear was caused by dispersive pressures between neutrally buoyant spheres undergoing shear (section 2.72). It was found that two distinct regions of behaviour existed; a grain inertia and a macroviscous zone, separated by a transition region. The laboratory flowslides in this experimental work were all in the macroviscous region, according to Bagnold's criteria using equation 2.13 (section 2.82). Bagnold (1954) found that the dispersive shear stress was proportional to the mean shear rate and the dispersive normal stress. This work has been extended by other researchers using ring shear apparatus (section 2.82), and the dispersive stress ratio has been related to a dynamic angle of friction, which remained nearly constant. Bagnold (1956) assumed that the dispersive normal stress at the bed was equal to the normal stress originating from the buoyant weight of grains above the bed level. The

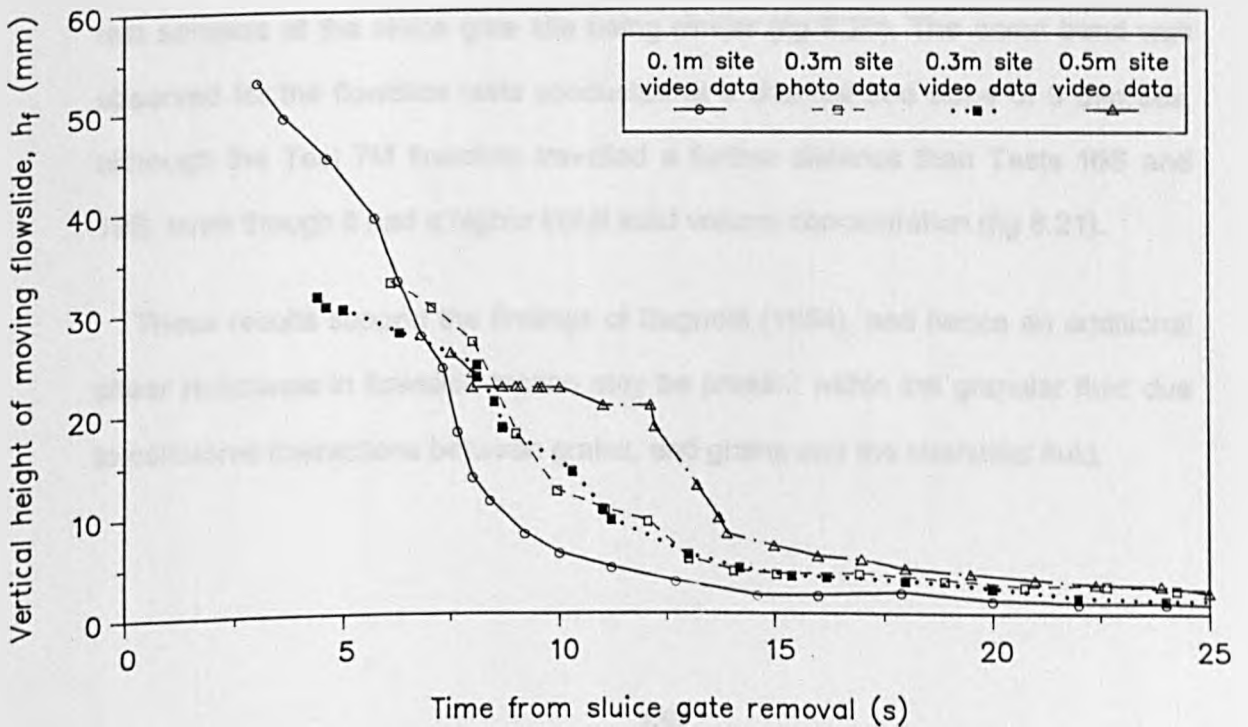
FIG 8.18

COMPARISON OF AVERAGE SURFACE VELOCITIES AND FLOW DEPTHS DURING FLOWSLIDE TEST 7M; CHANNEL BED SLOPE = 9 DEGREES

a) TEMPORAL VARIATION OF AVERAGE SURFACE VELOCITIES IN THE CENTRE OF THE CHANNEL



b) TEMPORAL VARIATION OF FLOW DEPTH AT THE THREE OBSERVATION SITES



variation of the magnitude of the excess pore water pressures with slip surface slope obtained during these experiments questions this concept. In addition, Bagnold (1954) obtained the expressions for the dispersive stresses from the shearing of neutrally buoyant spheres. These stresses have therefore been shown to exist even though the grains were weightless. The relationships between the dispersive normal stress at the bed, the depth of material above the bed and excess pore water pressures are not clear. It would be interesting to determine if any excess pore water pressures were present during ring shear experiments.

Despite this uncertainty, the dispersive shear and normal stress were proportional to the mean shear rate in the macroviscous zone. Comparison of the temporal variations of the flow depth and average surface velocities may support this observation. The dispersive shear stress was also found to be dependent on the solid volume concentration. The side elevations of the flowslides obtained in the final series of flowslide tests after all motion had ceased (fig 8.19) were compared to those obtained during the second series of experiments. It can be seen that at a channel bed slope of 6 degrees, increases in final run out distance occurred with decreases in solid volume concentration, the initial heights of the test samples at the sluice gate site being similar (fig 8.20). The same trend was observed for the flowslide tests conducted at a channel bed slope of 9 degrees, although the Test 7M flowslide travelled a further distance than Tests 16S and 19S, even though it had a higher initial solid volume concentration (fig 8.21).

These results support the findings of Bagnold (1954), and hence an additional shear resistance in flowslide motion may be present within the granular fluid due to collisional interactions between grains, and grains and the interstitial fluid.

FIG 8.19

SIDE ELEVATIONS OF SETTLED TEST SAMPLE AND CORRESPONDING FLOWSLIDE AFTER ALL MOTION HAS CEASED, FOR FLOWSLIDE TESTS AT VARIOUS BED SLOPES

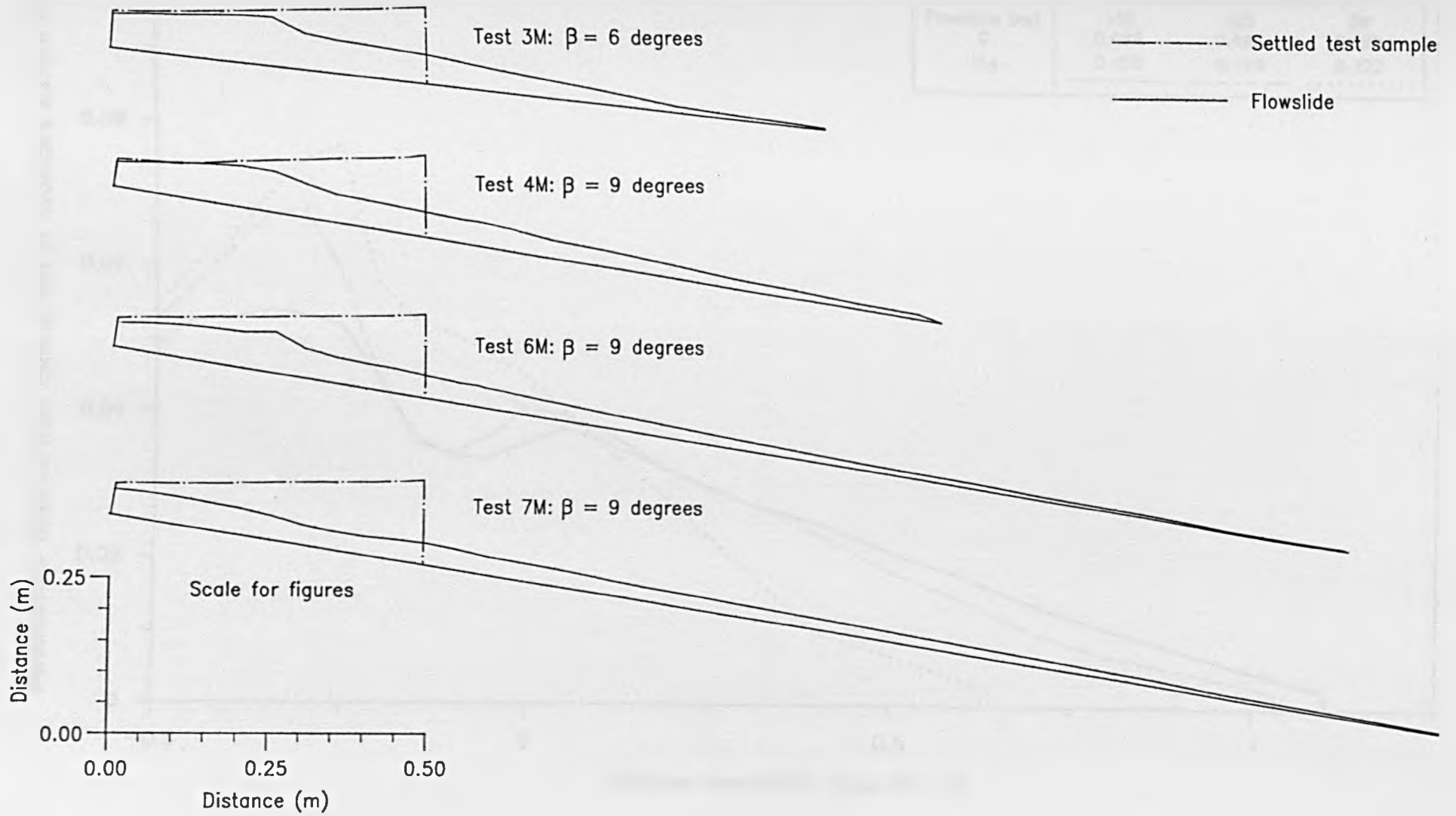


FIG 8.20

SIDE ELEVATIONS OF FLOWSLIDES AFTER ALL MOVEMENT HAS CEASED
(CHANNEL BED SLOPE = 6 DEGREES)

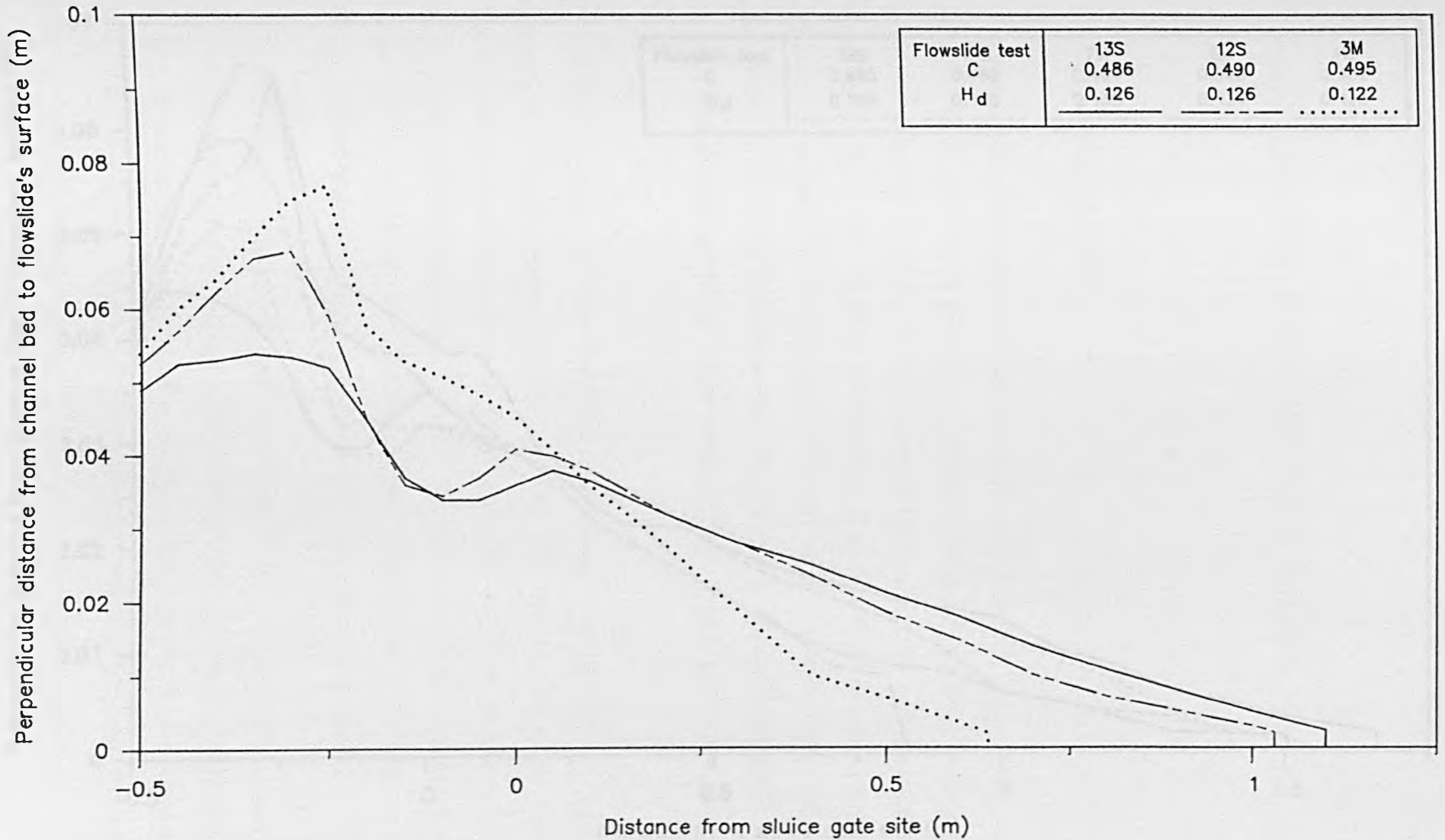
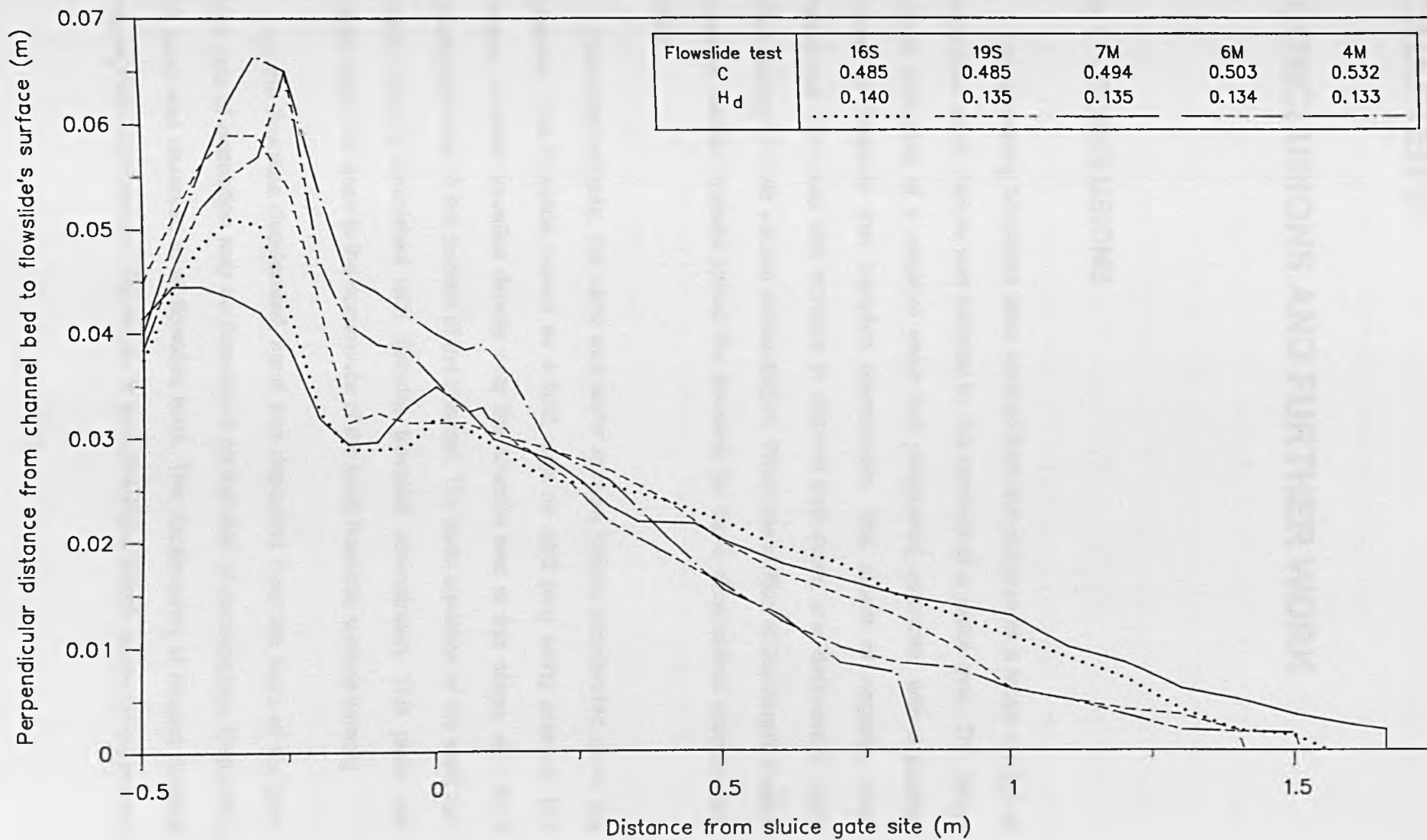


FIG 8.21

SIDE ELEVATIONS OF FLOWSLIDES AFTER ALL MOVEMENT HAS CEASED
(CHANNEL BED SLOPE = 9 DEGREES)



CHAPTER 9:

CONCLUSIONS AND FURTHER WORK

9.1 CONCLUSIONS

The laboratory flowslides were created from the collapse of a loose sample of saturated sand. Failure was initiated by the removal of a sluice gate. The failure mode consisted of a negative wave that progressed upstream, with a positive wave or flowslide that travelled downstream. The extent of negative wave behaviour increased with increase in channel bed slope, and decrease in initial bulk density or solid volume concentration. When the motion of the negative wave ceased, further material joined the flowslide by three dimensional retrogressive slips.

Following collapse, the sand and water mixture initially accelerated down the channel. The flowslide moved as a fluid, with no rigid plug being present. The flowing material travelled directly over the channel bed at this stage, with sand being deposited in the corners of the channel. The peak elevation of the sand and water mixture diminished with distance travelled downstream. This peak was observed to be close to the occurrence of the peak flowslide surface velocity.

As the flowslide decelerated, sand was deposited from the base of the flow. The rate of deposition may be dependent on the rate of deceleration. Deposition of sand was observed in all flowslide tests. The deceleration of flowing material propagated downstream. Deposition of sand therefore began at the upstream end

of the flowslide, and progressed downstream. As a result, the bed slope over which the flowing material was moving increased with the time.

The depth of flowing material, determined from the surface elevations of the flowing and static material at the channel wall, was found to be an underestimate of the flow depth in the centre of the channel. A transverse section through the flowslide would reveal that the lower boundary of the flowing material was concave in plan view. The magnitude of this underestimate may even have been as great as 90%. This curved lower boundary of the flowing material was a result of the flowing material minimising frictional contact, maximising its hydraulic radius. A slightly curved upper surface to the flowing material may have been present (convex in plan view), but no quantitative data was obtained.

Water was observed on the surface of the flowslide at varying times after sluice gate removal. This water was likely to be derived from the consolidation of material upstream that was not involved in the flow, and from an increase in density of the sand and water mixture as it was deposited. This surface water moved at a higher velocity than the flowslide, causing an additional shear force on the surface of the flowing sand and water mixture, which increased the velocity of the flowing sand and water mixture.

The deceleration and the rate of sand deposition decreased with time and the flowing sand and water mixture achieved nearly constant velocity. The flow depth here was small. Hereafter, the flow depth gradually decreased as further material was deposited at the base of the flowslide. The flowslide finally came to a halt when all the material had been deposited. Water continued to move over the surface of the flowslide at a decreasing rate, due to seepage from the body of static material under the influence of gravity. The distance that the flowslide travelled downstream from the sluice gate site was dependent on the gravitational

driving force and the saturated bulk density or solid volume concentration of the flowing material.

The results of pore water pressure measurements at the base of the laboratory channel showed that excess pore water pressures were definitely present within the moving material of the flowslide. Despite the limitations of measurement accuracy and underestimation of both the flow depth and slip surface slope, comparison of the predicted pore water pressure calculated at the base of a vertical element of the flowslide and the measured pressure suggested that the excess pore water pressure at the base of the flowing material sufficiently reduced the normal effective stress and intergranular friction to allow motion of the grains. This behaviour did not alter with change in either longitudinal distance at which the pore water pressure was measured or channel bed slope.

9.2 FURTHER WORK

Further study of flowslide motion should address several aspects, each of which may provide sufficient scope for research projects in their own right. It was noted during the literature study that several shear resistance mechanisms could influence granular fluid motion. These include turbulence, dispersive pressures and excess pore water pressures. Winterwerp et al (1990) stated that very little is known about the relations and interactions between the various phenomena. Further work to assess the importance of each type of flow mechanism is still necessary, even though this research project has elucidated certain aspects concerning the unsteady motion of flowslide. Work of this nature could be undertaken in different types of apparatus, such as open channels, viscometers, ring shear cells and triaxial apparatus. It has been noted that it is unclear how to

compare even the same particle sized material in ring shear cells of different size [Hanes/Inman (1985)]. Further attention is therefore required in this direction to establish the limitations of each measurement system. In order to establish model scale effects, a rigorous testing procedure of different particle sizes under an extensive range of experimental conditions would of course be necessary. A complete understanding of the underlying principles of granular fluid or flowslide motion is therefore only likely to emerge through the collation of the work of many.

Attention is now turned to the laboratory apparatus on which most guidance can be given. There are several improvements to the current laboratory apparatus that may prove useful to those anticipating to use open channels for laboratory work. The test sample preparation system would benefit from an increase in channel wall height. This would allow the fluidised sand bed to be raised to greater heights, and enable the overflow to be positioned a sufficient height above the sand bed to minimise loss of test material. A different test preparation system might be considered. This might involve keeping the base of the upstream section horizontal, with the downstream channel section being bolted to this at the desired test bed slope. This would allow a fuller investigation of the sample preparation procedure in-situ. More control over the test sample density may be obtained as the configuration of the sand in the upstream section would not alter with change in channel bed slope.

Open channel apparatus would be suitable for the study of the negative wave behaviour of the test sample failure. This has not, as yet, been investigated in a quantitative manner. This information obviously has important implications to the introduction of material to flowslides. Results obtained at the end the third series of these flowslide experiments have shown that this type of apparatus would be useful in the study of relationships between flowslide accelerations and material deposition.

Measurement of pore water pressure with pressure transducers of a more appropriate range would ensure a greater degree of accuracy. An increase in the number of pressure transducers would allow an arrangement of transducers in the vertical direction. This would yield information concerning the vertical distribution of pore water pressures in both the static and flowing material. The measurement of the pressure distribution within the static material would allow a more accurate assessment of the pressure contribution from this layer, rather than the assumption of pressures arising from seepage of water parallel to the bed. Measurement of the vertical distribution of pore water pressures in the flowing material may confirm the observations of Bezuijen/Mastbergen (1988), who found that this pressure decreased linearly with increase in height above the slip surface. It should be remembered that performance of the transducers during this research project was adversely affected by the movement of material directly over the pressure transducers' plastic discs. This problem may also occur with pressure transducers mounted at the channel wall. Investigation of the pore water pressure within the flowing material may be facilitated by use of a moving bed apparatus, in which there is no mean forward velocity relative to the channel walls. Mobile pressure transducers within the flowing material have also been used previously [Eckersley (1990)], and might be considered.

It is suggested that unless sophisticated video tape analysis facilities are available, measurement of the various flowslide elevations at the channel wall should be made using timed exposure photography rather than with video equipment. This is due to the greater accuracy and ease of data extraction that is obtainable. Measurement of vertical stresses has also been attempted elsewhere using load cells [Eckersley (1990)].

The investigation of the curved lower flow boundary should be a priority. The degree of curvature and the factors upon which it is dependent need to be

quantified. The inability to observe the interior of the granular fluid obviously pose difficulties. This problem might be overcome with the use of impedance tomography [Tozer et al (1992), Noel/Xu (1991), Turnbull/Griffiths (1985)]. Basically, this technique identifies areas that have different electrical properties, or conductivities. The previous success in determining solid volume concentrations for sand and water mixtures using conductivity probes [Bezuijen/Mastbergen (1988)] may mean it might be worth developing this instrumentation technique. It may be possible to obtain solid volume concentration data simultaneously. If progress is made with this system, possibilities exist with mounting the probes over a flat bed, to allow three-dimensional flowslide motion to be studied, in conjunction with timed exposure photography for surface velocity measurements. This latter technique proved to be useful during this research project, but improvements could perhaps be made through the controlled introduction of tracer particles. Data can also be obtained concerning the flowslide's surface elevation, and transverse and longitudinal variation of the flowslide's surface slope with this method [Johnson/Rodine (1984)]. Stereo photography could also be used.

Unfortunately, due to the nature of granular fluids, vertical velocity distributions obtained with any measurement device would still be restricted to the channel wall. Even so, this information would be important to ascertain shear strain rates and the effect of the surface water on flowslide motion.

It is proposed that until the uncertainties concerning the behaviour of granular fluid waves can be resolved, use of materials that are not of a granular fluid nature to represent flowslides would not be productive. Theoretical analysis of the flowslide problem would be greatly assisted by a large and extensive experimental database, as the reality of obtaining accurate and comprehensive field data during a flowslide event will always be remote.

APPENDICES

A.1 INFINITE LANDSLIDE MODEL

With reference to fig A.1:

Volume of element: $V_i = bh_f$

Weight of block $W = \rho_{sat}gh_f$

Resolving along slip plane, at failure

$$\tau \times 1 \times \frac{b}{\cos \beta_b} = W \sin \beta_b$$

$$\tau = \frac{W \sin \beta_b \cos \beta_b}{b}$$

Resolving perpendicular to slip plane

$$(\sigma'_n + u_b) \times 1 \times \frac{b}{\cos \beta_b} = W \cos \beta_b$$

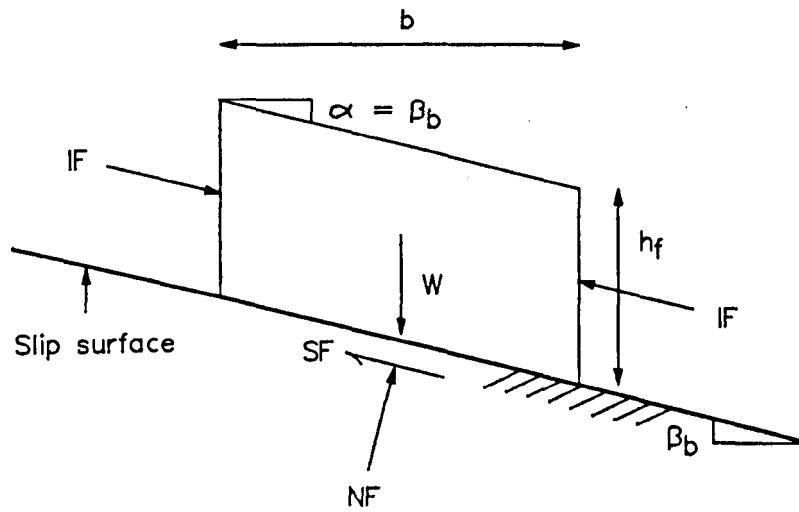
$$\sigma'_n = \frac{W \cos^2 \beta_b}{b} - u_b$$

Therefore

$$\frac{\tau}{\sigma'_n} = \frac{W \sin \beta_b / b}{(W \cos^2 \beta_b / b) - u_b}$$

$$= \frac{\tan \beta_b}{1 - (u_b / \rho_{sat}gh_f \cos^2 \beta_b)}$$

FIG A.1 SCHEMATIC DIAGRAM OF A VERTICAL ELEMENT OF SOIL CONSIDERED DURING INFINITE LANDSLIDE ANALYSIS



Assume unit width along strike and equal interslice forces

- α = surface slope of vertical element
- β_b = slope of slip surface
- b = length of vertical element
- h_f = height of vertical element
- W = weight of vertical element
- SF = shear resistance force
- NF = normal reaction force
- IF = interslice force

Defining

$\tan \phi'_{mob}$ = mobilised angle of friction

$$\begin{aligned}\tan \phi'_{mob} &= \frac{\tau}{\sigma'_n} \\ &= \frac{\tan \beta_b}{1 - (u_b / \rho_{sat} g h_f \cos^2 \beta_b)}\end{aligned}$$

Then, the factor of safety against landsliding is:

$$\begin{aligned}F &= \frac{\tan \phi'}{\tan \phi'_{mob}} \\ F &= \frac{\tan \phi'}{\tan \beta_b} \left(1 - \frac{u_b}{\rho_{sat} g h_f \cos^2 \beta_b} \right)\end{aligned}$$

When $F > 1$ means the slope is safe, and landslide occurs when $F = 1$

When $F = 1$,

$$u_{b,pred} = \left[1 - \frac{\tan \beta_b}{\tan \phi'} \right] \rho_{sat} g h_f \cos^2 \beta_b$$

A.2 EXPERIMENTAL DATA

A 2.1 LABORATORY TESTS PERFORMED

Notes:

SE = camera placed to observe all/large section of flowslide's side elevation

SGR = sluice gate removal

S = seepage artificially induced in sand by opening valve beneath porous plastic for a short period of time (0.5-11.5 seconds).
This method of assisting flowslide motion was only performed during the initial preliminary experiments

Meaning of letters after flowslide test numbers:

P = preliminary experiments

F = first series experiments in modified experimental apparatus

S = second series of experiments in modified experimental apparatus

M = main series of experiments in modified experimental apparatus

Test number	β_{prep} (degrees)	β (degrees)	Video position x (m)	Flowslide Initiation	Comments
0	-	0	-	manual	Visual observation of subaqueous flowslides in small perspex tank
1P	0	0	-	SGR & S	-
2P	0	0	SE	SGR & S	-
3P	0	9	SE	SGR & S	-
4P-9P	-	-	-	-	Information not available
10P	8	6	0.1	SGR	Small volume of pond water present
11P	6	6	SE	SGR & S	Downstream slope of test sample = 3:1, limited flowslide behaviour
12P	16	14	0.1	SGR	-
13P	16	14	-	SGR	Sluice gate failed whilst fluidising sand:- flowslide occurred with very high water content. Surface waves observed (amplitude \approx 15 mm)
14P	14	12	plan at 0	SGR & S	-
15P	14	12	0	SGR	-
16P	12	10	0	SGR	-
17P	11	9	SE	SGR	-
18P	11	9	SE at 0	SGR	-
19P	10	8	SE at 0	SGR	-
20P	12	10.25	-	SGR	-
21P	16	13	-	SGR	-
22P	14	11	-	SGR	-
23P	14	11	-	SGR	-

Test number	β_{prep} (degrees)	β (degrees)	Video position x (m)	Comments
1F	0	0	-	Poor performance of wave transmitter
2F	14	12	0.1	Video camera malfunction
3F	0	0	0.1	Build up of static material observed
4F	0	10	0.1	2 failures of test sample prior to sluice gate removal
5F	11	9	?	Video data unavailable
6F	11	9	-	Poor calibration of wave transmitter
7F	0	0	-	Sine wave superimposed on pressure transducer output
8F	14	12	-	2 kg mass fell into channel during flowslide event

Test number	β_{prep} (degrees)	β (degrees)	Video position x (m)	Wave tip velocity obtained	Comments
1S	14	12	0.1	-	Flowslide moved directly over channel bed for nearly all duration of motion
2S	0	0	-	-	Video camera malfunction
3S	14	12	-	-	Video camera malfunction, levées formed at $x = 0.1$ m
4S	14.6	12	0.5	-	>5 mm of static material observed at channel wall but instability of pressure transducer output suggested flowslide moved over channel bed in centre of channel
5S	14.6	12	-	yes	Video data unavailable
6S	14.6	12	-	-	Test aborted
7S	14.6	12	0.5	yes	>5 mm of static material observed at channel wall but instability of pressure transducer output suggested flowslide moved over channel bed in centre of channel
8S	0	0	0.1	yes	-
9S	14.6	12	0.5	yes	-
10S	14.6	12	0.5	-	-
11S	9	6	0.1	yes	-
12S	9	6	0.1	yes	-
13S	9	6	0.1	yes	-
14S	0	0	0.1	yes	-
15S	0	0	0.1	yes	-
16S	?	9	0.5	yes	-
17S	12	9	0.5	yes	-
18S	-	-	-	-	Test aborted
19S	11	9	0.5	yes	-

Test number	β_{prep} (degrees)	β (degrees)	Video position x (m)	Camera position x (m)	Comments
1M	9	6	0.3	plan	Side elevation photographs not obtainable using plan photography
2M	9	6	0.3	0.3	Quality of photographs poor due to presence of flare
3M	9	6	0.3	0.3	Insufficient detail on photographs due to camera being positioned too far from channel wall
4M	12	9	0.1, 0.5	0.3	Length of exposure on camera too short:- all flowslide material appeared to be static
5M	12	9	0.1, 0.5	0.3	Photographic data good, but density of flowslide unknown due to water not being removed from above test sample
6M	10.7	9	0.1, 0.3, 0.5	plan, 0.3	Video camera did not capture top of flowslide at 0.1 m, photographs at 0.3 m not obtained
7M	10.7	9	0.1, 0.3, 0.5	plan, 0.3	-
8M	10.7	9	0.1, 0.3, 0.5	plan, 0.3	Plasticene dams not removed from channel

A 2.2 SIDE ELEVATIONS OF INITIAL TEST SAMPLE AND FLOWSLIDE AFTER ALL MOTION HAS CEASED

FLOWSLIDE TEST 8S Channel bed slope = 0 degrees				FLOWSLIDE TEST 15S Channel bed slope = 0 degrees			
Side elevation of initial test sample		Side elevation of flowslide after all motion has ceased		Side elevation of initial test sample		Side elevation of flowslide after all motion has ceased	
x (m)	z (m)	x (m)	z (m)	x (m)	z (m)	x (m)	z (m)
-0.5	0	-0.5	0	-0.5	0	-0.5	0
-0.5	0.091	-0.5	0.09	-0.5	0.1	-0.5	0.091
-0.4	0.091	-0.45	0.0883	-0.45	0.102	-0.45	0.087
-0.35	0.0905	-0.4	0.0815	-0.4	0.104	-0.4	0.0785
-0.3	0.09	-0.35	0.0735	-0.35	0.105	-0.35	0.072
-0.25	0.0905	-0.3	0.0685	-0.3	0.106	-0.3	0.067
-0.1	0.092	-0.25	0.0635	-0.25	0.1065	-0.25	0.063
0	0.091	-0.2	0.0588	-0.2	0.107	-0.2	0.0595
0	0	-0.15	0.0545	-0.15	0.1075	-0.15	0.056
		-0.1	0.0505	-0.1	0.108	-0.1	0.054
		-0.05	0.0475	-0.05	0.1065	-0.05	0.051
		0	0.046	0	0.107	0	0.0485
		0.05	0.043	0	0	0.1	0.045
		0.1	0.0385			0.15	0.042
		0.15	0.0345			0.2	0.038
		0.2	0.03			0.25	0.0345
		0.25	0.025			0.3	0.0318
		0.3	0.02			0.35	0.028
		0.35	0.016			0.4	0.0245
		0.4	0.012			0.45	0.021
		0.45	0.008			0.5	0.0175
		0.5	0.004			0.55	0.0145
		0.521	0.0013			0.6	0.011
		0.5235	0			0.615	0.008
						0.7	0.005
						0.76	0

FLOWSLIDE TEST 12S Channel bed slope = 6 degrees				FLOWSLIDE TEST 13S Channel bed slope = 6 degrees			
Side elevation of initial test sample		Side elevation of flowslide after all motion has ceased		Side elevation of initial test sample		Side elevation of flowslide after all motion has ceased	
x (m)	z (m)	x (m)	z (m)	x (m)	z (m)	x (m)	z (m)
-0.5	0	-0.5	0	-0.5	0	-0.5	0
-0.5	0.0545	-0.5	0.0525	-0.5	0.056	-0.5	0.049
-0.45	0.062	-0.45	0.057	-0.45	0.064	-0.45	0.0525
-0.4	0.069	-0.4	0.0623	-0.4	0.0705	-0.4	0.053
-0.35	0.076	-0.35	0.067	-0.35	0.078	-0.35	0.054
-0.3	0.083	-0.3	0.068	-0.3	0.084	-0.3	0.0535
-0.25	0.0905	-0.25	0.059	-0.25	0.091	-0.25	0.052
-0.2	0.098	-0.2	0.045	-0.2	0.098	-0.2	0.045
-0.15	0.105	-0.15	0.036	-0.15	0.105	-0.15	0.037
-0.1	0.1135	-0.1	0.0345	-0.1	0.112	-0.1	0.034
-0.05	0.1205	-0.05	0.037	-0.05	0.119	-0.05	0.034
-0.0135	0.1265	0	0.041	-0.013	0.124	0	0.036
0	0	0.05	0.04	0	0	0.05	0.038
		0.1	0.038			0.1	0.0365
		0.2	0.032			0.2	0.032
		0.3	0.028			0.3	0.028
		0.4	0.0235			0.4	0.025
		0.5	0.0185			0.5	0.0212
		0.6	0.0147			0.6	0.0179
		0.7	0.01			0.7	0.014
		0.8	0.007			0.8	0.0107
		0.9	0.005			0.9	0.0078
		1.0	0.003			1.0	0.005
		1.03	0.002			1.1	0.0023
		1.03	0			1.1	0

FLOWSLIDE TEST 16S Channel bed slope = 9 degrees				FLOWSLIDE TEST 19S Channel bed slope = 9 degrees			
Side elevation of initial test sample		Side elevation of flowslide after all motion has ceased		Side elevation of initial test sample		Side elevation of flowslide after all motion has ceased	
x (m)	z (m)	x (m)	z (m)	x (m)	z (m)	x (m)	z (m)
-0.5	0	-0.5	0	-0.5	0	-0.5	0
-0.5	0.044	-0.5	0.0375	-0.5	0.05	-0.5	0.045
-0.45	0.054	-0.45	0.044	-0.45	0.059	-0.45	0.051
-0.4	0.0635	-0.4	0.0485	-0.4	0.0665	-0.4	0.056
-0.35	0.073	-0.35	0.051	-0.35	0.075	-0.35	0.059
-0.3	0.083	-0.3	0.0505	-0.3	0.084	-0.3	0.059
-0.25	0.0925	-0.25	0.042	-0.25	0.093	-0.25	0.054
-0.2	0.1025	-0.2	0.0327	-0.2	0.1025	-0.2	0.043
-0.15	0.112	-0.15	0.029	-0.15	0.111	-0.15	0.0315
-0.1	0.123	-0.1	0.029	-0.1	0.12	-0.1	0.0325
-0.05	0.1315	-0.05	0.0292	-0.05	0.1284	-0.05	0.0315
-0.0219	0.1383	0	0.032	-0.0211	0.1333	0	0.0315
0	0	0.05	0.031	0	0	0.05	0.0315
		0.1	0.0294			0.1	0.0305
		0.15	0.0275			0.2	0.029
		0.2	0.026			0.3	0.027
		0.3	0.0255			0.4	0.024
		0.4	0.024			0.5	0.02
		0.5	0.022			0.6	0.017
		0.6	0.0195			0.7	0.015
		0.7	0.018			0.8	0.013
		0.8	0.015			0.9	0.01
		0.9	0.013			1.0	0.006
		1.0	0.011			1.1	0.005
		1.1	0.009			1.2	0.004
		1.2	0.007			1.3	0.0035
		1.3	0.004			1.4	0.002
		1.4	0.002			1.413	0
		1.5	0.0015				
		1.56	0				

FLOWSLIDE TEST 9S Channel bed slope = 12 degrees				FLOWSLIDE TEST 10S Channel bed slope = 12 degrees			
Side elevation of initial test sample		Side elevation of flowslide after all motion has ceased		Side elevation of initial test sample		Side elevation of flowslide after all motion has ceased	
x (m)	z (m)	x (m)	z (m)	x (m)	z (m)	x (m)	z (m)
-0.5	0	-0.5	0	-0.5	0	-0.5	0
-0.5	0.024	-0.5	0.022	-0.5	0.022	-0.5	0.019
-0.45	0.0345	-0.45	0.03	-0.45	0.033	-0.45	0.029
-0.4	0.0435	-0.4	0.0357	-0.4	0.0435	-0.4	0.0325
-0.35	0.055	-0.35	0.039	-0.35	0.0545	-0.35	0.0455
-0.3	0.0665	-0.3	0.039	-0.3	0.066	-0.3	0.048
-0.25	0.079	-0.25	0.034	-0.25	0.078	-0.25	0.036
-0.2	0.091	-0.227	0.031	-0.2	0.0917	-0.2	0.021
-0.15	0.1035	-0.22	0.025	-0.15	0.103	-0.15	0.008
-0.1	0.1155	-0.2	0.02	-0.1	0.1107	-0.1	0.005
-0.05	0.1275	-0.15	0.015	-0.05	0.127	-0.05	0.007
-0.028	0.133	-0.1	0.0125	-0.0285	0.134	0	0.014
0	0	-0.05	0.012	0	0	0.05	0.0135
		0	0.013			0.1	0.0105
		0.1	0.012			0.2	0.012
		0.15	0.0105			0.3	0.009
		0.2	0.0105			0.4	0.01
		0.3	0.011			0.5	0.008
		0.4	0.01			0.6	0.0078
		0.5	0.01			0.7	0.0078
		0.6	0.01			0.8	0.008
		0.7	0.0105			0.9	0.009
		0.8	0.011			1.0	0.011
		0.9	0.011			1.1	0.009
		1.0	0.011			1.2	0.007
		1.1	0.009			1.3	0.0065
		1.2	0.009			1.4	0.008
		1.3	0.008			1.5	0.008
		1.4	0.008			1.6	0.006
		1.5	0.008			1.7	0.008
		1.6	0.008			1.8	0.008
		1.7	0.008			1.9	0.007
		1.8	0.008			2.0	0.008
		1.9	0.0055			2.1	0.008
		2.0	0.0055			2.2	0.0065
		2.1	0.006			2.3	0.0055
		2.2	0.006			2.4	0.0055
		2.3	0.006			2.5	0.0055
		2.4	0.0065			2.6	0.0055
		2.5	0.006			2.7	0.005
		2.6	0.004			2.8	0.005
		2.7	0.003			2.9	0.0055
		3.0	0.002			3.0	0.004
		3.0	0			3.1	0.004
						3.2	0.004
						3.3	0.0045
						3.4	0.004
						3.5	0.004

FLOWSLIDE TEST 3M Channel bed slope = 6 degrees				FLOWSLIDE TEST 4M Channel bed slope = 9 degrees			
Side elevation of initial test sample		Side elevation of flowslide after all motion has ceased		Side elevation of initial test sample		Side elevation of flowslide after all motion has ceased	
x (m)	z (m)	x (m)	z (m)	x (m)	z (m)	x (m)	z (m)
-0.5	0	-0.5	0	-0.5	0	-0.5	0
-0.5	0.059	-0.5	0.054	-0.5	0.0445	-0.5	0.04
-0.45	0.0645	-0.45	0.06	-0.45	0.05	-0.45	0.0485
-0.4	0.07	-0.4	0.064	-0.4	0.054	-0.4	0.0555
-0.35	0.076	-0.35	0.0697	-0.35	0.064	-0.35	0.062
-0.3	0.0825	-0.3	0.075	-0.3	0.075	-0.3	0.0685
-0.25	0.089	-0.25	0.077	-0.25	0.0845	-0.25	0.065
-0.2	0.0955	-0.2	0.058	-0.2	0.094	-0.2	0.054
-0.15	0.1015	-0.15	0.053	-0.15	0.104	-0.15	0.0455
-0.1	0.108	-0.1	0.051	-0.1	0.113	-0.1	0.044
-0.05	0.1155	-0.05	0.0485	-0.05	0.123	-0.05	0.042
-0.0127	0.121	0	0.0455	-0.0208	0.131	0	0.04
0	0	0.05	0.041	0	0	0.05	0.0385
		0.1	0.036			0.08	0.039
		0.2	0.028			0.09	0.0385
		0.3	0.019			0.1	0.038
		0.4	0.01			0.11	0.0372
		0.5	0.007			0.12	0.0365
		0.6	0.0035			0.13	0.036
		0.64	0.002			0.14	0.035
		0.64	0			0.2	0.029
						0.3	0.026
						0.4	0.0205
						0.5	0.0155
						0.6	0.013
						0.7	0.0085
						0.8	0.0075
						0.84	0

FLOWSLIDE TEST 6M Channel bed slope = 9 degrees				FLOWSLIDE TEST 7M Channel bed slope = 9 degrees			
Side elevation of initial test sample		Side elevation of flowslide after all motion has ceased		Side elevation of initial test sample		Side elevation of flowslide after all motion has ceased	
x (m)	z (m)	x (m)	z (m)	x (m)	z (m)	x (m)	z (m)
-0.5	0	-0.5	0	-0.5	0	-0.5	0
-0.5	0.046	-0.5	0.0385	-0.5	0.0505	-0.5	0.0415
-0.45	0.056	-0.45	0.046	-0.48	0.0545	-0.45	0.0445
-0.4	0.064	-0.4	0.052	-0.46	0.0575	-0.4	0.0445
-0.35	0.073	-0.35	0.055	-0.44	0.0605	-0.35	0.0435
-0.3	0.081	-0.3	0.057	-0.42	0.0635	-0.3	0.042
-0.25	0.09	-0.25	0.065	-0.4	0.0665	-0.25	0.0385
-0.2	0.099	-0.2	0.047	-0.38	0.07	-0.2	0.032
-0.15	0.1075	-0.15	0.041	-0.36	0.0735	-0.15	0.0295
-0.1	0.1165	-0.1	0.039	-0.34	0.0765	-0.1	0.0297
-0.05	0.1265	-0.05	0.0385	-0.32	0.08	-0.05	0.033
-0.021	0.1322	0.05	0.0325	-0.3	0.0845	0	0.035
0	0	0.08	0.033	-0.28	0.0875	0.05	0.033
		0.09	0.032	-0.26	0.091	0.1	0.03
		0.1	0.0317	-0.24	0.0945	0.15	0.029
		0.11	0.0313	-0.22	0.098	0.2	0.028
		0.12	0.031	-0.2	0.1015	0.25	0.026
		0.13	0.0302	-0.18	0.105	0.3	0.0235
		0.14	0.0295	-0.16	0.108	0.35	0.022
		0.16	0.029	-0.14	0.1115	0.45	0.0218
		0.18	0.028	-0.12	0.115	0.5	0.0202
		0.22	0.0265	-0.1	0.1185	0.6	0.018
		0.3	0.022	-0.08	0.1225	0.7	0.0165
		0.38	0.0195	-0.06	0.126	0.8	0.015
		0.5	0.016	-0.04	0.13	0.9	0.014
		0.6	0.0125	-0.0215	0.134	1.0	0.013
		0.7	0.01	0	0	1.1	0.01
		0.8	0.0085			1.2	0.0085
		0.9	0.008			1.3	0.006
		1.0	0.006			1.4	0.005
		1.1	0.005			1.5	0.0035
		1.2	0.0035			1.6	0.0025
		1.3	0.002			1.66	0.002
		1.5	0.0017			1.66	0
		1.51	0				

A 2.3 TEMPORAL VARIATION OF THE FLOWSLIDE SURFACE ANGLE

FLOWSLIDE TEST 3M Channel bed slope = 6 degrees		FLOWSLIDE TEST 4M Channel bed slope = 9 degrees	
Video records taken at the 0.3 m site		Video records taken at the 0.5 m site	
<i>t</i> (s)	<i>α</i> (degrees)	<i>t</i> (s)	<i>α</i> (degrees)
20	8.47	23.5	13.3
25	6.7	25.1	14.1
30	8.1	26	13.3
35	7.1	26.2	14.1
40	8.4	26.3	13.2
45	8.1	26.4	13.8
50	9.5	28.7	13.3
55	9.5	30.8	12.2
60	9.5	32	11.4
		34.2	10.6
		37.3	11.2
		38.7	11.2
		41	10.3
		45	10.8
		50	10.2
		55	11.2
		60	11.5
		65	10.5
		70	11.5

A.3 REFERENCES

- Alarcon-Guzman, A. / Leonards, G.A. / Chameau, J.L.
'Undrained monotonic and cyclic strength of sands'
A.S.C.E. Journal of Geotechnical Engineering,
v114, No 10, October 1988, pp 1089-1109
- Alarcon, A. / Leonards, G.A.
Discussion of 'Liquefaction evaluation procedure' [Poulos et al (1985);
A.S.C.E. Journal of Geotechnical Engineering, v111, No 6, June 1985, pp 772-792]
A.S.C.E. Journal of Geotechnical Engineering, v114, No 2, Feb 1988, pp 232-235
- Atkinson, J.H. / Bransby, P.L.
'The mechanics of soils, an introduction to critical state soil mechanics'
McGraw-Hill Book Company (UK) Ltd, 1978
- Augenstein, D.A. / Hogg, R.
'Friction factors for powder flow'
Powder Technology, v10, 1974, pp 43-49
- Augenstein, D.A. / Hogg, R.
'An experimental study of the flow of dry powders over inclined surfaces'
Powder Technology, v19, 1978, pp 205-215
- Bagnold, R.A.
'Experiments on a gravity-free dispersion of large solid spheres in a Newtonian fluid under shear'
Proceedings of the Royal Society of London, Series A, v225, 1954, pp 49-63
- Bagnold, R.A.
'Some flume experiments on large grains, but little denser than the transporting fluid and their implications'
Proceedings of the Institute of Civil Engineers, pt 111, 1955, pp 174-205
- Bagnold, R.A.
'Flow of cohesionless grains in fluids'
Phil. Trans. Royal Society of London, Series A, v249, 1956, pp 235-297
- Bagnold, R.A.
'The shearing and dilatation of dry sand and the 'singing' mechanism'
Proceedings of the Royal Society of London, Series A, v295, Dec 1966, pp 219-232
- Bailard, J.A. / Inman, D.L.
'A reexamination of Bagnold's granular-fluid model and bed load transport equation'
Journal of Geophysical Research, v84, No C12, December 1979, pp 7827-7833
- Bezuijen, A. / Mastbergen, D.R.
'On the construction of sand fill dams - Part 2: Soil mechanical aspects'
Proceedings of the International Symposium on Modelling Soil-Water-Structure Interactions, Delft, The Netherlands, 1988, pp 363-371

- Bishop, A.W.
 'The stability of tips and spoil heaps'
 Quarterly Journal of Engineering Geology, v6 1973, pp 335-376
- Bolton, M.
 'A guide to soil mechanics'
 MacMillan Publishers Ltd, 1984
- Bolton, M.D.
 'The strength and dilatancy of sands'
 Géotechnique 36, No 1, 1986, pp 65-78
- Britto, A.M. / Gunn, M.J.
 'Critical state soil mechanics via finite elements'
 Publishers: Ellis Horwood Ltd (1987)
- B.S. 1377: 1975
 'Methods of test for soils for Civil Engineering purposes'
 British Standards Institution, London, 1975
- Cannon, S.H. / Savage, W.Z.
 'A mass change model for the estimation of debris-flow runout'
 Journal of Geology, 1988, v96, pp 221-227
- Casagrande, A
 'On liquefaction phenomena'
 Report of lecture; Green, P.A. / Ferguson, P.A.S.
 Géotechnique 21, 1971, pp 197-202
- Castro, G. / Poulos, S.J.
 'Factors affecting liquefaction and cyclic mobility'
 A.S.C.E. Journal of Geotechnical Engineering,
 v103, No GT6, June 1977, pp 501-516
- Davies, T.R.H.
 'Debris flow surges - a laboratory investigation'
 Mitteilung No6 der Versuchsanstalt für Wasserbau,
 Hydrologie und Glaziologie an der ETH (1988) 122 pp
- Dobry, R. / Alvarez, L.
 'Seismic failures of Chilean tailings dams'
 A.S.C.E. Journal of Soil Mechanics and Foundations Division,
 v93, No SM6, November 1967, pp 237-260
- De Groot, M.B. / Silvis, F. / van Rossum, H. / Koster, M.J.
 'Liquefied sand flowing over a gentle slope'
 Ninth Eur. Conf. Soil Mech. Found. Eng., Dublin, Ireland, 1987
- De Groot, M.B. / Heezen, F.T. / Mastbergen, D.R. / Stefess, H.
 'Slopes and densities of hydraulically placed sands'
 Hydraulic Fill Structures, Specialty Conference,
 A.S.C.E. Geotechnical Division, Fort Collins, CO, August 1988, pp 32-51

- Eckersley, J.D.
 'Instrumented laboratory flowslides'
 Géotechnique 40, No 3, 1990, pp 489-502
- Fowler, D. / Russell, H.
 'Tip anarchy risks disaster'
 New Civil Engineer, 26 March 1992
- Griffiths, D.E. / Turnbull, J.
 'A multi-electrode array for resistivity surveying'
 First Break, Vol 3, No 7, July 1985, pp 16-20
- Griffiths, D.H. / Turnbull, J. / Olayinka, A.I.
 'Two-dimensional resistivity mapping with a computer-controlled array'
 First Break, Vol 8, No 4, April 1990, pp 121-129
- Kleiner, D.E.
 'Design and construction of an embankment dam to impound gypsum wastes'
 Proceedings of the ICOLD, 1976, pp 235-249
- Hanes, D.M. / Inman, D.L.
 'Observations of rapidly flowing granular-fluid materials'
 Journal of Fluid Mechanics, v150, 1985, pp 357-380
- Heidari, M. / James, R.G.
 'Centrifugal modelling of earthquake induced liquefaction in a column of sand'
 Soil Dynamics and Earthquake Engineering Conference,
 Southampton, July 1982, pp 271-281
- Hird, C.C. / Hassona, F.
 Discussion of 'A state parameter for sands' [Been/Jefferies (1985);
 Géotechnique 35, No 2, pp 99-112]
 Géotechnique 36, No 1, 1986, pp 124-127
- Hird, C.C. / Hassona, F.A.K.
 'Some factors affecting the liquefaction and flow of saturated sands in laboratory tests'
 Engineering Geology, 28 (1990), pp 149-170
- Hird, C.C. / Spence, K.J.
 Discussion of 'Instrumented laboratory flowslides' [Eckersley (1990); Géotechnique
 40, No 3, pp 489-502]
 Géotechnique 41, No 2, 1991, pp 277-279
- Hsu, K.J.
 'Catastrophic debris streams (sturzstroms) generated by rockfalls'
 Geological Society of America Bulletin, v86, January 1975, pp 129-140
- Hungr, O. / Morgenstern, N.R.
 'High velocity ring shear tests on sand'
 Géotechnique 34, No 3, 1984, pp 415-421

Hungr, O. / Morgenstern, N.R.

'Experiments on the flow behaviour of granular materials at high velocity in an open channel'

Géotechnique 34, No 3, 1984, pp 405-413

Hutchinson, J.N.

'A sliding-consolidation model for flow slides'

Canadian Geotechnical Journal, v23, No 2, May 1986, pp 115-126

Jeyapalan, J.K.

'Analyses of flow failures of mine tailings impoundments'

A dissertation presented to the University of California, at Berkeley, Calif., in 1980, in partial requirements for the degree of Doctor of Philosophy

Johnson, A.M. / Rodine, J.R.

'Debris flow'

from 'Slope instability'; Edited by Brunnsden, D. / Prior, D.B., John Wiley and Sons Ltd, 1984, pp 257-361

Kleiner, D.E.

'Design and construction of an embankment dam to impound gypsum wastes'

Proceedings of the ICOLD, 1976, pp 235-249

Kramer, S.L. / Seed, H.B.

'Initiation of soil liquefaction under static loading conditons'

A.S.C.E. Journal of Geotechnical Engineering, v114, No 4, April 1988, pp 412-430

Lucia, P.C.

'Review of experiences with flow failures of tailings dams and waste'

Dissertation presented to the University of California, at Berkley, Calif., in 1981 in partial requirements for the degree of Doctor of Philosophy

Mastbergen, D.R. / Bezuijen, A. / Winterwerp, J.C.

'On the construction of sand fill dams; Part 1: Hydraulic aspects'

Proceedings of the International. Symposium on Modelling Soil-Water-Structure Interactions, Delft, The Netherlands, 1988

New Civil Engineer

'China clay spoil slip alarms experts'

New Civil Engineer, 15 February 1990

Noel, M. / Biwen, X.

'Archaeological investigation by electrical resistivity tomography: a preliminary study'

Geophys. J. Int (1991) v107, pp 95-102

Pierson, T.C.

'Dominant particle support mechanisms in debris flows at Mt Thomas, New Zealand, and implications for flow mobility'

Sedimentology (1981), v28, pp 49-60

- Poulos, S.G.
 'The steady state of deformation'
 A.S.C.E. Journal of Geotechnical Engineering,
 v107, No GT5, May 1981, pp 553-562
- Poulos, S.G. / Castro, G. / France, J.W.
 'Liquefaction evaluation procedure'
 A.S.C.E. Journal of Geotechnical Engineering, v111, No 6, June 1985, pp 772-792
- Poulos, S.G. / Castro, G. / France, J.W.
 Closure on discussion of 'Liquefaction evaluation procedure' [Poulos et al (1985);
 A.S.C.E. Journal of Geotechnical Engineering, v111, No 6, June 1985, pp 772-792]
 A.S.C.E. Journal of Geotechnical Engineering, v114, No 2, Feb 1988, pp 251-259
- Rouse, W.C.
 'Flowslides'
 from 'Slope instability'; Edited by Brunnsden, D. / Prior, D.B.,
 John Wiley and Sons Ltd, 1984, pp 491-522
- Savage, S.B.
 'Flow of granular materials'
 from 'Theoretical and Applied Mechanics', pp 241-266
 Elsevier Science Publishers B.V. (North Holland), 1989
- Savage, S.B. / Hutter, K.
 'The motion of a finite mass of granular material down a rough incline'
 Journal of Fluid Mechanics (1989), v199, pp 177-215
- Savage, S.B. / Sayed, M.
 'Stresses developed by dry cohesionless granular materials sheared in an annular
 shear cell'
 Journal of Fluid Mechanics (1985), v150, pp 391-430
- Schofield, A / Wroth, C.P.
 'Critical state soil mechanics'
 Publishers: McGraw-Hill Book Co., New York, N.Y. 1968
- Scott, C.R.
 'An Introduction to Soil Mechanics and Foundations'
 Applied Science Publishers Ltd, 1980
- Seed, H.B.
 'Landslides during earthquakes due to soil liquefaction'
 A.S.C.E. Journal of Soil Mechanics and Foundations Division,
 v94, No SM5, September 1968, pp 1055-1122
- Silvis, F. / Lindenberg, J. / van Heteren, J.
 'A numerical model to describe the initiation of flowslides in under water sand
 slopes'
 Int. Symp. Modelling Soil-Water-Structure Interactions, Delft, The Netherlands, 1988

Sousa, J. / Voight, B.
'Continuum simulation of flow failures'
Géotechnique 41, No 4, 1991, pp 515-538

Tozer, R.C. / Simpson, J.C. / Freeston, I.L. / Mathias, J.M.
'Noncontact induced current impedance imaging'
Electronic letters, 9 April 1992, v28, No 8

Vaid, Y.P. / Chem, J.C. / Tumi, H.
'Confining pressure, grain angularity and liquefaction'
A.S.C.E. Journal of Geotechnical Engineering,
v111, No 10, October 1985, pp 1229-1235

Vick, S.G.
'Planning, Design, and analysis of Tailings Dams'
Publishers: John Wiley and Sons, Inc. (1983)

Whitham, G.B.
'The effects of hydraulic resistance in the dam-break problem'
Proceedings of the Royal Society of London, Series A, v227, 1955, pp 399-407

Winterwerp, J.C. / De Groot, M.B. / Mastbergen, D.R. / Verwoert, H.
'Hyperconcentrated sand-water mixture flows over flat bed'
A.S.C.E. Journal of Hydraulic Engineering, v116, No 1, January 1990, pp 36-54